Universitat Autònoma de Barcelona

Micro-RNAs in ovarian cancer as tools for diagnosis and therapy

Blanca Majem Cavaller

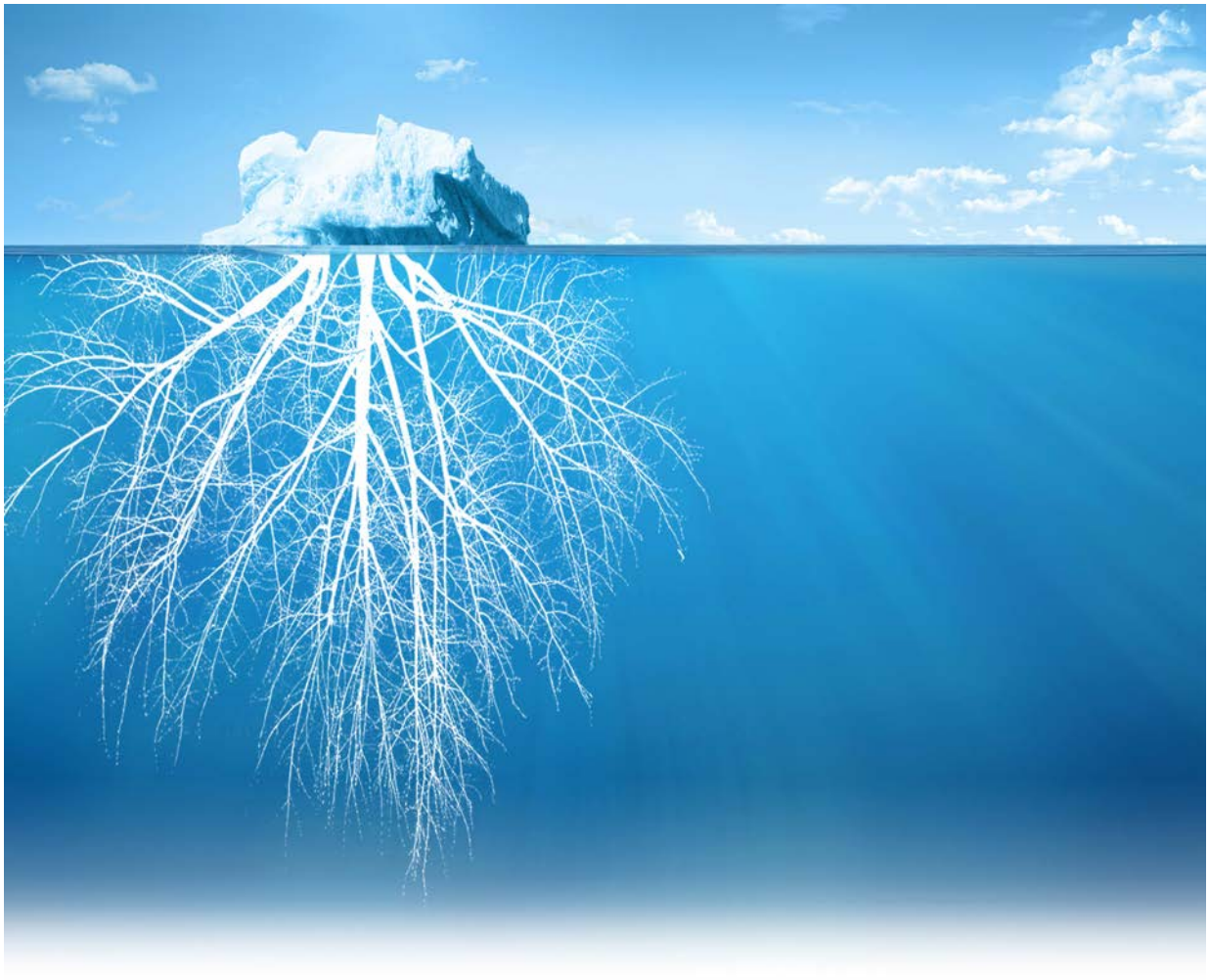

Micro-RNAs in ovarian cancer as tools for diagnosis and therapy

Blanca Majem Cavaller

Blanca Majem Cavaller

June 27th, 2017

Micro-RNAs in ovarian cancer as tools for diagnosis and therapy

PhD thesis presented by

Blanca Majem Cavaller

To obtain the degree of

PhD for the *Universitat Autònoma de Barcelona (UAB)*

PhD thesis done at the Cell Cycle and Cancer laboratory, within the Biomedical Research Group in Gynecology, at Vall d'Hebron Research Institute (VHIR) and University Hospital (HUVH), under the supervision of

Dr. Anna Santamaria, Dr. Marina Rigau and Dr. Marta Llauradó

Thesis affiliated to the Department of Cell Biology, Physiology and Immunology from the School of Medicine at UAB, in the PhD program of Cell Biology, under the tutoring of **Dr. Rosa Miró**

***Universitat Autònoma de Barcelona*, June 27th 2017**

Dr. Anna Santamaria
(Director)

Dr. Marina Rigau
(Director)

Dr. Marta Llauradó
(Director)

Dr. Rosa Miró
(Tutor)

Blanca Majem Cavaller
(Student)

“The triumph is not always to conquer but never to be discouraged”
(Anonymous)

"Courage is not the absence of fear, but the triumph over it”
(Nelson Mandela)

INDEX

ABBREVIATIONS

SRY _ sex-determining region Y protein
FOXL2 _ forkhead box protein L2
FST _ follistatin
OSE _ ovarian surface epithelium
OC _ ovarian cancer
SV _ survival
EMT _ epithelial-mesenchymal transition
FIGO _ International Federation of Gynecology and Obstetrics
HGSC _ high-grade serous carcinomas
EOC _ Epithelial Ovarian Cancer
CCC _ clear-cell carcinoma
MC _ mucinous carcinoma
LGSC _ low-grade serous carcinoma
STIC _ Serous tubal intraepithelial carcinoma
G1-3 _ histological grade 1-3
HR _ homologous recombination
TCGA _ The Cancer Genome Atlas
RRSO _ risk reducing bilateral salpingo-oophorectomy
FTE _ fallopian tube epithelium
CA125 _ cancer antigen 125
MUC16 _ mucin 16
US _ ultrasound
MRI _ magnetic resonance imaging
CT _ computed tomography
RMI _ risk of malignancy index
FDA _ Food and Drug Administration
NED _ no evidence of disease
hCG _ human chorionic gonadotropin
AFP _ alpha-fetoprotein
PLCO _ Prostate, Lung, Colorectal and Ovarian
UKTOCS _ United Kingdom Trial of Ovarian Cancer Screening
ROCA _ risk of ovarian cancer algorithm
PPV _ positive predictive value
HE4 _ Human Epididymis Protein 4
FSH _ follicular stimulating hormone
WS _ whole saliva
mRNA _ messenger RNA
RTqPCR _ Real Time quantitative PCR
SKB _ Salivaomics Knowledge Base
exRNA _ extracellular RNA
OFNASET _ Oral Fluid NanoSensor Test
ncRNAs _ non-coding RNAs
GCIG _ Gynecologic Cancer Inter Group
R0 _ No macroscopic residual disease
PDS _ Primary debulking surgery
CTH _ chemotherapy
NACT _ Neoadjuvant chemotherapy
IDS _ interval debulking surgery
PDX _ patient-derived xenografts
PFS _ progression-free survival
PFI _ platinum-free interval
AAs _ angiogenic agents
VDAs _ vascular-disrupting agents
PARP _ poly (ADP-ribose) polymerase
EMA _ European Medicines Agency
DDR _ DNA damage repair
CNA _ copy number alterations
siRNA _ small interfering RNA
piRNA _ PIWI - interacting RNA

miRNA _ microRNA
nt _ nucleotides
AGO _ Argonaute
TSS _ transcription start site
RNA Pol II _ RNA polymerase II
pri-miRNA _ primary miRNA
dsRNA _ double-strand RNA
ssRNA _ single-strand RNA
RIIID _ RNase III domains
pre-miRNA _ precursor miRNA
NLS _ nuclear localization signals
dsRBD _ dsRNA binding domains
EXP5_ exportin 5
RAN-GTP _ GTP-binding nuclear protein RAN
TRBP _ TAR RNA binding protein
RISC _ RNA-induced silencing complex
3'UTR _ 3' untranslated region
SNPs _ single nucleotide polymorphism
ctDNA _ circulating tumor cell-free DNA
CTCs _ circulating tumor cells
CFS _ cell-free saliva
FFPE _ formalin-fixed paraffin embedded
VNED _ alive, no evidence disease
P-QT _ primary tumor after NACT
Rec _ tumor implant of a recurrent OC
Cyst _ Cystadenoma
ATCC _ American Type Culture Collection
ECACC _ European Collection of Authenticated Cell Cultures
FBS _ fetal bovine serum
QCs _ quality controls
SE50 _ Single-End 50 bp
RT _ reverse transcription
TAC _ Transcription Analysis Console
GFP _ green fluorescent protein
BSA _ bovine serum albumin
PI _ Propidium iodide
PBS _ phosphate-buffered saline
SKE _ SKOV3-Explanted
DE _ Differential expression
circRNA _ circular RNA
PCA _ principal component analysis
SEM _ standard error of the mean
FDR _ adjusted p-value/false discovery rate
GSEA _ Gene Set Enrichment Analysis
HOMD _ human oral microbiome database
NES _ normalized enriched score
ceRNA _ competitive endogenous RNA
miR-34b*/c _ miR-34b-3p, miR-34c-3p and miR-34c-5p
AR _ androgen receptor
BH _ Bcl-2 Homology domains
ER _ endoplasmic reticulum
HAX1 _ HCLS1 Associated Protein X-1
RAB1B _ Ras-related protein Rab-1B
PBX3 _ pre-B cell leukemia homeobox 3
CDCP1 _ CUB domain-containing protein 1
PLAGL2 _ PLAG1 Like Zinc Finger 2
CDK2/4 _ cyclin dependent kinase 2/4
CSK1B _ the CDK regulatory subunit 1
CDKN1B _CDK inhibitor 1B

SKP2 _ the S-phase kinase associated protein 2

CCNE1 _ cyclin-E1

Rb _ retinoblastoma

p-Rb _ phosphorylated form of Rb

GSK3β _ glycogen synthase kinase 3β

SMURF2 _ SMAD Specific E3 Ubiquitin Protein Ligase 2

1. INTRODUCTION

1.1. OVARIAN CANCER GENERALITIES

The embryonic gonad is initially one tissue with two fates, which can develop into either testes or ovaries that in turn govern phenotypic sex through the production of hormones. Male differentiation program is induced by the presence of the Y chromosome and the expression of the sex-determining region Y protein (SRY) and the SOX9 transcription factor (among others)[1,2], the lack of which determines the embryonic gonad to develop into ovarian tissue through a tight balance of a genetic program coordinated by sex hormones (Figure 1), including forkhead box protein L2 (FOXL2), WNT4 and follistatin (FST)[2]. They are self-reinforcing and cross-inhibitory during gonadal development and in the adult gonads[3]. The predominant cells in the cortex of the differentiated gonad are ovarian stromal cells and ovarian follicles, which consist of oocytes and the surrounding granulose and theca cells[2]. The cortex of the female gonad is then covered by a specialized coelomic epithelium that is known as the ovarian surface epithelium (OSE) (Figure 1).

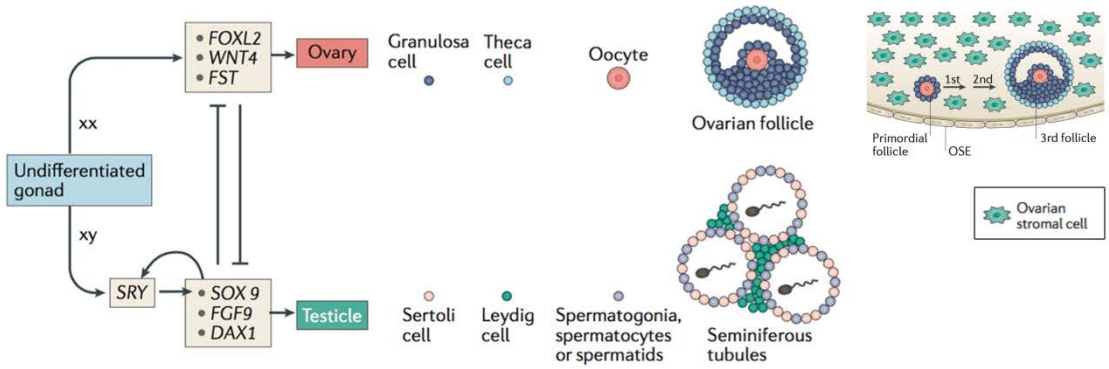

Figure 1: The development of the ovary. Adapted from Karnezis *et al* [2].

Early in development, the future OSE forms part of the coelomic epithelium, which is the mesodermal derived epithelial lining of the intraembryonic coelom, including the presumptive gonadal area and that, by proliferation and differentiation, gives rise to the external part of the gonad[4]. OSE acquires distinct characteristics to that of the extraovarian mesothelium (i.e. lining of the peritoneal wall, fallopian tubes, uterus, etc.) despite they are identical to their origin in the coelomic epithelium and face a similar environment as both line the pelvic cavity[4].

Since the early 90's, the functions of the OSE cells are well known such as contributing to the postovulatory repair of the ovarian cortex by proliferation and migration over the site of follicular rupture, by deposition of a basement membrane, and by the autonomous production of connective tissue-type extracellular matrix for the remodeling of the ovarian cortical stroma[5]. Taking into account that OSE is characterized as a non-canonical epithelia which contains at the same time mesenchymal markers (such as N-cadherin and Vimentin, but not E-cadherin) and epithelial markers (such as cytokeratin 7, 8, 18 and 19); incomplete tight junctions; low attachment to its basal membrane; and postovulatory wound healing and regenerative capacities[5,6]; OSE becomes a prone epithelia for metaplastic changes (i.e. invaginations, inclusions cysts, benign and malign ovarian neoplasms) due to the cellular plasticity associated to its features.

1.1.1. EPIDEMIOLOGY

Cancer is a major public health problem worldwide and is the second leading cause of death in the US, accounting for almost 1.7 million new cases for the 2017 regarding all cancer sites[7]. Of these, 22,440 accounts for estimated new cases diagnosed for ovarian cancer (OC), with around 63% of deaths (14,080 of estimated deaths). Despite the low incidence among female cancers (2.6%), OC is the most lethal gynecological malignancy and is situated in the 5th position of cancer-related deaths in women, below Lung, Breast, Colon and Pancreas[7].

1.1.2. STAGING AND SURVIVAL

OC is a particular disease due to its metastatic behavior because primary tumor cells do not have to go through anatomical barriers and do not follow the canonical pattern of dissemination by the hematogenous path (i.e. degradation of the extracellular matrix, intravasation, travel through the blood stream, extravasation, colonization of distant organs, etc.). Instead, tumors originated in the ovary metastasize directly through the peritoneal cavity to local (i.e. fallopian tubes, uterus), regional (i.e. bowel, peritoneal wall, etc.) and distant organs (i.e. liver, pancreas, lungs, etc.); what it is commonly known as transcoelomic metastasis[8,9]. Cell detachment of the primary tumor, survival (SV), resistance to anoikis, evasion of immunological surveillance, epithelial-mesenchymal transition (EMT), spheroid formation (including the interaction with the tumor-associated macrophages[9]), ascites formation (abnormal accumulation of fluid in

the peritoneal cavity due to the presence of inflammation and/or malignant cells) and peritoneal implantation (including omentum, pelvic and abdominal viscera), are the most common steps in the process of OC methastasis[8]. The stage of the disease is determined by the extent of the primary tumor cells into the peritoneal cavity and the organs affected (including lymph nodes), by using the International Federation of Gynecology and Obstetrics (FIGO) staging system (Table 1).

FIGO staging classification for cancer of the ovary, fallopian tube, and peritoneum	TNM classification
Stage I: Tumor confined to ovaries or fallopian tube(s)	**T1-N0-M0**
IA: Tumor limited to 1 ovary (capsule intact) or fallopian tube; no tumor on ovarian or fallopian tube surface; no malignant cells in the ascites or peritoneal washings	T1a-N0-M0
IB: Tumor limited to both ovaries (capsules intact) or fallopian tubes; no tumor on ovarian or fallopian tube surface; no malignant cells in the ascites or peritoneal washings	T1b-N0-M0
IC: Tumor limited to 1 or both ovaries or fallopian tubes, with any of the following:	T1c-N0-M0
IC1: Surgical spill intraoperatively	T1c1-N0-M0
IC2: Capsule ruptured before surgery or tumor on ovarian or fallopian tube surface	T1c2-N0-M0
IC3: Malignant cells in the ascites or peritoneal washings	T1c3-N0-M0
Stage II: Tumor involves 1 or both ovaries or fallopian tubes with pelvic extension (below pelvic brim) or peritoneal cancer	**T2-N0-M0**
IIA: Extension and/or implants on uterus and/or fallopian tubes and/or ovaries	T2a-N0-M0
IIB: Extension to other pelvic intraperitoneal tissues	T2b-N0-M0
Stage III: Tumor involves 1 or both ovaries or fallopian tubes, or peritoneal cancer, with cytologically or histologically confirmed spread to the peritoneum outside the pelvis and/or metastasis to the retroperitoneal lymph nodes	**T3**
IIIA: Metastasis to the retroperitoneal lymph nodes with or without microscopic peritoneal involvement beyond the pelvis	T1/T2/T3a-N1-M0
IIIA1: Positive retroperitoneal lymph nodes only (cytologically/histologically proven):	T3a/T3aN1-M0
IIIA1(i) Metastasis up to 10 mm in greatest dimension	
IIIA1(ii) Metastasis more than 10 mm in greatest dimension	
IIIA2: Microscopic extrapelvic (above the pelvic brim) peritoneal involvement with or without positive retroperitoneal lymph nodes	T3a2-N0/N1-M0
IIIB: Macroscopic peritoneal metastasis beyond the pelvis up to 2 cm in greatest dimension, with or without metastasis to the retroperitoneal lymph nodes	T3b-N0/N1-M0
IIIC: Macroscopic peritoneal metastasis beyond the pelvis more than 2 cm in greatest dimension, with or without metastasis to the retroperitoneal lymph nodes (includes extension of tumor to capsule of liver and spleen without parenchymal involvement of either organ)	T3c-N0/N1-M0
Stage IV: Distant metastasis excluding peritoneal metastases	Any T, any N, M1
IVA: Pleural effusion with positive cytology	
IVB: Parenchymal metastases and metastases to extra-abdominal organs (including inguinal lymph nodes and lymph nodes outside of the abdominal cavity)	

Table 1: FIGO staging of OC. FIGO: International Federation of Gynecology and Obstetrics. TNM: TNM classification of malignant tumors. (N) Regional nodes: (Nx) Regional lymph nodes cannot be assessed; (N0) No regional lymph node metastasis; (N1) Regional lymph node metastasis. (M) Distant metastasis: (Mx) Distant metastasis cannot be assessed; (M0) No distant metastasis; (M1) Distant metastasis (excluding peritoneal metastasis). Adapted from[10–12].

Actually, OC remains largely a surgically staged neoplasm, where tumor staging is based on surgical assessment and pathological examination of the cancer at initial diagnosis, including tissue biopsy, abdominal fluid, and if a malignant pathological examination is confirmed, then by the removal of lymph nodes and all the other macroscopic tumor specimens the stage is determined[10,11].

In addition, FIGO is updating the staging classification of OC and such classifications have considerably changed over the years. For example, as shown in Table 1, stage classification comprises cancers of the ovary, but also cancers aroused from the fallopian tube and the peritoneum. Lately (and discussed more extensively in section 1.1.5), there is data supporting the view that high-grade serous ovarian, fallopian tube, and peritoneal cancers should be considered collectively, and that the common convention of designating ovarian origin should no longer be used for the serous subtype, unless that is clearly the origination site, or at least since we have appropriate molecular determinants (if so) to differentiate between anatomical origins. It has been suggested by the FIGO that serous tumors arising in the ovary, fallopian tube or peritoneum might be described collectively as “serous carcinoma", most of these being high-grade serous carcinomas (HGSC)[11].

Due to the unspecific symptoms and the lack of effective screening strategies (see section 2), around 70% of the OC patients are diagnosed at late stages (III-IV) of the disease (Figure 2, left). Overall SV for all patients with OC is 46%[13], but this varies greatly based on stage at initial diagnosis; while 5-year survival in patients with stage I cancer is around 90%, it decreases to 25% for patients diagnosed at stage III - IV (Figure 2, right)[7], when the majority of the patients are diagnosed.

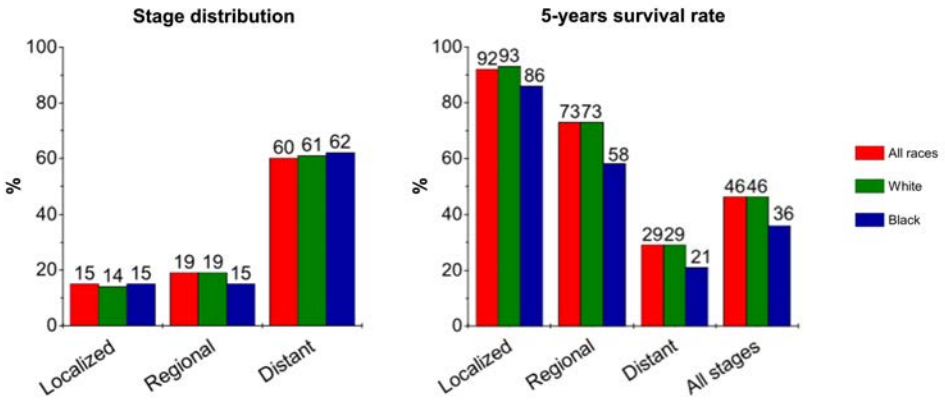

Figure 2: OC incidence and mortality. Stage distribution (left) and 5-years relative survival rates by stage at diagnosis (right). Adapted from Siegel *et al* [7].

1.1.3. HISTOLOGY

Histological subtypes

Depending on the cell of origin OC is subdivided into different histological types that have different identifiable risk factors, molecular profiles, clinical features and outcomes[12]. Those OCs that arise from the epithelium (Epithelial Ovarian Cancer, EOC) account for 90% of all OC cases, including HGSC [70%]; endometrioid carcinoma (EC [10%]); clear-cell carcinoma (CCC [10%]); mucinous carcinoma (MC [3%]); and low-grade serous carcinoma (LGSC [<5%]) (Figure 3) as the most common subtypes, and more rare but still aggressive types are small-cell carcinomas and carcinosarcomas. The 10% left account for non-epithelial OC, and includes tumors from germ cell and sex cord stromal origin[12,14].

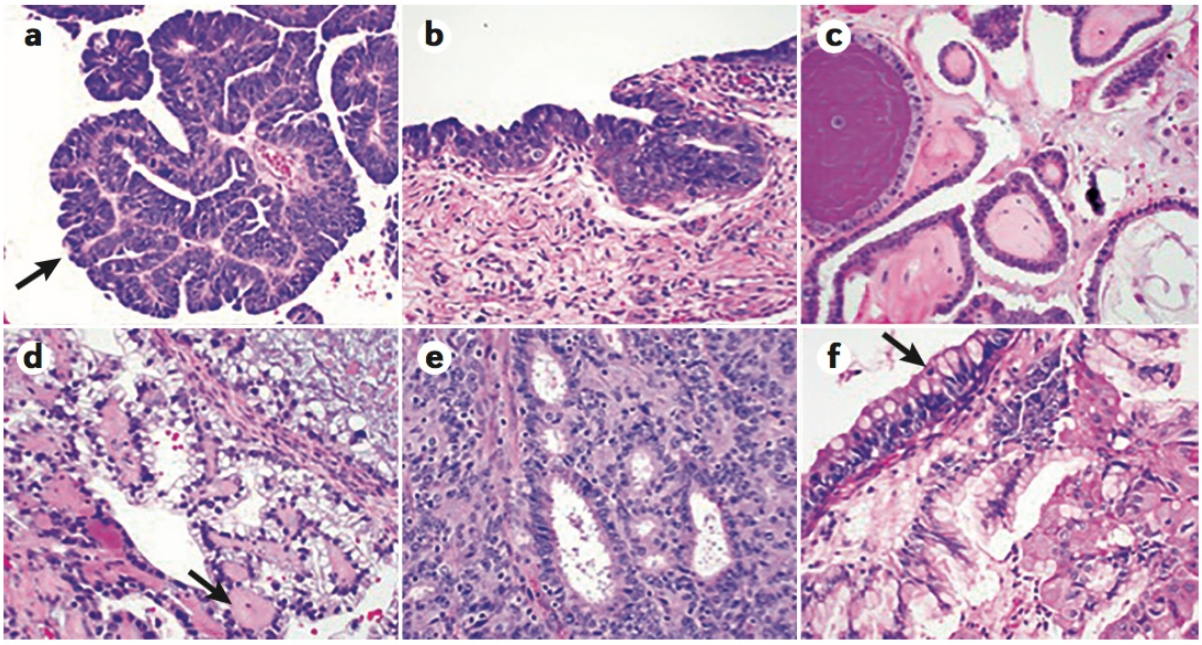

Figure 3: Morphological characteristics of the major epithelial OC histological subtypes. a) HGSC: severe nuclear atypia, high nuclear-to-cytoplasmic ratio, abundant mitoses, papillary architecture (arrow). **b) Serous tubal intraepithelial carcinoma (STIC) lesions:** precursor lesion of HGSC: morphology shared with HGSC. **c) LGSC:** papillary architecture, mild nuclear atypia, lower nuclear-to-cytoplasmic ratio. **d) CCC**: large atypical tumor cells, frequent clearing of the cytoplasm, stromal hyalinization (arrow). **e) EC:** recapitulates endometrial glands, graded based on cellular architecture and nuclear atypia. **f) MC:** mucin-filled tumor cells, frequent goblet cell forms (arrow). Adapted from Matulonis *et al.*[12].

Histological grading

Epithelial tumors are further sub-classified by histologic grading, which can be correlated with prognosis. This grading system does not apply to non-epithelial tumors. Two grading systems are applied by the FIGO:

1. For non-serous carcinomas, grading is based on cell architecture with a one-step upgrade if there is prominent nuclear atypia, as follows:

- GX: Grade cannot be assessed
- G1: Well differentiated
- G2: Moderately differentiated
- G3: Poorly differentiated

2. For serous carcinomas, a two-grade system is performed based on their biology. HGSC carry a high frequency of mutations in TP53[15,16]. Most "moderately differentiated" serous carcinomas carry mutations in TP53 and should be combined with the high-grade tumors. LGSC are often associated with borderline or atypical proliferative serous tumors, often contain mutations in BRAF and KRAS and contain wild-type TP53[11].

Clinical presentation and molecular alterations of the most relevant EOC

The prevalence of the EOC histological subtypes is different and they have distinct clinical presentation in terms of FIGO staging and age at diagnosis; they present different histological grading, have distinct mutations, and different response to therapies (table 2).

The high-grade subtypes have poorer prognosis than the low-grade counterparts of serous and EC. HGSC and high-grade (G3) EC usually present peritoneal carcinomatosis (ascites and pelvic masses), and present high genomic instability due to deficiencies in homologous recombination (HR) genes[12]. Generally, the response to therapies is poor for all histological subtypes (Table 2), being HGSC the poorest prognostic group[12].

Recurrent mutations: while **TP53** is the most commonly mutated tumor suppressor gene (96%) in HGSC[15], also genes regulating its degradation have also been found in EOC (e.g. MDM2 and MDM4; Table 2). Defects in HR genes were found in ~50% of analyzed HGSC[12], including both somatic and germ line **BRCA1/2** mutations, as well as alterations in other DNA repair pathway (Table 3). Interestingly, mutations in HR genes have been identified in approximately one-third of all EOC cases, not only including serous and but also non-serous histologies[12].

Despite the recurrent mutations in EOC, some tumors, particularly the HGSC and high-grade (G3) EC subtypes, are genetically heterogeneous (Table 2). Also, MCs are of such genetic complexity almost at the same level than of HGSC and high-grade (G3) EC subtypes. Despite they do not have such mutations in the DNA repair system; MCs are also very resistant to the standard treatments. In addition, LGSC and low grade (G1-2) EC and CCC, although less genetically complex (Table 2), they can also be resistant to the standard therapies. The mutational heterogeneity observed in EOC might be related to different still unknown drivers. Albeit genetic and other risk factors have been associated to the different histologies[17], the nature of this disease remains still not fully understood, mainly caused by the distinct mutations, clinical presentation and outcomes of this multiple disease.

EOC histology	Grade	%	Age (years)	FIGO stage	Response to therapy	Gene	Mutation
Serous (70-75%)	High-grade (HGSC)	70%	60-70	III-IV	Initially sensitive to the standard platinum-based therapy, but the majority of them will recur	TP53	Inframe or frameshift indel; missense or non-sense mutation
						"TP53-like"	Copy number gain of MDM2 or MDM4 genes (regulate p53 degradation)
						Defects in HR (50%); BRCA1/2 and genes from in Table 3	Germline and somatic mutations in *Table 3*
						Notch, PI3K, RAS-MEK, FOXM1, AURKA, ERBB3, CDK2, MTOR, BRD4, MYC, AKT2	Point mutations and copy number alterations
	Low-grade (LGSC)	<5%	45-55	I-IV	Respond better to the standard treatments	BRAF KRAS	Point mutations
Endometrioid (10%)	G3	<5%	40-50	III-IV	Initially sensitive to the standard platinum-based therapy, but the majority of them will recur	Similar mutational landscape as HGSC, ARID1A	Missense or non-sense mutation; gene rearrangement and indels for ARID1A
	G1-2	>5%	40-50	I-II	Can be resistant to platinum-based chemotherapy	PTEN, PI3K, KRAS, ARID1A	Inframe or frameshift indel; missense or non-sense mutation; gene rearrangement and homozygous deletion
Clear cell (10%)	Mainly G3	10%	55	III	Can be resistant to platinum-based chemotherapy	PI3KCA PTEN ARID1A	Missense muttions (oncogenes); base substitution, out-of-frame indel or a splice site mutation (tumor suppressors)
Mucionus (<5%)	Mainly G1-2	<5%	45-50	I-II	Tends to be insensitive to chemotherapy but is still treated initially with cytotoxic chemotherapy	p53, KRAS, BRAF, CDKN2A, RNF43, ELF3, GNAS, ERBB3, KLF5	C>T transitions mainly in an NpCpG trinucleotide context; inframe, indel and missense mutations

* EOC associated with endometriosis, such as CCC and EC, are associated with ARID1A mutations

Table 2: Clinical presentation and molecular features EOC subtypes: clinical characteristics and most common somatic mutations in EOC subtypes. HR: Homologous recombination system. Table adapted from Refs.[12,18–22].

Additional recurrent molecular alterations identified in HGSC include defective Notch, PI3K, RAS–MEK and FOXM1 signaling pathways[15], as well as other mutated genes that play a part in the pathogenesis of HGSC and that could also serve as potential therapeutic targets for EOC include AURKA, ERBB3, CDK2, MTOR, BRD4 and MYC and AKT2, among others[12,23]. Indeed, this molecular complexity characterized by the high number of mutations in genes affecting multiple signaling pathways may explain why the development of effective therapies for HGSC has been difficult to achieve.

Activation of the **PI3K/AKT/mTOR pathway** occurs in around 40% of the HGSC through alterations (amplifications and mutations) on PIK3CA and AKT1/2, or inactivating mutations and deletions of PTEN (more rarely; 7%)[15]. In addition, up to 30% of CCC and EC harbor PI3KCA[24]. However, it is unclear whether an aberration in this pathway is the critical driver of cancer growth and therefore susceptible to targeted inhibition in EOC[24].

Activation of the MAPK signaling pathway **(Ras/Raf/MEK/ERK pathway)** can occur either in HGSC (24%) and LGSC. For the last and rare subtype, its activation may be very important as BRAF and KRAS mutations were reported in around 65% of cases[24]. Therefore, Ras/MEK pathway is an attractive therapeutic target either for HGSC or for LGSC. In primary MC, which is frequently resistant to conventional chemotherapy, the Ras/MEK pathway represents also an appropriate therapeutic target since it harbors mutations in KRAS and BRAF[24].

Additionally, although increased expression of EGF receptor (EGFR) (**ErbB family)** is common in OC (up to 60%) but mutations are rare in HGSC; however, single-agent EGFR inhibitors or HER2-targeted therapy are not very successfull[24]. ErbB3 (HER3) forms a heterodimer with HER2 and stimulates cell survival through activation of MAPK and AKT pathways[24], suggesting that combinational therapies would yield in better responses to therapy.

Interestingly, The Cancer Genome Atlas (TCGA) analysis showed that the **RB1 pathway** was deregulated in around 70% of HGSC[15]; more than 20% of the tumors had somatic amplifications of **MYC** gene[15]; and **FOXM1 transcription factor network** was significantly overexpressed in 87% of the cases while no DNA amplification was found, indicating a transcriptional regulation, suggesting that the high rate of TP53 mutation contributes to FOXM1 overexpression in HGSC, since p53 represses FOXM1 after DNA damage[15].

1.1.4. RISK FACTORS

Several factors can increase the risk of developing EOC, including age, postmenopausal hormonal therapy and oral contraceptives use, infertility, nulliparity, endometriosis and genetic factors (Table 3). Other factors such as lifestyle (NSAIDS consumption and smoking), obesity and dietary factors might affect the risk of EOC[12]. Interestingly, a recent study evaluated prospectively the association between several risk factors abovementioned and the EOC histological subtypes[17]. Higher parity, age at menopause, endometriosis, and tubal ligation were only associated with EC and CCC. Family history of breast cancer had modest heterogeneity among subtypes. Most risk factors exhibited significant heterogeneity by histology. Unsupervised clustering by risk factors separated EC, CCC, and LGSC from HGSC and MC, supporting that subtypes are different diseases and, indeed, strongly associated with non-serous EOC rather than with serous, which challenges risk prediction for HGSC, the most fatal subtype[17].

Gene	Protein	Protein function
BRCA1	Breast cancer type 1 susceptibility protein	• Crucially involved in the repair of double-strand breaks by homologous recombination
BRCA2	Breast cancer type 2 susceptibility protein	• Serves as a scaffold for other proteins involved in double-strand DNA repair, mostly through defective homologous recombination • Stabilizes RAD51–ssDNA complexes
BARD1	BRCA1-associated RING domain protein 1	• Forms a heterodimer with BRCA1 • The BRCA1–BARD1 complex is essential for mutual stability
BRIP1	BRCA1-interacting protein 1 (Fanconi anaemia group J protein)	• Binds to BRCA1 • The BRCA1–BRIP1 complex is required for S phase checkpoint activation
PALB2	Partner and localizer of BRCA2	• A bridging protein that connects BRCA1 and BRCA2 at sites of DNA damage • Helps load RAD51 onto ssDNA
RAD51C	DNA repair protein RAD51 homologue 3	• Strand exchange proteins that bind to ssDNA breaks to form nucleoprotein filaments and initiate DNA repair
RAD51D	DNA repair protein RAD51 homologue 4	
MSH2	MutS protein homologue 2	• Mismatch repair proteins that recognize and repair base-pairing errors occurring during DNA replication
MLH1	MutL protein homologue 1	
MSH6	MutS protein homologue 6	
PMS2	Mismatch repair endonuclease PMS2	• Mutations in mismatch repair genes are associated with Lynch syndrome

Table 3: Genetic risk factors. Functions of commonly mutated inherited genes associated with increased risk of EOC. Adapted from Matulonis *et al*.[12]

Germ line BRCA1 and BRCA2 mutations are the most significant known genetic risk factors for OC and are found in up to 17% of patients with EOC[12], as well as in other cancer types including melanoma (BRCA2), breast (BRCA1 and BRCA2), pancreatic (BRCA2) and prostate (BRCA2) cancers[12]. While BRCA1 is crucial for DNA repair, cell cycle checkpoint control and apoptosis, among other functions; BRCA2 is important in HR repair system[25].

Some EOC subtypes are associated with germ line BRCA mutations. While HGSC is the most common subtype presenting these mutations, MC subtype is rarely associated. Better overall SV is associated to women with EOC carrying germ line BRCA mutations compared to women harboring wild-type BRCA1/2[12]. Germ line BRCA2 mutations are associated with increased overall SV compared with germ line BRCA1 mutations, probably because BRCA2 results in enhanced platinum sensitivity than BRCA1[26]. The location and the type of mutation in BRCA genes can also influence the risk of developing EOC[27], but the response to treatment seems to do not associate to these factors (clinical evidence, unpublished).

Patients with a strong family history of EOC particularly if there is a documented germ line mutation, are advised to have a risk reducing bilateral salpingo-oophorectomy (RRSO) after appropriate counseling and at the completion of childbearing. Additionally, young age patients diagnosed with HGSC or high-grade EC, should be offered for genetic testing. BRCA mutations may also occur in women without a family history of breast/OC and in women with HGSC under the age of 70 years genetic, in which genetic testing should be considered too[11].

Mutations in other DNA repair genes can increase the risk of developing EOC, including RAD51C, RAD51D, BRIP1, BARD1 and PALB2 (genes that are part of the Fanconi anemia), MLH1, PMS2, MSH2 or MSH6 (genes associated to inherited disorders, such as Lynch syndrome), as well as other genes involved in DNA repair, such as CHEK2, MRE11A, RAD50, ATM and TP53[12,28]. Patients with EOC associated to Lynch syndrome mutations use to appear at a younger age and at earlier stages at diagnosis (usually stage I), being EC and CCC the most common subtypes associated to this syndrome. Even though, both BRCA1/2 and the DNA mismatch repair genes are involved in DNA repair, the specific mechanisms that underlie why cancers arise in specific organs associated with these inherited mutated genes are still unknown[12].

1.1.5. ETIOLOGY

Historically, one of the main reasons why the biology and evolution of the most common OC have been so difficult to understand is because most tumor cells do not phenotypically resemble any normal cells in the ovary. It has been postulated several hypothesis founded by recent discoveries supporting different origins for the EOC subtypes[2]. Recent evidences indicate that most of the HGSC, CCC and EC primarily arise from tissues that are not normally present in the ovary, while germ cell and sex cord stromal tumors have clearly an anatomical origin within the ovary, which have been extensively reviewed by Cools *et al.*[29] and Karnezis *et al.*[2] respectively. Also, it is thought that the majority of MCs are metastasis from gastrointestinal cancers[30]. For CCC and EC, many studies support that precursor lesions of these diseases are retrograde endometriosis, since it was found benign and malign lesions coexisting in the ovarian tumors, but it is still not known how the precursor develops[2]. For HGSC, the most common EOC, no credible histological precursor lesion has been identified until 15 years ago, when patients with BRCA1/2 germ line mutations underwent into RRSO, in which some precursor lesions were found in the fallopian tube epithelium (FTE), and was postulated as the anatomical site of origin for many HGSC. In turn, the precursor lesions called STIC have a presumed precursor lesion, the "p53-signature" lesion (a histologically normal lesion in the FTE but TP53-mutant), which was found in the fimbria of the FTE of these risk-reducing surgeries. STICs have been found also in sporadic advanced-stage HGSC, supporting them as the precursor lesions of most HGSC[2,11]. A recent study aiming to decipher common molecular patterns between HGSC and cells of origin, revealed that HGSC and FTE DNA methylomes are significantly and consistently more highly conserved than those of HGSC and OSE, thus supporting the hypothesis that HGSC arise from the fallopian tube[31]. However, there are still some conservative authors that proved that not all HGSC arise from STICs but, instead, there are also some HGSC that arise from OSE cells. In particular, Coscia *et al*.[32] recently identified a protein signature that separated HGSC into a two predominantly epithelial and mesenchymal tumor clusters, resembling and clustering with FTE and OSE cells, respectively, suggesting that a possible origin of HGSC either from the FTE or from the OSE is possible.

1.2. OVARIAN CANCER DIAGNOSIS

1.2.1. BACKGROUND

The fact that the most common OC types arise from cells that are not normally located in the ovary challenges the concept of what a 'true' OC is. However, OC is still treated almost as a single disease in terms of diagnostic procedures and treatment options (see section 3). As abovementioned, most women are already diagnosed with late-stage OC (70%), caused mainly by the lack of early warning symptoms and appropriate diagnostic tests for early detection[14]. Also, the nonspecific symptoms of the disease at late stage (Table 4) are easily confused with those of various benign pathologies and those related to the gastrointestinal tract, potentially delaying further the diagnosis.

General Symptoms	
Gastrointestinal dysfunction	constipation
	bowel obstruction
	diarrhoea
	nausea
	vomiting
	gastrointestinal reflux
Abdominal discomfort	Increased abdominal size
	Pelvic pain and/or pressure
	Abdominal bloating
Respiratory symptoms	Fatigue
	Shortness of breath
Urinary symptoms	Frequent urination

Table 4: General Symptoms for advanced stage OC.

Most women are symptomatic at late stage presentation and have ascites (Figure 4) (fluid in the peritoneal cavity), which causes mostly all the symptoms numbered in Table 4. Respiratory symptoms can result from extensive intra-abdominal cancer with ascites, causing diaphragmatic pressure, pleural effusions and/or a pulmonary embolus. Finally, abnormal vaginal bleeding is an uncommon symptom[11,14]. Until symptoms become apparent and require intervention (abdominal pressure, pleural effusion, etc.), patients undergo a long process of clinical examinations by several specialists until the existence of a tumor is finally confirmed.

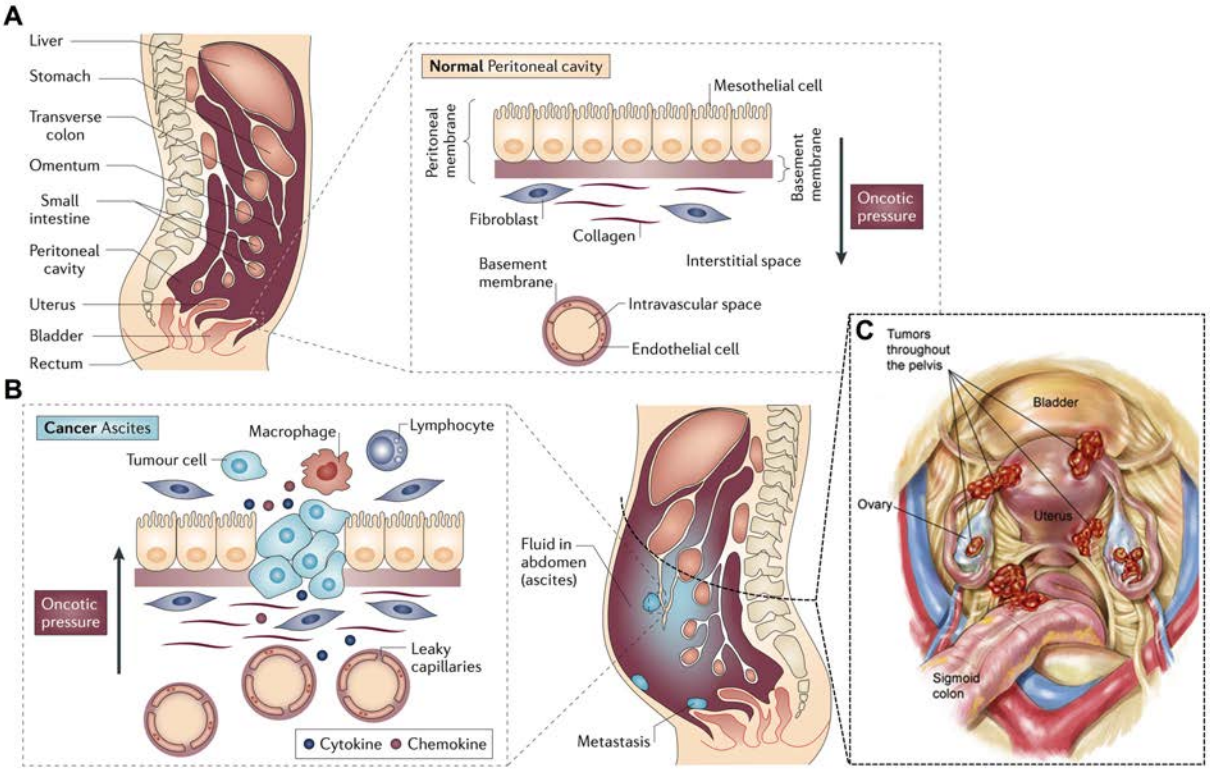

Figure 4: Ascites formation by peritoneal dissemination: the cause of the unspecific symptoms. A) The peritoneal membrane covers the visceral organs, as well as the abdominal and pelvic cavities. In physiological conditions, the difference in oncotic pressure across the peritoneal membrane limits capillary fluid filtration and prevents edema (due to water reabsorption into the capillaries). **B)** In malignant ascites, the area of micro-vessels lining the peritoneal cavity is increased, which together with the high protein concentration of the ascites increased capillary permeability by changing the oncotic pressure to the peritoneal cavity. **C)** Transversal view of the peritoneal cavity with the invasive implants typical from an advance stage OC presenting ascites. Adapted from Refs.[33,34]

Usually, all these symptoms account for all the histological subtypes of EOC; although they behave different, the etiology of the symptoms differ slightly[12]. As HGSC and high-grade (G3) EC usually metastasize quickly, all the symptoms are caused by the rapid accumulation of the ascitic fluid in the peritoneal cavity, as well as the tumor spread to the peritoneal wall and the adjacent organs (bowel, uterus, etc.). In contrast, CCC, MC and LGSC become symptomatic at an earlier stage (bigger adnexal masses of the primary tumor, less spreading at diagnosis) and, although they are also associated with many of the symptoms mentioned, they are usually caused by the pressure of the ovarian mass onto the bowel, urinary tract system and pelvis[11,12].

1.2.2. CURRENT DIAGNOSTIC TOOLS

In patients with indicative symptoms, diagnostic workflow includes:

(I) Pelvic examination of the patient

(II) Radiographic imaging

(III) Blood test for the tumor biomarker cancer antigen 125 (CA125)

(IV) Surgery

Results from diagnostic testing, especially imaging, can provide information about the ovarian mass, such as size, location and level of mass complexity, which can help clinicians to determine the level of suspicion for cancer. Laparoscopic surgery with removal of the mass and peritoneal biopsies will give further information on the tumor histology[11]. Other factors can point to the presence of a malignancy, and are useful in the clinical assessment of masses such as age (young for germ cell, older for EOC) and bilateralism of the adnexal mass. Importantly, since the **final diagnosis** is not determined until the **surgery** is performed, and since most of the patients are diagnosed at **late stage** of the dissemination process, there is an urgent need to develop **non-invasive diagnostic tools** able not only to determine the final diagnosis by means of non-invasiveness but also to improve the early detection of the disease.

Pelvic examination

Physical signs associated with early stage OC may be limited to palpation by pelvic examination of a mobile, but somehow irregular, pelvic mass (stage I). Because the lack symptoms at early-stage, these cases almost occur only by chance, having a sensitivity of 45% and a specificity of 90%[35]. As the disease spreads into the pelvic cavity, nodules may be found in the *cul-de-sac*, particularly on bimanual recto-vaginal examination (stage II). As the disease involves the upper abdomen, ascites may be evident. A physical examination of the abdomen may demonstrate flank bulging and fluid waves associated with the ascites. Metastatic disease is commonly found in the omentum, such that the latter may be readily identified in the presence of advanced stage OC (stage III) as a ballot table or palpable mass in the mid-abdomen, usually superior to the umbilicus and above the palpable pelvic mass. The disease may spread through lymphatic ganglia to either the inguinal or left supraclavicular lymph nodes, which may be readily palpable. It may advance into the pleural cavity as a malignant effusion, usually on the right side or bilateral, in which case the lung bases exhibit

dullness to percussion and decreased breath sounds and egophony to auscultation (stage IV)[14].

Imaging

Due to its wide availability, ultrasound (US) is the imaging method of choice to assess an ovarian lesion and to determine the presence of solid and cystic elements, as well as the presence of ascites. The distinction between benign and malignant tumors is generally not possible by US, either alone or in combination with magnetic resonance imaging (MRI) or computed tomography (CT). The sensitivity and specificity for US is 75.0%, 98.2%; for MRI is 91% and 88%, and for CT is 90% and 75%, respectively[35,36]. However, none of these methods has a clearly established role in pre-operative tumor staging. As mentioned above, surgical exploration remains the standard approach for staging, following the FIGO parameters based on the postoperative pathological examination for histological control and confirmation of the disease[11,14].

CA125 blood test

Currently, the only biomarker that is widely used in clinical practice is the CA125[37]. This protein is a high molecular weight cell-surface glycoprotein, also known as mucin 16 (MUC16), antigen normally expressed in tissues derived from coelomic epithelia, such as ovary, fallopian tube, peritoneum, pleura, pericardium, colon, kidney, and stomach. It has also been directly involved in the development of the disease[38]. CA125 blood test is performed when the results of the two other diagnostic tests accompany a suspicion of cancer. However, the test is not sensitive enough when used alone, since CA125 is elevated (>35 U/mL) in 80% of patients with advanced stage disease, but it does so only in 50% of stage I cases[37]. In addition, CA125 lacks of specificity (50-60%) since it is also elevated in benign disorders, such as uterine fibroids, ovarian cysts, endometriosis and other cancer types[39,40]. Regarding the different EOC histologies, increased levels of CA125 are more frequently observed in HGSC than in non-serous subtypes[12]. In fact, it is accepted since the late 80's that CA125 is a better marker for recurrence than for newly diagnosed EOC, thus having clinical value for follow-up monitoring, earlier detection of the recurrent lesions and early retreatment[41,42].

In contrast to its poor utility as a screening and diagnostic biomarker, CA125 is useful in assessing the risk of a malignant versus benign tumor in women who debut with an adnexal mass[43]. Identifying women at higher risk of malignancy not only enables

clinicians to choose patients who will benefit from more specialized care, but it also decreases morbidity and mortality and increases overall SV in the patients referred for surgical intervention. In particular, CA125 concentrations >95 U/mL in postmenopausal women may help distinguish benign from malignant masses[43].

CA125 combined with US features of the adnexal mass is another tool for risk stratification. The **risk of malignancy index (RMI)** uses the CA125 concentration multiplied by menopausal status and US score for risk calculation. Clinicians refer patients with higher scores to specialized gynecology/oncology teams[43].

The Food and Drug Administration (FDA) initially cleared CA125 assays for predicting the likelihood that women previously diagnosed with EOC would have evidence of residual tumor after surgical intervention[44]. In fact, residual disease is usually correlated to CA125 levels (>35 U/mL with >95% accuracy) in women who have had surgery to remove the tumor, which are referred to chemotherapy[43]. Although there are no specific guidelines for disease monitoring, oncologist commonly use CA125 to monitor patients' response to chemotherapy as follows:

- 2 weeks before initiating treatment
- 2–4 weeks afterwards
- Every 2–3 weeks during follow-up.

For long-term follow-up, current guidelines suggest monitoring every 2–4 months for 2 years and then less frequently if there is no evidence of disease (NED)[11].

The FDA never approved CA125 for preoperative use in the United States, but only for cancer surveillance for women diagnosed with EOC. Ironically, the majority of CA125 tests ordered today are for the evaluation of an ovarian tumor prior to surgery. The use of serum CA125 has also never been associated with a survival benefit, whether utilized before or after diagnosis[45].

Besides CA125, tumor markers such as human chorionic gonadotropin (hCG) and alpha-fetoprotein (AFP) are mandatory to exclude germ cell tumors in young patients with a pelvic mass or enlargement of an ovary[11]. Also, carcinoembryonic antigen (CEA) should be considered to test, since a gastric or colonic primary tumors with metastases to the ovaries may mimic EOC; and if the CEA is elevated, a colonoscopy should be considered when indicated symptoms suggest possible bowel cancer[11].

Surgery

Even if all tests performed indicate a suspicion of EOC, to confirm the diagnosis a tissue biopsy must be performed, normally by laparoscopy. To date, due to the lack of specificity of the current diagnostic tools and the intrinsic general symptomless of the disease, still only 1 out of 10 women that undergo into a surgery of suspicion is finally diagnosed with EOC (through surgery and pathological examination of the extracted specimens)[11].

1.2.3. SCREENING TOOLS AND DIAGNOSTIC BIOMARKERS

No current screening strategy has affected the survival rate of patients with EOC. Due to the lack of sensitivity and specificity in a single determination, CA125 is not recommended for screening asymptomatic women. Experts agree that potential biomarkers for early cancer detection should be validated on samples taken before diagnosis — the stage at which the test would be used in the clinic — that is a step that few groups attempt and no biomarker for EOC has render good success, as discussed by Lizzie Buchen in *Missing the mark*[46]. Up to that point, most biomarkers for detecting early EOC had only been shown to distinguish patients with already diagnosed cancer from healthy controls, but they were intended to detect the disease in women whose cancer is just budding and confined to the ovary, before symptoms develop.

What the field awaits is for a 'prospective' study, run on blood samples or other body fluid from apparently healthy women, in order to find biomarkers that would pinpoint those who will later be diagnosed for EOC. Such samples, from large numbers of women who are tracked over months or years, are extremely difficult to obtain, because of the low prevalence of the disease and the wide range of histological subtypes, each with different biological and clinical properties. Therefore, the generation of a successful screening strategy for EOC is challenging. Some of the most important efforts done in order to improve the early diagnosis of EOC are summarized in Figure 5.

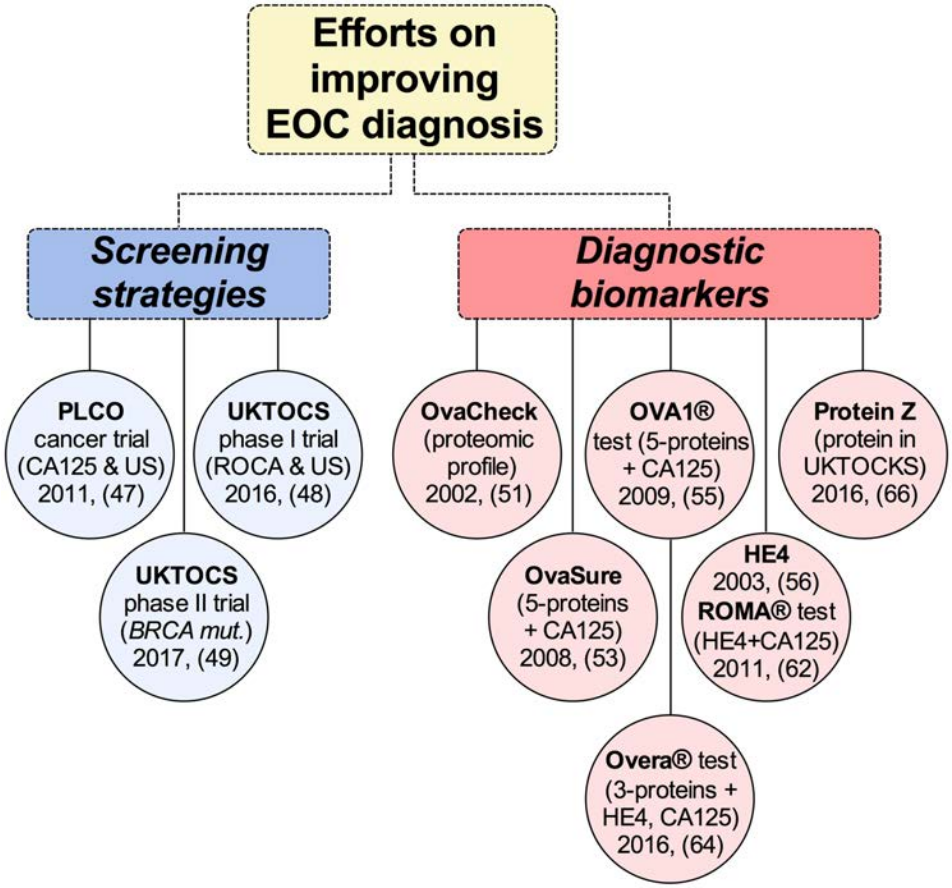

Figure 5: Most relevant screening strategies and diagnostic tools developed to improve EOC early diagnosis.

PLCO and UKTOCS screening studies

To date, two major screening studies have been carried out prospectively to improve early detection of OC and thus reducing mortality. On one hand, the **PLCO** (Prostate, Lung, Colorectal and Ovarian) cancer screening trial in the United States population (NCT00002540) followed a strategy by combining the CA125 blood test and radiographic imaging (US) annually, with a median follow up of 12.4 years and in 78,237 healthy women. Results showed no differences in terms of stage distribution and overall mortality among screened group and the usual care group[47].

On the other hand, the **phase I** trial of the **UKTOCS** (United Kingdom Trial of Ovarian Cancer Screening) evaluated prospectively the levels of CA125 in an algorithm termed 'risk of ovarian cancer algorithm' (ROCA). ROCA was the primary screening modality, with transvaginal US used as a secondary screening measure based on CA125 levels. In this study, 202,638 women were randomly assigned into one of three groups (screening based on ROCA, US alone or no screening), with a median follow up of 11.1

years. The proportion of women diagnosed with OC was similar between groups but more patients at lower stages (stage I–IIIA) of disease were detected in the ROCA-screened group. However, no differences were found between patients in the ROCA group and US group, and there was no reduction of the overall mortality in any of the groups. Thus, the ROCA test cannot currently be recommended as a screening strategy for OC[48].

Despite no significant and translatable results were obtained in the phase I trial, a **phase II** trial of the **UKTOCS** has been recently carried out in high-risk patients (i.e. carrying BRCA1/2 mutations) finding and evidence of stage shift in women diagnosed with OC[49]. Nineteen patients were diagnosed with invasive OC/fallopian tube cancer within 1 year of screening (13 diagnoses were screen-detected and six were occult at RRSO). Around 50% of the total patients diagnosed were stage I to II, and of the six occult cancers at RRSO, five were stage I to II. RRSO remains the treatment of choice for women at high-risk of OC, but in those not up for surgery, multimodal screening using ROCA and US every 4 months appears to be a better option than symptom awareness alone. Such screening should not be viewed as an alternative to surgery, but it does seem to offer a better chance of avoiding a diagnosis of advanced incompletely resectable OC for high-risk patients[49].

Diagnostic biomarkers tests

Through the last decades, many efforts have been done in order to find new biomarkers for EOC diagnosis and screening. Due to the handicaps mentioned, the FDA has approved none of them because did not demonstrate improved overall SV and run into the market very quickly before clinical validation. OvaCheck and OvaSure are two examples that failed to translate into successful tests for early detection of EOC, where FDA cleared them but then rejected from the market for several reasons explained below[46,50].

OvaCheck was a test developed from a proteomic blood signature able to discriminate early and late stage EOC from patients with benign disease of the ovary[51]. Commercial rights to develop the test were quickly licensed, but in a relative short period of time several authors tried to reanalyze the data obtained by Petricoin *et al.*[51], founding inconsistent results and technical proteomic considerations that invalidated the results[50].

Several years later, the **OvaSure** test, which was initially based on blood levels of 4 proteins[52], followed by the introduction of CA125 and the protein macrophage migration inhibitory factor[53] to make the test more sensitive to cancer, was rapidly marketed by LabCord. Meanwhile, the panel entered for validation in the PLCO cohort, but the authors do not wait for it to publish and licensing the patent. Some collaborators supporting the statistical part of the second paper found errors (biased results with a higher positive predictive value (PPV) than the correct one, with higher rate of false-positives and unnecessary surgeries therefore)[46], as well as other authors who failed in reproducing the data from Visintin *et al.*[53]. Finally, the FDA asked to LabCord to remove the test from the market due to the possible harm of the test to the women, even though they argued that in that way they were already testing the screening capacity of the test[46].

In 2009, the FDA approved the first preoperative serum biomarker test called **OVA1®**, developed by Vermillion Inc. It is based on a combination of several serum proteins biomarkers including the CA125, transferrin, β-2-microglobulin, apolipoprotein A1 and transthyretin[54,55]. It can help to detect EOC among pelvic masses already requiring surgery, but there is not enough data on the benefits on improving early diagnosis, might increasing also false-positive results. Primary care physicians/gynecologists should not use OVA1 test to replace but complement the diagnostic procedures.

The newest serum biomarker is the **Human Epididymis Protein 4 (HE4)**, also known as WFDC2 and identified in the epithelium of the distal epididymis (originally involved in sperm maturation), which was firstly found increased by ELISA in sera from postmenopausal patients with early and late stage OC, with an advantage over the CA125 assay in that it is less frequently positive in healthy patients and nonmalignant diseases of the ovary[56–58]. It was also found HE4 to be elevated in more than half of the EOC patients who did not have elevated CA125 levels; therefore, the combination of both biomarkers provided improved sensitivity in discriminating benign from malignant pelvic masses[58]. Although it has been found expressed in many tissues including normal glandular epithelium of the female genital tract and breast, it was found overexpressed in many cancer types including EOC[59]. Actually, HE4 was recently found as a useful biomarker able to discriminate cytogenetically between ascites coming from EOC (especially HGSC) and gastrointestinal tumor[60]. HE4 was cleared by the FDA for use in monitoring patients with a known diagnosis of EOC, able to detect

recurrence of epithelial cancers 2 to 3 months in advance of CA125, but like CA125, it does not have a preoperative diagnostic indication from the FDA[45]. Lately, it has been demonstrated that the overexpression of HE4 promoted tumor growth and chemoresistance against cisplatin resulting in reduced survival rates in animal models, and also correlated with chemoresistance and decreased survival rates in EOC[61], suggesting a role in EOC tumorigenesis and that selective targeting directed towards the HE4 protein would have therapeutic benefits for the treatment of EOC. In addition, the FDA cleared HE4 as a biomarker for the detection of EOC in women already presenting an ovarian cyst or pelvic mass as part of the Risk of Ovarian Malignancy Algorithm, **ROMA® test**[62], and for monitoring[63] women diagnosed with EOC.

Interestingly, **Overa® test**[64], the second generation OVA1 test, has been cleared by the FDA for determining EOC risk in conjunction with independent clinical and imaging assessment prior to planned surgery for a women with a pelvic mass[65]. Overa replaces two of the five OVA1 biomarkers with HE4 and follicular stimulating hormone (FSH) in order to improve specificity independently of menopausal status.

The incessant efforts accompanied by a very low rate of success has not stop the scientific community from continue trying to give answer to one of the major issues for EOC. The latest work was published last year, in which they discovered Protein Z, a novel biomarker for the early detection of EOC, by using serum samples from the UKTOCS cohort[66]. Protein Z is a novel independent early detection biomarker that demonstrated improved sensitivity compared to CA125 alone and potentially to ROCA algorithm in the detection of EOC[66,67]. However, it is important to mention that CA125, HE4, OVA1®, and ROMA® and Overa® tests are not diagnostic/screening tests, since they are used to determine the likelihood of malignancy of an already existing adnexal mass that requires surgery[43]. For the last decades, the scientific community has been trying to overcome this biomarker's inadequacy by combining CA125 with other markers and with imaging, or monitoring its behavior over time: all ultimately without epic success[45]. Hence, success will arise from the identification of biomarkers in the earliest EOC stages where treatment can have a lasting impact on SV. Interestingly all FDA approved diagnostic markers for EOC use blood as a source of biomarkers, but research in other body fluids, such as saliva, might help to improve EOC diagnosis.

Year of discovery	Biomarker/Test	Sensitivity	Specificity	Ref.	FDA approval	Market
1981	CA125[&]	50%-80%	50-60%	(43)	1997[+]	✔
2002	Ovacheck[$]	100%	94%	(51)	-	✖
2008	Ovasure[#]	95%	99%	(53)	-	✖
2009	OVA1®	94%	54%	(45)	2009[@]	✔
2003	HE4	73%	95%	(57)	2008[+]	✔
2011	ROMA®	90%	63%	(62)	2011[@]	✔
2016	Overa®	91%	69%	(54)	2016[@]	✔
2016	Protein Z algorithm*	72%	95%	(67)	-	✖

Table 5: Diagnostic accuracy of the developed test/biomarkers. & CA125 has a sensitivity of 50% in early stage EOC, and increases to 80% in late stage EOC; + It was approved for monitoring disease progression and response to therapy; @ It was approved for prediction of malignancy of a present adnexal mass; $ Technical limitations (proteomic m/z values of less than 500) and lack of reproducibility invalidated the test[50] (50); # Higher prevalence than the real for OC was used to calculate PPV, invalidating the test (46); *Combined algorithm with other protein markers including CA125 and age; Not yet approved by the FDA.

1.2.4. SALIVA AS SOURCE OF BIOMARKERS

Saliva comes primarily from three major paired salivary glands (parotid, submandibular and sublingual) where specialized cells take up water, salts and macromolecules from the blood that add up to their individual gland secretions. Hence, most blood compounds are also present in saliva, which has recently termed the “mirror of the body”[68,69]. Upon release of glandular secretions into the oral cavity, the fluid is mixed with a variety of exocrine, non-exocrine, cellular, and exogenous components to ultimately form whole saliva (WS).

Saliva has a critical role in maintaining the oral health and homeostasis, and the function of the upper gastrointestinal tract. Saliva is mostly water but it also contains post-translationally modified proteins (e.g., glycoproteins, phosphoproteins), lipids, minerals, and other small compounds that lubricate our tongues, thereby facilitating the chewing, speaking and swallowing processes, preventing excessive swings in pH, and beginning the process of digestion[70,71].Unfortunately, the importance of saliva is often appreciated only when it is gone, as commonly happens in patients with oral cancer or undergoing radiation treatments[72].

Saliva is a highly desirable body fluid for biomarker development, as it provides a non-invasive, simple and low-cost method for disease detection and screening[73,74]. Many efforts have been made in elucidating the molecular profiles in healthy saliva, both at protein and messenger RNA (mRNA) levels[75]. The overall low concentration of saliva markers hindered the development of salivary biomarkers over the last decade. However, the use of high-throughput strategies helped to overcome this problem (Figure 6).

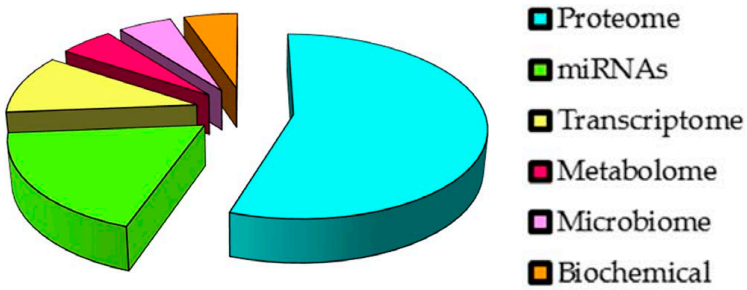

Figure 6: Leading "omics" in salivary biomarker development. Adapted from Rapado O. *et al*.[76].

The use of several proteomic techniques, such as 2-D gel electrophoresis and mass spectrometry, were used to define the salivary proteome[77–81]. The use of transcriptomic techniques, such as Real Time quantitative PCR (RTqPCR), microarray analysis and deep sequencing analysis allowed the definition of the salivary transcriptome[82–87], thereby contributing to the foundation of salivary biomarker development. In addition, the salivary microbiome[88,89], methylome[90] and metabolome[91–93] have also been determined and shown a promising potential as disease-related biomarkers for oral and systemic diseases. The vast amount of "salivaomics" data has led to the development of the Salivaomics Knowledge Base (SKB)[94], a data management system and Web resource supporting salivary diagnostics research[95,96]. In addition to salivary molecular content, a great deal of effort has been made to standardize procedures for saliva collection and storage[97,98], as well as for increasing stability of salivary proteins and mRNAs[99–101].

Saliva reflects disease status

Although saliva fulfills the goal of the holy grail of diagnostics — non-invasiveness — salivary diagnostics is so far only recognized for oral diseases; its clinical utility and scientific credibility for systemic diseases is still biologically and scientifically unsubstantiated. However, the potential use of saliva has been demonstrated not only

for detecting various local diseases, including Sjögren's syndrome[102,103], oral[104–107] and head and neck[108,109] cancers, but also for detecting systemic diseases, such as HIV[110,111], hepatitis C virus[112,113], type-2 diabetes[114], cardiovascular diseases[115,116], lung cancer[117–120], pancreatic cancer[121–123], breast cancer[124,125], gastric cancer[126] and OC[127], among others (Figure 7). After a decade of scientific and technological advancements, the incipient maturation of these basic and translational outcomes is driving to the development of clinical tests that will benefit patients, based on the use of saliva as a source of biological information.

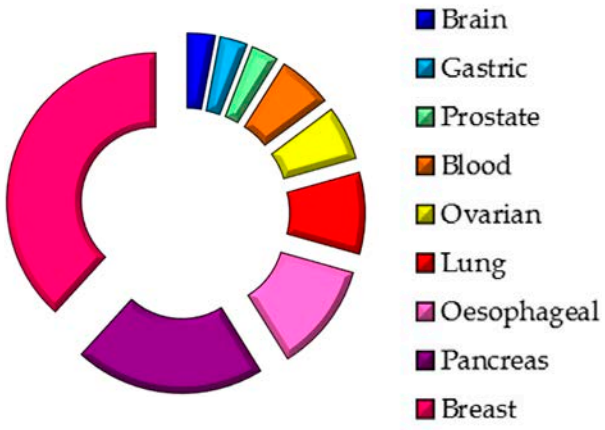

Figure 7: Salivary biomarkers depending on the site of origin. Adapted from Rapado O. *et al.*[76].

The identification of biological markers for specific diseases is one of the driving forces in the current research. An ideal diagnostic biomarker should enable unbiased determination of the disease, especially in patients with early-stage disease and without specific symptoms. Clinically, it should fulfill several criteria, such as high specificity, high sensitivity, easy use, standardized protocols, and readability of the results for the clinicians. Theoretically, every disease may be detected by its unique biomarker. However, a more complete view for a diagnostic signature is a panel of up- and down-regulated molecules that differ in their disease and normal states.

Human saliva has been increasingly used for biomarker development to enable non-invasive detection of diseases. The term "salivaomics" was coined to highlight the *omics* constituents in saliva that can be used for biomarker development and personalized medicine[96]. Most of the studies abovementioned have demonstrated the potential use of salivary extracellular RNA (exRNA) not only to detect local diseases but also systemic diseases. Saliva collection is non-invasive, easy, and low-cost method for disease detection and screening, reasons that make saliva a desirable body fluid for clinical applications, with particular interest in large population screening,

children, geriatric patients, and in cases where repeated samplings are needed (i.e. response to treatment and disease monitoring). However, without proper study design, implementation of robust analytical techniques and prospective clinical trials, the efforts and expectations may very easily be hampered.

Saliva is a proximal body fluid in the oral cavity and therefore is intuitively sound for detection of oral diseases. Currently, there are several theories and studies (including animal models) supporting why saliva is termed as “liquid biopsy”, useful to detect non-oral diseases. Some studies hypothesize that molecules can travel from the primary tumor to the blood and appear altered in cancer salivas (Figure 8).

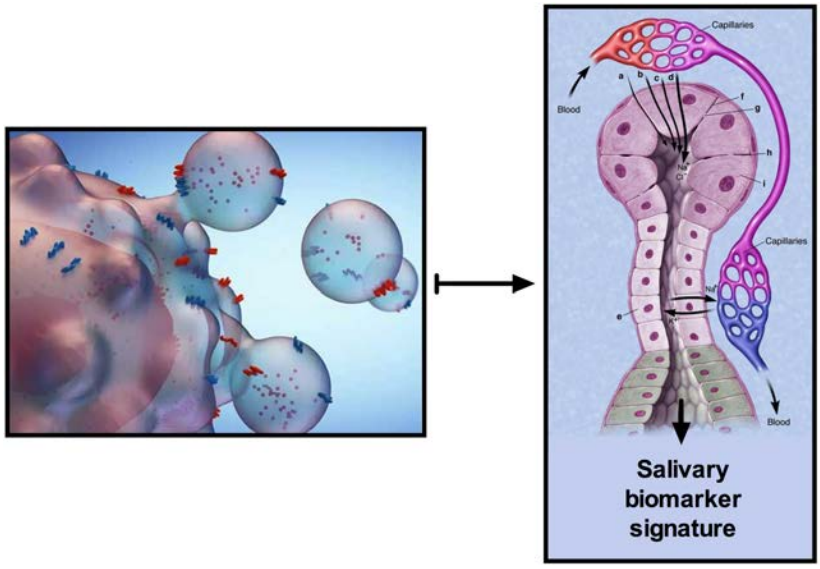

Figure 8: Proposed model of the fundamental biology of salivary biomarkers. One of the hypothesis is that saliva can travel from the primary tumor to the circulation and appeared altered in saliva, either directly from the tumor or by modifying the salivary gland transcriptome[117,128]. Image adapted from Refs.[128,129].

Supporting this hypothesis, Gao *et al.*[117] used induced tumor-bearing mice models of melanoma and lung cancer and defined a salivary transcriptome profile associated to each tumor-type. In addition, Lau *et al.*[122], by using a pancreatic tumor-bearing mice model, revealed the basic mechanisms underlying the rationale of salivary biomarkers through the hypothesis that exosome-like vesicles carry, drive, and deliver tumor markers into the saliva (Figure 8). The lack of sustained and clear mechanisms showing how salivary biomarkers can reflect disease states elsewhere in the body has compromised the scientific acceptance of this emerging field in the clinics[96]. The clinical and scientific credentialing of saliva for systemic disease detection would present a groundbreaking technology that would transform molecular diagnostics globally. Some

achievements have been made pursuing the development of a device for specific salivary biomarkers detection. In particular, the "Oral Fluid NanoSensor Test (OFNASET)" is a prototype nanotechnology point-of-care sensor developed by David T. Wong, an expert on the field[130]. OFNASET have the ability to detect multiplex analytes in saliva for oral cancer detection, through the combination of mRNA and protein electrochemical detection[130]. In addition, his group has developed a device able to detect EGFR mutation at DNA level by using patients' saliva for lung cancer diagnosis[120], in order to reduce the current invasive procedures and reduce unnecessary biopsies (licensed to RNAmeTRIX® company, under the patent WO2015187855, property of UCLA). More recently, another device for oral cancer detection was published based on a novel optical microfluidic biosensor with highly sensitive organic photodetectors for absorbance-based detection of salivary protein biomarkers[131]. The results of measuring IL-8 and IL-1E protein levels were in agreement with those provided by two commercial assays of ELISA hereby offering an attractive and cost-effective tool for diagnostic or screening purposes at the point of care. Several biosensors allowed the detection of multiple analytes including DNA, RNA and proteins for either oral and systemic diseases[132], but continuous research is needed to translate salivary diagnostics into a routine clinical practice. In addition, the generation of point-of-care systems will benefit health system and quality life of patients. Nonetheless, the majority of all these efforts have been focused on revealing the presence of mRNA and proteins as powerful diagnostic biomarkers, but little is known about the emerging classes of non-coding RNAs (ncRNAs) in saliva[133].

In EOC, two studies have reported the use of saliva as a non-invasive diagnostic body fluid. In the early 90's, a linear correlation was observed between serum and saliva CA125 levels from patients with EOC[134]. Interestingly, while serum CA125 had a high false-positive rate for detecting benign ovarian pathologies, the salivary CA125 had a lower false-positive rate (~82% compared to ~12% for serum and saliva, respectively)[134], which suggested that saliva might be more specific than the serum CA125 in detecting EOC. In addition, Lee Y. *et al.*[127] described that the combination of 5 salivary downregulated mRNA (AGPAT1, B2M, BASP2, IER3, and IL1B) could significantly discriminate EOC patients from the healthy controls. Overall, these results suggest the promising utility of saliva samples for improving EOC diagnosis.

1.3. OVARIAN CANCER THERAPY

1.3.1. BACKGROUND

It is clear that the lack of early symptoms hamper the early diagnosis, which mainly causes the high mortality rate of OC. Therefore, the primary aim of treatment for advanced stage OC is to maximize cancer control and palliate disease symptoms for as long as possible. The two main tools for OC treatment are **surgery** and **chemotherapy**, with unanimous consensus by the Gynecologic Cancer InterGroup (GCIG) regarding the importance of surgery for patients newly diagnosed with OC[135]. Although personalized treatments are currently envisioned for cancer therapy and besides the beneficial treatment with PARP1 inhibitors for BRCA mutation carriers (discussed below), all OC are generally "equally" treated, regardless of the molecular features, the histology (serous and non-serous), and the etiology of the malignancy (ovary, fallopian tube and peritoneum)[12].

1.3.2. CURRENT THERAPEUTIC TOOLS

After initial diagnosis by the current diagnostic tools, patients face the challenge of choosing appropriate medical care, including the adherence to standard guidelines of care and specialized gynecological oncologist[136,137], which has been recommended to provide high-quality of care and reduced mortality in patients with gynecological cancers.

Surgical strategies

When the cancer is already developed, either at an early or late stage, the surgery is essential. The goal-standard of surgery is macroscopic complete resection. Accordingly, three clinical subgroups emerge, and the surgeon must document the extent of residual disease:

- No macroscopic residual disease (R0)
- Optimal: <1 cm macroscopic residual disease (R1)
- Suboptimal: >1 cm macroscopic residual disease (R2)

Despite these categories abovementioned, it has been recently accepted as "optimal" only if an R0 is achieved[138]. It is universally accepted that the amount of residual

disease after surgery is the key determinant of patient outcome with survival being best in patients with no gross residual disease at the end of surgery[135]. Different surgical strategies are followed depending on the spread of the tumor and its potential resectability. For early stages, the tumor confined to one or both ovaries is removed normally in the laparoscopic surgery and after histo-pathological examination it is determined for chemotherapy or not depending on the histological grade and stage (Figure 9).

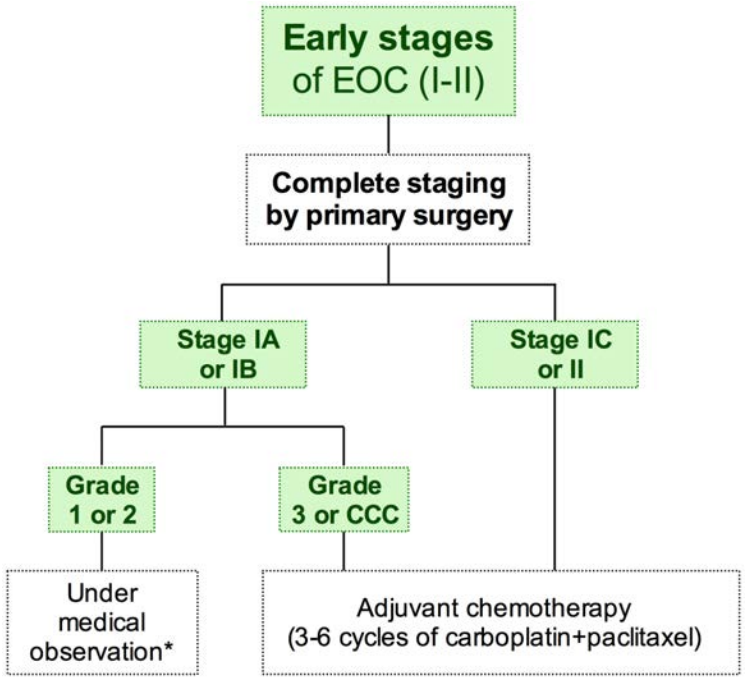

Figure 9: Treatment strategy for early stage (I-II) EOC. Adapted from Ref. SEGO oncology guide[139]. *Patients treated by surgery and diagnosed with G1-2 early stage EOC do not undergo into adjuvant therapy, but remain under medical observation periodically.

For advanced FIGO stage (70%) of EOC a qualified gynecologic oncology surgeon should decide between two lines of treatment[135] (Figure 10):

- Primary debulking surgery (PDS) + chemotherapy (CTH)
- Neoadjuvant chemotherapy (NACT) + interval debulking surgery (IDS) + CTH

What trends to the clinicians to go through one or another strategy is basically the feasibility to remove the metastatic disease observed in the laparoscopic surgery[139], to achieve R0 of residual disease (no macroscopic residual disease). At that time, the surgery by laparoscopy provides diagnostic insights for staging, a biopsy for histological analysis, and an impression of the metastatic pattern allow to determine its potential resectability:

- Localized, big, “single” and isolated nodules of metastasis located in close and distant organs (mainly peritoneum, bowel, liver, etc.)
- Small, multiple implants in a “carpet-like” metastatic spread throughout the serous layer[12] (peritoneum, omentum genital system, bowel, etc.)

When the last situation occurs, clinicians tend to go through the NACT to reduce the tumor burden, where the IDS are more successful (Figure 10).

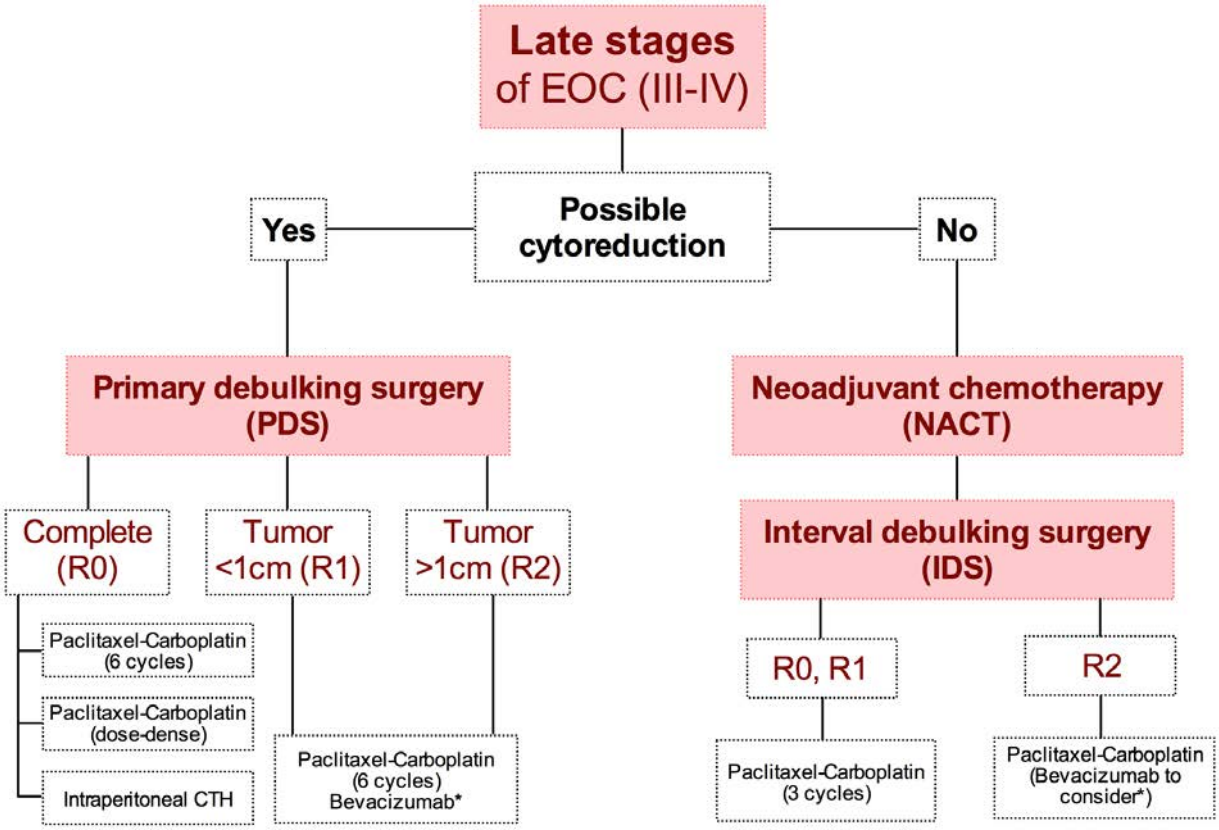

Figure 10: Treatment strategy for late stage (III-IV) EOC. Adapted from Ref. SEGO oncology guide[139]. *Administration of bevacizumab can be considered after first-line therapy (see below).

The use of NACT (three cycles of chemotherapy) is increasing partly because it has become clear that a complete resection of tumor confers a better prognosis. After NACT, as shown in Figure 10, two clinical subgroups emerge regarding response to treatment (determined by CA125 and imaging):

- Those who are candidates for IDS, decreased and resectable tumor burden
- Those who are not suitable for IDS, because the tumor does not respond to the treatment or it progressed even worse during the treatment

Similarly, two prognostic subgroups emerge following IDS:

- Patients with no gross residual disease
- Patients with gross residual disease

Patients undergoing NACT should be considered for 'window-of-opportunity' studies that offer access to tumor biopsies at diagnostic laparoscopy followed by second tumor biopsies at IDS[12,135]. Such biopsies are of high value since they can give valuable information about the molecular status and, therefore, testing targeted therapies using patient-derived xenografts (PDX) animal models will improve the development of targeted therapies and personalized medicine for OC[140,141].

These strategies (PDS and NACT/IDS) represent two major clinical subgroups. However, no advantage was found in terms of OS and progression-free survival (PFS) benefit supported by CHORUS, EORTC55971 and JCOG0602 clinical trials[138,142,143], although NACT resulted in a higher rate of optimal cytoreduction[144], less blood and ascites loss, as well as less invasiveness and adverse effects of the surgery[145]. Recently, a review and meta-analysis suggested that advanced stages OC should be divided in several categories according to the response to treatment and prognosis[146], and proposed that HGSC are more suitable for NACT/IDS, while non-serous histologies (which have favorable prognosis but are initially less chemosensitive) might be more suitable for PDS. This proposal intend to individualize surgical approach for each patient (histology) in order to stratify which patients would benefit from such lines of treatments.

Chemotherapy

The accepted standard is 6 cycles of platinum-based combination chemotherapy, with platinum (carboplatin or cisplatin) and taxane (paclitaxel or docetaxel)[11]. Platinum derivatives, which have been administrated to OC since more than 50 years ago, are DNA binding compounds interfering in DNA duplication and producing DNA damage; cells that are not able to repair DNA breaks undergo apoptosis[147]. It was around late 90's when taxanes were included in the management of OC, where an increase of the initial response to CHT was observed[147]. Taxanes are molecules that block cell division through stabilizing microtubules and therefore blocking tubulin dynamics and cytoskeleton rearrangement during cytokinesis (that is physical cell division)[148].

The use of adjuvant chemotherapy after the surgery depends mainly on the cancer stage and grade. Many patients with grade I or II – stage Ia-Ib OC are not treated with chemotherapy post-surgery, but those with grade III at early stages (Ia-Ib) or Ic and II (Figure 9) and all-grades at advanced stages OC undergo into adjuvant chemotherapy (Figure 10)[11].

For advanced stage OC the standard chemotherapy is intravenous (IV) 3-weekly carboplatin (AUC 5–6)[149] and paclitaxel (175 mg/m^2). Acceptable alternatives include dose-dense weekly paclitaxel (80 mg/m^2) plus 3-weekly carboplatin[150], still being robustly cost-effective for the healthcare system[151]. However, this is somehow controversial since an improvement in OS and PFS was observed in patients receiving dose-dense therapy compared with conventional treatment in JGOG 3016 trial[152] but not in GOG0262 (NCT01167712) clinical trial[153].

Intraperitoneal (IP) chemotherapy administration remains the preferred treatment for those patients with optimal (<1 cm) PDS of stage III OC as it increases PFS and OS[154], but some toxicity has been observed and, therefore, no standardized regimen for IP therapy has been established. However, women with suboptimal (>1 cm) PDS should be treated with IV chemotherapy[150], caused by the reduced penetrance of the drug into the tumors by IP administration.

Although initially 80% of the patients are sensitive to the standard treatments, only 15% have a complete response, and 85% of the patients usually become resistant and die of recurrence[155]. Since more than 30 years ago, OC has been analyzed on the basis of platinum sensitivity[156], defined as the period of time “free of recurrence” elapsed between the last dose of platinum-based CTH and evidence of disease progression, called platinum-free interval (PFI). Currently, platinum sensitivity can be divided into 3 main groups:

- Recurrence during treatment, called “platinum-refractory disease”
- PFI <6 months, considered as “platinum-resistant disease”
- PFI ≥6 months, considered as “platinum-sensitive disease”

This classification schema based on PFI was incorporated in the design of hundreds of clinical trials and the inclusion criteria, and since the early 1990′s has served as the basis of drug approvals by regulatory agencies for patients with recurrent OC[157].

Second-loop surgery is usually performed aiming also macroscopic complete resection for patients with recurrent OC. In addition, several **second-line treatments** for platinum-sensitive and platinum-resistance OC has been used (Table 6), which are used in multiple combinations[150], sustained by multiple trials summarized in Matulonis *et al*[12].

Compound	Mode of action	Platinum-sensitive	Platinum-resistant
Cisplatin	DNA binding	×	
Carboplatin		×	
Paclitaxel	microtubule stabilization	×	×
Docetaxel		×	×
nanoparticle albumin-bound paclitaxel			×
liposomal doxorubicin	topo isomerase 2 inhibitor	×	×
gemcitabine	anti-metabolite, pyrimidine antagonist	×	×
bevacizumab	anti-angiogenesis	×	×
Topotecan	topoisomerase inhibitors		×
Etoposide			×

Table 6: Second-line treatment options for OC. See Refs.[12,150,157].

It is important to mention that the time to detect the recurrence disease depends on the adherence of the patients and clinicians to the follow-up procedures[157], monitored by CA125 and imaging after first-line treatment. Despite the improvements in imaging, a patient can be assigned as “platinum-sensitive” if it is detected later than sooner due to non-rising levels of the serum CA125. This designation relies only on a time line frame, which is very limited by the lack of accurate biomarkers and technical standards to detect recurrence[11,135]. Significantly, this can impact on how patients with recurrent disease are classified and clinically managed for second-line treatments[157].

One of the explanations of the low success on improving response rate to treatment and survival is the poor knowledge of the molecular levels and biological properties of the different EOC and the recurrence diseases. Histology, as mentioned, is one of the factors; it is known that the different histologies do not respond equally to the chemotherapy[12]. HGSC and high-grade (G3) EC initially are sensitive but most of them become resistant suffering recurrence, while the low-grade counterparts are generally already resistant to the standard treatment, and can be subjected for hormonal therapy. For CCC and MC histologies, the tumors use to be initially very resistant to the standard chemotherapy but still are treated with cytotoxic agents[11,12].

The discovery that BRCA1/2 mutation status as a factor that affects OC patients' treatment response helped to establish protocols for the management the patients[158]. Several lines of evidence suggest that OC patients with a somatic or germ line BRCA1/2 mutation are highly responsive to platinum and other DNA-damaging chemotherapy regimens, such as platinum derivatives, liposomal doxorubicin and PARP inhibitors, among others[157,159,160].

1.3.3. TARGETED THERAPIES

Although several rounds of CTH based in platinum derivatives and taxanes are usually administrated to most of the OC patients, the majority of them will become resistant and recur. New therapies for recurrent OC to target specific pathways include anti-angiogenic agents (AAs) and vascular-disrupting agents (VDAs)[161], poly (ADP-ribose) polymerase (PARP) inhibitors[160] (which block the repair of DNA damage) and immunotherapy agents (anti- PD-1 and PD-L1)[162] among others (Figure 11), and are still under investigation.

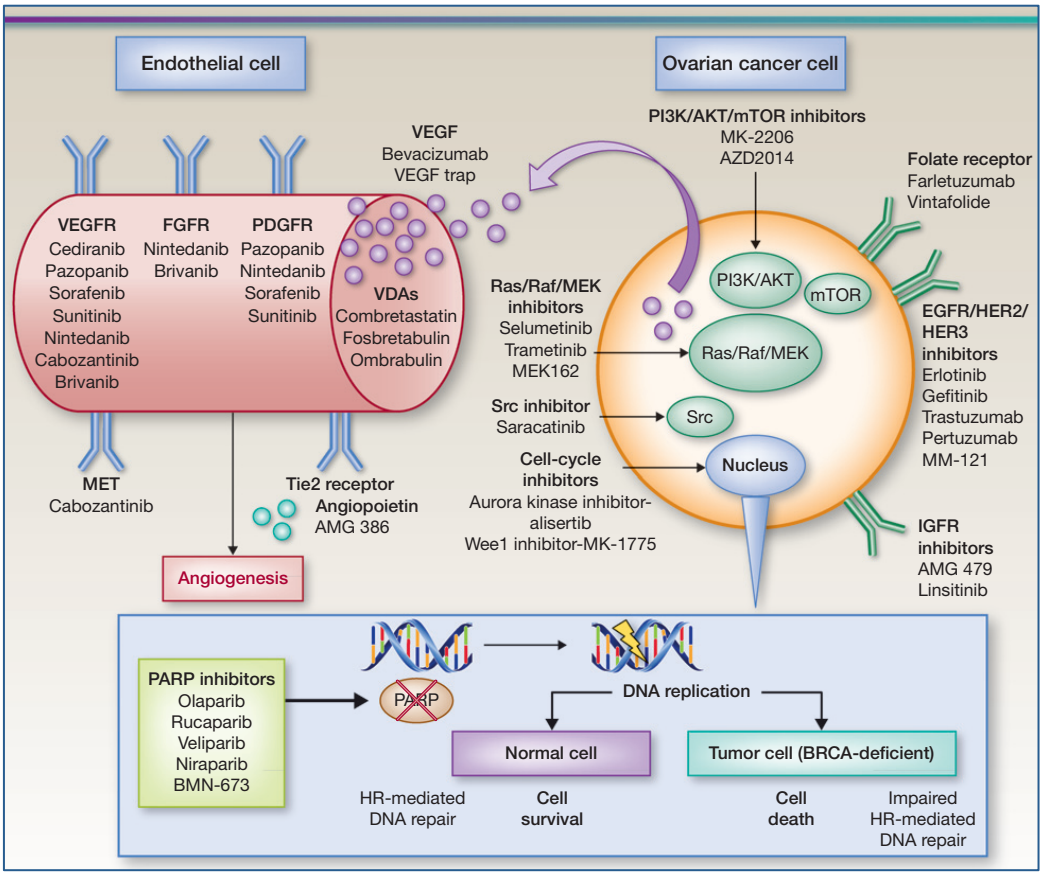

Figure 11: Targeted therapies in OC. Adapted from Banerjee S. *et al.* [24]

Recently, the AAs called **Bevacizumab**, an anti-vascular endothelial growth factor (anti-VEGF), was introduced as an option for recurrent OC as a second-line treatment in combination with the standard treatment and/or gemcitabine[150]. Alternatively, the addition of bevacizumab to consolidate the 3-weekly carboplatin and paclitaxel first-line treatment appeared to improve PFS[161,163]. Consolidation is treatment given after completion of first-line therapy with a complete clinical/pathologic response. However, improvements in OS appear to be restricted to poor-prognosis subgroups[163], and despite being available in Europe (approved by the European Medicines Agency (EMA)), bevacizumab has not been approved for patients in the United States, neither for newly diagnosed nor recurrent OC[12].

In addition, a new successful generation of drugs has emerged targeting **PARP** enzymes. PARP-1 and -2 are the most abundant of the 17-member superfamily nuclear enzymes that are activated upon DNA damage, and have a major role in the repair of the DNA breaks. PARP inhibition results in the accumulation of double-strand DNA brakes that are repaired by the HR pathway, in which BRCA1 and BRCA2 are key proteins[164]. Mutations in BRCA1 and BRCA2 also compromise DNA damage repair (DDR) machinery, and so patients with such mutations are more likely to respond to PARP inhibition, through synthetic lethality[164,165]. This process of synthetic lethality is a condition where simultaneous mutation and/or inhibition of two genes –but not either alone– leads to cell death, conceptually similar to therapeutic strategies involving synergistic effects[165]. Additionally, putative anticancer mechanisms of action have been described for PARP inhibitors in wild-type and mutant BRCA cells, in which other genes in the HR pathway play important roles in the "*BRCAness*" phenotype that could also lead to synthetic lethality[166].

Currently, germ line BRCA mutation status is established as a predictive biomarker of potential benefit to guide therapy with PARP inhibitors[166]. BRCA testing was previously offered only to women with a family or personal history of breast and/or OC. Since it is known that almost 20% of women with HGSC harbor a germ line BRCA mutation, and that around 40% of them might not have a family history, the test is being implemented for all non-mucinous OC, to guide treatment decisions and further give benefit not only to all patients bearing germ line but also to patients bearing somatic BRCA mutations (50%)[166]. Recently, Davies H. *et al.*[167] developed *"HRDetect"*, a predictor test able to detect germ line and somatic BRCA1/2 deficiencies (including SNPs, CNV, LOH, *indel*,

etc.) demonstrating its efficacy over alternative sequencing strategies, and independently validated in breast, pancreatic and OC patients[167].

Olaparib is the first PARP inhibitor approved by the EMA and FDA for BRCA-mutated OC patients, who have been treated with three or more chemotherapy regimens regardless of PFI[164]. It has shown single-agent response rate of up to 30% in recurrent OC, with the greatest activity in cancers with BRCA mutations and platinum-sensitive disease[166]. Very recently, a phase I-II study supported clinical and translational investigation of **rucaparib**, another PARP inhibitor, in patients with HR repair deficiency (germ line BRCA1/2 mutations) and platinum-sensitive disease, but potentially extending applicability beyond BRCA-mutated cancers, that is tumors with other HR deficiencies[168].

Despite the great results on the promising field, resistance to PARP inhibitors after a good response the treatment have been observed[169]. One of the mechanisms is the somatic BRCA1/2 recovery by copy number gain and/or up-regulation of the remaining functional allele[170] or reversion of a methylated BRCA allele[16], while bi-allelic somatic deletion and loss-of-function mutation lacked of a functional allele for recovery of BRCA activity, thus having a prolonged OS[170].

In conclusion, cells that repair DNA damage less efficiently are particularly sensitive to PARP inhibitors, and this will delay the resistance to standard chemotherapy. Thus, further studies are needed to evaluate the HR status in tumors (other deficiencies/mutations in the DDR machinery/HR pathway beyond BRCA1/2 genes) in order to know which patients will benefit from the synthetic lethality of the PARP inhibitors, and to generate novel combinational therapies for OC, especially for HGSC[160,169,171]. Since OC –especially HGSC– lack of clear driver mutations (regardless of p53, which is not sufficient to drive tumorigenesis) and have a high rate of somatic copy number alterations (CNA)[172] in part due to defects in HR pathways[16] (translated into chromosomal instability), some authors have made some efforts in this regard. Delaney *et al.*[172] developed a tool for identifying patterns of somatic CNA that together in cooperation could potentially drive OC tumorigenesis leading to targetable pathways[172].

Interestingly, several therapies targeting specific pathways (Figure 11) have been emerged thanks to the molecular knowledge of each histological subtype; however these therapies are still under study for their use in combination with standard regimens for recurrent OC[24]. Some of the examples are summarized below.

As previously mentioned, the activation of the **PI3K/AKT/mTOR pathway** occurs in around 40% of the HGSC[15]; and in up to 30% of CCC and EC[24]. Patients with PIK3CA mutations treated with PI3K/AKT/mTOR inhibitors demonstrated a higher response rate than patients without mutations[173]. Currently, a phase-II trial is investigating the efficacy of ***Temsirolimus***, carboplatin and paclitaxel as first-line therapy in patients with newly diagnosed stage-III–IV CCC[173]. Other inhibitors of the PI3K and AKT genes (***Everolimus*** and ***Ridaforolimus***) have entered in phase I-II clinical trials[173].

In addition, **Ras/Raf/MEK/ERK pathway** activation can occur either in HGSC (24%) and LGSC (65%)[24]. Therefore, Ras/MEK pathway is an attractive therapeutic target either for HGSC or for LGSC. In a phase-II study, recurrent LGSC were treated with ***Selumitinib*** and about 15% of patients demonstrated objective response rate[173]. In primary MC, which is frequently resistant to conventional chemotherapy, the Ras/MEK pathway is also an appropriate therapeutic target since it harbors mutations in KRAS and BRAF[24].

Also, the activation of EGFR signaling by overexpression of **EGFR** is up to 60%; however, single-agent EGFR inhibitors or HER2-targeted therapy (such as ***Trastuzumab***) are not very successfull[24]; while ***Pertuzumab*** (another HER2 inhibitor) in combination with gemcitabine in platinum-resistant OC showed a response rate of 13.8% as compared to 4.6% in patients receiving only gemcitabine; thus, other clinical trials are ongoing based on the combination of Pertuzumab and standard CTH[173]. Dual blockade of the VEGF and EGFR pathways by bevacizumab in combination with ***Erlotinib*** in recurrent OC was not superior to bevacizumab alone with severe adverse effects[173]. Additionally, there are multiple ongoing clinical trials for PARP inhibitors in combination with therapies against PI3K/AKT, VEGF, CDK and mTOR inhibitors, among others[166]. Thus, the study of “driving patterns” of tumorigenesis including cooperative mutations in HR system, somatic CNA and mutations in genes of the abovementioned pathways in order to gain understanding on resistance disease, and to generate new regimens of combinatorial therapies[174].

1.4. MIRNAS: NOVEL STRATEGIES FOR DIAGNOSIS AND THERAPY

1.4.1. MiRNA MOLECULES

Small non-coding RNAs (ncRNAs) are defined by their length (20–30 bp); they are classified into three classes: small interfering RNA (siRNA), PIWI-interacting RNA (piRNA) and microRNA (miRNA); and play important roles in biological pathways. The lack of these RNAs, may cause jumping of transposons (causing DNA damage), loss of stem cells, brain and muscle development failures, impaired cell division, deregulation of insulin secretion among many other processes[175], thus supporting that small ncRNAs play widespread key functions in development and in regulation of normal physiology across all organisms[175].

Specifically, miRNAs are ~22 nucleotides (nt) in length and constitute a dominating class of small ncRNAs in most somatic tissues[176]. Despite their size, their production, maturation, and regulatory function require the action of a large number of proteins, including the two RNase III proteins, DROSHA and DICER[176], and Argonaute (AGO) proteins[177] (Figure 12).

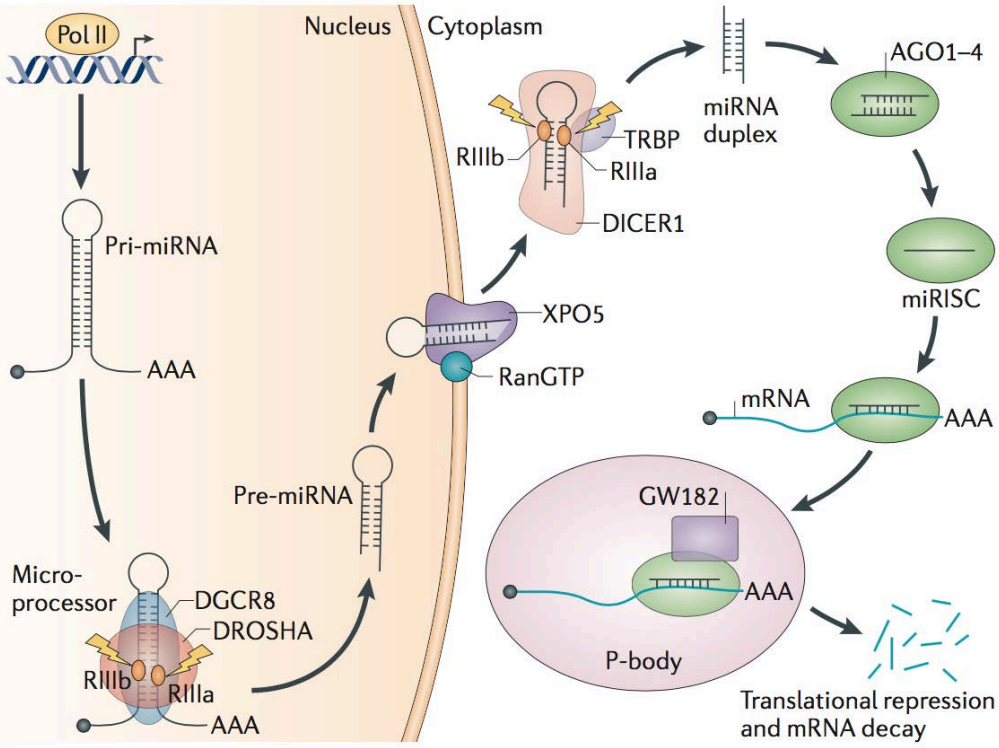

Figure 12: MiRNA-processing machinery in eukaryotes. The processing of pri-miRNA to pre-miRNA occurs within the nucleus by the microprocessor complex and after exportation to the cytoplasm, pre-miRNA is processed to the mature miRNA that along with AGO proteins form miRISC complex, which drives the specific silencing of target mRNAs. Adapted from Shuibin L. *et al.*[178].

MiRNAs can be located at intergenic regions, either from coding and non-coding genes. Some miRNAs can also be found within exons and introns, and both exonic and intronic miRNAs can share promoter and transcription start site (TSS) with the host protein-coding gene[176]. Alternative TSS and miRNA promoters have been postulated for miRNAs located in non-coding genes and for some intronic miRNAs (CpG islands mapping), but precise mapping of miRNA promoters still needs to be elucidated[176]. MiRNAs are eventually organized in clusters, i.e. miRNAs located in close proximity (<10Kb) to each other in a particular chromosome. These miRNAs are generally co-transcribed constituting a polycistronic transcript unit. However, the individual miRNAs can be additionally regulated independently at a post-transcriptional level[176].

MiRNA processing

MiRNAs transcription can be modulated epigenetically by DNA methylation and/or histone modifications. They are generally transcribed by RNA polymerase II (Pol II). The first transcript obtained is usually larger than 1Kb and is called primary miRNA (**pri-miRNA**). It contains stem–loop hairpin structure, in which mature miRNA sequences are embedded[176]. Typically, a pri-miRNA consists of a double-strand RNA (dsRNA) stem of 33–35 bp, a terminal loop and two single-strand RNA (ssRNA) segments at both the 5' and 3' ends (Figure 12).

Then, the **microprocessor complex**, formed by the RNase III-type endonuclease DROSHA (which contains two RNase III domains (RIIID)) and its essential cofactor DGCR8, initiates the maturation process in the nucleus by cutting specifically the dsRNA stem at 3' and 5' by the RIIID*a* and *b*, respectively. The released transcript is a small dsRNA hairpin (including the terminal loop) of ~65 bp in length, called precursor miRNA (**pre-miRNA**)[176]. Both DROSHA and DGCR8 contain nuclear localization signals (NLS) to remain in the nucleus and 3 dsRNA binding domains (dsRBD) that efficiently bind the pri-miRNA to help miRNA processing. Deficiencies in both genes cause lethality and defects in embryonic development in mice and humans[176]. Additionally, post-traductional modifications (i.e. acetylations and phosphorylations) in both factors, as well as other RNA-binding proteins (p68 and p72) that interact with DROSHA and/or the pri-miRNA, interfere in the stability and localization of the microprocessor complex, modifying the affinity to and the processing activity of the pri-miRNA and, ultimately, determine the abundance of the mature miRNA[176]. Of note, while the processing of intronic miRNA (co-transcriptional process) does not affect

splicing of the host gene (pre-mRNA), the exonic miRNA processing affects the stability of the mRNA by inducing RNA cleavage, thus antagonizing the levels of the host gene.

Nuclear export and DICER cleavage: after pri-miRNA processing, the nuclear pre-miRNA is exported to the cytoplasm by the help of two proteins: exportin 5 (EXP5) and the GTP-binding nuclear protein RAN (RAN-GTP). The **transport complex** includes these two proteins and the pre-miRNA. After translocation to the cytoplasm through the nuclear pore complex, a GTP is hydrolyzed, thereby resulting in the dissociation of the transport complex and the release of the pre-miRNA into the cytoplasm. Mutations in *XPO5* (gene encoding EXP5)[179] caused decreased levels of mature miRNA. Further investigation needs to be done in regard to find potential partners of EXP5 and regulators of nuclear exportation. This fact highlights that the regulation of miRNA levels is very complex and relies not only at a transcriptional level but also on the multiple factors and steps of the processing machinery.

The last step of miRNA processing is controlled by the RNase III endonuclease **DICER** that also contains two RIIID (*a* and *b)*, which form the catalytic center for the cleavage (by intramolecular dimerization of the two RIIID). DICER recognizes pre-miRNA by the terminal loop. It contains two pockets (PAZ domain) for the positioning of the 5' (phosphorylated) and the 3' (two single ribo-nucleotides overhang) ends of the pre-miRNA, like a person standing in a pair of shoes. Once there, DICER cleaves pre-miRNA near the terminal loop, at a distance of 22nt, and 21-25nt away from the 5' and 3' end, respectively, liberating a small RNA duplex (**mature miRNA**)[176]. Like DROSHA, DICER interacts with dsRBD proteins, such as the TAR RNA binding protein (TRBP) that also participates in the control of pre-miRNA cleavage and length of the mature miRNA. Mutations in and modifications of DICER also produce defects in embryonic development and deficiencies in spermatogenesis and hematopoietic stem cell lineage[180].

RISC formation: the mature miRNA delivered after DICER cleavage is then associated with **AGO** proteins to form the RNA-induced silencing complex (**RISC**). AGO proteins contain two RNA-binding domains: the Piwi domain, which binds the miRNA guide at its 5' end, and the PAZ domain, which binds the single-stranded 3' end of miRNA[181]. The endonuclease that cleaves the targeted mRNA resides in the Piwi domain of the AGO proteins[181]. Of the dsRNA mature miRNA loaded into the AGO protein, one strand

becomes the “guide strand” and the other is called the “passenger” strand. The guide strand is the only one retained in the RISC complex. The strand guide is determined during the AGO loading step, mainly on the basis of the relative thermodynamic stability of the two ends of the small RNA duplex. The passenger strand is removed from the RISC complex to generate a mature RISC able to complementary target the mRNA for gene silencing in the P-bodies[176,181]. Generally, the guide strand is the 5’ strand of the pre-miRNA, while the passenger strand is the 3’ of the pre-miRNA and is unusually common. Modifications in AGO proteins such as hydroxylation, phosphorylation, ribosylation and ubiquitynation contribute to their stability and localization into the P-bodies as well as to regulate their degradation, thus regulating the levels of mRNA silencing activity[176].

AGO proteins load mature miRNAs into their structure, in a conformation that facilitates efficient scanning of target mRNAs for complementary sequences[176,181]. All human AGO proteins (AGO1-4) are capable of inducing translational repression and decay of target mRNAs through interaction with the translation machinery and mRNA decay factors[176], but only AGO2 does directly cleave mRNAs that are matched with the miRNA[182].

MiRNA function

MiRNAs are acting *in trans* on mRNA stability blocking translation and triggering RNA silencing. They act hierarchically regulating multiple pathways in a cell, a theory that was firstly proposed by Britten and Davidson in the late 60’s[183]. Their translational repression function has been widely studied, pinpointing that complementary RNA-guide sequences within the mature miRNA structure are needed for its binding to the RNA-specific sequence located at the 3’ untranslated region (3’UTR) of the target gene, commonly known as **“seed sequence”**. The domain at the 5' end of the miRNA (from nucleotide position 2 to 7) is crucial for target recognition and has been termed the **“miRNA seed”**. Within the mature miRNA the first nucleotide of the RNA guide is usually unpaired[175]. The downstream nucleotides of the miRNA (particularly nucleotide 8 and nucleotides 13–16) also contribute to base pairing with the target mRNA[176]. While miRNA functions as a guide by base pairing the target mRNA, AGO proteins function as effectors by recruiting factors thus promoting mRNA degradation and/or blocking protein production of the targeted mRNAs[177].

Families, clusters and nomenclature

As abovementioned, miRNAs located in close proximity to each other in a particular chromosome belong to the same cluster and are generally co-transcribed constituting a polycistronic transcript unit[176]. In a situation where transcription factors or epigenetic modifications are regulating the activity of the promoter for a particular "**miRNA cluster**", the levels of all miRNAs in the cluster would thereby be proportional to the activity of the promoter.

Although several miRNAs in a cluster can be transcriptionally regulated as one unit, it does not mean that all miRNAs in a cluster must regulate the same target genes. Actually, what confers specificity for the target gene is the seed sequence within the mature miRNA. Hence, those miRNA molecules across the genome that contain the same seed sequence will generally regulate the same target genes, and are considered to belong to the same "**miRNA family**", a fact already described in 2000 by the discovery of the first miRNAs[184,185].

Additionally, several miRNAs can belong to the same family due to gene duplication resulting in paralogous miRNA loci (i.e. let-7 family). For instance, if two miRNAs of the same family generated by gene duplication are found in the same chromosome, they are called miR-1a and miR-1b; however, if both miRNAs are in separate loci, a numerical suffix is added to their nomenclature (miR-1a-1 and miR-1a-2). Furthermore, each locus produces two mature miRNAs: one from the 5' strand and one from the 3' strand of the pre-miRNA (for example, miR-1b-5p and miR-1b-3p). However, one arm (called the 'guide' strand; e.g. miR-1b-5p) is usually more abundant than the other arm (the 'passenger' strand), which is known as miRNA-3p (e.g. miR-1b-3p).

The latest release of the miRNA database (miRBase) has catalogued 2661 miRNAs in humans although not for all these annotations there is information about the functional importance.

Regulation of miRNA levels in cancer

Several studies reported that a particular miRNA can synchronously regulate multiple genes, but in turn, multiple miRNA can be orchestrated to regulate a single gene. It is known that ~60% of the coding genes have, at least, one conserved miRNA-binding site plus other non-conserved ones[176], thus suggesting that many genes are under control of miRNAs. Therefore, it is not surprisingly that deregulation of miRNA biogenesis is associated to pathological states such as cancer[178]. MiRNAs are catalogued as "oncomiRs" if they silence tumor suppressor genes, and tumor suppressor miRNAs if they target the expression of oncogenes, and have been found deregulated in cancer[186]. One of the mechanisms affecting miRNA activity in cancer is explained by the fact that miRNA biogenesis is often impaired in cancer, enrolling alterations in the main regulatory factors of the miRNA core processing machinery[178]:

- **Pri-miRNA processing:** somatic mutations in the RNase IIIb domain of DROSHA and deregulated expression of DROSHA levels have been found to act as oncogenic or tumor suppressor depending on the cancer type and the impaired miRNA processed. Also, somatic mutations in de dsRBD have been found for the other component of the microprocessor complex, DGCR8[178].
- **Nuclear export:** deregulated levels of EXP5, heterozygous-inactivating mutations and epigenetic silencing in *XPO5* have also been associated to several cancer types[178] as well as the balance of RAN-GTP/GDP state[187].
- **Pre-miRNA processing:** recurrent somatic mutations in the RNase IIIb domain of DICER are commonly found in cancer, and although they do not produce a truncated protein, the 5' side of the pre-miRNA hairpin is not correctly processed leading to a downregulation of the "-5p" but not the "-3p" forms of the miRNA. Like DROSHA, deregulated levels of DICER are usually found in many cancer types[178,180]. In addition, DICER syndrome is an inherited disorder caused by germ line DICER1 mutation that predisposes to a broad range of tumors (benign and malign), including a rare pediatric lung tumor, a cystic nephroma and ovarian Sertoli-Leydig tumors, among others[188]. In agreement, it has been found that Dicer can function as a haploinsufficient tumor suppressor in mice[189]. Also, frameshift mutations in the dsRBD of TRBP produce DICER destabilization and are found in several cancer types[178].

- **RISC:** in response to cellular stress such as hypoxia, phosphorylation of AGO2 is induced, thereby inhibiting the interaction with DICER1 and leading the accumulation of miRNA in the cytoplasm[178].

In addition to the particular alterations in the core components of the miRNA processing machinery, other genetic alterations affecting the pri-miRNA transcription *per se* have been observed in cancer. Briefly, **genomic variations** in fragile sites[178] (deletions, amplifications, translocations, point mutations) and **epigenetic modifications** (miRNA specific promoter and gene promoter hypermethylation, and histone modifications)[190] alter pri-miRNA transcription and/or processing, thus undergoing into aberrantly mRNA expression and contributing to cancer progression.

Deregulated miRNA expression can also arise from **alterations in tumor suppressor or oncogenic factors** that function as transcriptional activators or repressors controlling pri-miRNA transcription and also miRNA processing[176,178]. Here, there are some examples:

- The tumor suppressor **p53,** in response to DNA damage, enhances the post-transcriptional maturation of several miRNAs with growth-suppressive function, including miR-16-1, miR-143 and miR-145, increasing the fidelity of the RNA-binding proteins (p68 and p72) to interact with DROSHA[191]. Additionally, genes encoding miR-34 family members are direct transcriptional targets of p53[192]. Upon DNA damage, the p53 network suppresses tumor formation not only through multiple transcriptional targets, but also increasing miR-34 family, which acts in concert with p53 blocking CCNE1, CDK4, MET and p-RB to inhibit inappropriate cell proliferation[192]. Additionally, the loss of the tumor suppressor **p63** (an homolog of p53) and its microRNA-205 target results in enhanced cell migration and metastasis in prostate cancer[193].
- In contrast, the potent oncogene **MYC** activates the expression of well-known oncogenic miRNAs such as the miR-17-92 cluster, which represses a set of chromatin regulatory and pro-apoptotic genes, thereby maintaining cell survival, autonomous proliferation, and self-renewal capacity[194,195].
- **ZEB1/2,** well-known repressors of E-cadherin and inducers of EMT, are direct targets of the miR-200 family members but, at the same time, ZEB1/2 can inhibit the expression of miR-200 members in a negative feedback loop, thus

contributing to the epithelial cell plasticity and regulating the metastatic spread[196].

- Finally, **NF-kB** transcriptionally activates miR-21, miR-30c, and miR-100, which silence pro-apoptotic genes such as caspase-8/3, strengthening the activation of the pathway and contributing to drug resistance and higher aggressive cancerous disease[197].

In addition to modifications in miRNA processing machinery either at genetic, epigenetic, transcriptional and post-transcriptional levels, **modifications in miRNA sequence** itself can be found causing defects in miRNA biogenesis or target specificity. Such modifications can be single nucleotide polymorphism (SNPs), RNA tailing, RNA editing, RNA methylation and active miRNA degradation, and they have been postulated to regulate the stability, abundance and, therefore, the activity of certain mature miRNAs[176].

1.4.2. MiRNAs IN OVARIAN CANCER

It was firstly reported that a general downregulation of miRNAs levels was found in cancer, that miRNA levels are directly related to the levels of cell differentiation and inversely associated with pluripotency (a hallmark of cancer), and that miRNA signatures reflect more accurately than mRNA levels the developmental lineage and tissue origin of human cancers, including OC[186]. As expected, OC also has some of the miRNA alterations abovementioned influencing the miRNA processing machinery and governing miRNA activity.

- **Alterations in the miRNA processing machinery**: one of the explanations of the lower miRNA levels in EOC would be the low level of functional DROSHA and/or DICER. On one hand, Merritt WM *et al*. reported that DROSHA and DICER were downregulated in EOC and that low expression correlated with advanced stages and associated with poor clinical outcome[198]. Additionally, germ line mutations in *DICER1* have been associated to sex-cord stromal tumors of the ovary[180]. On the other hand, DROSHA DGCR8, DICER1 and AGO1-2 have been shown to be upregulated in HGSC and associated with advanced tumor stages[178]. Additionally, Zhang L. et a. reported no differences in the levels of DROSHA and DICER between early and late-stage EOC[199].

Interestingly, most EOC have mutations in p53, which regulates the activity of DROSHA through its interacting RNA binding protein p68 (also known as DDX5). P53 enhances DROSHA-mediated processing of several miRNAs under DNA-damage conditions, activity that would be abrogated in p53 mutant OC[191]. Similarly, miR-34 family members are increased at transcriptional and post-transcriptional level in p53-wt cells but not in p53-null cells[192], suggesting that one of the multiple reasons for why OC has a general downregulation of miRNAs would be, in part, the deficiency in the p53-dependent miRNA biogenesis pathway.

- **Alterations in exportation mechanisms:** SKG is a serine/threonine protein kinase that regulates the levels of the GTP-bound state of RAN, the partner of EXP5. SKG1 was found overexpressed in OC[187], and that its inhibition results in reducing pre-miRNA nuclear export, thereby suggesting that could be a therapeutic target in EOC[187].
- **Other alterations:** core components of the miRNA processing machinery are not the only ones responsible for the deregulation of miRNAs levels in OC. As in other cancer types, other featured alterations in OC that induce miRNA silencing are genomic copy number loss and DNA hypermethylation of a vast number of tumor suppressor miRNAs[190,199], with the consequent up-regulation of genes related to cell proliferation, cell signaling and cancer pathways.

Giving the heterogeneity of the disease, it is necessary to consider wider scenario of the mutations and levels of expression of the core components of the miRNA processing machinery compiled with the genomic and epigenetic alterations for the different histological and molecular subtypes to help in the understanding of the OC biology. Together, these insights remark the importance of miRNA function in understanding the initiation and progression of OC, to valuably contribute improving the early diagnosis and finding new targeted-therapies for specific molecular subtypes of EOC.

Recently, the current status of miRNAs as a diagnostic, prognostic and therapeutic strategies in OC has been reviewed, highlighting that although substantial results have been obtained to date, the heterogeneity among the studies, platforms, cohorts (stages, grades, histological subtypes, etc.) include variability on and difficult the interpretation of the results across the studies[200].

Generally, let-7, miR-200, miR-30, miR-34 family members and two miRNA clusters located at Chr.X and Chr.14 (among other important miRNAs) are mostly downregulated in advanced EOC and associated to poor prognosis and shorter OS and PFS[199,200]. Also, several miRNAs are associated with chemoresistance that upon restoration of the levels of some of them (specially for the miR-200 family[201] that regulates EMT) increased sensitivity to the standard treatments[200].

Interestingly, a recent study using TCGA data from CNA, methylation and mRNA and miRNA expression, described a miRNA-regulatory network that defined an OC mesenchymal subtype associated with poor OS[202]. This miRNA signature included two important downregulated miRNAs in OC that belong to the miR-200 family and regulate EMT through targeting *ZEB1* and *ZEB2*. It also includes 3-downregulated miRNAs (miR-25, miR-29c and miR-506) that regulate transcriptional repressors of E-cadherin, which are targets involved in invasion and metastasis. In addition, the overexpression of miR-506 abolished TGFβ-induced EMT/mesenchymal phenotype *in vitro* and *in vivo*, and correlated with increased OS and epithelial markers in OC patients[202]. MiR-506 is located in the miRNA cluster at Chr.X and, importantly, it is downregulated in OC chemoresistant cells acting through CDK4/6-FOXM1 axis, *SNAI2*, and RAD51, which are key player genes in OC development and aggressiveness[15,200].

Efficient OC management relies on early diagnosis of the disease and efficient treatments. Since miRNAs are the tip of the iceberg over a high complex regulatory network within a tumor cell constituting a good source of biological information and, therefore, they are important not only as diagnostic biomarkers but also future therapeutic targets. Below, and as the relevant topic that this thesis deals with, some of the relevant studies recently performed on miRNAs as novel diagnostic biomarkers and therapeutic strategies are highlighted.

1.4.2.1. MiRNAs as a diagnostic tool

Circulating nucleic acids are released by tumor cells into the bloodstream as a result of apoptotic and necrotic cell death or by active secretion[203], and, in principle, contain genetic defects identical to the tumor cells they originate from, including DNA and RNA molecules[204]. Although they are usually fragmented, the circulating tumor cell-free DNA (ctDNA) is stable, while other cell-free RNAs are not so, with the exception of miRNAs[204].

Many diagnostic miRNAs have been discovered through deep sequencing technologies, and although further research is needed to elucidate the complexity of the heterogeneous origin of miRNAs in body fluids, they provide precise information that could lead to early diagnosis of cancer, and eventually could provide insights into the biology of the tumor[203]. Additionally to blood, their presence has been confirmed in many body fluids including urine, saliva, cerebrospinal, pleural, amniotic, seminal and peritoneal fluid, as well as tears, colostrum and breast milk among others[205].

The advantages of using cell-free miRNAs in cancer diagnosis include the low cost and easy-to-use assays for cell-free miRNA analyses, as well as quick results can be obtained using PCR-based methods for daily diagnosis and disease monitoring[203]. Furthermore, miRNAs are small RNA molecules that are stable in circulation and protected from RNases degradation[206]. Several systems have been proposed for circulatory miRNA protection against degradation either by forming ribonucleoproteins complexes (i.e. with AGO2 or HDL proteins) or contained in extracellular vesicles (apoptotic bodies, shedding vesicles and exosomes)[203].

Most of the studies postulating miRNAs as diagnostic biomarkers for OC are found in serum and/or plasma samples (Table 7). The implementation of miRNAs into the clinical practice as a liquid biopsy has exponentially increased, much as for ctDNA and circulating tumor cells (CTCs), the latter two ranking in top positions as a means of diagnostic tools[204,207,208] and with a high potential of aiding to clinical decisions (e.g. the detection of EGFR mutation in ctDNA guides the treatment for a type of lung cancer, a strategy approved by the FDA and EMA)[207].

Year	Reference	Sample type	Sample size	EOC histology	FIGO Stage	Upregulated miRNAs	Downregulated miRNAs
2008	Taylor DD. *et al.* Gynecol Oncol *(Reviewed in Prahm et al.[200] (Ref.62))*	Exosomal serum miRNA	Patients 50 Benign 10 Control 10	serous	I-IV	miR-21, miR-141, miR-200a, miR-200b, miR-200c, miR-203, miR-205, miR-214	
2009	Resnick KE. *et al.* Gynecol Oncol *(Reviewed in Prahm et al.[200] (Ref.63))*	Serum miRNA	Patients 28 Controls 15	serous, endometrioid, clear cell, mucinous	I-IV	miR-21, miR-92, miR-93, miR-126, miR-29a	miR-155, miR-127, miR-99b
2010	Hausler SF. *et al.* Br J Cancer *(Reviewed in Prahm et al.[200] (Ref.76))*	Whole blood	Patients 24 Controls 15	serous and endometrioid	-	miR-30c1	miR-342-3p, miR-181a, miR-450b-5p
2012	Kan CW. *et al.* BMC Cancer *(Reviewed in Prahm et al.[200] (Ref.64))*	Serum miRNA	Patients 28 Controls 28	serous	IIc-IV	miR-200a, miR-200b, miR-200c	
2013	Hong F. *et al.* J Int Med Res *(Reviewed in Prahm et al.[200] (Ref.69))*	Serum miRNA	Patients 96 Controls 35	serous and others	I-IV	miR-221	
2013	Xu YZ. *et al.* Asian Pac J Cancer Prev *(Reviewed in Prahm et al.[200] (Ref.70))*	Serum miRNA	Patients 94 Controls 40	serous and others	I-IV	miR-21	
2013	Guo F. *et al.* J Int Med Res *(Reviewed in Prahm et al.[200] (Ref.71))*	Serum miRNA	Patients 50 Controls 50	-	I-IV	miR-92	
2013	Suryawanshi S. *et al.* Clin Cancer Res *(Reviewed in Prahm et al.[200] (Ref.77))*	Plasma miRNA	Patients 54 Endometriosis 33 Controls 20	serous, endometrioid and clear cell	I-IV	miR-15b, miR-16, miR-21, miR-195	
2013	Zheng H. *et al.* Plos One *(Reviewed in Prahm et al.[200] (Ref.36))*	Serum miRNA	Patients 360 Controls 200	serous, endometrioid, clear cell, mucinous	I-IV	miR-205	Let-7f
2014	Ayaz L. *et al.* J Obstet Gynaecol *(Reviewed in Prahm et al.[200] (Ref.65))*	Serum miRNA	Patients 18 Controls 24	serous	I-IV	miR-191-5p, miR-206, miR-548-3p, miR-320a, miR-574-3p, miR-590-5p, miR-34c-5p, miR-106b-5p. Only in OC: miR-140-3p, miR-133a, miR-34a-5p, miR-146b-5p, miR-125a-3p, miR-95, miR-16-5p, miR-138-5p, miR-17-5p, miR-323a-3p	miR-19a-3p, miR-30a-5p, miR-645, 150-5p
2014	Ji T. *et al.* Asian Pac J Cancer Prev. *(Reviewed in Prahm et al.[200] (Ref.68))*	Serum miRNA	Patients 31 Benign 23 Controls 8	-	I-IV	miR-22, miR-93, miR-106, miR-451	
2014	Xie J. *et al.* Cell Mol Immunol *(Reviewed in Prahm et al.[200] (Ref.72))*	Serum miRNA	Patients 34 Benign 10 Controls 20	serous and others	I-IV	miR-20a	

Table 7: Illustrative list of circulating miRNAs as OC diagnostic tool. Adapted and extended from Refs.[200,209–214].

Table 7 (cont.)

Year	Reference	Sample type	Sample size	EOC histology	FIGO Stage	Upregulated miRNAs	Downregulated miRNAs
2014	Shapira I. *et al.* Br J Cancer *(Reviewed in Prahm et al.[200] (Ref.74))*	Plasma miRNA	Patients 42 Benign 36 Controls 23	serous	IIa-IV	miR-1274a, miR-625-3p, miR-720	miR-106a, miR-126, miR-146a, miR-150, miR-16, miR-17, miR-19b, miR-20a, miR-223, miR-24, miR-921, miR-106b, miR-191, miR-193a-5p, miR-30b, miR-20a-5p, miR-30c,miR-320, miR-328
2014	Shen W. *et al.* Plos One *(Reviewed in Prahm et al.[200] (Ref.78))*	Plasma miRNA	Patients 17 Controls 13	serous, endometrioid, clear cell, mucinous	I-IV	miR-26a	
2015	Langhe R *et al.* Cancer Lett. *(Reviewed in Prahm et al.[200] (Ref.66))*	Whole blood, serum miRNA	Patients 25 Benign 25	serous	Ic-IV		Let-7i, miR-122-5p, miR-152-5p, miR-25-3p
2015	Liang H *et al.* Tumor Biol. *(Reviewed in Prahm et al.[200] (Ref.67))*	Serum miRNA	Patients 84 Benign 51 Controls 135	serous, endometrioid, clear cell, mucinous	I-IV		miR-145
2015	Gao YC. *et al.* Tumor Biol *(Reviewed in Prahm et al.[200] (Ref.73))*	Serum miRNA	Patients 74 Benign 19 Controls 50	serous, endometrioid, clear cell, mucinous, undiferentiated	I-IV	miR-200c, miR-141	
2015	Meng X. *et al.*[209] Br J Cancer	Serum miRNA	Patients 180 Controls 66	serous, endometrioid, clear cell, mucinous	I-IV	miR-7, miR-429	miR-25, miR-93
2015	Zhang Y. *et al.*[211] Sci.Rep.	Serum miRNA	Patients 20 Controls 20	-	-	miR-16-2*, miR-2861, miR-195	
2016	Meng X. *et al.*[210] Oncotarget	Exosomal serum miRNA	Patients 163 Benign 20 Controls 32	serous and others	I-IV	miR-373a, miR-200a, miR-200b, miR-200c	
2016	Zuberi M. *et al.*[212] Plos One	Serum miRNA	Patients 70 Controls 70	serous, mucinous and others	I-IV	miR-125b	
2017	Todeschini P. *et al.*[213] Cancer letters	Serum miRNA	Patients 168 Controls 65	serous	III-IV	miR-1246	
2017	Zhu T. *et al.*[215] Int J Gyn Ca	Serum miRNA	Patients 135 Benign 54	serous, endometrioid, clear cell, mucinous	I-IV	miR-125b	

1.4.2.2. MiRNAs as a therapeutic tool

So far miRNAs as a diagnostic tool have not been implemented into a feasible test for cancer detection in general; however, miRNAs as a novel therapeutic approach have made some advances during the last years. The ability of a particular miRNA to target multiple mRNAs that are altered in disease conditions makes these molecules interesting candidates to use them as a therapy (in the form of miRNA mimics) or as a targeted therapy (in the form of antagomiRs/antimiRs)[215]. MiRNA mimics are synthetic small dsRNA molecules that match the corresponding miRNA sequence and therefore functionally aim to replenish the lost miRNA expression. AntimiRs are synthetic small ssRNA molecules that have a complementary sequence and bind to the target miRNA inhibiting its function. They are based on first-generation antisense oligonucleotides (ASOs), which were designed to target mRNAs, or modified with locked nucleic acids (LNAs)[215].

One of the challenges for RNA-based therapeutic strategies (including ssRNA or dsRNA) is their potential for degradation by RNases present in serum or in the endocytic compartment of the cells. To avoid this, two different but converging strategies have been pursued: (i) alter oligonucleotide chemistry; (ii) engine delivery systems to encapsulate RNAs, and protect from RNases and endosomal degradation (Table 8). Both strategies have been developed not only to increase the stability of the miRNA molecules but also to improve the efficacy of specific target delivery[215].

A considerable number of preclinical studies involving miRNA therapeutics have been conducted over the last years, from which a number of therapeutic miRNA have so far moved into clinical development through clinical trials (recently reviewed by Rupaimoole R. *et al*[215]). Some of the examples followed strategies to replenish tumor suppressor miRNAs: miR-34 encapsulated with lipid nanoparticles for local and systemic delivery; miR-200c, miR-506 and miR-520 in DOPC liposomal carriers; miR-26a with adeno-associated virus; and nanocell EDV systems coupled with EGFR targeted molecules[215].

However, some challenges in the development of miRNA-based therapeutics still remain[215]: (i) to identify the best miRNA candidates or miRNA targets for each disease; (ii) To design a miRNA delivery vehicle that confers high stability; (iii) to enable tissue-specific targeting; (iv) to avoid potential toxicities and off-target effects.

Chemical modifications		Delivery systems	
miRNA mimics	Addition of **methyl groups** to the passenger strand to increase the stability	**Viral vectors**	Adenoviral vectors that encode small RNA molecules of interest (difficult to bring to the clinics)
AntimiRs	**2'-O-methoxyethyl** modification resulted in improved target modulation **(antagomiRs)**	**PLGA:** Poly(lactide-co-glycolide) particles	PLGA polymers can be altered thus controling delivery rate (high safety profile but low miRNA loading)
	Chemically locked by a bridge that connects the 2'-oxygen and 4'-carbon in a ribonucleotide **(LNA-modified antimiRs)**	**NLEs:** Neutral lipid emulsions	Consist of 1,2-dioleoyl-sn-glycero-3-phosphocholine (DOPC), squalene oil, polysorbate 20 and an antioxidant (low toxicity but low efficiency in tumor delivery)
	Two deoxyribonucleotides pattern, followed by one locked ribonucleotide (**called LNA mixmers**)	**DOPC-based nanoparticles** (neutral liposomes)	DOPC-based nanoparticles widely tested in preclinical setting for the delivery of miRNAs and siRNAs. Phase I trials for siRNA-based approaches
	Complexed by **disulfide bond** to pH low insertion peptide **(pHLIP)**; enters to the cells upon low pH conditions through non-endosomal route	**EDV/TargomiRs :** EnGeneIC Delivery Vehicle nanocells	Bacterium-derived 400 nm particles that have the capacity to deliver chemotherapeutic agents. Can be conjugated with antibodies (e.g. EGFR) to target specific sites
ASOs	Addition of **methyl groups** at different locations in the RNA backbone increases stability	**PEI**: Synthetic polyethylenimine	PEI is an early-generation polymer. Upon forming complex with nucleic acids, enter into the cell by endocytosis (in preclinical development)
	Addition of a **2'-O-methoxyethyl** modification also improved nuclease resistance and binding affinity	**Dendrimers**	Poly(amidoamine)- or poly(propylenimine)-conjugated nucleic acids (high efficiency in delivery but toxicity associated to the cationic
	Phosphorothioate nucleotides (replacing the non-bridging oxygen in the phosphate group with sulfur), allowing internucleotide linkages resistant to nucleases degradation	**PEG:** Poly(ethylene glycol)	Nucleic acids are conjugated to PEG via a disulfide linkage. Advanced delivery systems currently in clinical trials (superior gene-silencing efficacy compared with the PEI system)
	Addition of a **2'–O-methyl group** to phosphorothioate nucleotides resulted in increased binding affinity to the target mRNA and significant nuclease resistance	**Chitosan**	Cationic polymer derived from a natural polysaccharide composed of glucosamine and N-acetylglucosamine residues, called chitin (low toxicity and biodegradable)
		GalNAc: N-acetyl-D-galactosamine	GalNAc-miRNA-conjugates delivered without the need of lipid carriers and uptaked by clathrin-mediated endocytosis (currently in phase I and phase II trials, but limited to liver diseases)

Table 8: Mechanisms to increase stability and delivery of miRNA mimics or antimiRs. See Ref.[215].

Systematic studies using large cohorts of patients (TGCA-like sources), multiple biopsies to avoid the intra-tumoral heterogeneity, miRNAs that resensitize chemoresistant cancer cells, CHIP-seq assays and target prediction tools to find the relevant miRNA "*targetome*", among others, are proposed strategies to find the best miRNAs that can then be therapeutically manipulated[215]. The ability of miRNAs to target multiple genes is attractive, as it may facilitate the targeting of multiple compensatory pathways. However, a particular miRNA targetome might include oncogenes and tumor suppressors, as well as a number of targets not involved in cancer, which complicates the development of selective miRNA-directed therapeutics[215]. Moreover, miRNAs, especially at non-physiological concentrations, can have off-targets that could potentially lead to adverse effects by targeting normal cell homeostasis genes. Functional studies precede and are necessary to verify the therapeutic role of interesting miRNAs in EOC. Such miRNA reports become prime candidates to further investigate the potential for EOC intervention. Most relevant and latest studies postulating miRNAs as putative therapies for EOC are listed in Table 9.

miRNAs		Alteration described in EOC	Cellular function	miRNA target	Study type	Year	Reference
miR-200 family	miR-141, 200a	Overexpressed in responders	Oxidative stress response, paclitaxel sensitivity upon overexpression	MAPK14 (p38a)	*In vitro* and *in vivo*	2011	Mateescu B. et al. Nat Med *(Reviewed in Prahm et al.[200] (Ref.44))*
	miR-200a	Downregulated in resistant cells	Decreased migration and invasion upon overexpression	ZEB2	*In vitro*	2011	Wu Q. et al. Gynecol Oncol *(Reviewed in Prahm et al.[200] (Ref.115))*
	miR-141	Overexpressed in non-serous resistant	Inhibition increases platinum sensitivity through NF-kB inactivation	KEAP1	*In vitro* and *in vivo*	2012	van Jaarsveld M. et al. Oncogene *(Reviewed in Prahm et al.[200] (Ref.57))*
	miR-200c, 200a	Downregulated in advanced stages	EMT, migration and invasion	ZEB2, ZEB1	*In vitro and in vivo*	2013	Chen D. et al. Int J Gyn Can (Reviewed in Prahm et al.[200] (Ref.117))
	miR-200b	Downregulated	miRNA delivery inhibits metastasis and angiogenesis	IL8, CXCL1	*In vitro* and *in vivo*	2013	Pecot CV. et al. Nat Com *(Reviewed in Prahm et al.[200] (Ref.99))*
	miR-200a/b	Downregulated in mesenchymal types	Downregulation increases EMT, migration and poor survival	ZEB1	*In vitro*	2016	Chung VY et al. Sci Rep[216]
Let-7 family	Let-7i	Downregulated	Overexpression increases platinum sensitivity	H-RAS, HMGA2	*In vitro*	2008	Yang N. et al. Cancer Res *(Reviewed in Prahm et al.[200] (Ref.37))*
	Let-7e	Downregulated	Overexpression increases platinum sensitivity	EZH2, CCD1	*In vitro* and *in vivo*	2013	Cai J. et al. Oncogenesis *(Reviewed in Prahm et al.[200] (Ref.83))*
miR-506		Low in chemoresistant cells, poor prognosis and serous	Suppresses tumor growth and EMT	SNAI2	*In vitro and in vivo*	2013	Yang D. et al. Cancer cell *(Reviewed in Prahm et al.[200] (Ref.22))*
			Overexpression increases platinum sensitivity, inhibits proliferation and increases senescence	CDK4, CDK6	*In vitro* and *in vivo*	2014	Liu G. et al. J Pathol *(Reviewed in Prahm et al.[200] (Ref.86))*
				RAD51	*In vitro* and *in vivo*	2015	Liu G. et al. J Natl Cancer Inst *(Reviewed in Prahm et al.[200] (Ref.87))*
			miRNA delivery suppressed invasion and metastasis	SNAI2, VIM, N-cadherin	*In vitro and in vivo*	2015	Sun Y. et al. J Pathol *(Reviewed in Prahm et al[200] (Ref.100))*
miR-199/214 cluster	miR-199a	Elevated	Overexpression reduces NF-kb activation and increases chemosensitivity	IKKb	*In vitro*	2008	Chen R. et al. Oncogene[217]
	miR-199a, miR-214	Increases upon cell differentiation	Overexpression reduces stemness, induces chemosensitivity but increases proliferation	IKKb, PTEN	*In vitro*	2010	Yin G et al. *Oncogene (Reviewed in Prahm et al.[200] (Ref.93))*
	miR-214	Elevated	Overexpression increases AKT activation and platinum resistance	PTEN	*In vitro*	2014	Yang H. et al. Cancer Res *(Reviewed in Prahm et al.[200] (Ref.89))*
	miR-199	Downregulated	Overexpression inhibited cell growth and migration and increases drug sensitivity	PTPN3	*In vitro*	2016	Li S. et al. Sci Rep[218]
miR-34 family	miR-34a,b*/c	Downregulated	Overexpression reduced proliferation, motility, and invasion	MET	*In vitro*	2010	Corney DC. et al. Clin Cancer Res *(Reviewed in Prahm et al.[200] (Ref.49))*
miR-31		Downregulated in chemoresistant and poor prognosis	Overexpression inhibits proliferation and induces apoptosis	E2F2, STK40, CEBPA	*In vitro*	2010	Creighton CJ. et al. Cancer Res *(Reviewed in Prahm et al.[200] (Ref.96))*
			Overexpression increases chemosensitivity	MET	*In vitro* and *in vivo*	2013	Matimura T. et al. Oncogenesis *(Reviewed in Prahm et al.[200] (Ref.94))*
			Overexpression increase microtubule polymerization, G2 phase delay, and sensitivity to taxane	STMN1	*In vitro*	2015	Hassan MK. et al. Oncoscience *(Reviewed in Prahm et al.[200] (Ref.95))*
miR-137		Downregulated	Overexpression reduces OC growth (induces G1 arrest and cell apoptosis), migration, and invasion	AEG1	*In vitro* and *in vivo*	2013	Guo J et al. BBRC *(Reviewed in Prahm et al.[200] (Ref.105))*
			Overexpression increased cisplatin-induced apoptosis	XIAP	*In vitro*	2016	Li X. et al. Br J Cancer[219]

Table 9: Illustrative list of miRNAs as putative OC therapeutic tools. Adapted and extended from Refs.[200,216–230].

Table 9 (cont.)

miRNAs	Alteration described in EOC	Cellular function	Target	Study type	Year	Reference
miR-134	Upregualted	Activated JNK and ERK and reduced chemosensitivity	SDS22	*In vitro* and *in vivo*	2016	W J et al. Cell Death and Dis[220]
miR-134-3p	Downregulated	Downregulation is associated with poor prognosis and its overexpression reduces cell growth, migration and angiogenesis	RAB27A	*In vitro* and *in vivo*	2017	Chang C. et al. Gene[221]
miR-520d-3p	Low expression associated with shorter survival	Overexpression inhibits proliferation, migration, and invasion	EPHA2, EPHB2	*In vitro* and *in vivo*	2013	Nishimura M. et al. Cancer Disc *(Reviewed in Prahm et al.[200] (Ref.88))*
miR-138	Downregulated	Overexpression inhibits EMT	SOX4, HIF-1a	*In vitro* and *in vivo*	2013	Yeh YM. et al. Int J Cancer *(Reviewed in Prahm et al.[200] (Ref.103))*
miR-92a	Downregulated	Overexpression inhibits proliferation, cell adhension and invasion and reduces peritoneal metastasis	ITGA5	*In vitro* and *in vivo*	2013	Ohyagi-Hara C. et al. Am J Pathol *(Reviewed in Prahm et al.[200] (Ref.107))*
miR-484	Downregulated	Overexpression increased chemosensitivity, necrosis and control angiogenesis	VEGFB, VEGFR2	*In vitro* and *in vivo*	2013	Vecchione A. et al. PNAS *(Reviewed in Prahm et al.[200] (Ref.58))*
miR-152, miR-185	Downregulated	Overexpression increased cisplatin sensitivity	DNMT1	*In vitro* and *in vivo*	2013	Xiang Y et al. Oncogene[222]
miR-7	Downregulated in metastatic EOC	Overexpression inhibits invasion, migration, and EMT	EGFR	*In vitro*	2014	Zhou X. et al. Plos One *(Reviewed in Prahm et al.[200] (Ref.104))*
miR-491-5p	Downregulated	Overexpression induced inhibition of AKT and MAPK pathways	BCL-XL, EGFR	*In vitro*	2014	Denoyelle C. et al. Cell Death and Dis[223]
miR-106b	Downregulated	Overexpression reduces cell proliferation, migration and invasion, promoted G1 or S arrest and apoptosis, and supressees tumor development	RhoC	*In vitro* and *in vivo*	2015	Chen S. et al. Plos One *(Reviewed in Prahm et al.[200] (Ref.108))*
miR-1271	Downregulated	Overexpression inhibited cell growth	Cyclin G1 (CCNG1)	*In vitro*	2015	Liu X. et al. Med Sci Monit[224]
miR-145	Downregulated	Overexpression markedly induced apoptosis	TRIM2	*In vitro* and *in vivo*	2015	Chen X. et al. Gynecol Oncol[225]
miR-193b	Downregulated	Overexpression enabled the metastasizing cells to invade and proliferate into the omental	uPA	*In vitro* and *in vivo*	2015	Mitra AK et al. Oncogene[226]
miR-23a	Upregulated	Activated NF-kB and WNT/MAPK pathways	IKKa, ST7L	*In vitro*	2016	Yang Z. et al. Br J Cancer[227]
miR-124	Downregulated	Overexpression induced G1 arrest and sensitize cells to etoposide through p27/Myc/phospho-Rb signature	p27 (activation)	*In vitro* and *in vivo*	2016	Seviour EG et al. Oncogene[228]
miR-101, miR-26	Upregulated	Imposed glucose restriction on T cells and dampened their function via Notch inactivation (poor antitumor immunity)	EZH2	*In vitro*	2016	Zhao E. et al. Nat Immunol[229]
miR-216b	Downregulated	Overexpression increased cisplatin sensitivity	PARP	*In vitro*	2017	Liu Y. et al. Can Gene Ther[230]

2. HYPOTHESIS AND OBJECTIVES

About 70% of all OC cases are diagnosed at late stage of the disease where the 5-years SV is ~25%. Among other reasons, late stage diagnosis occurs because current diagnostic methods are not sufficient to diagnose OC at an early stage of the dissemination process, when the tumor is still confined to the ovary and when the 5-years SV is ~90%. Among the different histological subtypes of EOC, HGSC is the most common subtype (~70%) and the worse in terms of metastatic behavior, contributing in gran part to the high mortality rate of the disease. Other histologies, such as CCC and low-grade EC, are of better prognosis since they are usually detected at an early stage of the disease. Although the current treatments are intended to eliminate macroscopic and microscopic residual disease, 85% of the patients will become resistant and die of recurrence. Therefore, the therapy given to the patients is mostly palliative and pursues the better quality of life.

MiRNAs are small RNA molecules that regulate multiple cellular processes by silencing of the specific target mRNAs, and have been found deregulated under pathological conditions, including cancer. In addition, they are stable in circulation and are protected from degradation, therefore being potential non-invasive diagnostic tools. Thus, it is hypothesized that miRNAs can be useful to improve the early diagnosis by a non-invasive method and that can be new elements to find new targeted therapy for OC patients. The **general goal** of the thesis is **to explore the utility of the miRNAs for the management of OC**. Specifically, the two main specific objectives of the thesis are:

Objective 1. To identify new miRNA biomarkers in saliva as a tool to improve the early diagnosis of HGSC, based on the facts that miRNAs are stable molecules in many body fluids, and that saliva has been used as a source of biological information harboring pathological signatures regarding disease status.

Objective 2. To identify new miRNA-based therapies as a tool for the treatment of late-stage OC, based on the facts that the development of new targeted therapies has became the Holy Grail for cancer therapy due to the better outcomes explained by patients' stratification gathering specific molecular patterns, and that miRNA molecules govern multiple physiological pathways within a cell that can be altered in disease conditions such as cancer.

3. MATERIALS AND METHODS

3.1. MATERIALS

3.1.1. HUMAN OVARIAN CANCER SAMPLES

Salivas

The ethical committee approved saliva collection from patients of the Gynecological department at Vall Hebron University Hospital (VHUH) from Barcelona, Spain. Written informed consent was obtained for all patients. Saliva samples utilized were collected prospectively and final diagnoses were obtained by the Pathology department and following the FIGO classification (Table 10).

Group*	#	TYPE	FIGO stage	Grade	Chemo-therapy
1	1	Mucinous cistadenome of the ovary			
1	2	Fibrome of the ovary			
1	3	Fibrome of the ovary			
1	4	Mucinous cistadenome of the ovary			
1	5	Papilar mucinous cistadenome of the ovary			
1	6	Mucinous cistadenome of the ovary			
1	7	Benign ovarian fibrotecome			
1	8	Folicular cyst			
1	9	Serous para-tubal cyst			
1	10	Torsion of the ovary			
2	11	HGSC	IB	2	Yes
2	12	HGSC	IC	3	Yes
2	13	HGSC	IC	3	Yes
2	14	HGSC	IC	3	Yes
2	15	HGSC	IIa	3	Yes
2	16	HGSC	IIA	3	No
2	17	HGSC	IIA	3	Yes
2	18	HGSC	IC	3	Yes
3	19	HGSC	IIIC	3	Yes
3	20	HGSC	IIIC	3	Yes
3	21	HGSC	IIIC	3	Yes
3	22	HGSC	IIIC	3	Yes
3	23	HGSC	IIIC	3	Yes
3	24	HGSC	IIIC	3	Yes
3	25	HGSC	IIIC	3	Yes
3	26	HGSC	IIIC	3	Yes
3	27	HGSC	IIIC	3	Yes
3	28	HGSC	IIIC	3	Yes
3	29	HGSC	IIIC	3	UCI
3	30	HGSC	IIIC	3	Yes
3	31	HGSC	IV	3	Yes
3	32	HGSC	IV	3	Yes

**Group 1. Benign; 2. Early HGSC; 3. Late HGSC*

Table 10: Human salivary samples included in the study

Usually, subjects are asked to refrain from eating, drinking, smoking, or oral hygiene for at least 1 h prior to collection, exclusion criteria that were unnecessary to apply since saliva were collected in fasting before surgery, following the procedures previously reported[87]. Following collection, saliva samples were vortex for 30 sec to reduce the viscosity of the saliva (mucin-rich), and centrifuged at 2600 x *g* for 15 min at 4 °C. Saliva supernatants (cell-free saliva, CFS) were then separated from the cellular phase. To preserve the RNA from degradation, SUPERase-In RNase inhibitor was added at a ratio of 1 µL/mL of CFS. Aliquots of 1 mL CFS were then stared at −80 °C for further analysis.

Tissues

OC formalin-fixed paraffin embedded (FFPE) tissues were obtained from the repository of the Department of Pathology of VHUH under protocols approved by the institutional review board. Additionally, four Spanish collaborative hospitals proportionated FFPE tissues for the multicenter validation, including Hospital del Mar, Barcelona; Institut de Recerca Biomèdica (IRB), Lleida; MD Anderson Caner Center, Madrid; Intstitut Valencià d'Oncologia (ICO), Valencia; and Institut Català d'Oncologia (ICO) de Bellvitge, Barcelona. A total of 107 FFPE primary tumor tissues from advanced stage OC patients were collected, and used for the miRNA array analysis. Clinical data and outcome information were obtained from patients' records (Table 11).

In addition, a total of 84 fresh tissues, including 29 benign ovarian diseases (BOD) and 55 tumors, were obtained from patients from VHUH (Table 12). All patients gave their written informed consent and fresh tissues were collected under ethical committee approval from patients of the Gynecological department at VHUH. Tissues were immediately collected after surgery and stored at -80 ºC until processed and used for RTqPCR (miRNA and mRNA) analysis.

Patient	Phase	CENTER	Age	Dx (hystology)	Disease stage	CA125 at Dx	Status	SV (years)
1	Discovery	HUVH	56	Papillary serous	IIIC	567	Dead	< 1
2	Discovery	HUVH	76	Mucinous	IV	17	Dead	< 1
3	Discovery	HUVH	77	Papillary serous	IIIC	809	Dead	< 2
4	Discovery	HUVH	58	Clear cell	IIIC	-	Dead	< 1
5	Discovery	HUVH	72	Papillary serous	IIIC	1890	Dead	< 2
6	Discovery	HUVH	53	Endometrioid	IIIC	25	Dead	2
7	Discovery	HUVH	59	Endometrioid	IIIC	316	Dead	< 1
8	Discovery	HUVH	56	Papillary serous	IIIC	3417	Dead	1
9	Discovery	HUVH	53	Papillary serous	IIIC	1466	Dead	3
10	Discovery	HUVH	46	Papillary serous	IIIC	1029	Dead	> 3
11	Discovery	HUVH	52	Undiferenciated	IIIC	539	Dead	3
12	Discovery	HUVH	75	Papillary serous	IIIC	300	Dead	>3
13	Discovery	HUVH	77	Papillary serous	IIIC	145	Dead	> 1
14	Discovery	HUVH	64	Papillary serous	IIIC	1181	Dead	> 1
15	Discovery	HUVH	50	Papillary serous	IIIC	6992	VNED	> 10
16	Discovery	HUVH	50	Indiferenciado	IIIC	125	VNED	> 9
17	Discovery	HUVH	62	Papillary serous	IIIC	5000	VNED	> 13
18	Discovery	HUVH	61	Papillary serous	IIIC	100	VNED	> 13
19	Discovery	HUVH	56	Papillary serous	IIIC	-	VNED	> 12
20	Discovery	HUVH	65	Endometrioid	IIIC	270	VNED	> 12
21	Discovery	HUVH	55	Clear cell	IIIC	90	VNED	11
22	Discovery	HUVH	66	Clear cell	IIIC	731	VNED	> 10
23	Discovery	HUVH	67	Papillary serous	IIIC	498	VNED	> 11
24	Discovery	HUVH	55	Papillary serous	IIIC	998	VNED	> 11
25	Discovery	HUVH	53	Papillary serous	IIIC	2856	VNED	> 8
26	Discovery	HUVH	62	Papillary serous	-	348	VNED	8-9
27	Discovery	HUVH	45	Endometrioid	IIIC	1276	VNED	9
28	Validation	HUVH	51	Undiferenciated	IIIC	-	Dead	4.5
29	Validation	HUVH	56	Mucinous	IV	-	Dead	< 4.5
30	Validation	HUVH	54	Clear cell	IIIC	723	Dead	3
31	Validation	HUVH	73	Papillary serous	IIIC	780	Dead	3
32	Validation	HUVH	56	Papillary serous	IIIC	862	Dead	<3
33	Validation	HUVH	63	Papillary serous	IV	-	Dead	> 1
34	Validation	HUVH	62	Papillary serous	IIIC	654	Dead	> 1
35	Validation	HUVH	73	Papillary serous	IIIC	1927	Dead	< 1
36	Validation	HUVH	52	Endometrioid	IIIC	834	Dead	9
37	Validation	HUVH	49	Papillary serous	IIIC	-	Dead	> 8
38	Validation	HUVH	56	Papillary serous	IIIC	126	Dead	7,5
39	Validation	HUVH	40	Papillary serous	IIIC	834	Dead	> 7
40	Validation	HUVH	60	Undiferenciated	IIIC	1403	Dead	> 6
41	Validation	HUVH	73	Clear cell	IIIC	298	Dead	6
42	Validation	HUVH	69	Papillary serous	IV		Dead	> 5
43	Validation	HUVH	49	Papillary serous	IIIC	1028	Dead	5
44	Validation	HUVH	71	Papillary serous	IIIC	5500	Dead	5
45	Validation	HUVH	71	Mucinous	IIIC	2395	Dead	5
46	Validation	HUVH	59	Papillary serous	IV	-	Dead	5
47	Validation	HUVH	56	Endometrioid	IIIC	-	Dead	5
48	Validation	HUVH	71	Papillary serous	IIIC	2256	Dead	5
49	Validation	HUVH	65	Papillary serous	IIIC	246	VNED	> 6
50	Validation	HUVH	43	Papillary serous	IIIC	2260	VNED	> 6
51	Validation	HUVH	43	Clear cell	IIIC	-	VNED	> 6
52	Validation	HUVH	68	Papillary serous	IIIC	-	VNED	> 11
53	Validation	HUVH	63	Undiferenciated	IIIC	950	VNED	> 11
54	Validation	HUVH	-	Papillary serous	IIIC	-	VNED	10
55	Validation	HUVH	47	Clear cell	IIIC	53	VNED	> 9
56	Validation	HUVH	46	Endometrioid	IIIC	371	VNED	9
57	Validation	HUVH	70	Undiferenciated	IIIC	156	VNED	8
58	Validation	H.Mar	74	Papillary serous	IIIC	15.1	VNED	12
59	Validation	H.Mar	76	Papillary serous	IV	929	VNED	11
60	Validation	H.Mar	43	Papillary serous	IIIC	3190	VNED	6
61	Validation	H.Mar	77	Papillary serous	IIIC	449	Dead	< 3.5
62	Validation	H.Mar	63	Papillary serous	IV	1011	Dead	3.5
63	Validation	H.Mar	77	Endometrioid	IIIC	731	Dead	3
64	Validation	H.Mar	61	Papillary serous	IIIC	1148	Dead	< 2
65	Validation	H.Mar	71	Papillary serous	IV	1523	Dead	1
66	Validation	H.Mar	70	Papillary serous	IIIC	1836	Dead	< 1
67	Validation	H.Mar	53	Papillary serous	IIIC	2821	VNED	3
68	Validation	H.Mar	48	Endometrioid	IIIC	4074	VNED	1
69	Validation	IRB-Lleida	Post	Clear cell	IIIC	11	VNED	> 10
70	Validation	IRB-Lleida	Post	Papillary serous	IIIC	449	VNED	> 8

Table 11 ***(Cont.)***

Patient	Phase	CENTER	Age	Dx (hystology)	Disease stage	CA125 at Dx	Status	SV (years)
71	Validation	IRB-Lleida	Post	Papillary serous	IIIC	763	VNED	> 8
72	Validation	IRB-Lleida	Post	Papillary serous	IV	4253	Dead	3
73	Validation	IRB-Lleida	Post	Papillary serous	IIIC	881	Dead	2-3
74	Validation	IRB-Lleida	Post	Endometrioid	IV	910	Dead	> 2
75	Validation	IRB-Lleida	Post	Papillary serous	IIIC	1432	Dead	< 2
76	Validation	IRB-Lleida	Post	Papillary serous	IV	3089	Dead	< 1
77	Validation	IRB-Lleida	Post	Papillary serous	IV	1122	Dead	> 1
78	Validation	IRB-Lleida	Post	Endometrioid	IIIC	3660	Dead	< 1
79	Validation	IRB-Lleida	Post	Papillary serous	IIIC	7	VNED	5
80	Validation	MDA-Madrid	54	Papillary serous	IV	545	VNED	> 6
81	Validation	MDA-Madrid	79	Papillary serous	IIIC	-	VNED	7
82	Validation	MDA-Madrid	58	Papillary serous	IV	-	VNED	6
83	Validation	MDA-Madrid	50	Papillary serous	IIIC	353	VNED	5
84	Validation	MDA-Madrid	75	Papillary serous	IIIC	-	Dead	2
85	Validation	MDA-Madrid	61	Papillary serous	IIIA	130	VNED	2
86	Validation	IVO - Valencia	61	Papillary serous	IV	206	VNED	2
87	Validation	IVO - Valencia	52	Papillary serous	IIIB	4119	VNED	3
88	Validation	IVO - Valencia	27	Papillary serous	IIIC	844	VNED	12,5
89	Validation	IVO - Valencia	51	Papillary serous	IV	7	VNED	12
90	Validation	IVO - Valencia	62	Mucinous	IIIA	1513	Dead	2,5
91	Validation	IVO - Valencia	61	Transicional cells	IIIC	859	VNED	< 11
92	Validation	IVO - Valencia	45	Mucinous	IIIC	212	Dead	< 1
93	Validation	IVO - Valencia	34	Papillary serous	IIIA	243	VNED	7,5
94	Validation	IVO - Valencia	60	Papillary serous	IIIC	723	VNED	> 2
95	Validation	IVO - Valencia	45	Transicional cells	IV	6335	VNED	< 5
96	Validation	IVO - Valencia	76	Papillary serous	IIB	38	VNED	< 4
97	Validation	IVO - Valencia	69	Undiferenciated	IIIC	-	VNED	6,5
98	Validation	IVO - Valencia	53	Papillary serous	IIIA	339	VNED	2,5
99	Validation	IVO - Valencia	41	Papillary serous	IIIB	42	VNED	1,5
100	Validation	ICO - Bellvitge	79	Papillary serous	IIIC	334	VNED	10
101	Validation	ICO - Bellvitge	62	Clear Cell	IIIC	18	VNED	9
102	Validation	ICO - Bellvitge	77	Mixte	IIIC	713	Dead	1,5
103	Validation	ICO - Bellvitge	64	Clear Cell	IIIC	128	Dead	0,5
104	Validation	ICO - Bellvitge	67	Indifernc	IIIC	367	VNED	10
105	Validation	ICO - Bellvitge	58	Papillary serous	IIIC	402	VNED	14
106	Validation	ICO - Bellvitge	68	Endometroide	IIIC	1514	VNED	13
107	Validation	ICO - Bellvitge	51	Indifernciated	IIIC	502	VNED	10

Table 11: FFPE tissues from advanced stage OC. "Post" indicates postmenopausal women-no age available. Units of CA125 levels are by U/mL. VNED: alive – no evidence disease.

N	Group*	TYPE	N	Group*	TYPE	FIGO stage	G	N	Group*	TYPE	FIGO stage	G
1	B	Folicular cyst	30	Early	Mucinous	IIB	2	59	Late	Papillary serous	IIIC	3
2	B	Folicular cyst	31	Early	Mucinous	IC	2	60	Late	Papillary serous	IIIC	3
3	B	Folicular cyst	32	Early	Mucinous	IC	2	61	Late	Papillary serous	IIIC	3
4	B	Folicular cyst	33	Early	Papillary mucinous	Ia	2	62	Late	Papillary serous	IIIC	3
5	B	Folicular cyst	34	Early	Clear cell	IIB	3	63	Late	Papillary serous	IIIC	3
6	B	Folicular cyst	35	Early	Clear cell	IIB	3	64	Late	Papillary serous	IV	3
7	B	Simple serous cyst.	36	Early	Clear cell	IC	3	65	Late	Papillary serous	IV	3
8	B	Simple serous cyst.	37	Early	Endometrioid	IC	2	66	Late	Papillary serous	IV	3
9	B	Simple serous cyst.	38	Early	Endometrioid	IC	2	67	Late	Papillary serous	IIC-IIIA	-
10	B	Simple serous cyst.	39	Early	Endometrioid	IA	1	68	Late	Papillary serous	IIIC	3
11	B	Simple serous cyst.	40	Early	Endometrioid	IA	2	69	Late	Papillary serous	IIIA	3
12	B	Simple serous cyst.	41	Early	Endometrioid	IC	3	70	P-QT	Papillary serous	IIA	3
13	B	Simple serous cyst.	42	Early	Endometrioid	IC2	1	71	P-QT	Papillary serous	IIIC	3
14	B	Papilar serous cyst.	43	Early	Papillary serous	IA	1	72	P-QT	Papillary serous	IIIC	3
15	B	Papilar mucinous cyst.	44	Early	Papillary serous	IC	3	73	P-QT	Papillary serous	IIIC	3
16	B	Papilar mucinous cyst.	45	Early	Papillary serous	IC	3	74	P-QT	Papillary serous	IIIC	3
17	B	Simple mucinous cyst.	46	Early	Papillary serous	IC	3	75	Rec	Papillary serous	IIb	3
18	B	Simple mucinous cyst.	47	Early	Papillary serous	IC1	3	76	Rec	Papillary serous	IIC	3
19	B	Simple mucinous cyst.	48	Early	Papillary serous	IIA	3	77	Rec	Mucinous	IA	3
20	B	Simple mucinous cyst.	49	Early	Papillary serous	IIA	3	78	Rec	Not typified	IIIC	3
21	B	Simple mucinous cyst.	50	Early	Papillary serous	IC	2	79	Rec	Papillary serous	IIIC	3
22	B	Simple mucinous cyst.	51	Early	Papillary serous	IIa	3	80	Rec	Papillary serous	IIIC	3
23	B	Simple mucinous cyst.	52	Early	Papillary serous	IIA	3	81	Rec	Papillary serous	IV	3
24	B	Adnexal torsion	53	Late	Clear cell	IIIC	3	82	Rec	Papillary serous	-	-
25	B	Fibroma	54	Late	Clear cell	IIIC	3	83	Rec	Papillary serous	IIIC	3
26	B	Fibroma	55	Late	Papillary serous	IIIC	3	84	Rec	Papillary serous	IIIC	3
27	B	Fibroma	56	Late	Papillary serous	IIB	3					
28	B	Fibroma	57	Late	Papillary serous	IIIC	3					
29	B	Fibroma	58	Late	Papillary serous	IVB	3					

Table 12: Fresh-frozen tissue samples of the ovary. *B: benign ovary; Early and Late: stage of the primary tumors; P-QT: primary tumor after NACT; Rec: tumor implant of a recurrent OC; “cyst.” means cystadenoma, a type of benign cyst of the ovary; “G” means grade of the differentiation.

3.1.2. CELL CULTURES

OC cell lines

SKOV3 OC cells were acquired from American Type Culture Collection (ATCC, Manassas, VA, USA). OAW42, 59M, OAW28, OVCAR4, TOV112 and OV90 OC cell lines were acquired from European Collection of Authenticated Cell Cultures (ECACC, Salisbury, UK). A2780p and A2780cis OC cells were a generous gift from Dr. Francesc Viñals (IDIBELL, Barcelona, Spain). BIN67 OC cell lines were also a kindly gift from Dr. Barbara Vanderhyden (Ottawa Hospital Research Institute, Canada), and IGROV1 from Dr. Antonio Rosato (Istituto Oncologico Veneto, Padova, Italy). Also, IOSE-503 and IOSE-385 immortalized OSE cell lines were obtained from (Ovarian Cancer Research Team, OvCaRe (Vancouver, Canada). HEK293T were obtained form Dr. Eric Nigg (Universität Basel, Switzerland) (Table 13). All culture mediums were supplemented with 10% of heat-inactivated fetal bovine serum (FBS) except for BIN67 cells that 20% of FBS was used. All media were supplemented with 2 mM L-glutamine, 100 U/mL penicillin and 100 µg/mL streptomycin (Invitrogen, CA, USA). No penicillin/streptomycin were used to supplement cell cultures when cells were

transfected. All cultures were maintained at 37 °C in a saturated atmosphere of 95% air and 5% CO_2. Cells were regularly tested for mycoplasma contamination and were authenticated by short tandem repeat profiling High Tech Core at the high technology unit from VHIR. All cell lines were amplified and stored in liquid nitrogen.

Cell line	Histological type	Source	Culture conditions
SKOV3	EOC	Ascites	McCoy's 5A (Invitrogen?)
A2780 A2780cis* IGROV1	high-grade EC	Primary tumor Primary tumor Primary tumor	RPMI (* plus 1uM cisplatin every 2 passages)
OVCAR4 TOV112 OV90 IOSE-503 IOSE-385	HGSC high-grade EC HGSC Immortalized OSE cells Immortalized OSE cells	Primary tumor Primary tumor Ascites normal ovary normal ovary	Mix medium: mixture (1:1) of MCDB 105 and M-199 mediums (Biological Industries, Israel)
OAW42 OAW28 59M HEK293T	EOC HGSC HGSC Human Embryonic Kidney Cells	Ascites Ascites Ascites -	DMEM High Glucose
BIN67	Small cell OC, hypercalcemic type	Metastatic foci	Mixture (1:1) of DMEM and DMEM-F12 (Biological Industries)

Table 13: General characteristics of the used human cell lines.

Patient-derived ascites primary cultures

Primary cultures were established from tumoral cells in the peritoneal ascitic fluid from 4 advanced stage OC patients (Table 14) and cultured as previously described[231]. Except from patient VH-04 that presents a recurrence disease, all ascites were collected prior to chemotherapy. Immediately after surgery, the ascitic fluid containing tumor cells was mixed (1:1) in a corresponding flask with Mix medium (Biological industries) containing 15% of FBS, 2mM L-glutamine, 100 U/mL penicillin and 100 µg/mL antibiotics. After one week, culture medium was changed to remove blood and adherent cells were grown with Mix medium until 80% confluence. It is not recommended to move the flask or change the media before one week of seeding the primary ascitic cells, since it is the time that usually take the tumor spheroids/cells growing in the ascitic fluid to adhere to the surface of the culture plate and disaggregate. All primary cultures were maintained at 37 °C in a saturated atmosphere of 95% air and 5% CO_2. All primary cell cultures were amplified and stored in liquid nitrogen. Cells from 2-6 passages were used for the tumor sphere assays.

#	TYPE	FIGO stage	Grade
VH-01	Papillary serous	IVa	3
VH-02	Papillary serous	IIIC	3
VH-03	Papillary serous	IIIC	3
VH-04	Clear cell	Rec*	3

*Ascites from a recurrent OC

Table 14: Patient-derived primary cultures of ascites from advanced stage OC.

3.1.3. ANTIBODIES

The antibodies and conditions used are listed in table 15.

Antibody	Catalog Number	Source	Application	Conditions
PARP1	#9542	Cell Signalling	WB	1:3000 dilution, 5% BSA
Caspase-3	#9665	Cell Signalling	WB	1:1000 dilution, 5% BSA
Cyclina B	#05-373	Merk Millipore	WB	1:1000 dilution, 5% nonfat milk
p27 Kip1 (D69C12)	#3686	Cell Signalling	WB	1:1000 dilution, 5% nonfat milk
Cyclin D1	#2978	Cell Signalling	WB	1:1000 dilution, 5% nonfat milk
p21 Waf1/Cip1 (12D1)	#2947	Cell Signalling	WB	1:1000 dilution, 5% nonfat milk
HAX1	610825	BD Transduction	WB	1:500 dilution, 5% nonfat milk
RAB1B	ab116336	Abcam	WB	1:1000 dilution, 5% nonfat milk
CDCP1	#4115	Cell Signalling	WB	1:1000 dilution, 5% nonfat milk
PBX3	ab109173	Abcam	WB	1:1000 dilution, 5% nonfat milk
PLAGL2	ab139509	Abcam	WB	1:1000 dilution, 5% nonfat milk
p-Rb (S795)	#8516P	Cell Signalling	WB	1:1000 dilution, 5% BSA
Rb	C15, sc-50	Santa Cruz	WB	1:1000 dilution, 5% BSA
p-AKT (S473)	#9271	Cell Signalling	WB	1:1000 dilution, 5% BSA
CDK2	#2546	Cell Signalling	WB	1:1000 dilution, 5% BSA
CDK4	#12790	Cell Signalling	WB	1:1000 dilution, 5% BSA
MYC	-	hybridome E910	WB	1:10 dilution, 5% nonfat milk
α-Tubulin	T9026	Sigma Aldrich	WB	1:5000 dilution, 5% nonfat milk
anti-Rabbit IgG	A0545	Sigma Aldrich	WB	1:5000 dilution, 5% nonfat milk
anti-Mouse IgG	A9044	Sigma Aldrich	WB	1:5000 dilution, 5% nonfat milk; 1:10000 for α-Tubulin
Ki67	790-4286	Roche	IHQ	-

Table 15: List of antibodies used for Western Blot and Immunohistochemistry.

3.1.4. PRIMERS AND PROBES

The primers used for gene detection by Sybr-Green RTqPCR technology were designed using Universal Probe Library (Diagnostics, Roche) and purchased from Invitrogen (Thermo Fisher Scientific) (Table 16). For miRNA expression levels detection by RTqPCR, TaqMan® assays were purchased from Thermo Fisher Scientific (Table 17). The hsa-miR-572 was used as endogenous control.

#	Gene name	NM_number (GeneCards)	Catalog #	Amplicon lenght	Primer position	Primer sequence (5'- 3')	Quality / Intron spanning / In silico PCR
1	AKT3	NM_005465	04686969001	75nt	Left primer Right primer	ttgctttcagggctcttgat cataatttcttttgcatcatctgg	Good / Yes / Yes
2	PBX3	NM_006195	04688627001	88nt	Left primer Right primer	agcgtcctgtgtgagatcaa gtctcattagctggggatcg	Good / Yes / Yes
3	PLAGL2	NM_002657	04687574001	93nt	Left primer Right primer	ttttgcttccaaatacaagctg cggtgaaacatcttatcacagtaca	Good / Yes / Yes
4	CDCP1	NM_022842	04685091001	79nt	Left primer Right primer	cttaccccaaggactgtgga cgagggcagacagcagtaa	Good / Yes / Yes
5	SMARCE1	NM_003079	04689054001	78nt	Left primer Right primer	cgacgagaacattccgatg ccttcttcaccattctgttgg	Good / Yes / Yes
6	KIF21B	NM_017596	04685075001	105nt	Left primer Right primer	caagtgcattcggactctca atctgatgctcgccctga	Good / Yes / Yes
7	MEF2D	NM_005920	04688066001	91nt	Left primer Right primer	aacgccgacatcatcgag ggctctgttccagcgagt	Good / Yes / Yes
8	BCL7A	NM_020993	04685059001	95nt	Left primer Right primer	gggccaaagatgatatcaagag tcgtagggatgtgtcaccaa	Good / Yes / Yes
9	GATA4	NM_002052	04688554001	103nt	Left primer Right primer	gtcatctcactacgggcaca cttcagggccgagaggac	Good / Yes / Yes
10	HAX1	NM_006118	04686926001	90nt	Left primer Right primer	acagtaacccgacacgaagc caggatggaaaaggcatcat	Good / Yes / Yes
11	STK38	NM_007271	04688643001	93nt	Left primer Right primer	tgatgaactggaaagaaactttga cccattcacagcagaacctc	Good / Yes / Yes
12	PHF8	NM_015107	04685008001	78nt	Left primer Right primer	gggtagcctctattgagacaggt tcttttgggccttctgtagc	Good / Yes / Yes
13	RAB1B	NM_030981	04688996001	95nt	Left primer Right primer	accaagaaggtggtggacaa acattggtggcattcttgg	Good / Yes / Yes
14	KIAA0141/DE	NM_014773	04688503001	87nt	Left primer Right primer	tacaatgcgggcttgtgtc gctggcagccaactgataa	Good / Yes / Yes
15	MAGEA3	NM_005362.3	04689097001	100nt	Left primer Right primer	gtgaggaggcaaggttctga gggcaatggagacccact	Good / Yes / Yes
16	GBGT1	NM_021996.5	04685059001	94nt	Left primer Right primer	tatctcccctgcccagagat tgggctgagggtactgtga	Good / Yes / Yes
17	MEG3	NR_002766.2	04688007001	80nt	Left primer Right primer	gtggaagcacgctcacaa tcttccgcagcttccatc	Good / Yes / Yes
18	GAPDH	NM_002046	04689003001	115nt	Left primer Right primer	caacgaccactttgtcaagc ggtggtccaggggtcttact	Good / Yes / Yes

Table 16: Primer sequences for genes detected by Sybr-Green RTqPCR technology.

#	TaqMan Assay ID	miRBase ID	miRBase Accession Number	Mature miRNA Sequence	Chromosome location (on Build GRCh38)
1	001611	hsa-miR-654-5p	MI0003676	UGGUGGGCCGCAGAACAUGUGC	Chr.14: 101040219 - 101040299 [+]
2	001522	hsa-miR-554	MI0003559	GCUAGUCCUGACUCAGCCAGU	Chr.1: 151545796 - 151545891 [+]
3	002332	hsa-miR-409-3p	MI0001735	GAAUGUUGCUCGGUGAACCCCU	Chr.14: 101065300 - 101065378 [+]
4	000452	hsa-miR-127-3p	MI0000472	UCGGAUCCGUCUGAGCUUGGCU	Chr.14: 100882979 - 100883075 [+]
5	001614	hsa-miR-572	MI0003579	GUCCGCUCGGCGGUGGCCCA	Chr.4: 11368827 - 11368921 [+]

Table 17: TaqMan® assays purchased for miRNA expression levels detection by RTqPCR.

3.1.5. OLIGONUCLEOTIDES

The following oligonucleotides in Table 18 and Table 19 were used to genetically modulate miRNA and gene expression, respectively.

#	Item	miRNA Mimics Catalog #	miRNA Hairpin Inhibitors (AntagomiRs) Catalog #	Sequence (Accession)
1	miRIDIAN microRNA Negative Control #1	CN-001000-01	IN-001005-01	Based on cel-miR-67, mature sequence: UCACAACCUCCUAGAAAGAGUAGA (MIMAT0000039)*
2	miRIDIAN microRNA Negative Control#2	CN-002000-01	IN-002005-01	Based on cel-miR-239b, mature sequence: UUGUACUACACAAAAGUACUG (MIMAT0000295)*
3	miRIDIAN microRNA Human hsa-miR-654-5p	C-300988-01	IH-300988-03	UGGUGGGCCGCAGAACAUGUGC (MIMAT0003330)
4	miRIDIAN microRNA Human hsa-miR-554	C-300871-01	IH-300871-03	GCUAGUCCUGACUCAGCCAGU (MIMAT0003217)
5	miRIDIAN microRNA Human hsa-miR-409-3p	C-300738-05	IH-300738-06	GAAUGUUGCUCGGUGAACCCCU (MIMAT0001639)
6	miRIDIAN microRNA Human hsa-miR-127-3p	C-300627-03	IH-300627-05	UCGGAUCCGUCUGAGCUUGGCU (MIMAT0000446)
7	miRIDIAN microRNA Transfection Control	CP-004500-01	-	Dy547-labeled microRNA mimic based on the C. elegans miRNA cel-miR-67

** They have been confirmed to have minimal sequence identity with miRNAs in human, mouse, and rat*

Table 18: MiRIDIAN miRNA mimics and antagomirs, purchased from Dharmacon.

siRNA	Gene name	Target sequence (5′-3′)	Reference	Source
1	CDCP1_1	GTCCTGAGAATCACTTTGT	Orchard-Webb DJ *et al.,* BMC Cancer, 2014	Sigma Custom
2	CDCP1_2	TAATGTTGCTTTCTCGTGGCAGAGC	Uekita T *et al*. Cancer Science, 2013	Sigma Custom
3	PLAGL2_1	GCTCTGTTATGGAGCCTTA	Sekiya R *et al*. Carcinogenesis, 2014	Sigma Custom
4	PLAGL2_2	GCTCTTGATTAGAAGCAAT	Sekiya R *et al*. Carcinogenesis, 2014	Sigma Custom
5	HAX1	ACAGACACTTCGGGACTCAAT	Cavnar PJ *et al*. J Cell Biol, 2011	Sigma Custom
6	RAB1B	GCCAGCGAGAACGTCAAT	Halberg N *et al.* Cancer Cell, 2016	Sigma Custom
7	PBX3	CAAAGTGGAGGTGGATAGT	-	Sigma Pre-designed
8	Lamin A*	GGACCTGGAGGTCTGCTGT	-	Dharmacon

*Custom-scramble siRNA (siLamin A) used as a siRNA control

Table 19: Control siRNA and siRNAs for the putative miR-654 target genes.

3.2. METHODS

3.2.1. HIGH-THOUGHPUT DATA

3.2.1.1. Small RNA sequencing analysis of saliva

Thirty-two salivas were subjected to RNA sequencing by using the CFS fraction (Table 10). Salivary RNA extraction, library preparation and sequencing processes were performed at UCLA, in collaboration with Dr. David T. Wong's lab. All procedures performed were firstly set up and recently published[87]. Samples were randomized per groups of study in 4 batches for RNA extraction, and the ordering of the sample group was also different between batches. RNA extraction was done by a combined method of organic extraction (QIAZOL/chloroform) and spin filter clean up (miReasy micro Kit, QIAGEN), followed by in-solution DNase treatment (in the eluted RNA), and a

glycogen-and-ethanol precipitation step to purify and concentrate the RNA. After the RNA extraction of each batch of samples, quality controls (QCs) and first-day library preparation were performed with the fresh RNA. On one hand, the extracted RNA was quantified by Ribogreen assay (Thermo Fisher Scientific) adapted to a low-range concentration standard in a dark microplate as described[87]. On the other hand, quality and size of the RNA was measured by RNA Pico Chip Bioanalyzer (Agilent Technologies). Several thresholds based on the QCs were applied to all samples before RNA sequencing. Thus, all the samples included yielded higher than 5 ng of total RNA measured by Ribogreen, and no intact ribosomal RNA peaks should appear indicating of residual cell contamination (eukaryotic: 18S (1869 nt), 28S rRNA (5070 nt); prokaryotic: 16S (1542 nt), 23S rRNA (2906 nt)) in the Bioanalyzer profile. cDNA libraries were generated from the salivary RNA extracted by using *NEBNext Small RNA library Prep Set for Illumina* (NEB# E7330L) as reported[87]. The cDNA libraries were pooled by 8 samples/pool following the instructions of the Sequencing Core at UCLA, CA, USA. Briefly, all samples were brought to 10 nM concentration with EB Buffer (QIAGEN) 0.1% Tween-20, and 2.5 µL of each 10 nM sample was pooled into a new tube (8 samples/pool) in a final volume of 20 µL, thus contributing to 2.5 nM each library. Pools generation aims to sequence several samples at the same time (that is, in the same lane), and in this case 4 lanes were sequenced in total (4 lanes x 8/samples = 32 libraries). In the case of small ncRNAs, sample pooling can be until 8 samples, thanks to the specific DNA sequences (barcodes 1-8) that are ligated during library generation[87]. The platform used was HiSeq Illumina® system, and stranded and Single-End 50 bp (SE50) was used for the procedure (5 days long). The 23 GB of data was subjected to bioinformatic and statistical analysis by miARma-seq tool[232] (see section 3.2.4.1).

3.2.1.2. Human miRNA microarray analysis

For miRNA expression profiling, TaqMan® Array Human MicroRNA A+B Cards Set v3.0 (Applied Biosystems, CA, USA) were used, which are based on TaqMan® RTqPCR technology and allow the analysis of a total of 768 miRNA sequences by ΔΔCT method. RNA from 30 FFPE tumor samples (Table 11) was used for the "discovery phase". Briefly, 300 ng of total RNA was used for the reverse transcription (RT) of the 768 miRNAs, by using the TaqMan MicroRNA RT Kit (Applied Biosystems, Foster City, USA), and the commercial pool of Megaplex™ RT Primers, Human Pool

Set v3.0 (Applied Biosystems, CA, USA). Then, 2.5 µL of cDNA was targeted preamplified in a 25 µL reaction volume with the Megaplex™ PreAmp Primers, Human Pool Set v3.0 (Applied Biosystems, CA, USA) and TaqMan® PreAmp Master Mix 2X (Applied Biosystems, CA, USA), to enhance the yield of the 768 miRNAs of analysis. Each sample was reverse transcribed and preamplified for pool A and B primers separately in a Thermal Cycler, and following the manufacture instructions. RTqPCR was performed in a 7900 ABIPrism System, with special adaptor for microfluidic cards. Two miRNA array cards were done per patient, with a total of 60 RTqPCR reactions (n=60; 30 pool A, 30 pool B).

For the miRNA "validation phase", Custom TaqMan® Array MicroRNA Cards were used. The same steps were done as in the discovery phase but custom RT and Preamp primer pools were used for the 32 differentially expressed miRNAs selected for validation (see section 4.2.1). Total RNA from 80 FFPE tumor samples collected from 6 different Spanish Hospitals was used for this purpose (Table 11). All RT, PreAmp and RTqPCR reactions were done following the manufacture instructions for Custom TaqMan® Array MicroRNA Cards. Eight patients per RTqPCR reaction were included in each card, with a total of 10 custom array cards (n=80).

3.2.1.3. Human mRNA microarray analysis

Triplicates of the SKOV3 siControl (siLamin A), SKOV3-siCDCP1 and SKOV3-siPLAGL2 were used to carry out the microarray analysis. RNA concentration and quality of extracted RNA were measured by Nanodrop and RNA Nano Chip Bioanalyzer (Agilent Technologies), respectively. The efficiency of CDCP1 and PLAGL2 depletion was measured by RTqPCR. Human Clariom^{TM} S assay (Affymetrix, Thermo Fisher Scientific) was used to analyze gene-level whole-transcriptome expression profiling, which accurately detects > 20,000 well-annotated genes, with > 200,000 probes. The High Technology Unit (UAT) at VHIR performed all the steps after RNA extraction, including the first and second strand cDNA production, biotinylation, hybridization, labeling and scanning of the chips, following the manufactures instructions. Raw data was obtained and used for the differential expression analysis by Expression Console and Transcription Analysis Console (TAC) softwares, publicly available (see section 3.2.4).

3.2.1.4. DNA methylation microarray analysis

All data analyzed come from DNA methylation microarrays (Illumina Infinium HumanMethylation450 BeadChip arrays) and analyses were performed in collaboration with Dr. Manel Esteller and Dr. Sebastian Moran (IDIBELL, Bellvitge, Barcelona, Spain). Data was obtained as previously described[233]. Briefly, the software from Illumina (GenomeStudio 2010.3, Methylation Module 1.8.5) was used to calculate the methylation beta values of the 485577 CpG islands interrogated in the microarray. By using the manufacture annotations, CpG islands were selected according to the miR-654 chromosomal location. For OC primary tumors (n = 35), raw methylation data was downloaded from TCGA portal[15] and GSE81224 dataset[31], and also was obtained from PEBC dataset from Dr. Esteller's lab (unpublished). For OC cell lines (n = 43), the methylation data was downloaded from the GSE68379 dataset recently published[234]. A total of 13 CpG islands associated to the target region (that is the human Chr.14 where miR-654 is located) were evaluated for a total of 35 and 43 OC tissues and cell lines, respectively.

3.2.2. *IN VITRO* EXPERIMENTS

3.2.2.1. Transient transfections

MiRIDIAN miRNA Mimic and Hairpin Inhibitors (antagomirs) were purchased from Dharmacon (Table 18) and utilized to modulate miRNA levels in several OC cell lines. Cells were transfected with Lipofectamine 2000 ® (Invitrogen) at 25 nM concentration of control and miRNA mimics and antagomirs with OPTIMEM and corresponding cell culture medium for each cell line. For p96-well plates, 0.2 µL of lipofectamine per well was used in a total volume of 150 µL (100 µL of cells plus 50 of transfection reaction) for all cell lines used. For p24-well plates, 3 µL of lipofectamine was used in a total of 500-µL volumes for all cell lines used. In p60 plates, 6 µL and 9 µL of lipofectamine was used for SKOV3 and A2780p cells, respectively, in a total volume of 2 mL (1.5 mL of cells and 500 µL of transfection reaction). In p100 plates, 15 µL and 20 µL of lipofectamine was used for SKOV3 and A2780p cells, respectively, in a total volume of 8 mL (6 mL of cells and 2 mL of transfection reaction). Cells were plated and transfected at the same time (reverse transfection) and culture medium was changed after overnight incubation. Transfection efficiency was monitored using the fluorescent

miRNA Transfection Control labeled with Dy547 with the same conditions. The same protocol was followed for siRNA transient transfection but the final concentration of the antisense oligonucleotides was 50nM. The siRNAs for HAX1, RAB1B, CDCP1, PBX3, PLAGL2 were purchased from Sigma-Aldrich (Table 19). The efficiency of the siRNA-silencing was evaluated by Western Blot.

3.2.2.2. Constructs generation

3'UTR constructs: custom DNA fragments containing the miR-654-5p binding sites within each 3′UTR region of HAX1, CDCP1, PBX3, PLAGL2 genes were purchased (GeneArt™ String™ fragments, ThermoFisher Scientific) and ligated into the pCR™II-Blunt-TOPO® vector (Zero Blunt® PCR Cloning Kit, Invitrogen). 3′UTR fragments of the putative target RAB1B were directly purchased cloned into a pMA-T vector backbone (Invitrogen) (Table 20). Afterwards, psiCHECK^{TM}-2-HAX1, CDCP1, PBX3, PLAGL2 and RAB1B 3'UTR vectors were generated by cloning the specified fragments into the psiCHECK^{TM}-2 vector by XhoI and NotI restriction sites. For CDCP1 and PLAGL2 putative target genes two constructs for each 3'UTR were generated due to the length of their 3'UTR region. PsiCHECK^{TM}-2 vector was kindly provided by Miguel F. Segura (VHIR, Spain).

TARGET		miR-654 binding site			
Name	**Gene ID**	**Position**	**Sequence**	**3'UTR fragment length**	**Vector**
HAX1	NM_006118	50-57	CACCTCTCACCCATT**GCCCACCA**	187bp	psiCHECK™-2_HAX1
RAB1B	NM_030981	517-523 708-714 751-757 858-865	CACAGGGGCCCAGCA**GCCCACC**C ACCCATGCGCTGCCT**GCCCACC**G AGGCGGAGGCGGAAG**GCCCACC**G CACTCCGTCTCTGGA**GCCCACCA**	574bp	psiCHECK™-2_RAB1B
PBX3	NM_006195	83-90 821-827	GAAAGCGTTTTTGTA**GCCCACCA** AGAGTATTTATACAT**CCCACCA**A	924bp	psiCHECK™-2_PBX3
CDCP1	NM_022842	1171-1178	TCTTTGACTTACAAA**GCCCACCA**	504bp	psiCHECK™-2_CDCP1_A
		2972-2978	CTGGAACAAGCACAA**GCCCACC**G	504bp	psiCHECK™-2_CDCP1_B
PLAGL2	NM_002657	390-396 515-521	GAAATTGCCCAAGAA**GCCCACC**T AGGCCTTTATTTCTC**GCCCACC**C	510bp	psiCHECK™-2_PLAGL2_A
		3059-3065	AACCCCCGCCCTCCA**GCCCACC**G	434bp	psiCHECK™-2_PLAGL2_B

Table 20: 3'UTR binding sites cloned for the 5 putative target genes

pGIPZ / pGIPZ-miR-654 construct: custom DNA fragments containing pre-miR-654 flanked with cel-miR-31 sequences was designed (140bp) and directly purchased into a pMA-T vector backbone (GeneArt™ String™ fragments, ThermoFisher Scientific). Then, pGIPZ-pre-miR-654 vector was generated by cloning the fragment into the

pGIPZ vector by XhoI and HpaI restriction sites. The pGIPZ vector was kindly provided by Miguel F. Segura (VHIR, Spain).

3.2.2.3. Lentivirus production and transduction

Lentivirus were propagated using previously described methods[235]. Briefly, HEK293T cells were transfected with 3 plasmids (pMD2.G and psPAX2 from Addgene, and the pGIPZ-Control or the pGIPZ-pre-miR-654), the first two corresponding to the viral envelope packaging system. After 6 h, media was replaced by DMEM and after 36h green fluorescent protein (GFP) signal was observed under the microscope and viral supernatant was collected and used to transduce SKOV3 cells. Reverse transduction was performed (i.e. at the same day of seeding 900.000 SKOV3 cells in p60 plate), and after 24h incubation, the media of the infected cells was replaced with growth medium. pGIPZ-Control or pGIPZ-miR-654 stably-transduced SKOV3 cells were selected with 3 µg/mL puromycin (Sigma-Aldrich) prior to use in experiments.

3.2.2.4. Protein extraction and Western Blot

Pelleted cells, either from OC cell lines and from ascites primary cultured spheres (see section 3.2.2.12.), were harvested in homemade 1X RIPA buffer (Tris HCl 1.5M pH=8.8, NaCl 5M, Triton X-100, EDTA 500mM) supplemented with 1:100 complete protease inhibitor cocktail (Sigma Aldrich), and phosphatase inhibitor cocktail (P5726, P0044 Sigma Aldrich) was used when indicated in the particular experiment. Lysis was performed on ice for 1 h incubation with a 30 sec vortex every 15 min. Cell lysates were obtained after centrifugation at 14000 x g for 15 min at 4 ºC. Among 20-80 ug of protein were resolved on homemade 8-15% tris-glycine polyacrylamide electrophoresis gels or Bis-Tris 10% MOPS or MES running buffer with pre-cast electrophoresis gels (Invitrogen, Thermo Fisher Scientific), and transferred onto PVDF membranes. Membranes were blocked for 1 h with 5% non-fat milk (Panreac), 5% bovine serum albumin (BSA) (Sigma Aldrich) and probed with the indicated antibodies overnight at 4 ºC (Table 15). Membranes were incubated with horseradish peroxidase-conjugated secondary antibodies for 1h before developing with Chemiluminescent horseradish peroxidase substrate Immobilon Western (Millipore) or ECL (GE Healthcare).

3.2.2.5. Immunohistochemistry

Immunohistochemistry was performed in a BenchMark Ultra (Ventana Medical Systems, Tucson, AZ, USA) following the recommended protocol, in collaboration with the Pathology Department from VHUH. Antigen retrieval was performed with CC1 buffer for 20 minutes. The primary antibody used was the monoclonal rabbit antibody 30-9 (Ventana Medical Systems, Inc) and the incubation time was of 32 minutes. Detection system was Ultraview DAB, used following the recommended protocol. Percentage tumoral cells and Ki67 positive cells was evaluated by an attending pathologist, taking into account the number of tumor cells in 3 high power fields, detected morphologically, and counting the number of nuclear stained cells with Ki67 immunohistochemistry.

3.2.2.6. RNA extractions and RTqPCR

***FFPE tissues**:* total RNA (including miRNAs) was extracted using FFPE miRNeasy Mini Kit (Qiagen, Hilden, Germany) following the manufacture instructions. Firstly, all hematoxylin and eosin staining were examined for each ovarian tumor and the section including 80% of tumoral area was chosen for the corresponding paraffin tissue. Then, 4 sections of 10 μm per tumor were used for RNA extraction. For each tumor, the sections were placed in a p60-well plate and the extremes were cut with a scalpel to remove the excess of the paraffin. Deparaffinization was done by adding 1 mL of xylene and vigorously vortex to the 4 sections in a new eppendorf plus a centrifugation at 15000 x g (two times). Protein Kinase and DNase treatments were done as suggested by the manufacture instructions, as well as the rest of the steps with the spin column included in the kit.

***Fresh-frozen tissues**:* total RNA (including miRNAs) was extracted using miRNeasy Mini Kit (Qiagen, Hilden, Germany) following the manufacture instructions. Firstly, 2 to 3 mm^3 of tissue was cut in smaller pieces in dried ice and homogenized using FastPrep-24 Lysing Matrix tubes (MP Biomedicals) with 700 μL of QIAzol Lysis Reagent (Qiagen), with the FastPrep®-24 Classic Instrument (116004500 MP Biomedicals) 30 sec at 6.5 r/p for 3 times. Then, homogenates were centrifuged for 5 min at 12000 rpm and 4ºC to get rid of the cell and tissue debris. Supernatant was then transferred to a 1.5 mL eppendorf and 140 μL of chloroform was added to continue with the standard protocol of the kit.

***Cell lines**:* for SKOV3, A2780p and OAW28 cell lines total RNA (including miRNAs) was extracted using miRNeasy Mini Kit (Qiagen, Hilden, Germany). Cell cultures were scrapped, washed once with 1X phosphate-buffered saline (PBS), and cell lysates were obtained by adding 700 µL of QIAZOL to the pelleted cells. Total RNA was then extracted following the manufacture instructions. All RNAs from FFPE tumors, fresh tissues, and cell lysates were subjected to DNase treatment, and RNA was eluted in 30 µl RNase-free water (pre-heated at 50 ºC for 5 min). Then, RNA concentration was measured by Nanodrop and the samples with a ratio A260:A280 between 1.8 and 2.0 were accepted for subsequent analyses.

RTqPCR of miRNAs: for verification analysis in FFPE tissues, miRNA TaqMan probes were used for the analysis (Table 17). RNA samples were brought to 12.5 ng/µL and 2 µL of RNA was used for RT using TaqMan MicroRNA RT Kit (Applied Biosystems, Foster City, USA). The cDNA was obtained for each individual miRNA by using the RT primers included with the TaqMan probes purchased. Verification of the 4 validated miRNAs was done in 40 FFPE samples (including some samples from the discovery and the validation phases). Levels of miR-654-5p were measured in 84 fresh ovarian tissues by the same TaqMan probe (001611) including 29 benign and 55 ovarian cancer tissues, following the same procedures explained below.

RTqPCR of mRNAs: for mRNA target analysis, 1 µg of total RNA from SKOV3 and A2780 cells was used for RT using SuperScript III enzyme (Invitrogen). Primer sequences (Table 16) and Power SybrGreen Master MIX (Cat# 4367659) was used for the RTqPCR reactions to detect mRNA levels using the corresponding designed primers at a 0.1 uM-final reaction concentration. Same protocol was used to evaluate the levels of the putative direct miR-654-5p target genes in 84 fresh ovarian tissues, as well as to evaluate the levels of the selected genes as contorls for the DNA demethylating experiments.

3.2.2.7. Proliferation assay

Proliferation assays were performed with OC cell lines as previously reported[236]. Liposomal transfection complexes without miRNA (MOCK), with miRIDIAN microRNA mimics or antagomirs and Negative Controls (Dharmacon, GE Healthcare) were generated with Lipofectamine® 2000 (Life technologies, Thermo Fisher Scientific, 0.2 µL per well) in 96-well plates (6 replicates/condition) following the manufacturer's

recommendations. Cells were seeded at specific densities (SKOV3: 3 × 10^3 cells/well; A2780p: 10 × 10^3 cells/well; OAW42: 3 × 10^3 cells/well; OVCAR4: 3.5 × 10^3 cells/well) into wells containing liposomal complexes followed by overnight incubation in a humidified incubator at 37°C and 5% CO_2. Then, media were changed and at the indicated time points media was removed by sharp blow of the plate, and cells were fixed with 4% formaldehyde (VWR Chemicals) for 20 min. Wells then were washed with 1X PBS and stored at 4°C (for the time-course experiments). After washing, cells were stained with 0.5% crystal violet (Sigma Aldrich) for 20 min followed by extensive washing with H_2O. Crystals were dissolved with 15% acetic acid (Sigma Aldrich) and optical density was measured at 590 nm using a microplate spectrophotometer.

For the evaluation of the siRNA effect in SKOV3 cells, viability assays were performed in p96-well plates as explained below but at 50 nM final concentration of each siRNA.

3.2.2.8. Cell death assay

Cell death assays were done as previously reported[236] with minor modifications. SKOV3, A2780p, OAW42 and OVCAR4 cells were seeded at 15 × 10^3, 10 × 10^4, 15 × 10^3 and 15 × 10^3 cells/24-well plates, respectively. Cells were reverse transfected using Lipofectamine® 2000 with MOCK, miRIDIAN microRNA Mimic Negative Control and miRIDIAN microRNA Mimic miR-654 (25 nM) in triplicate and 12-16 h later media was changed. 96 h post-transfection, cell were stained with 0.05 mg/ml Hoechst 33258 and 2.5 µM Propidium iodide (PI) staining. Cells that uniformly stained chromatin were scored as healthy whereas those with fragmented and/or condensed chromatin accompanied with positive PI staining were scored as apoptotic. For the evaluation of the siRNA effect in SKOV3 cells, apoptosis assays were performed in p24-well plates as explained below but at 50 nM final concentration of each siRNA. Quantification of apoptotic cells was made from 4 representative images/well (n=3 replicates per condition).

3.2.2.9. Cell cycle assay

SKOV3 and A2780p cells were reverse transfected in p100 plates at a cell density of 9 x 10^5 and 3 x 10^6 cells, respectively, with the miR-654 mimic and negative control following the abovementioned conditions. Cells were incubated in a time course schedule for 24, 72 and 96 h. For each time-point, two replicates were obtained. The medium in the cell culture was collected to include the floating cells and these were

harvested together with the adherent cells. Pelleted cells were washed twice with 1X PBS and fixed with 70% ice-cold ethanol overnight at a concentration of 1 x 10^6 cells/mL. Samples were stained by a treatment solution with sodium citrate (38 mM), Propidium iodide (500 ug/mL) and RNase A (10 mg/mL) at 4°C overnight. A total of 10000 cells per sample were counted by flow cytometry (FACS Calibur; Becton–Dickinson, San Jose, CA, USA) and cell cycle phase distribution was analyzed with the FACS software (Becton–Dickinson).

3.2.2.10. DNA demethylating assay

OAW28 and A2780 cells were seeded in p6 plates at a cell density of 4.5 x 10^5 and 1 x 10^6, respectively, and treated with 5'AZA-2'-desoxycytidine (A3656, Sigma Aldrich) demethylating agent for 24 and 48 hours, and with DMSO as a control. At the specific time points after treatment cells were collected and subjected for RNA extraction, and the levels of miR-654 were evaluated. As a control for demethylation, MEG3, GBGT1 and MAGE-A3 expression levels were evaluated by RTqPCR.

3.2.2.11. 3'UTR luciferase reporter assay

3'UTR luciferase reporter assays were performed as previously described[236]. HEK293T cells were seeded in 96-well plates at 20,000 cells/well in 100 µL/well of complete media without antibiotic. Cells were co-transfected 16‑24 h later using Lipofectamine® 2000 with 50 ng of psiCHECK2-3'UTR vector for each putative target gene cloned and 25 nM of miR-654 mimic or negative control. Liposomal complexes containing 3'UTR and liposomal mimic miRNAs were prepared separately in 50µL volume and then added consecutively to 96-well seeded HEK293T cells. Cells were incubated at 37 °C and 5% CO_2 for 20–24 h. Luciferase assay was performed using the Dual-Glo® Luciferase Assay System (Promega) following the manufacturer's recommendations. Luminescence was measured in an Appliskan (Thermo Fisher Scientific) microplate reader. Renilla luciferase activity was normalized to corresponding firefly luciferase activity and plotted as a percentage of the control.

3.2.2.12. Spheroid formation assays

Five patient-derived ascitic cells from advanced stage OC were grown in anchorage independent conditions for tumor sphere formation assays as previously reported[237] with some minor modifications. Firstly, cells were reverse transfected using

Lipofectamine 2000 with miRIDIAN microRNA Mimic Negative Control and miRIDIAN microRNA Mimic miR-654 (25 nM) and seeded in a cell density of 15 × 10^3 in non-adherent 24-well plates (coated with 0.5% agar with non-supplemented medium) in serum-free medium (mix medium 1:1, MCDB105: M199, Biological Industries) supplemented with B27 1X (Invitrogen), 2mM L-glutamine (Invitrogen), 20 ng/mL EGF (ProSpec-Tany Technogene Ltd) and 20 ng/mL FGF2 (ProSpec-Tany Technogene Ltd). Ninety-six hours later, the **number of spheres was scored** (spheres between 50-100 μm, ≥100 μm, and ≥200 μm if applicable, in diameter) and counted.

The variation between the number of spheres treated with miR-Control versus the number of spheres treated with miR-654 was represented, scored with the applicable diameters depending on each patient. The variation between the numbers of spheres treated with the miR-Control versus the number of spheres treated with miR-654 was represented, scored with the applicable diameters depending on each patient.

For **tumor spheres protein extraction**, 4 x 10^5 cells were seeded in p6 well plate coated with 1 mL of 0.5% agarose-medium, and 1 mL of cells and 500 μL of transfection mixture was added (25 nM final concentration for each miRNA). Spheres were collected at 96 h post-transfection and proceeded for protein lysate and WB as explained in the section 3.2.2.4.

For **viability assay of the tumor spheres**, MTS assay was performed using spheres at 96h post-transfection with miR-Control and miR-654. Tumor spheres were collected, pelleted and washed once, and disaggregated with 0.5 mL of 1X StemPro® Accutase® Cell Dissociation Reagent (Gibco™, Thermo Fisher Scientific) prior to the MTS assay. PMS and MTS reagents were mixed at a ratio of 1:20, and mixture was added to each well containing 100 μL of disaggregated cells (in culture medium) at a ratio of 1:10. MTS was measured between 2-5 h of incubation at 490 nm, depending on each patient.

3.2.3. *IN VIVO* EXPERIMENTS

For animal studies, no randomization or blinding was applied. All procedures were approved by the ethical committee of Vall d'Hebron Research Institute (protocol number 85/12). SKOV3 cells were reverse transiently transfected with miRIDIAN microRNA Mimic Negative Control and miRIDIAN miR-654 Mimic and after 24h cells were injected (2 x 10^6/mouse) in the flank of 8-week-old female NMRI-nude mice (Janvier, n = 12/group) in 300 µL of 1X PBS and Matrigel (1:1). The levels of miR-654 overexpression were measured in SKOV3 cells before mice injection. In addition two mice per group were sacrificed at day 5 and miR-654 levels were measured as well. Hematoxylin and eosin and Ki67 staining was done in these tumors to evaluate the engraftment capability and the percentage of tumoral cells in both groups. Tumor volume was measured every 2–3 days for 25 days using an electronic caliper. At the respective scheduled surgery, mice were killed and tumors removed and weighed. Each tumor was then longitudinally split in two and one half of each tumor was fixed in 10% formalin, paraffin-embedded, and 5 µm sections were performed for hematoxylin and eosin and Ki67 staining. The other half was used for RNA extraction to measure miR-654 expression levels, as described for fresh-frozen tissues, explained in section 3.2.2.6.

Due to the transient transfection method used for mouse xenografts, two *in vivo* pilot studies were performed in order to examine the window of tumor appearance and the exponential growth. First, SKOV3 cells were injected in the flank of the mice at 5 x 10^5 (n = 3), 1 x 10^6 (n = 3) and 5 x 10^6 (n = 4) cellular densities in 300 µL of 1X PBS and Matrigel (1:1). At day 43, all mice were sacrificed and 5 x 10^6 generated tumors were explanted and primary cultured. SKOV3-Explanted (SKE) cells were then injected at 1 x 10^6 (n = 4), 2 x 10^6 (n = 2) and 5 x 10^6 (n = 2) cellular densities, and tumor volume was evaluated, reducing to half-time window the tumor growth. SKE cells were transfected with miR-654 miRIDIAN mimic and reduction of cell viability was confirmed by crystal violet assay, and used for the above presented mouse xenograft model.

3.2.4. STATISTICAL ANALYSIS

3.2.4.1. Salivary biomarkers data

Differential expression (DE) analyses in saliva were performed by using the comprehensive tool recently published called miARma-Seq[232], in collaboration with the two bioinformaticians who developed it, Dr. Ana Rojas (IBiS - CSIC, Sevilla, Spain) and Eduardo Andrés León (IPBLN, CSIC, Granada, Spain). This software has been designed specially for the analysis of high throughput data coming from next generation sequencing technologies, either for miRNA, circular RNA (circRNA) and mRNA expression data. Firstly, miARma-Seq has been utilized to eliminate low quality nucleotides and/or reads containing sequences aroused from PCR amplification during library generation and sequencing processes, as indexing codes (barcodes) for the sample pooling and adaptors to hybridize the library to the flow cell (sequencing surface matrix). After this initial data processing, DE analysis is different depending on the type of RNA evaluated. Hereafter we refer only to miRNA.

For miRNAs DE analysis, miARma-Seq has utilized the sequence alignment tool called Bowtie1[238]. This alignment tool is specialized to identify the genomic coordinates of each sequenced read, if this is smaller than 50nt, thus being the most suitable for miRNA genes analysis. After the identification of the genomic coordinates, miARma-Seq summarizes all the reads and count the total number of reads per each known miRNA within the human genome by using featureCounts[239]. Because the expression of a certain miRNA is proportional to the number of sequences attributed by featureCounts, these are appropriate measures to statistically compare miRNA expression levels between salivas from benign (controls) and early/late OC patients. Additionally, by using miRDeep2 tool that is a completely overhauled application that discovers miRNA genes by analyzing sequenced RNAs[240]. The tool reports known and hundreds of novel microRNAs with high accuracy in seven species representing the major animal clades[240] and was incorporated in miARma pipeline[232] for such analysis. The last step included the statistical analysis for each miRNA to compare the behavior between groups of study: control, early stage OC and late stage OC. In that step, miARma-Seq utilized edgeR[241], which compares each of the miRNAs between control and cancer groups (early and late stage OC) providing a fold change of expression and an statistical p-value.

3.2.4.2. MiRNA array data from FFTE tumors

Row data from the TaqMan® Array Human MicroRNA A+B Cards Set v3.0 and Custom TaqMan® Array MicroRNA Cards were obtained from the Expression Suite software (publicly available online, Thermo Fisher Scientific), and statistical analysis were performed by the Bioinformatic and Statistical Unit (UEB) from VHIR. Briefly, QCs of the row data were performed to show the behavior of the samples based on: (i) the Principal component 2D plot which shows the distribution of the patients in 2 dimensional plots regarding their levels of expression in general; (ii) the Density of Row Ct values plot; and (iii) the Ct spatial layout plots. With all of the above two patients were excluded from the following statistical analysis as technical outliers because the RNA was more degraded. Several steps of normalization were performed, starting with the intra-plate normalization. Firstly, since the commonly used endogenous miRNAs (U6 and U48) present in A and B cards were not stable across the samples, the stability of all the miRNAs was checked across the samples and groups to chose the more stable ones as endogenous controls for this study. The chosen miRNAs as endogenous controls had a variation coefficient under 0.03, and were expressed in all the samples. Therefore, 5 and 8 miRNAs fitting these criteria for A and B cards, respectively, were chosen as endogenous controls (Table 24). Delta CT system was used to normalize the data, by subtracting the mean of the chosen controls from all the other miRNA values. Data was also submitted to a non-specific filtering to increase the statistical power and reduce unnecessary noise, filtering out those miRNAs with more than 20 undetermined values for the subsequent analysis. Fold change values for each of the miRNAs were obtained after the calibration step, in which the long-term overall SV patients were chosen as a reference group, what lead to the obtaining of the DDCT value.

3.2.4.3. Microarray analysis of CDCP1 and PLAGL2 silencing

Raw data was obtained from the High Technology Unit (UAT, VHIR) and was processed by Expression Console and TAC software, both publicly available. Briefly, normalization of the raw data (CEL files) and generation of principal component analysis (PCA) were done with Affymetrix Expression Console software. To perform DE analysis between control and siCDCP1 or siPLAGL2 data, Affymetrix TAC software was used, which automatically analyze the fold change and statistical p-values based on one-way ANOVA t-test.

3.2.4.4. Human samples, *in vitro* and *in vivo* assays

Experimental sample size for in vitro and in vivo experiments was chosen following the criteria of the UEB and UAT. Unless otherwise indicated, mean ± SEM values are the average of three independent experiments. Statistical significance was determined by two-sided unpaired Student's t-test or ANOVA Tukey's test (GraphPad Prism Software, La Jolla, CA, USA). *P<0.05, **P<0.01 and ***P<0.001. The normal distribution of the data was verified (Shapiro-Wilk and Kolmologrov tests) and accordingly, non-parametric tests (Mann Whitney) were used for comparisons between groups when analyzing human ovarian tissues. *P < 0.05, **P < 0.01, ***P < 0.001, ****P < 0.0001 and ***** adjusted p-value (FDR) <0.05.

3.2.5. BIOINFORMATIC TOOLS

MiRWalk common algorithms: this bioinformatic tool is available online (http://zmf.umm.uni-heidelberg.de/apps/zmf/mirwalk2/miRretsys-self.html) and was used for the miRNA target prediction analysis, which led us to obtain a list of putative hsa-miR-654-5p target genes.

DAVID: for functional annotation bioinformatics of the microarray analysis, deregulated genes upon CDCP1 and PLAGL2 depletion with an adjusted FDR < 0.25 were introduced in the DAVID database (available online, https://david.ncifcrf.gov) to identify the most significant deregulated KEGG pathways.

GSEA: Gene Set Enrichment Analysis (GSEA) was performed using javaGSEA Desktop Application (Broad Institute)[242]. All collections of publically available gene sets used were extracted from Molecular Signatures Database v6.0 (MSigDB). GSEA was carried out by comparing siControl against siCDCP1 or siPLAGL2 expression data. Nominal *p*-value < 0.05 or FDR < 0.25 were chosen as the cut-off criteria to identify the significantly enriched gene sets. Heatmaps were generated for pathways enriched in both conditions by normalization to the median and log2 transformation of the array expression values. Heatmaps include genes contained in the enriched gene sets and differentially expressed in at least one of the two conditions (fold change > ± 1.5, FDR < 0.25). Genes differentially expressed in opposite ways in siCDCP1 and siPLAGL2 were ruled out.

4. RESULTS

Results are divided in two sections related to the two main objectives of the thesis.

4.1. MIRNAS IN SALIVA AS A DIAGNOSTIC TOOL

4.1.1. Salivary RNA from HGSC and benign patients are suitable for RNA sequencing

In order to find new non-invasive biomarkers for early detection of OC, saliva samples from 32 patients (control, n=10; early-stage HGSC, n=8; and late-stage HGSC, n=14) were included in this study (Table 10). A workflow of the sample preparation procedure is exemplified in Figure 13. CFS was subjected to RNA extraction, QCs and library preparation as explained in the corresponding section of the methodology (3.2.1.1.). Samples were randomized per groups (1: control; 2: early; 3: late) in 4 batches, and the order of the sample group was also different between batches (Figure 14).

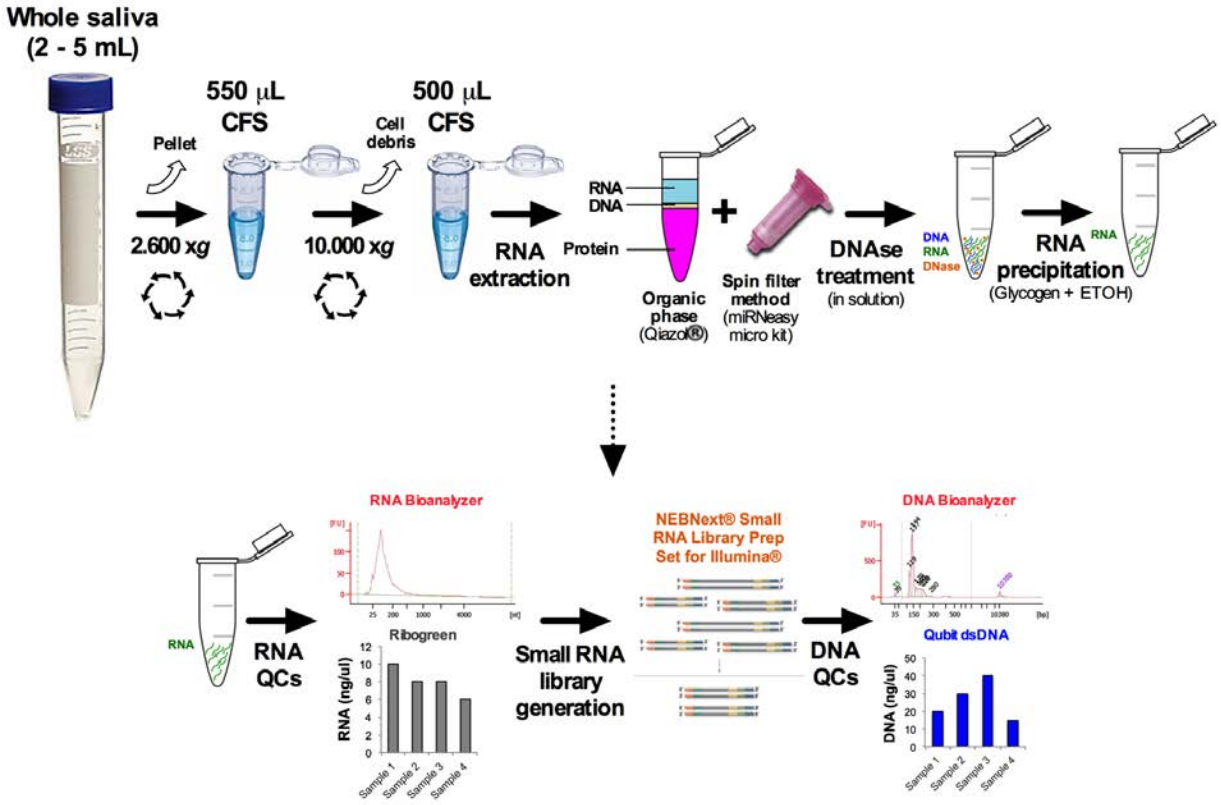

Figure 13: Saliva processing for small RNA sequencing analysis. CFS: cell-free saliva fraction.

Saliva samples			
Group	#	TYPE	FIGO stage
1	1	Benign	
1	2	Benign	
1	3	Benign	
1	4	Benign	
1	5	Benign	
1	6	Benign	
1	7	Benign	
1	8	Benign	
1	9	Benign	
1	10	Benign	
2	11	HGSC	IB
2	12	HGSC	IC
2	13	HGSC	IC
2	14	HGSC	IC
2	15	HGSC	IIa
2	16	HGSC	IIA
2	17	HGSC	IIA
2	18	HGSC	IC
3	19	HGSC	IIIC
3	20	HGSC	IIIC
3	21	HGSC	IIIC
3	22	HGSC	IIIC
3	23	HGSC	IIIC
3	24	HGSC	IIIC
3	25	HGSC	IIIC
3	26	HGSC	IIIC
3	27	HGSC	IIIC
3	28	HGSC	IIIC
3	29	HGSC	IIIC
3	30	HGSC	IIIC
3	31	HGSC	IV
3	32	HGSC	IV

→

Randomization and QCs data						
	Group	#	RNA ng/ul	input RNA amount (ng)	Library ng/ul	Average size (bp)
Batch-1	1	1	5.0	27.7	16.1	180
	1	2	9.5	52.1	13.6	174
	1	3	7.9	43.7	14.4	175
	2	11	7.8	42.9	21.9	188
	2	12	7.6	41.9	24.6	183
	3	19	7.1	39.1	27.3	185
	3	20	5.6	30.9	34.2	185
	3	21	8.7	47.6	59.1	256
Batch-2	2	13	8.5	46.9	20.1	189
	2	14	8.7	47.6	29.3	178
	1	4	1.9	10.6	20.2	177
	1	5	6.5	35.5	14.5	162
	1	6	5.0	27.4	13.6	175
	3	22	0.2	1.2	19.0	194
	3	23	0.8	4.3	9.9	157
	3	24	6.6	36.5	12.2	170
Batch-3	3	25	3.3	18.2	9.5	161
	3	26	6.8	37.2	22.8	180
	3	27	10.1	55.8	24.2	183
	3	28	10.4	57.3	22.2	186
	1	7	7.1	39.3	16.9	179
	1	8	5.3	29.3	14.9	177
	2	15	8.9	48.7	39.6	167
	2	16	9.7	53.3	23.6	182
Batch-4	2	17	4.7	25.7	16.0	193
	2	18	2.8	15.6	8.4	173
	3	29	7.4	40.6	13.0	171
	3	30	8.1	44.5	30.7	175
	3	31	7.1	38.8	31.3	202
	3	32	10.1	55.4	31.9	185
	1	9	5.2	28.6	5.6	159
	1	10	1.0	5.5	8.7	161

Figure 14: **Saliva samples randomization and QCs data.** Summary of the patients included (left) and data after sample processing (Right): (i) Batch number of sample processing (1-4); (ii) Group (1-3); (iii) Randomized patients (1-32); (iv) RNA concentration (ng/μL) measured by Quant-iT^{TM} Ribogreen® assay; (v) RNA input was calculated by multiplying the RNA concentration (ng/μL) and the starting volume of RNA used for the small RNA library (5.5μL of total RNA); (vi) Library concentration (ng/μL) calculated by Qubit® dsDNA BR assay. (vii) Average size (bp) for each library extracted from the High Sensitivity DNA Chip Bioanalyzer.

The QCs for all samples in the study are summarized in Figure 14. As observed in Figure 15, the RNA concentration of saliva varied between patients (Figure 15A, left) but no significant differences were observed when comparing groups of study (Figure 15A, right). The average RNA concentration of all samples was around 6 ng/μL, which correspond to an average of 100 ng of RNA per 1 mL of initial saliva. Thus, as on average saliva samples accounts for 500 uL of CFS, the total amount of RNA was considered sufficient to proceed with RNA sequencing. In addition, to prove that sample manipulation in randomized batches did not bias the sample performing, a comparison was carried out, resulting in no statistical differences between batches regarding the RNA input for library construction (Figure 15B).

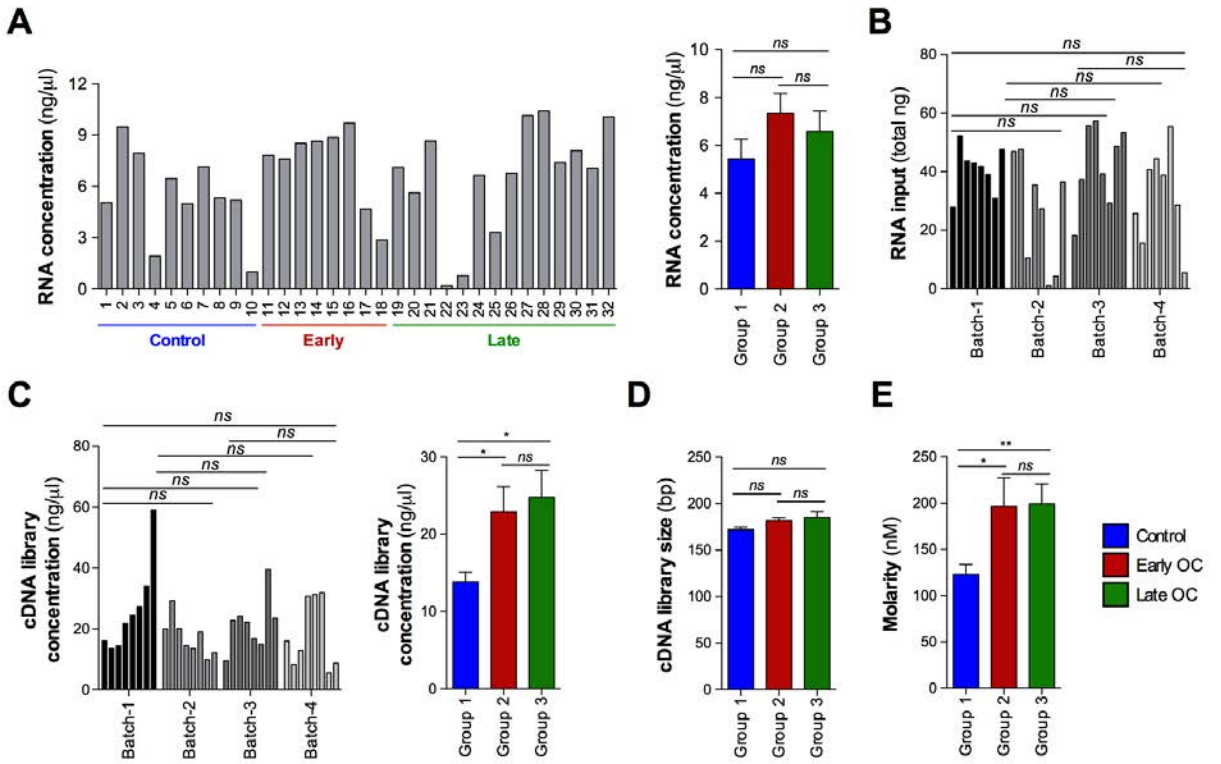

Figure 15: Quality controls (QCs) for RNA samples and small RNA libraries. A) Sample values for RNA concentration measured by Quant-iT^{TM} Ribogreen® assay. **B)** RNA input data plotted for each batch of samples processed. **C)** Library concentration for each batch of samples processed (left) and average for each group (right). **D)** Average size (bp) for each group. **E)** Molarity (nM) for each library was obtained using the tool from MolBiol[243], and library concentration and average size parameters. Plot represented the average molarity for each group. *p<0.05; **p<p0.01; "ns": non-significant.

Although two samples from batch-2 presented low RNA concentration (Figure 15B), they were considered to proceed with library preparation resulting in enough cDNA concentration material (Figure 15C, left). When comparing library concentration between groups of study, control patients (blue) appeared of lower concentration compared to cancer patients (red and green) (Figure 15C, right). However, library size was comparable between groups of study (Figure 15D). This suggested that the quality of the libraries was comparable between groups of study, and composed by the same size of RNA species. Similarly to cDNA library concentration, molarity was lower in control compared to HGSC salivas (Figure 15E), yet it did not suppose a problem as equimolar concentrations were loaded for RNA sequencing.

In order to prove the reproducibility of salivary RNA processing for RNA sequencing, the RNA and cDNA library profile of four random samples are shown in Figure 16. The majority of the RNA species presented in saliva sized between 25-200 nt (Figure 16A), which included the size of the miRNAs and confirmed the small RNA enrichment of the

standardized procedures used. In addition, a size selection step (~140-300 bp) was performed after the adaptor ligation to the RNA (Figure 16B). Size selection allowed to avoid the enrichment of longer RNA species and also to get rid of the excess of adaptors (Figure 16B), which are favored in the PCR amplification and sequencing processes.

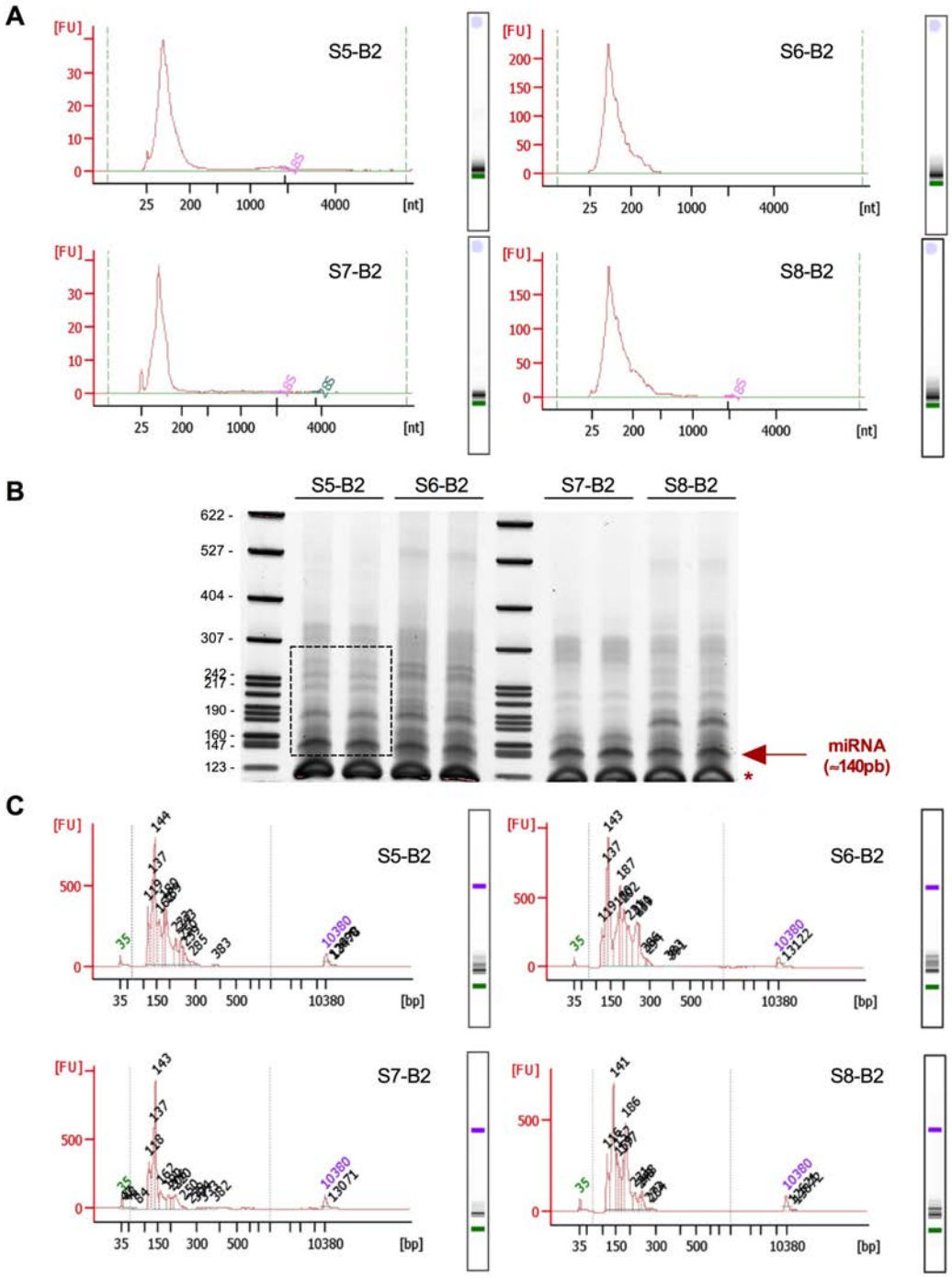

Figure 16: Salivary RNA profile. A) RNA profile obtained from RNA Pico Chip Bioanalyzer. **B)** Size-selection step by 6% PAGE-Urea gel (140-300 bp) after adaptor ligation step of the library generation. Red asterisk indicates the excess of the adaptors after running the gel. **C)** Small RNA library profile from High Sensitivity DNA Chip Bioanalyzer.

As abovementioned, molarity value (nM) was obtained for each library (fourth column of Table 21). As observed, all of them presented a molarity higher than 10 nM and, therefore, they were diluted to 10 nM and pooled in batches, thus contributing each library to 1.25 nM in the 10nM pool of 8 cDNA libraries. This could be performed since each library was tagged with a different index (9^{th}, 10^{th} and 11^{th} column of Table 21), which are specific sequences introduced during the library generation and that allow the sequencing of multiplexed samples (pools). Here, 4 different pools were sequenced in 4 lanes comprising the 32 saliva-randomized samples (Table 21).

After sequencing, pools were de-multiplexed using the expected index primer sequence read (next to last column of Table 21) and analyzed as explained in section 3.2.4.1. All samples passed QCs and had a good number of processed reads (Figure 17A) with an average of 16.2 million reads across all samples. Upon alignment with the human genome, an average of 36% of overall alignment was achieved, with no differences between groups (Figure 17B). Despite the apparent low alignment to the human genome (normally it is around 85-99% for cellular mRNA), this percentage of alignment in saliva was acceptable as compared to salivas form healthy individuals previously profiled[244]. In addition, oral microbiome has been previously detected by alignment of the CFS sequencing data to the human oral microbiome database (HOMD)[244]. Despite pelleted cells (buccal or bacterial) are also not included in this study, a possible contribution of RNA species from physiological and/or mechanical cell lysates could be incorporated from the CFS into the libraries, thus reducing the percentage of the alignment with the human genome.

P	L	G	Library Molarity (nM)	cDNA library (ul)	EB buffer 0,1% Tween20 (ul)	Final Molarity (nM)	Library Name	Index	Index Primer Sequence	Expected Index Primer Sequence Read	Name of the lane
Pool 1	L1	1	137.5	7.3	92.7	10nM	OvCaPool1-B1-1	I-1	5´-CAAGCAGAAGACGGCATACGAGAT**CGTGAT**GTGACTGGAGTTCAGACGTGTGCTCTTCCGATC-s-T-3´	ATCACG	SxaQSEQs VB092L1:k E3waru9
	L2	1	120.2	8.3	91.7	10nM	OvCaPool1-B1-2	I-2	5´-CAAGCAGAAGACGGCATACGAGAT**ACATCG**GTGACTGGAGTTCAGACGTGTGCTCTTCCGATC-	CGATGT	
	L3	1	127.1	7.9	92.1	10nM	OvCaPool1-B1-3	I-3	5´-CAAGCAGAAGACGGCATACGAGAT**GCCTAA**GTGACTGGAGTTCAGACGTGTGCTCTTCCGATC-	TTAGGC	
	L4	2	179.3	5.6	94.4	10nM	OvCaPool1-B1-4	I-4	5´-CAAGCAGAAGACGGCATACGAGAT**TGGTCA**GTGACTGGAGTTCAGACGTGTGCTCTTCCGATC-	TGACCA	
	L5	2	207.3	4.8	95.2	10nM	OvCaPool1-B1-5	I-5	5´-CAAGCAGAAGACGGCATACGAGAT**CACTGT**GTGACTGGAGTTCAGACGTGTGCTCTTCCGATC-	ACAGTG	
	L6	3	227.3	4.4	95.6	10nM	OvCaPool1-B1-6	I-6	5´-CAAGCAGAAGACGGCATACGAGAT**ATTGGC**GTGACTGGAGTTCAGACGTGTGCTCTTCCGATC-	GCCAAT	
	L7	3	284.5	3.5	96.5	10nM	OvCaPool1-B1-7	I-7	5´-CAAGCAGAAGACGGCATACGAGAT**GATCTG**GTGACTGGAGTTCAGACGTGTGCTCTTCCGATC	CAGATC	
	L8	3	355.8	2.8	97.2	10nM	OvCaPool1-B1-8	I-8	5´-CAAGCAGAAGACGGCATACGAGAT**TCAAGT**GTGACTGGAGTTCAGACGTGTGCTCTTCCGATC-	ACTTGA	
Pool 2	L1	2	163.5	6.1	93.9	10nM	OvCaPool2-B2-1	I-1	5´-CAAGCAGAAGACGGCATACGAGAT**CGTGAT**GTGACTGGAGTTCAGACGTGTGCTCTTCCGATC-s-T-3´	ATCACG	SxaQSEQs VB092L2:Y CU3pXk7
	L2	2	253.9	3.9	96.1	10nM	OvCaPool2-B2-2	I-2	5´-CAAGCAGAAGACGGCATACGAGAT**ACATCG**GTGACTGGAGTTCAGACGTGTGCTCTTCCGATC-	CGATGT	
	L3	1	175.5	5.7	94.3	10nM	OvCaPool2-B2-3	I-3	5´-CAAGCAGAAGACGGCATACGAGAT**GCCTAA**GTGACTGGAGTTCAGACGTGTGCTCTTCCGATC-	TTAGGC	
	L4	1	138.2	3.6	46.4	10nM	OvCaPool2-B2-4	I-4	5´-CAAGCAGAAGACGGCATACGAGAT**TGGTCA**GTGACTGGAGTTCAGACGTGTGCTCTTCCGATC-	TGACCA	
	L5	1	120.0	4.2	45.8	10nM	OvCaPool2-B2-5	I-5	5´-CAAGCAGAAGACGGCATACGAGAT**CACTGT**GTGACTGGAGTTCAGACGTGTGCTCTTCCGATC-	ACAGTG	
	L6	3	150.8	3.3	46.7	10nM	OvCaPool2-B2-6	I-6	5´-CAAGCAGAAGACGGCATACGAGAT**ATTGGC**GTGACTGGAGTTCAGACGTGTGCTCTTCCGATC-	GCCAAT	
	L7	3	96.7	5.2	44.8	10nM	OvCaPool2-B2-7	I-7	5´-CAAGCAGAAGACGGCATACGAGAT**GATCTG**GTGACTGGAGTTCAGACGTGTGCTCTTCCGATC	CAGATC	
	L8	3	110.4	4.5	45.5	10nM	OvCaPool2-B2-8	I-8	5´-CAAGCAGAAGACGGCATACGAGAT**TCAAGT**GTGACTGGAGTTCAGACGTGTGCTCTTCCGATC-	ACTTGA	
Pool 3	L1	3	90.9	5.5	44.5	10nM	OvCaPool3-B3-1	I-1	5´-CAAGCAGAAGACGGCATACGAGAT**CGTGAT**GTGACTGGAGTTCAGACGTGTGCTCTTCCGATC-s-T-3´	ATCACG	SxaQSEQs VB092L3:e 7ZrcrmW
	L2	3	194.9	5.1	94.9	10nM	OvCaPool3-B3-2	I-2	5´-CAAGCAGAAGACGGCATACGAGAT**ACATCG**GTGACTGGAGTTCAGACGTGTGCTCTTCCGATC-	CGATGT	
	L3	3	204.0	4.9	95.1	10nM	OvCaPool3-B3-3	I-3	5´-CAAGCAGAAGACGGCATACGAGAT**GCCTAA**GTGACTGGAGTTCAGACGTGTGCTCTTCCGATC-	TTAGGC	
	L4	3	184.2	5.4	94.6	10nM	OvCaPool3-B3-4	I-4	5´-CAAGCAGAAGACGGCATACGAGAT**TGGTCA**GTGACTGGAGTTCAGACGTGTGCTCTTCCGATC-	TGACCA	
	L5	1	145.4	6.9	93.1	10nM	OvCaPool3-B3-5	I-5	5´-CAAGCAGAAGACGGCATACGAGAT**CACTGT**GTGACTGGAGTTCAGACGTGTGCTCTTCCGATC-	ACAGTG	
	L6	1	129.7	7.7	92.3	10nM	OvCaPool3-B3-6	I-6	5´-CAAGCAGAAGACGGCATACGAGAT**ATTGGC**GTGACTGGAGTTCAGACGTGTGCTCTTCCGATC-	GCCAAT	
	L7	2	365.1	2.7	97.3	10nM	OvCaPool3-B3-7	I-7	5´-CAAGCAGAAGACGGCATACGAGAT**GATCTG**GTGACTGGAGTTCAGACGTGTGCTCTTCCGATC	CAGATC	
	L8	2	199.6	5.0	95.0	10nM	OvCaPool3-B3-8	I-8	5´-CAAGCAGAAGACGGCATACGAGAT**TCAAGT**GTGACTGGAGTTCAGACGTGTGCTCTTCCGATC-	ACTTGA	
Pool 4	L1	2	127.7	7.8	92.2	10nM	OvCaPool4-B4-1	I-1	5´-CAAGCAGAAGACGGCATACGAGAT**CGTGAT**GTGACTGGAGTTCAGACGTGTGCTCTTCCGATC-s-T-3´	ATCACG	SxaQSEQs VB092L4:Y KpL43YZ
	L2	2	74.5	6.7	43.3	10nM	OvCaPool4-B4-2	I-2	5´-CAAGCAGAAGACGGCATACGAGAT**ACATCG**GTGACTGGAGTTCAGACGTGTGCTCTTCCGATC-	CGATGT	
	L3	3	116.8	4.3	45.7	10nM	OvCaPool4-B4-3	I-3	5´-CAAGCAGAAGACGGCATACGAGAT**GCCTAA**GTGACTGGAGTTCAGACGTGTGCTCTTCCGATC-	TTAGGC	
	L4	3	270.1	3.7	96.3	10nM	OvCaPool4-B4-4	I-4	5´-CAAGCAGAAGACGGCATACGAGAT**TGGTCA**GTGACTGGAGTTCAGACGTGTGCTCTTCCGATC-	TGACCA	
	L5	3	238.7	4.2	95.8	10nM	OvCaPool4-B4-5	I-5	5´-CAAGCAGAAGACGGCATACGAGAT**CACTGT**GTGACTGGAGTTCAGACGTGTGCTCTTCCGATC-	ACAGTG	
	L6	3	265.3	3.8	96.2	10nM	OvCaPool4-B4-6	I-6	5´-CAAGCAGAAGACGGCATACGAGAT**ATTGGC**GTGACTGGAGTTCAGACGTGTGCTCTTCCGATC-	GCCAAT	
	L7	1	54.1	4.6	20.4	10nM	OvCaPool4-B4-7	I-7	5´-CAAGCAGAAGACGGCATACGAGAT**GATCTG**GTGACTGGAGTTCAGACGTGTGCTCTTCCGATC	CAGATC	
	L8	1	83.4	6.0	44.0	10nM	OvCaPool4-B4-8	I-8	5´-CAAGCAGAAGACGGCATACGAGAT**TCAAGT**GTGACTGGAGTTCAGACGTGTGCTCTTCCGATC-	ACTTGA	

Table 21: Molarity of the library and sample pooling for RNA sequencing. First column (P): Pool number (1-4); Second column (L): library number (1-8)/pool; Third column (G): group of study (1: control; 2: early-stage HGSC; 3: late-stage HGSC).

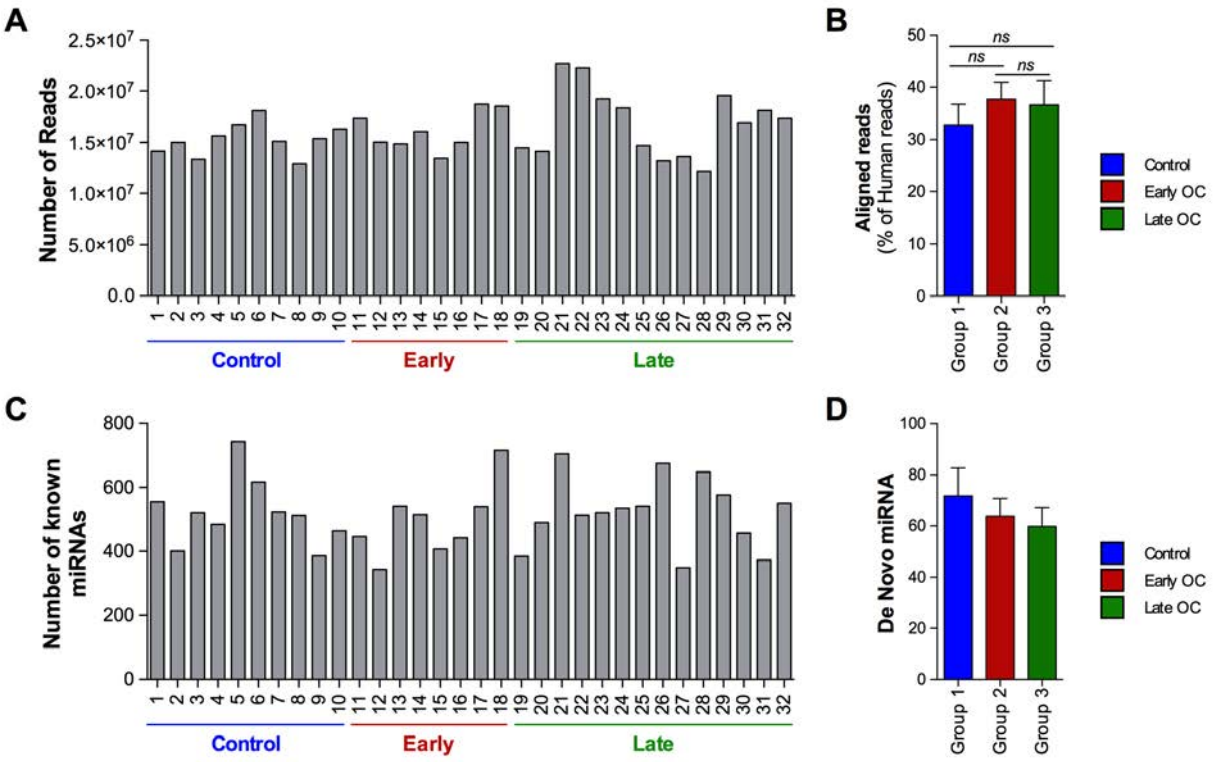

Figure 17: Number of reads and miRNAs identified in patients' salivas. A) Number of processed reads per library to use for the alignment. **B)** Average of the % of aligned reads for each library. **C)** Number of miRNAs detected in each saliva sample counted by FeatureCounts. **D)** Average number of De Novo miRNAs identified in each group of study. "ns": non-significant.

Prior to the DE analysis, the number of miRNAs detected per sample was obtained by FeatureCounts[239] (Figure 17C), with an average number of 520, 493 and 522 known miRNAs detected in salivas from control, early and late HGSC patients, respectively (p=0.61 for control *vs.* early; p=0.96 for control *vs.* late; and p=0.57 for early *vs.* late). Additionally, by using miRDeep2[240], a tool integrated in the miARma-seq pipeline[232], an average of 72, 64 and 60 novel miRNAs were identified *de novo* in saliva from control, early and late HGSC patients, respectively. These putative novel miRNAs were obtained as previously described[232,240] through mapping the reads against the potential miRNA precursors and by predicting RNA hairpin structures of the aligned sequences situated in different chromosomal locations previously unknown and/or not referred as miRNAs (Figure 17D).

Altogether, saliva from benign and HGSC patients had enough RNA concentration and similar RNA size, acceptable for cDNA library preparation. In addition, similar miRNA enrichment was obtained between samples and groups, which supported the feasibility for the DE analysis.

4.1.2. Small RNA sequencing revealed increased levels of new miRNA in saliva from HGSC patients

After having proved de good quality of the obtained data, DE analysis were performed. Through clustering analysis 4 outliers were identified (1 control (p113), 1 early (p163), and 2 late (p260 and p310) patients) that were excluded from the following analyses (Figure 18). Technical manipulations were excluded as a cause of being outliers, since all samples passed the QCs established. Also, smoking condition and CA125 levels were not variables related to the different behavior of these samples. It was found that these 4 samples had much higher number of aligned reads used to count miRNAs than the rest of the samples (from 3 x 10^5 to 1.2 x 10^6 reads while the majority of the samples had 5 x 10^4 to 9 x 10^4). This resulted in a much higher number of miRNAs detected and expressed in higher proportions, which perturbed the DE analysis, being outliers as shown in Figure 18.

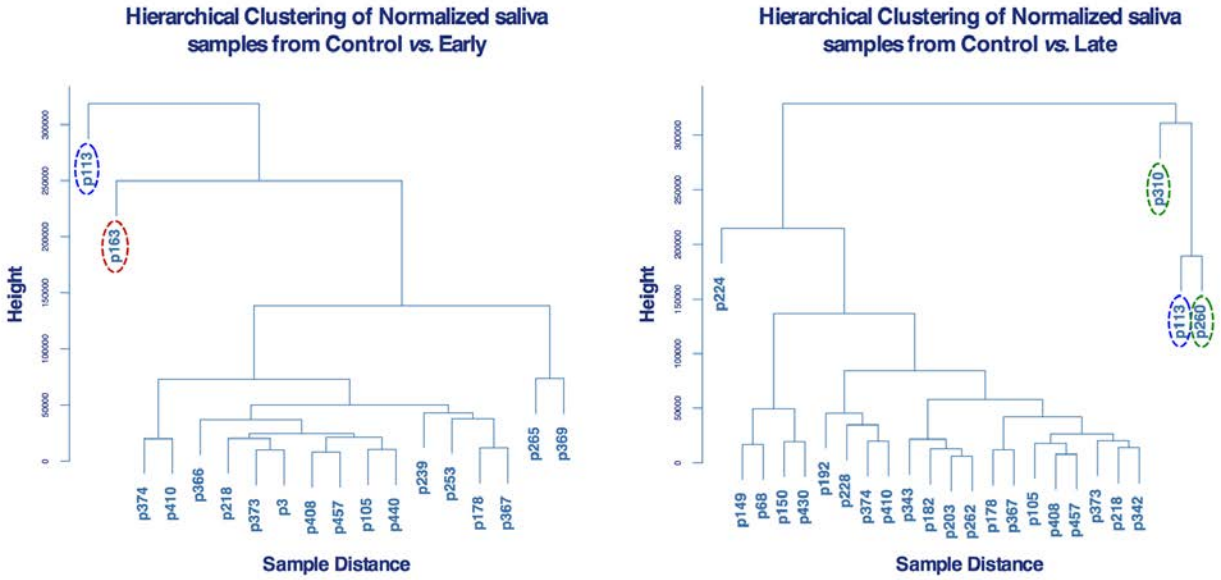

Figure 18: Hierarchical clustering specifies the dissimilarity of normalized data for all patients. Euclidean distance was used for hierarchical clustering of the samples. Sample outliers are rounded (blue=control; red=early; green=late).

Finally, after removing these outliers, the groups used for the DE analysis by miARma-Seq tool were composed by n=9, n=7 and n=12 for control patients, early and late HGSC patients, respectively. Unsupervised hierarchical clustering analysis was performed for the different comparisons analyzed (Figure 19A) showing the expression of the 50 top miRNAs. The statistical analysis performed showed a great number of known miRNAs differentially expressed with statistical significance (Figure 19B, top).

When comparing control and early HGSC salivas, 49 miRNAs were differentially expressed with a $p < 0.05$ and a fold change $> \pm 2$, with 32 of them being overexpressed in early HGSC salivas (Figure 19B, left panel). Similarly, 45 miRNAs were significantly deregulated between control and late HGSC salivas, with 28 of the miRNAs overexpressed in late salivas compared to controls (Figure 19B, mid panel). Surprisingly, when analyzing the DE miRNAs in salivas between early an late OC patients only 3 miRNAs were significant (Figure 19B, right panel), suggesting that these salivas might be not very different in reflecting the presence of this disease. Interestingly, a Venn diagram analysis showed 29 miRNAs commonly altered in both early and late stages of the disease compared to controls (Figure 19C), 20 of them being overexpressed in early and late HGSC compared to control salivas.

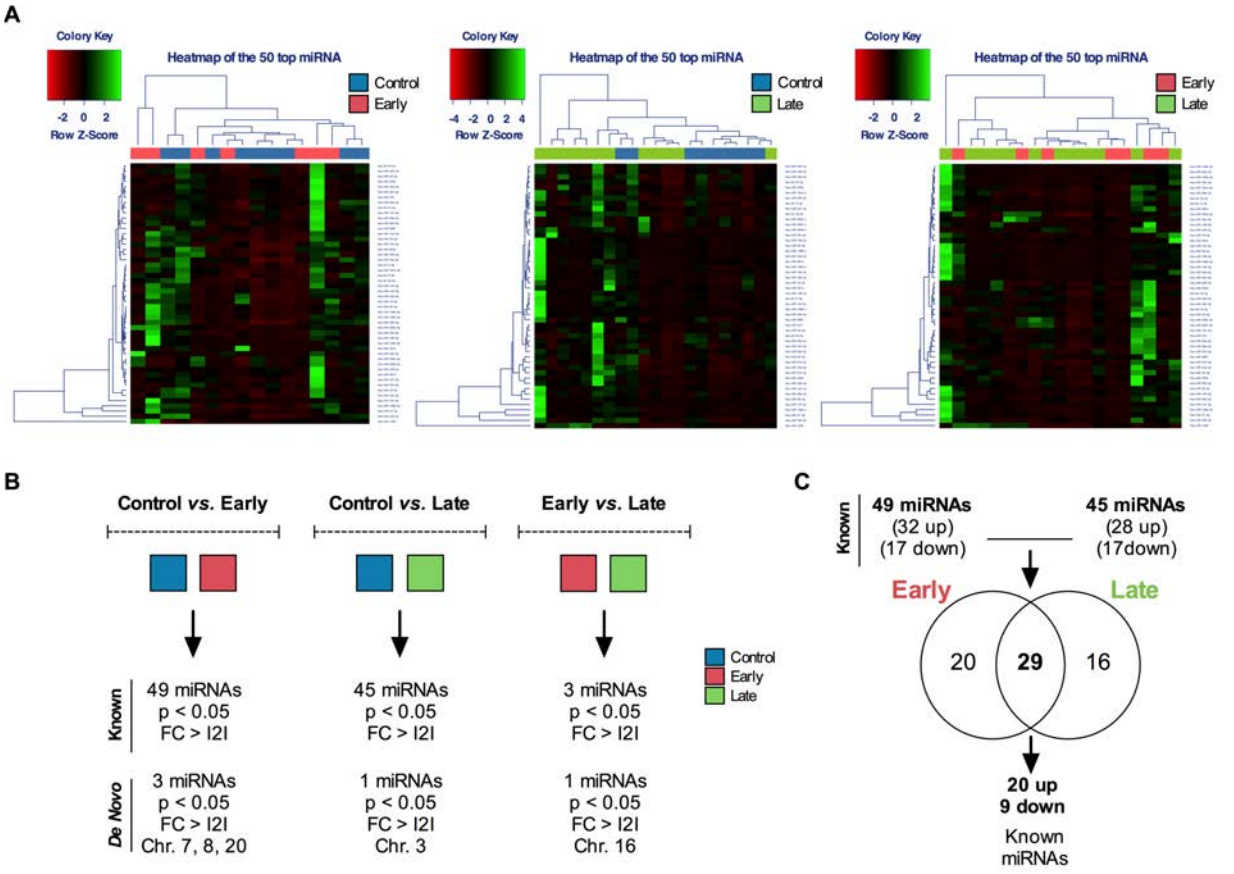

Figure 19: Salivary miRNAs appeared altered in saliva from OC patients. A) Hierarchical clustering between control-early (left panel), control-late (mid panel), and early-late (right panel) patients. Euclidean distances were used to perform the analysis. **B)** Summary of the DE known and unknown miRNAs in the three comparisons (FC: fold change). **C)** Venn diagram showing the overlapping on the significant known miRNAs ($p < 0.05$) altered in control-early and control-late comparisons.

Additionally, from the 72, 64 and 60 novel miRNAs identified in control, early and late HGSC patients' saliva, respectively, 5 novel miRNAs appeared significantly deregulated in HGSC compared to control salivas (Figure 19B, bottom). These miRNAs are located in chromosomes 20, 7, 8, 3 and 16, respectively. The putative miRNA transcript sequences of the novel miRNAs were extracted from the human GRCh37 (Table 22), which will need further annotation and functional validation.

#	Chr.	Coordinates	Fold Change	p-value	Putative miRNA sequence	Status
1	Chr.20	chr20:24789379..24789453:+	-21.6	0.004	CACGTGGGGGCTGCGGGTTGTGAGATCCTGTGGGGGCTGC TGGCTGTGAGATCGCATGGGGACTGTGGGCTGTGA	Down in Early vs. Control
2	Chr.7	chr7:5582546..5582619:+	-16.8	0.006	CAGGTGGGACTTAGCAGTGAGCCAGCTGTGCACAGGCCAG GGTGCTAAGCGTTGGGCCCTCTTAGCTCAGCAAA	Down in Early vs. Control
3	Chr.8	chr8:104383802..104383862:-	-10.2	0.017	CGGAGCTGGAGGCGGAGGAGACCGAGGAGAGGAACGTGG TCAGCGTCTGGCTCCGCCGCGC	Down in Early vs. Control
4	Chr.3	chr3:50712891..50712968:+	-7.9	0.035	GCGGGTGCGGGGGTGGGCGCGGGTCTCTGTGCAGAGAGG GCGGCAGGGGGCGCTGGCGGTGCGGCCTTGGCAGGTGCG	Down in Late vs. Control
5	Chr.16	chr16:85496411..85496469:-	-2.5	0.035	GAGGGGCCGGGGCGCCTGGGGGCCCCGCAGCCGCTCACG CCGCCCCCCGGCCCCGCGCC	Down in Late vs. Early

Table 22: Novel miRNAs identified *de novo* in saliva. Putative miRNA sequences correspond to the putative miRNA gene sequences attributed to the coordinates introduced in the human GRCh37.

Among the 49 miRNAs DE with a p-value < 0.05 in early HGSC compared to control salivas, 11 miRNAs were DE with an FDR < 0.05 (Table 23). Among them, 10 miRNAs were increased in early HGSC compared to control salivas (ranging from 3 to 85 fold change difference). In addition, among the 45 miRNAs DE with a p-value < 0.05 in late HGSC compared to control salivas, 5 miRNAs were significantly increased in late HGSC saliva with an FDR < 0.05 (Table 23), which presented fold changes ranging from 27 to 70.ç

Control vs. Early					Control vs. Late				
#	miRNA	Fold Change	FDR < 0.05	Status	#	miRNA	Fold Change	FDR < 0.05	Status
1	**hsa-miR-34c-5p**	50.5	0.0000	Up in Early	1	**hsa-miR-34c-5p**	39.8	0.0006	Up in Late
2	**hsa-miR-34b-3p**	85.7	0.0000	Up in Early	2	**hsa-miR-34b-3p**	81.0	0.0044	Up in Late
3	**hsa-miR-34c-3p**	44.8	0.0002	Up in Early	3	**hsa-miR-34c-3p**	27.7	0.0165	Up in Late
4	hsa-miR-449c-5p	49.0	0.0002	Up in Early	4	hsa-miR-34b-5p	69.3	0.0018	Up in Late
5	hsa-miR-92b-3p	8.3	0.0024	Up in Early	5	hsa-miR-449a	38.9	0.0259	Up in Late
6	hsa-miR-100-5p	4.5	0.0064	Up in Early					
7	hsa-miR-184	20.6	0.0165	Up in Early					
8	hsa-miR-210-3p	3.4	0.0165	Up in Early					
9	hsa-miR-3168	-6.5	0.0249	Down in Early					
10	hsa-miR-200a-3p	3.0	0.0420	Up in Early					
11	hsa-miR-218-5p	3.3	0.0479	Up in Early					

Table 23: Top DE miRNAs in saliva from early and late OC patients. MiRNAs in bold indicate that they are increased in both early and late OC salivas compared to controls.

Importantly, when looking to the miRNAs altered in early stage, the levels of expression of the 11 miRNAs with FDR < 0.05 were able to separate the control from early HGSC group by unsupervised hierarchical clustering analysis (Figure 20A),

suggesting the potential of these salivary miRNAs as biomarkers for early detection of OC. Interestingly, miR-34 family was overrepresented, with 3 family members overexpressed in HGSC salivas regardless of the disease stage (Table 23). As shown in Figure 20B, the three miR-34 family members were significantly increased in early and late HGSC compared to control salivas. The average number of normalized reads for miR-34c-5p, miR-34c-3p and miR-34b-3p in early HGSC salivas was 3569, 195 and 270 (SEM ± 2500, 113 and 175) respectively, while the number of reads dramatically decreased in control salivas to 70, 3 and 2, respectively (SEM ± 20, 2 and 2) (Figure 20B, left). Similarly, the average number of normalized reads in late HGSC salivas was 2921, 122 and 254 (SEM ± 1923, 84 and 200) for miR-34c-5p, miR-34c-3p and miR-34b-3p, respectively, while in control salivas was 73, 3 and 2 (SEM ± 21, 2, and 2), respectively (Figure 20B, right). Additionally, the normalized reads for the other top miRNA candidates (FDR < 0.05, Table 23) showed clear increased levels except miR-3168 that was downregulated in HGSC compared to control salivas (Figure 20C).

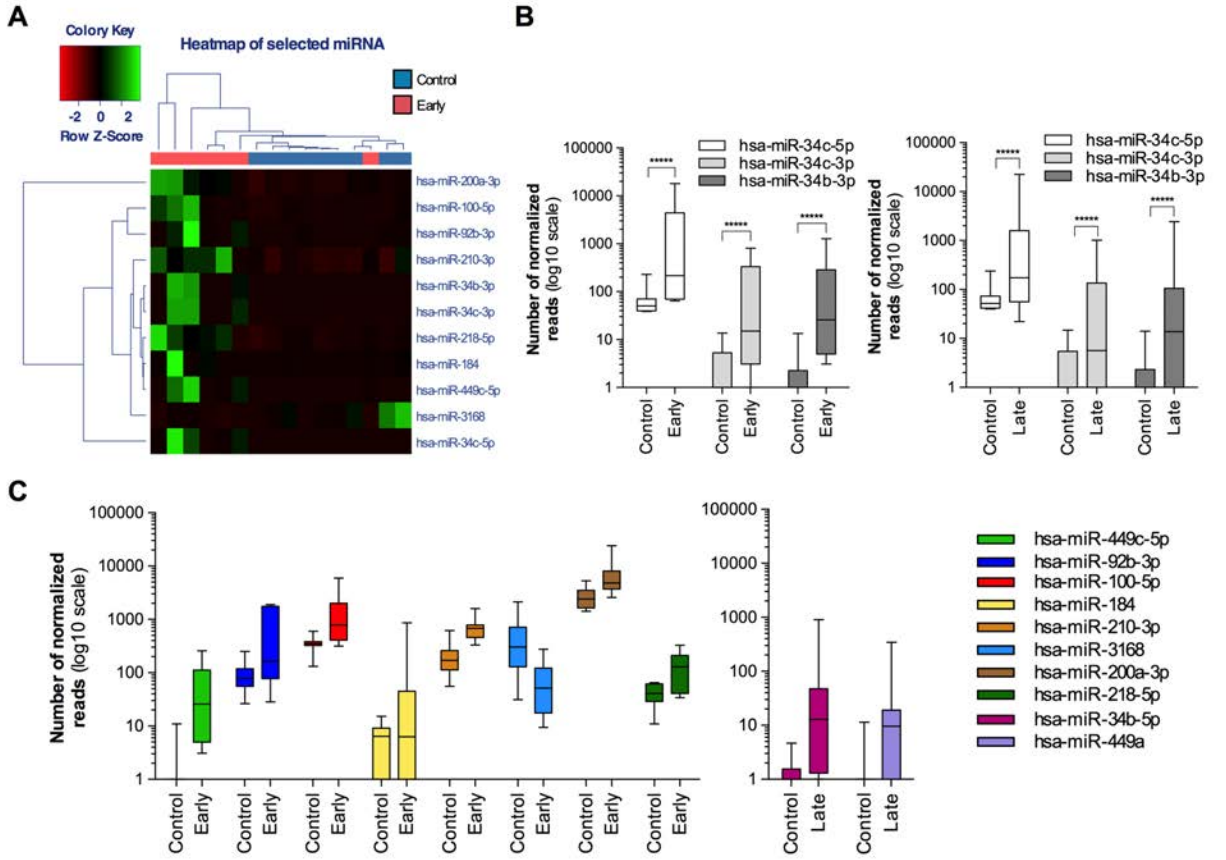

Figure 20: Top DE miRNAs are overexpressed in early and late stage OC. A) Hierarchical clustering analysis of selected miRNAs altered in early OC salivas compared to control salivas (miRNAs with FDR < 0.05). **B)** Normalized number of reads for miR-34 family members in early (left panel) and late (right panel) OC salivas compared to control salivas. ****FDR < 0.05. **C)** Normalized number of reads for miRNAs with FDR < 0.05 in early and late OC salivas compared to control salivas.

Altogether, it can be suggested that the miRNAs present in saliva may serve as potential diagnostic biomarkers as the levels of several miRNAs have been found very increased in saliva form HGSC patients. Very importantly, the salivas form early-stage HGSC used in this study could reflect the presence of OC as well as those from late-stage. In particular, the miR-34 family, although it can act as a tumor suppressor in OC cells[245–247], it is upregulated in saliva either from early and late stage HGSC patients, suggesting that they could indeed be used as new biomarkers for the disease, and might provide biological information about the biology of OC as discussed below. Therefore, it can be hypothesized that the use of saliva as a non-invasive diagnostic body fluid could potentially be useful to improve the early detection of OC, in particular for the HGSC histology, the most fatal subtype of OC. Currently, the top salivary miRNAs are under validation in a bigger cohort of samples in order to robustly confirm the potential diagnosis of these miRNAs and, in the future, a prospective multicenter validation will be carried out to further establish a miRNA profile able to improve the early diagnosis of HGSC.

4.2. MIRNAS AS A TOOL FOR OC TREATMENT

4.2.1. Identification of 4 deregulated miRNAs in advanced stage OC patients

As introduced earlier, miRNAs-based therapies are emerging. In an attempt to identify new targets for OC therapy, we analyzed miRNA changes in late-stage OC patients, the prognosis of which is already compromised due to the disease spread at that point of the ovarian carcinomatosis. The study was done retrospectively in 107 human OC FFPE primary tumor tissues by using TaqMan® Array Human MicroRNA Cards (Figure 21A). Twenty-seven samples were used in an initial discovery phase and a subsequent multicenter validation was carried out with 80 samples. For selection purposes, short-term SV was defined as overall SV of less than 3 years, and long-term SV was defined as more than 8 years (Figure 21B). The tumor selection criteria and the associated clinical data are provided in Table 11 and summarized in Figure 21B.

A

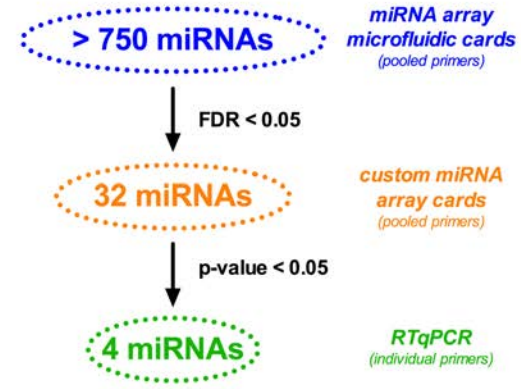

B

Discovery phase	Patients	
	N	**Average SV**
Short-term SV	14	1.8 years
Long-term SV	13	10.3 years

Validation phase	Patients	
	N	**Average SV**
Short-term SV	38	2.6 years
Long-term SV	42	8.3 years

Figure 21: Workflow and patients criteria for identification of deregulated miRNAs in late-stage OC. A) Workflow including the methodology used in the different phases and statistical criteria followed for the subsequent analysis. **B)** Summary of the patients' cohort. From the 27 patients used in the discovery phase, 2 patients were excluded as technical outliers as explained in methods section (see section 3.2.4.2.).

Since standard miRNAs used as endogenous controls included in the microfluidic cards by the manufacture (U6 snRNA, RNU44 and RNU48) were not stable across the samples' cohort, the Vandesompele J. *et al.* method was used for normalization[248]. Thus, the most stable miRNAs among the >750 miRNAs analyzed in the array card, were selected and used for the discovery and the validation phases (Table 24).

Endogenous controls Cards A	Variation coefficient	Ct mean	NA	Endogenous controls Cards B	Variation coefficient	Ct mean	NA
hsa-miR-636-002088	0.024	25.7	0	hsa-miR-520D-3P-002743	0.021	27.8	0
hsa-miR-518f-002388	0.024	28.6	0	**hsa-miR-1267-002885**	0.023	26.6	0
hsa-miR-518d-001159	0.025	24.8	0	hsa-miR-645-001597	0.024	30.7	0
hsa-miR-548c-5p-002429	0.028	28.2	0	**hsa-miR-572-001614***	0.025	26.3	0
hsa-miR-548d-5p-002237	0.029	27.2	0	hsa-miR-1303-002792	0.026	23.6	0
				hsa-miR-1233-002768	0.027	20.3	0
				hsa-miR-320B-002844	0.030	25.1	0

Table 24: miRNA selected as endogenous controls to perform the statistical analysis. Variation coefficient cutoff was 0.03 and NA=0 were established for controls selection (e.i. all samples must have a Ct value; NA: Not Available Ct value). Geometric mean of endogenous miRNAs from cards A and B were used for normalization of the discovery phase results; miRNAs in bold were used in the validation phase; *miRNA used for technical verification by RTqPCR and subsequent experiments.

A total of 32 miRNAs were found DE (n=25) with high confidence (Figure 22A), where SV groups clustered together in unsupervised hierarchical clustering analysis (Figure 22B). Subsequently, a cohort of 80 independent samples was used to validate the previously identified miRNAs. Four miRNAs (miR-654-5p, miR-554, miR-409-3p and miR-127-3p) showed increased levels in short SV patients by both custom miRNA array (Figure 22C) and RTqPCR analysis (Figure 22D).

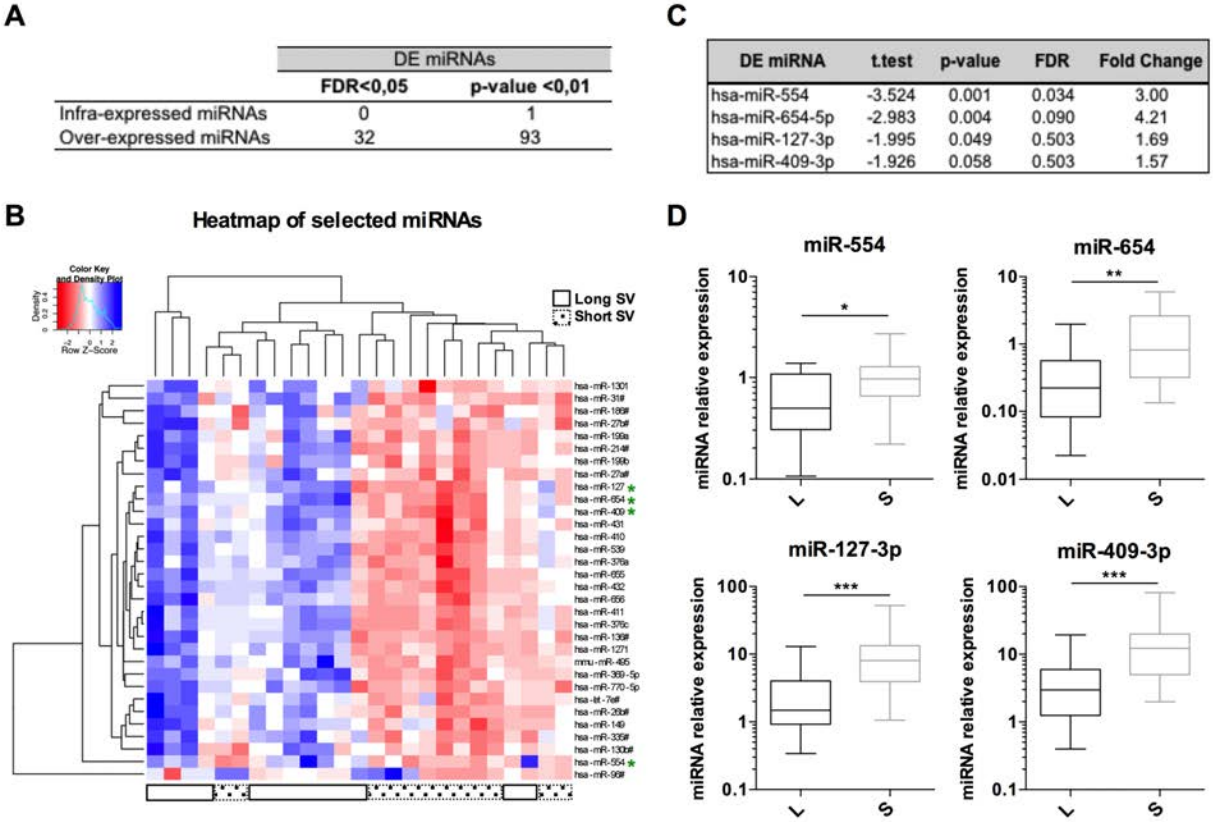

Figure 22: MiRNA levels are deregulated in late-stage OC patients. A) Summary of the discovery phase (n=25) depending on statistical criteria. **B)** Hierarchical clustering of the 32 DE miRNAs in the discovery phase. **C)** Summary of the results of the validation phase. **D)** Technical verification by RTqPCR including patients (n=40) from the discovery and validation phases. *p<0.05; **p<0.01; ***p<0.001.

4.2.2. Evaluation of the oncogenic/tumor suppressor role of the validates miRNAs

In order to evaluate the potential therapeutic role of the 4 validated miRNAs in OC, they were functionally tested *in vitro* by over- and infra- expressing them by miRNA mimics and antagomiRs in multiple OC cell lines. Surprisingly, and in apparent contradiction with the observation that miR-654 levels were higher in short SV patients, overexpression of miR-654 impaired cell proliferation with consistent effects in all OC cell lines tested (Figure 23A), while increased proliferation was observed upon miR-654 inhibition in 3 of the 4 OC cell lines tested (Figure 23B). This suggested that at least *in vitro*, miR-654 has a tumor suppressor role in OC.

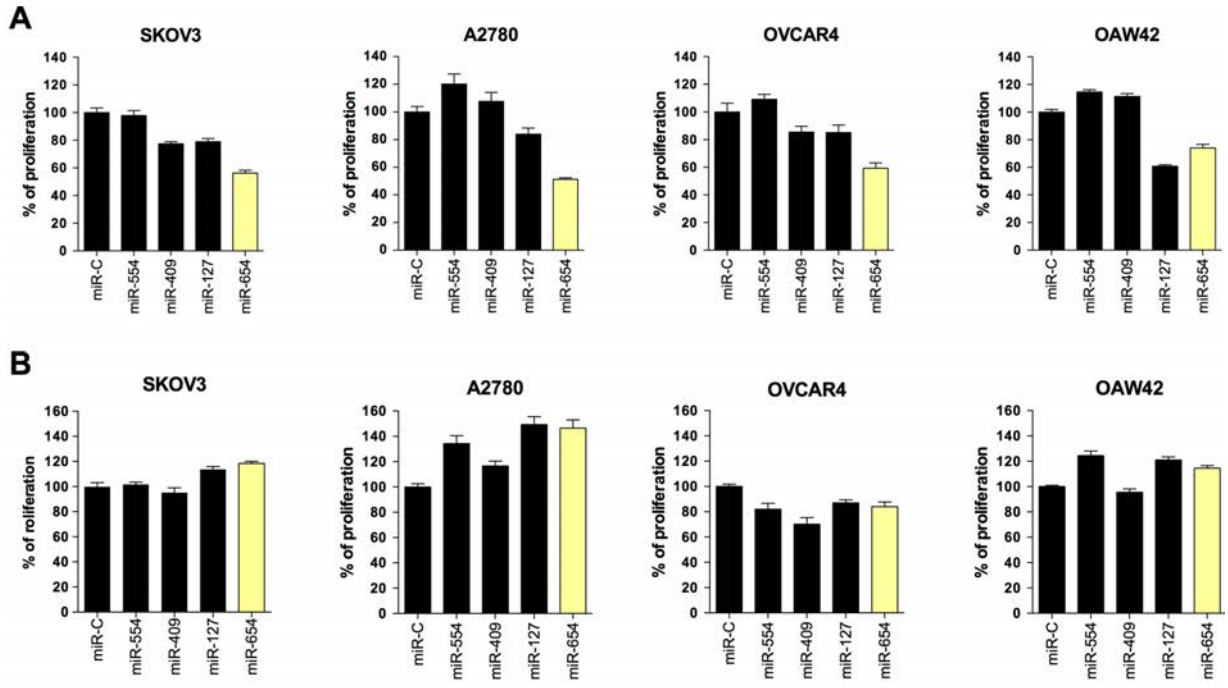

Figure 23: Modulation of the deregulated miRNAs in OC cell lines. A) miRNA mimics and **B)** antagomiRs were used to overexpress (A) and infraexpress (B) miRNA levels in 4 OC cell lines. For SKOV3 and A2780 cells the experiments using miRNA mimics were done in triplicate, while for OVCAR and OAW42 the average of two experiments is shown. Mean+SEM is plotted; *p<0.05; **p<0.01; ***p<0.001; ****p<0.0001.

4.2.3. MiR-654 levels were decreased in OC tumor samples

In order to confirm if miR-654 has indeed a role in OC initiation and progression, the expression levels of miR-654 were evaluated in benign ovaries (n=29) and tumoral samples (n=55) (Table 12). While miR-654 levels were increased in tumors form short- compared to long-SV advanced OC patients (Figure 22), in benign specimens miR-

654 levels were significantly higher than in overall tumoral samples (Figure 24A). This rather indicated a possible tumor suppressor role for miR-654 and it is in agreement with the reduced proliferation observed upon miR-654 overexpression (Figure 23A).

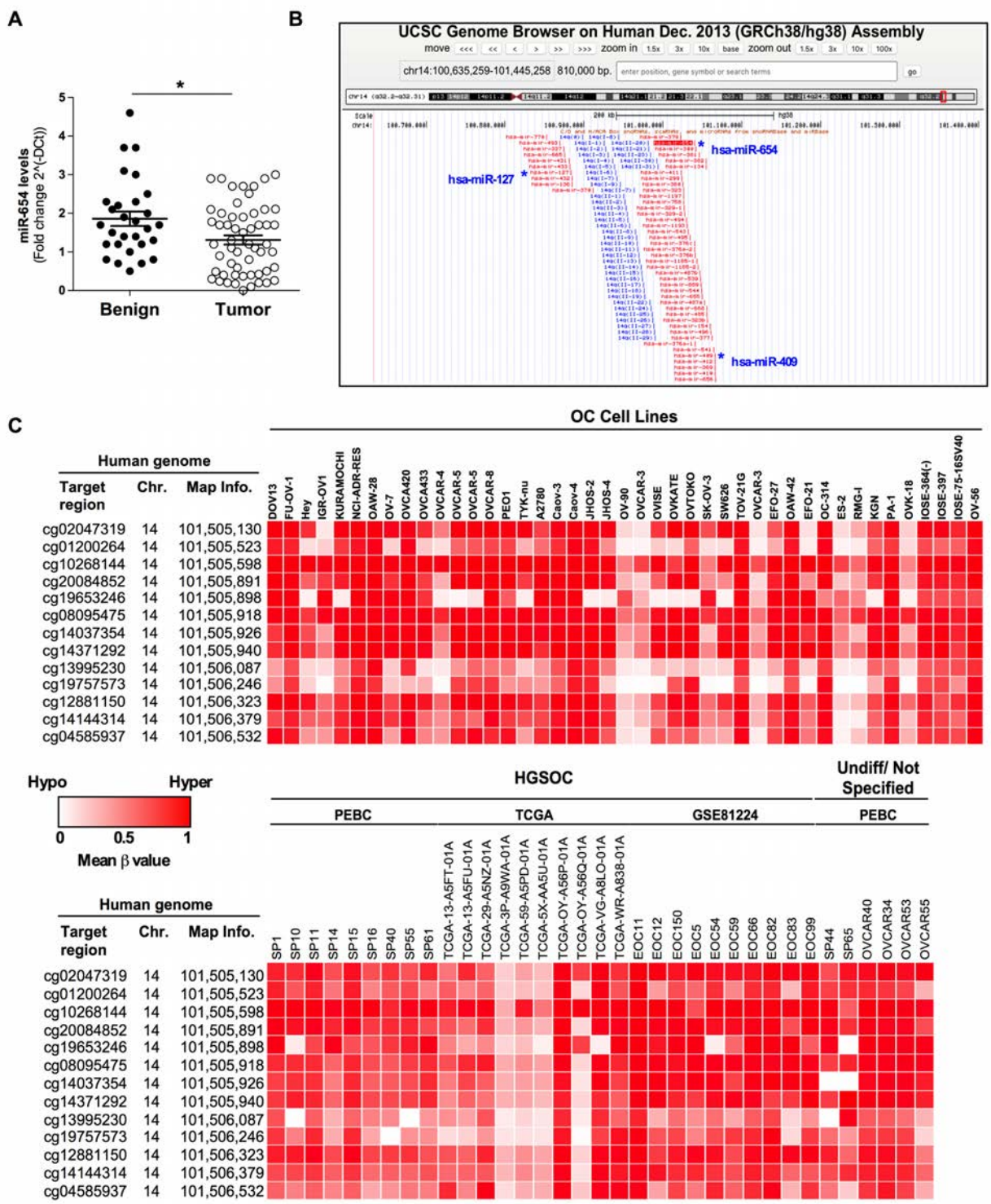

Figure 24: Decreased miR-654-5p expression and hypermethylation of its locus was found in OC. **A)** MiRNA levels in benign compared to tumoral ovaries. **B)** Chromosome 14 contained miR-654, miR-409 and miR-127 in the same region (q32.31). **C)** Methylation analysis of the CpG islands in the miR-654 locus in OC cell lines (top) and tumors (bottom).

To explore the possible mechanism by which miR-654 was reduced in tumors, an assembly analysis was performed. By using the UCSC Human Genome Browser (GRCh38/hg38, Dec. 2013) miR-654-5p was found to be located in chromosome 14, within the q32.31 chromosomal region (Figure 24B), a region frequently altered in cancer[249–251], including OC[199]. Using methylation data from the TCGA[15], GSE81224 dataset[31], GSE68379[234] and PEBC (unpublished) datasets, the methylation status of CpG islands within 14q32 was evaluated in OC cell lines (n=43) and ovarian tumors (n=35), and hypermethylation was found in 79% and an 89% of them, respectively (Figure 24C). This suggested that miR-654 levels could be decreased in OC due to hypermethylation of its locus.

In fact, miR-654 levels of A2780 and OAW28 (two of the OC cell lines that presented the region hypermethylated and expressed low levels of miR-654; Figure 25A), were higher upon treatment with the demethylase 5'AZA-2'-desoxycytidine when compared to untreated (C) cells (Figure 25B). This phenomenon was accompanied by increased levels of MEG3 (Chr.14), GBGT1 (Chr.9) and MAGE-A3 (Chr.X), genes that have been previously reported to be regulated epigenetically in OC through methylation status[252–254] (Figure 25C). Taken together, miR-654 levels were reduced in ovarian tumors possibly through the hypermethylation of the 14q32 locus.

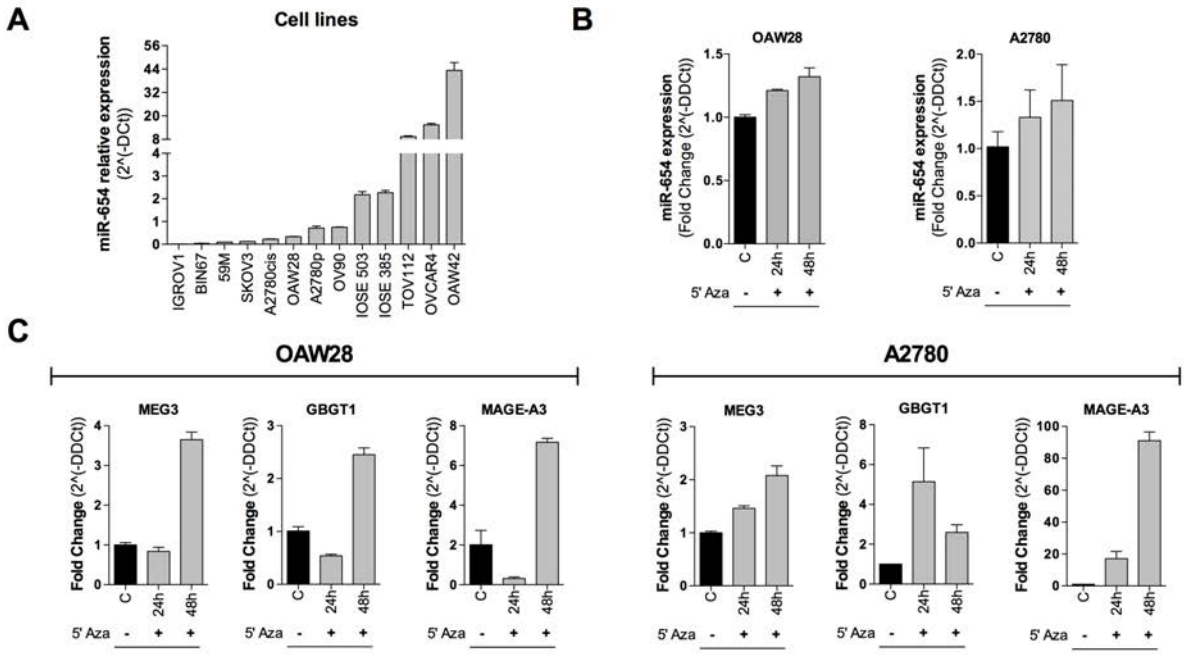

Figure 25: Epigenetic regulation of miR-654 in vitro. A) Levels of miR-654 in a panel of OC cell lines and IOSE cells, analyzed by RTqPCR. **B)** Levels of miR-654 upon treatment with the demethylase agent 5'AZA-2'-desoxycytidine over time in two cell lines that presented low miR-654 levels and high levels of hypermethylation. **C)** Levels of epigenetic-regulated genes MEG, GBGT1 and MAGE-A3 in two OC cell lines upon demethylating.

4.2.4. MiR-654 overexpression reduced cell proliferation and induced apoptotic cell death

SKOV3 and A2780p cell lines were chosen to further analyze the effects of miR-654 overexpression in cell viability in a time-course assay (Figure 26A and B). Fifty per cent reduction was already quantifiable at 72 and 96 h post-transfection in A2780 and SKOV3 cells, respectively (Figure 26B), with a visible decrease in cell density for both cell lines under optical microscope (Figure 26C). To further ascertain whether the effects of miR-654 overexpression in decreasing cell viability were due to an increase in cell death and/or a cell cycle arrest, the induction of apoptosis was firstly analyzed in four OC cell lines transfected with miR-654. The number of cells with condensed or fragmented chromatin (one of the hallmarks of apoptotic cell death) was found to be significantly increased upon miR-654 transfection in the four OC cell lines tested (Figure 26D, bottom images; and Figure 26E), while cells transfected with miR-Control displayed uniform patterns of chromatin staining (Figure 26D, top images; and Figure 26E). Furthermore, cell death was confirmed at molecular level by the marked cleavage of PARP-1 and Caspase-3 in SKOV3 and A2780 cell lines (Figure 26F).

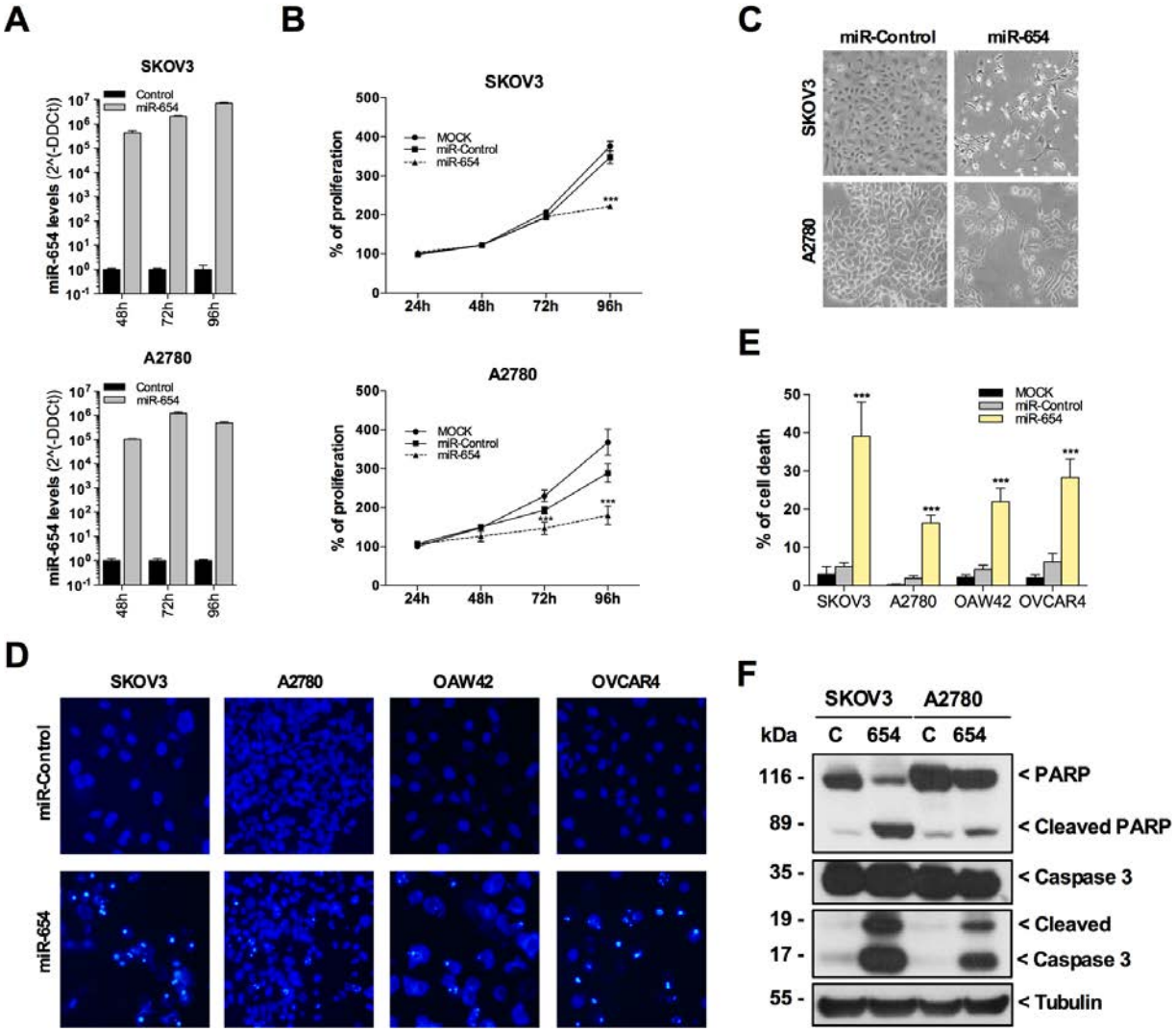

Figure 26: miR-654 reduced proliferation and induced apoptotic cell death. A) Levels of miR-654 at specific time points upon miR-654 over-expression. **B)** Time course proliferation assay (n=3 independent experiments). **C)** Representative phase contrast images of SKOV3 and A2780 cells at 96h post-transfection with miR-654 and miR-control. **D)** Representative images of Hoechst nuclear staining upon overexpression of miR-654. For SKOV3 and A2780 cells n=3 independent experiments, while for OVCAR and OAW42 the average of two experiments is shown. **E)** Quantification of D. **F)** Western Blot of PARP and Caspase-3 in SKOV3 and A2780 cells at 96h post-transfection with miR-654 and miR-control. Mean+SEM is plotted in B and E; *p<0.05; **p<0.01; ***p<0.001; ****p<0.0001.

Secondly, cell cycle analysis in a time-course assay was performed in SKOV3 and A2780 OC cell lines. An apoptotic pick appeared at 96h post-transfection n both OC cells lines (not shown), in agreement with the increased cell death observed upon miR-654 overexpression. In addition, a slight increase in the percentage of cells in G1 was found at different times in both cell lines (Figure 27), suggesting that overexpression of miR-654 caused an initial cell cycle delay that may add to the reduced proliferation observed. Taken together, miR-654 overexpression resulted in

decreased viability due to induced caspase-dependent apoptosis and reduced proliferation, accompanied by a modest cell cycle delay.

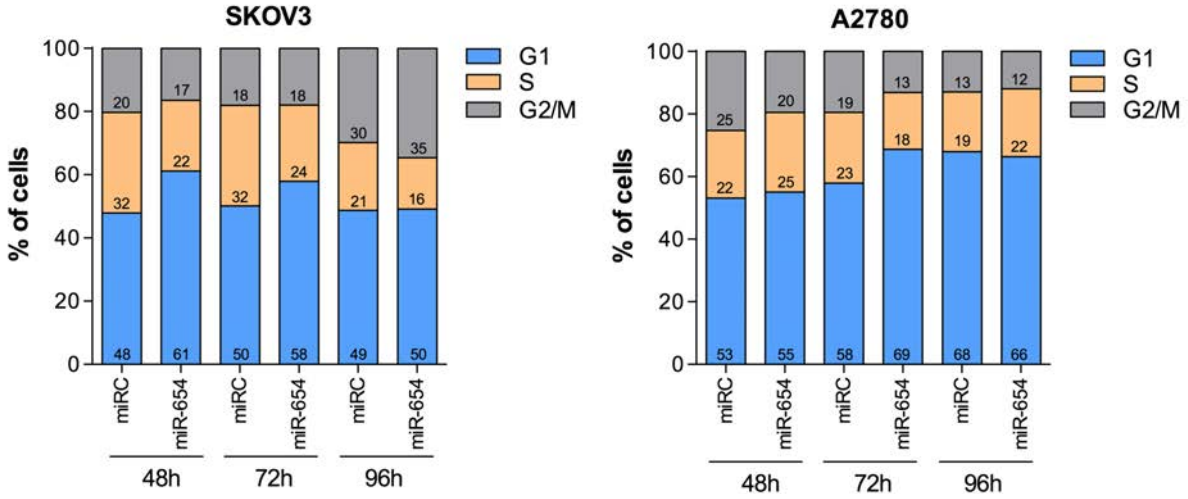

Figure 27: miR-654 overexpression caused a modest cell cycle delay. Cell cycle analysis over a time-course period in SKOV3 (left) and A2780 (right) cell lines transfected with miR-654 mimic.

4.2.5. MiR-654 overexpression impaired tumor growth *in vivo*

To enforce the therapeutic potential of miR-654 against OC, the effects of miR-654 overexpression were analyzed *in vivo.* Initially, pGIPZ-Control or pGIPZ-miR-654 stably transduced SKOV3 cells were established to perform the *in vivo* model. In these cells miR-654 overexpression was found 1.3 x 10^4 times higher in pGIPZ-miR-654 SKOV3 cells than in pGIPZ-Control ones (data not shown). However, no significant reduction in proliferation or increased apoptosis was observed in SKOV3 cells stably transduced with pGIPZ-miR-654 (data not shown). In addition, 50% of pGIPZ-Control or pGIPZ-miR-654 stably transduced SKOV3 cells were combined with 50% of non-GFP SKOV3 cells (parental cells) and let them grow together in the same culture plate in order to evaluate if miR-654 stably expression was inducing a delay in cell growth and, therefore, and advantage of parental cells to grow *in vitro*. FACS analysis was performed over a time-course period and revealed that pGIPZ-miR-654 SKOV3 cells did not give cell growth advantage to the parental cells (data not shown). This suggested that, in this model, pGIPZ-miR-654 stably expression in SKOV3 was not reproducing the results obtained by transiently overexpressing miR-654 *in vitro*.

Therefore, a transient model by overexpressing miR-654 in SKOV3 cells was designed for the *in vivo* experiment. To do that, SKOV3-Explanted (SKE) cells (see methods,

section 3.2.3) were transiently transfected with miR-654 and miR-Control and a portion of transfected cells was first used to monitor the levels of miR-654 by RTqPCR (Figure 28A), as well as to evaluate the effect of miR-654 on SKE cells *in vitro* (Figure 28B). After 24h of miR transfection, 2 x 10^6 viable SKE cells were injected in the flank of the mice (n=12/group), and mice were monitored as shown in Figure 28C. Eleven days post-injection, differences in tumor volume were already visible between miR-Control and miR-654 groups, with an average volume of 142.0 and 34.2 mm^3, respectively (Figure 28D). Moreover, the tumors detected in the miR-654 group did not progress or did so at a very low pace (Figure 28D), with 40% of the mice form the miR-654 group still not bearing tumors at day 8 while all mice bearing miR-Control transfected cells developed tumors (Figure 28E). All mice were sacrificed at day 25 and tumors were weighted and imaged. The excised tumors of the miR-654 group had significantly lower weight and were smaller in size compared with miR-Control tumors (Figure 28F and 28G, respectively).

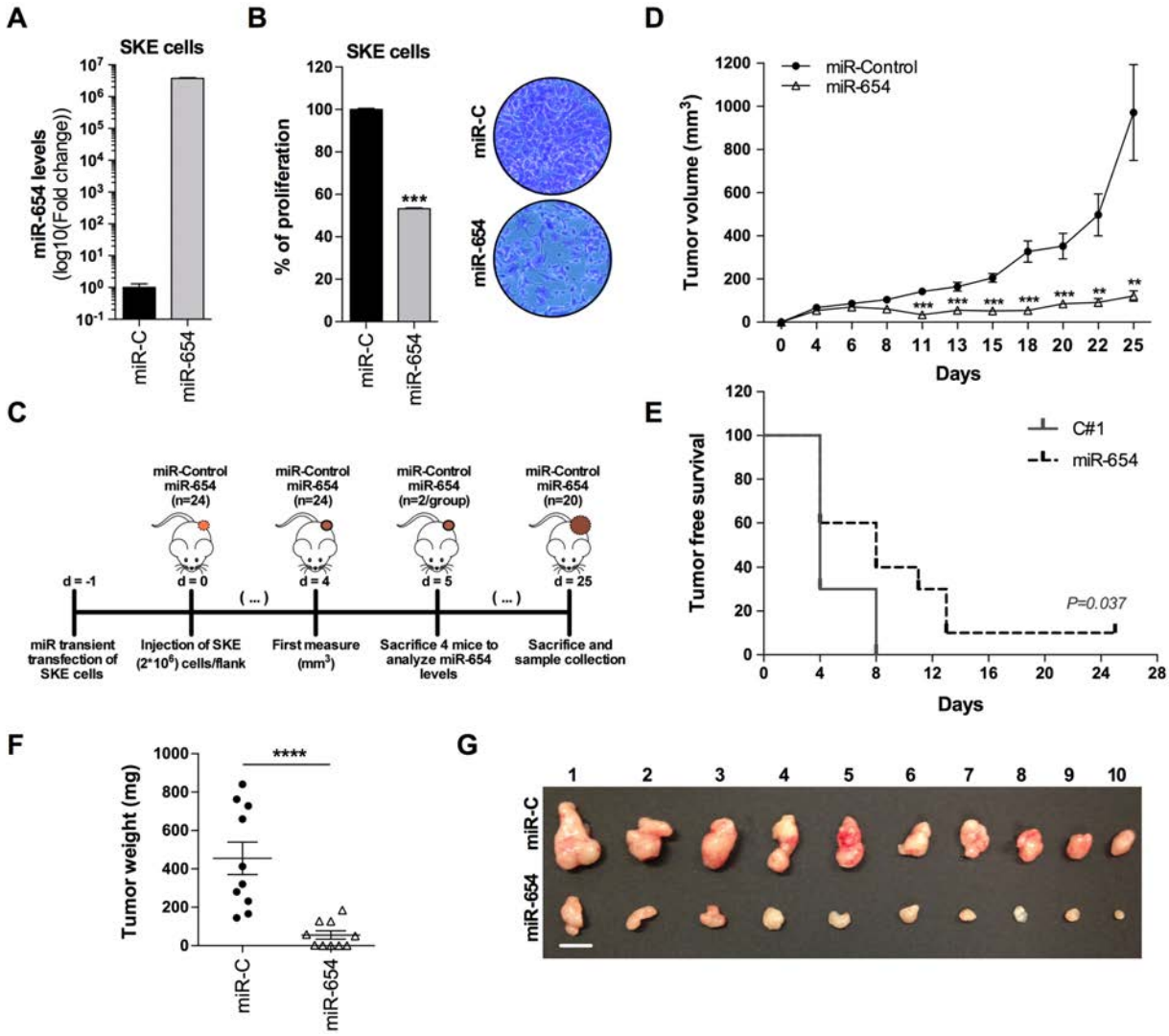

Figure 28: miR-654 reduced tumor growth *in vivo*. A) Levels of miR-654 analyzed by RTqPCR in SKE cells before mice injection. **B)** *In vitro* effect of a portion of transfected cells used for the *in vivo* model showing almost a 50% of reduction in proliferation (left), ***P<0.001. Representative images of the crystal violet assay used (right). **C)** Schematic representation of the *in vivo* model. **D)** Tumor volume of mice injected with either miR-Control or miR-654 transfected SKOV3 cells (n = 10/group), measured for 25 days. **P<0.01, ***P<0.001. **E)** Tumor-free survival curve of mice bearing OC xenografts transfected with miR-Control (continuous line) or miR-654 (dotted line). **F)** Average weight of resected tumors. ****P<0.0001. **G)** Macroscopic image of resected tumors at the conclusion of the experiment. Bar: 1 cm.

To test if miR-654 levels in tumors decreased over time, a result of the transient transfection, miR-654 levels were evaluated by RTqPCR in two mice per group that were sacrificed at 5 days post-injection and in the rest of tumors (n=20) at the end of the experiment (Figure 28C). MiR-654 levels prior injection and 5 days after injection were comparable (Figure 28A and Figure 29A). Interestingly, albeit with two lower orders of magnitude, tumors from the miR-654 group still expressed up to 10^4-10^5

more miR-654 than miR-Control tumors (Figure 29B). Strikingly, tumor volume inversely correlated with the remaining miR-654 levels within this mice group by 95% (r= -0.95, Figure 29C), with the highest miR-654 levels in the smallest tumor. Furthermore, tumor weight also inversely correlated with miR-654 levels by 86.19% (r= -0.8619, Figure 29D), resulting in a positive correlation between tumor volume and weight of 82.85% (r=0.8285, Figure 29E).

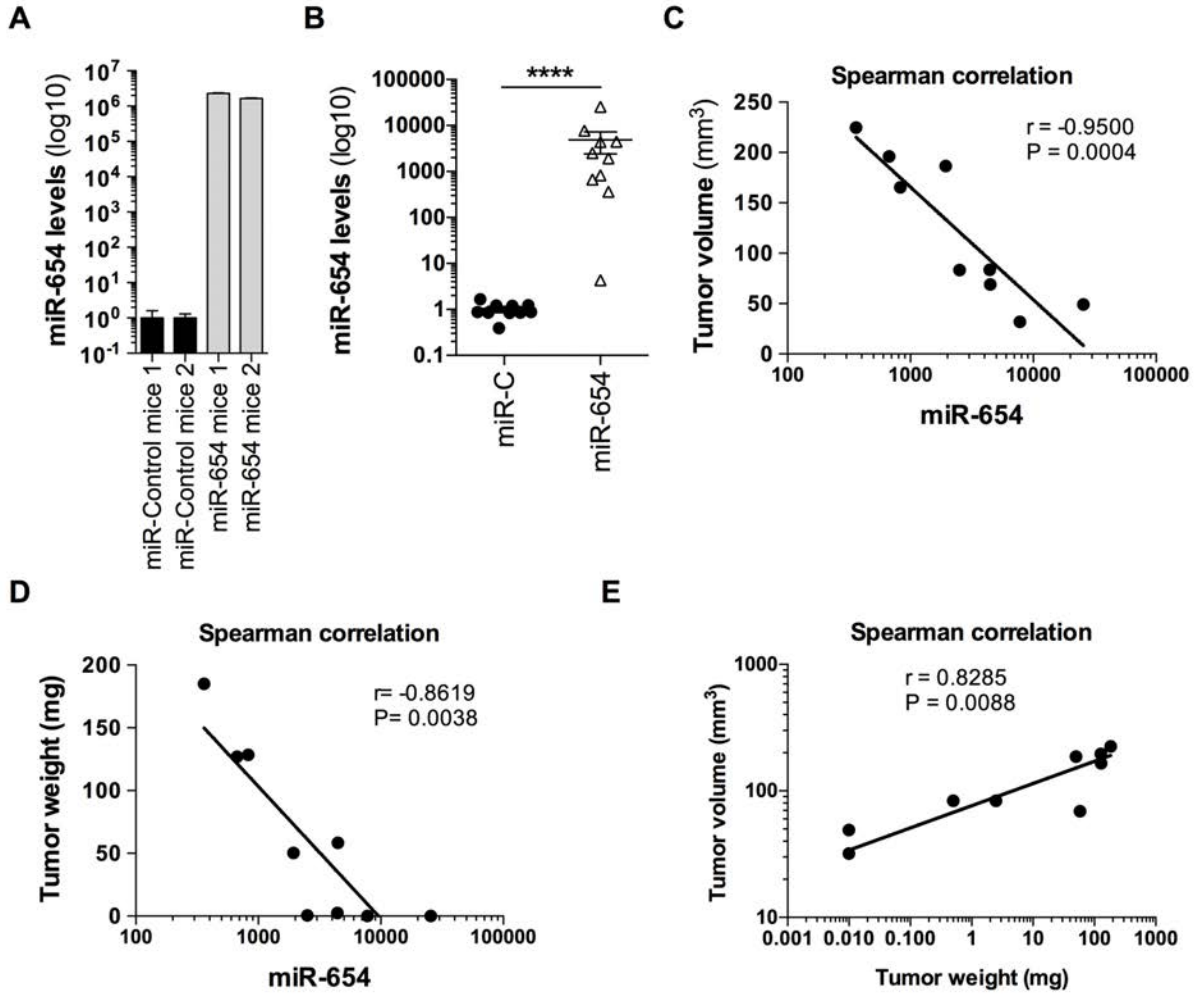

Figure 29: miR-654 levels were maintained *in vivo* and correlated with tumor volume and tumor weight. A) and **B)** Relative expression of miR-654 levels analyzed by RTqPCR in two mice per group and in 20 mice xenografts at the end-point of the experiment, respectively**. C)** and **D)** Spearman correlation between miR-654 levels and tumor volume or tumor weight of miR-654 mice group, respectively. **E)** Positive correlation between tumor volume and tumor weight of miR-654 mice group.

Immunohistochemical analysis of the tumors from the 4 mice sacrificed at day 5 revealed a decrease in the cellularity of the tumors and larger areas of collagen deposition upon miR-654 overexpression (Figure 30A). These phenotypes are reminiscent of the regressive cellular behavior commonly observed after chemotherapy, where the extracellular matrix (e.g. collagen) fuels the empty spaces left by death cells. Furthermore, upon miR-654 expression, not only the total number of tumoral cells was reduced in tumors at day 5, but also the percentage of Ki67 positive ones (Figure 30B). Together, these results show that ectopic expression of miR-654 reduced tumor growth of OC cells *in vivo*, inducing regressive changes at initial steps after the engraftment, and that these changes determined the fate of the tumors.

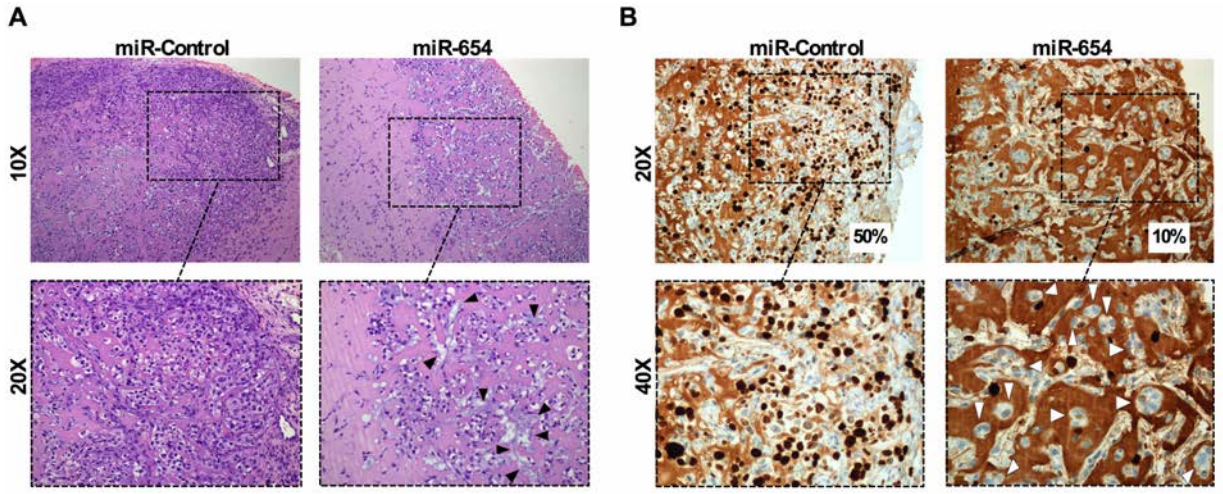

Figure 30: miR-654 levels were sustained after 5 days post-injection and cellularity of the xenografts was decreased upon miR-654. A) Representative microscopic hematoxylin and eosin (H&E)-stained images of OC xenografts. **B)** Representative microscopic Ki67 staining of the OC xenografts.

In addition, some tumors from miR-Control group invaded the dermis and muscle layer, while none of the miR-654 mice group did so (Figure 31A). Differences in cellularity and decreased percentage of Ki67 positive cells was still observed in tumors from the miR-654 group at the time of experiment completion (Figure 31B).

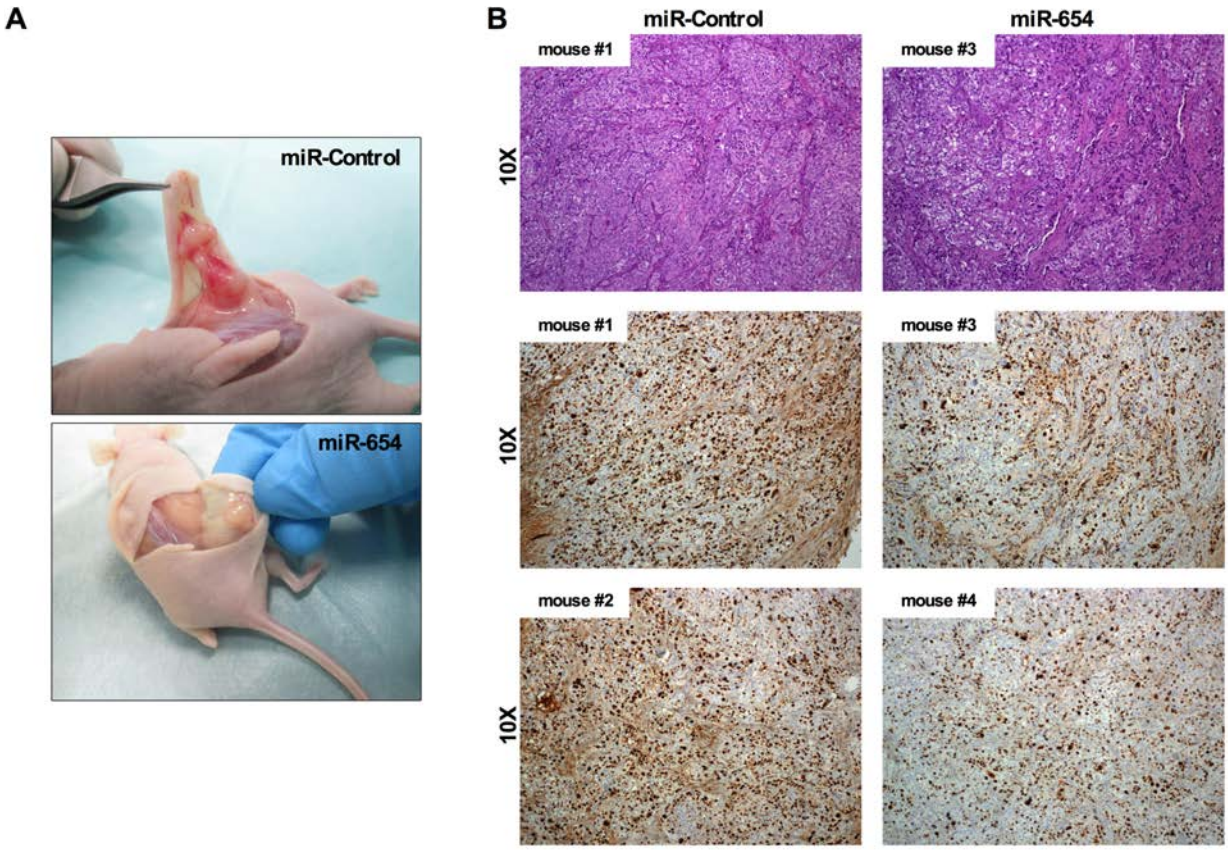

Figure 31: miR-654 overexpression reduced the tumor capability of invading the dermis. A) Macroscopic representative images of two mice from miR-Control (top) and miR-654 (bottom) group. **B)** Microscopic representative images of H&E and Ki67 staining of mice xenografts from miR-Control (left) and miR-654 (right) groups.

4.2.6. MiR-654 reduced spheres viability of patient-derived ascitic cells

In an attempt to get closer to the clinics, a pre-clinical *ex vivo* model was established. Patient-derived ascitic cells from four advanced OC patients were obtained from ascites collected at the time of the surgery (Table 14). Patient-derived ascitic cells were used to evaluate the therapeutic effect of overexpressing miR-654 in the sphere forming capacity and viability. In the four patients analyzed, miR-654 overexpression significantly reduced not only the number, but also the size of the spheres formed from patient-derived ascitic cells when grown under anchorage independent conditions in all cases (Figure 32A). In addition to the role of miR-654 in sphere formation, the viability of the remaining spheroids was evaluated. On one hand, spheroids were collected after 96h post-transfection and the cleavage of PARP-1 and Caspase-3 was evaluated by Western Blot. In agreement with the increased apoptosis seen upon miR-654 in clinically representative OC cell lines growing in monolayer, increased caspase-

dependent apoptosis was observed in spheroids transfected with the miR-654 from 3 patients-derived ascitic cells (Figure 32C). On the other hand, an MTS assay was also performed on spheroids from the same 3 patients and a significant reduction in cell viability (of around 50%) in all cases (Figure 32D). This suggested not only that the spheroid formation capacity was impaired by the ectopic expression of miR-654, but also that the remaining spheroids died due mechanisms governed by miR-654.

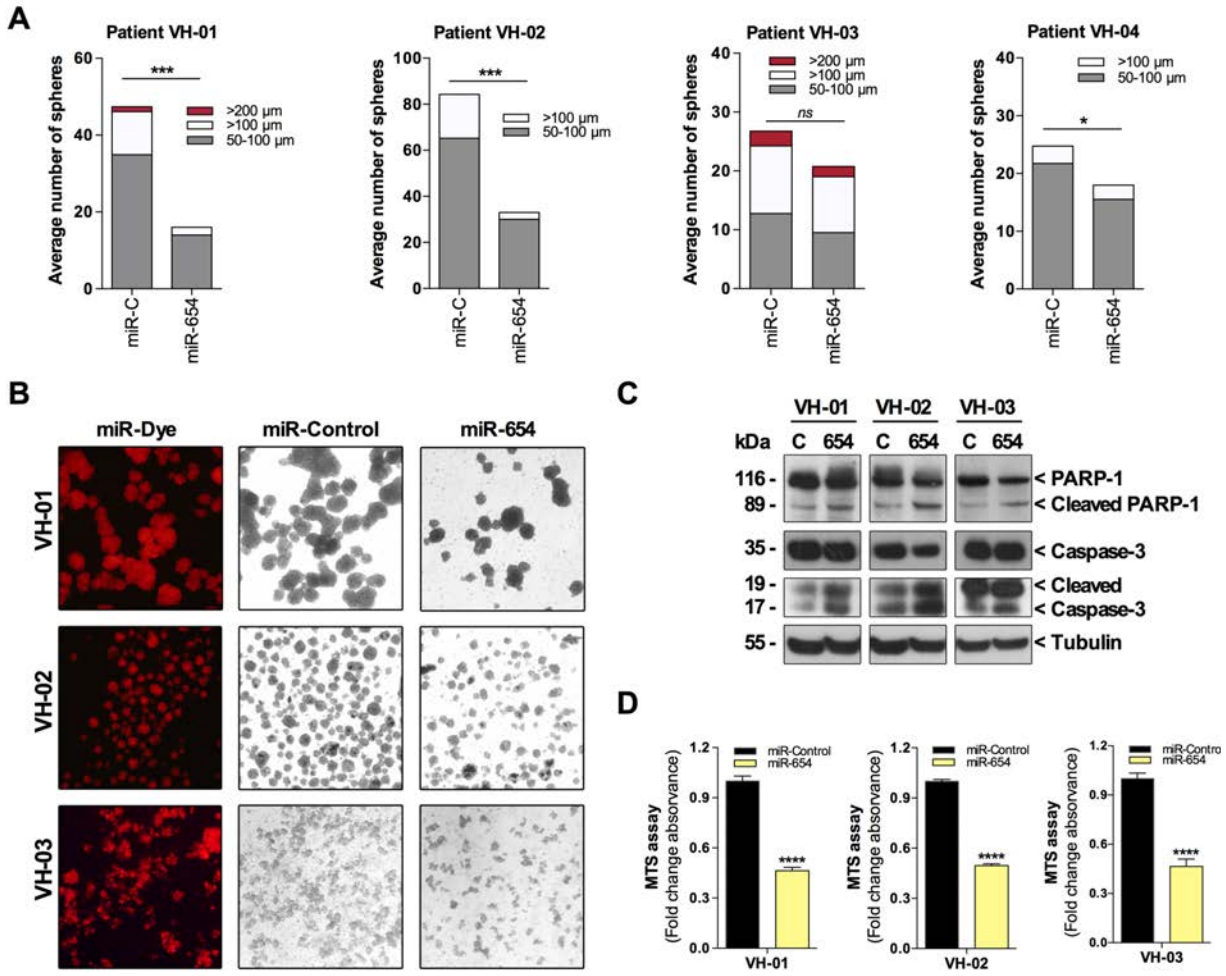

Figure 32: Ectopic expression of miR-654 reduced the number and viability of OC tumor spheroids from patient-derived ascitic cells. A) The number of spheres was scored after 96h post-transfection with miR-Control and miR-654 in 4 OC patient-derived ascitic cells grown under anchorage independent conditions and classified as in between 50-100 µm, ≥100 µm, and ≥200 µm in diameter. **B)** Representative microscopic images of the indicated ascitic primary cells used for the sphere forming capacity assay. The miRNA transfection control with Dy547 was used to monitor transfection in all patient-derived ascitic cells used. Spheres were used for protein extraction and Western Blot analysis with the indicated antibodies after 96h post-transfection with miR-Control and miR-654. **D)** Viability assay (MTS) was performed at 96h post-transfection with miR-Control or miR-654 in the indicated OC patient-derived ascitic cells cultured under anchorage independent conditions.

4.2.7. MiR-654 targeted multiple cancer-related genes involved in apoptosis, cell proliferation and survival pathways

In order to understand the molecular mechanisms that are regulated by miR-654 and that explain the observed phenotypes, its putative target genes were elucidated following the scheme shown in Figure 33A. First, a miRNA target analysis was conducted using the *in silico* platform *miRWalk2.0*[255]*.* A whole transcriptome 3'UTR search for miR-654 (-5p) binding revealed a list of 2302 putative target genes. This list was narrowed down to 46 putative target genes selecting only those predicted by at least 5 different algorithms (i.e. DIANAmT, miRanda, miRDB, miRWalk and Targetscan). Among them, 14 candidates were selected according to the miR-654 phenotype, and based on literature due to their implication in apoptosis, cell cycle, AKT and Wnt pathways and cancer-initiating cells, among other functions. The mRNA levels of these 14 genes were analyzed by RTqPCR to ascertain whether they were truly modulated by miR-654 in the OC context. The overexpression of miR-654 in SKOV3 and A2780 cells (Figure 33B) caused a reduction in the mRNA levels of several candidates (Figure 33C).

To further confirm whether the reduction in mRNA was followed by a decrease in protein levels, a Western Blot was performed at different time-points post-miR-654 transfection only on those potential targets that were downregulated at mRNA levels in both OC cell lines, and that a greater than 50% of reduction was obtained in at least one of the two cell lines (Figure 33C, red asterisks). Western Blot analysis showed that HAX1, RAB1B and CDCP1 protein levels decreased as early as 48h post-transfection in SKOV3 cells, while PLAGL2 started to decrease at 72h post-transfection, and PBX3 protein levels deceased at 96h post-transfection in SKOV3 cells (Figure 33D, left panel). HAX1 and RAB1B protein levels decreased already at 48h post-transfection in A2780 cells and PLAGL2 did so at 96h post-transfection. No reduction on protein levels were observed for CDCP1 and PBX3 genes, maybe due to the stability of the protein in A2780 cell line (Figure 33D, right panel).

Since all of the miR-654 putative targets were shown to be reduced in at least one cell line upon miR-654 overexpression, its direct binding was analyzed by a luciferase-reporter assay, to sought out if any of the 5 abovementioned candidates was directly modulated by miR-654. Luciferase-reporter vectors were engineered for all of the 5 candidates, within the same or in different vectors, depending on the candidate (Table

20). Each of the psiCHECK^{TM}-2-3'UTR vectors was co-transfected with miR-654 or miR-Control in HEK293T cells. Significant reduction in luciferase activity was observed upon miR-654 transfection for HAX1, RAB1B, CDCP1, PLAGL2 and PBX3 (Figure 33E), thereby indicating a direct modulation of these target genes by miR-654.

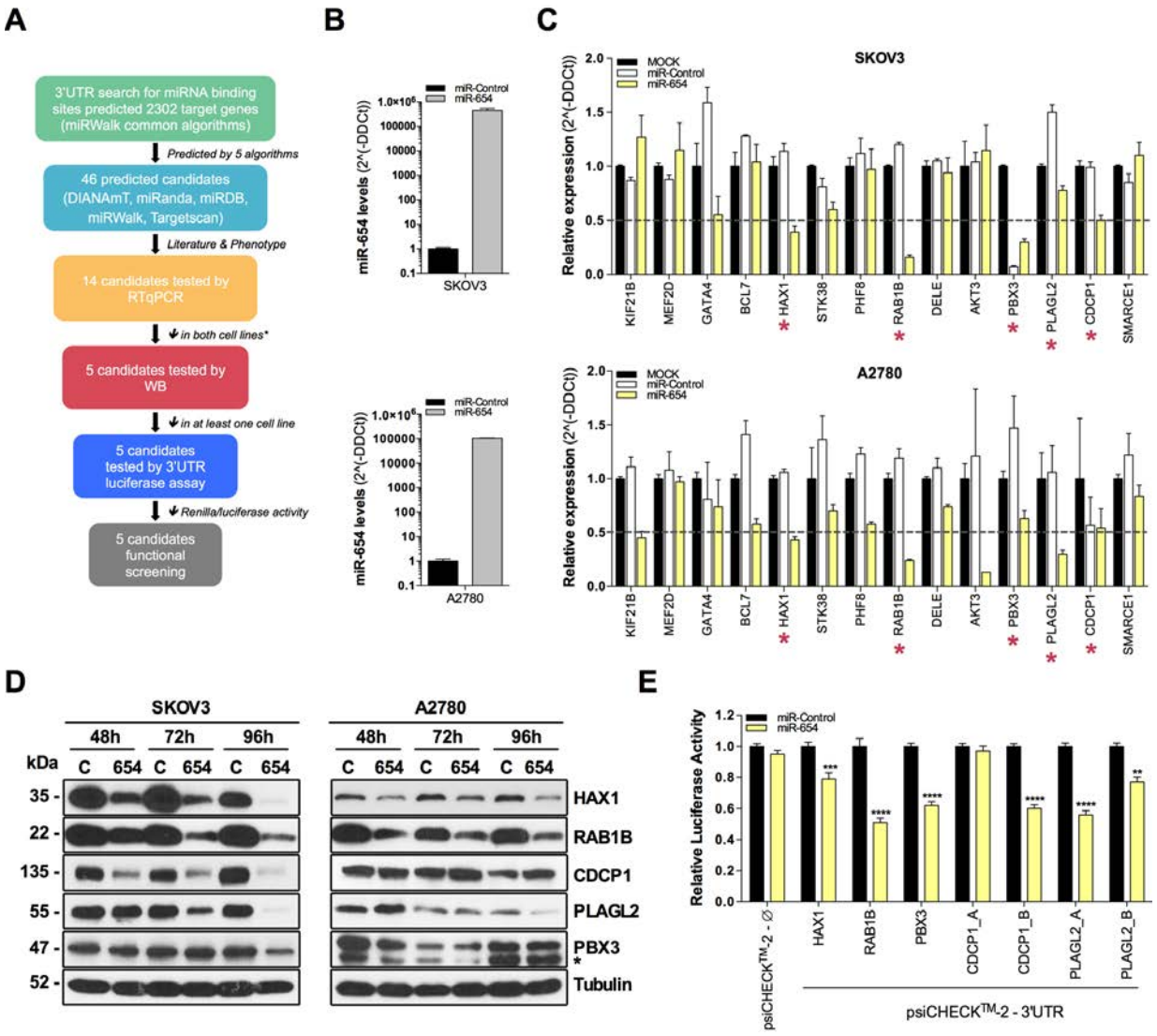

Figure 33: MiR-654 targeted multiple cancer-related genes involved in apoptosis, cell proliferation and survival pathways A) Schematic representation of the workflow followed to find miR-654 direct target genes**. B)** Confirmation of the miR-654 overexpression levels by RTqPCR in SKOV3 and A2780 cells at 48h post-transfection with miR-Control and miR-654. **C)** The expression of the indicated putative miR-654 target genes was determined by RTqPCR at 48h post-transfection of miR-654, miR-Control or MOCK-non-transfected SKOV3 (top panel) and A2780 (bottom panel) cells. Red asterisks point to the putative miR-654 targets that were selected for protein levels determination. **D)** Representative Western Blot for the indicated proteins at 48, 72 and 96 h post-transfection in SKOV3 (left panel) and A2780 (right panel) cells. Asterisk points at the specific band. **E)** Luciferase assay performed in HEK-293T cells co-transfected with the indicated luciferase-reporter vector and miR-654 or miR-Control. Data represented the mean ± SEM of three independent experiments (six replicates per experiment). **p<0.01 and ***p<0.001.

4.2.8. CDCP1 and PLAGL2 knockdown phenocopied miR-654 *in vitro*

In order to get deeper into the molecular mechanisms by which miR-654 acts through the 5 direct target genes, the expression of HAX1, RAB1B, CDCP1, PLAGL2 and PBX3 was knocked-down by siRNAs in SKOV3 cells (Figure 34A) and the effect on proliferation and cell death was assayed. Interestingly, CDCP1 and PLAGL2 silencing were the only ones that recapitulated the effects of miR-654 overexpression (Figure 34B). Likewise, CDCP1 and PLAGL2 knockdown significantly increased the percentage of apoptotic cell death comparably to miR-654 overexpression (Figure 34C and 34D).

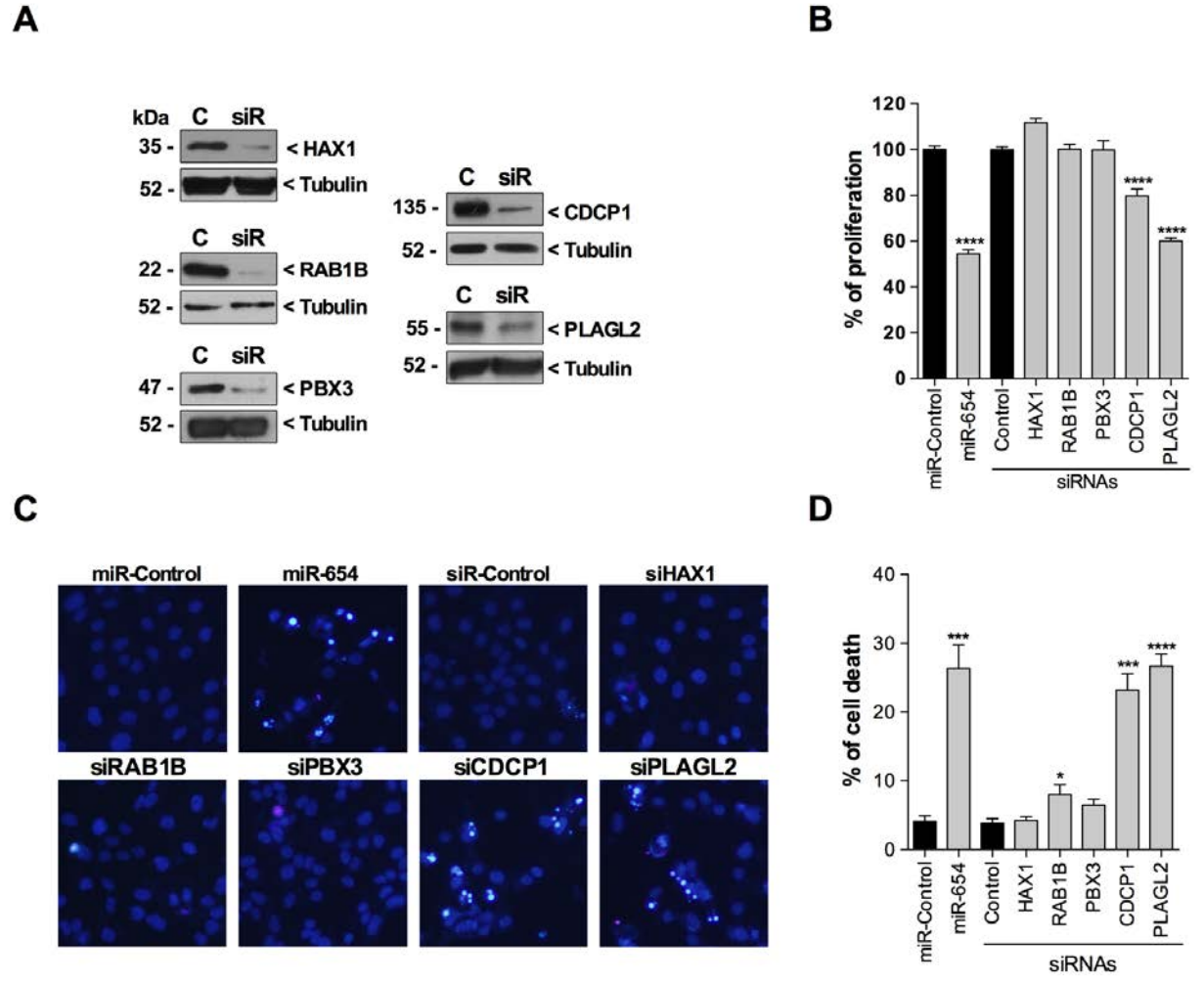

Figure 34: CDCP1 and PLAGL2 depletion reduced proliferation and increased apoptosis *in vitro*. **A)** Levels of the 5 direct target genes detected by Western Blot in SKOV3 cell line at 72h post-transfection with siR-Control or the corresponding siRNA for each of the target genes. **B)** Proliferation assay measured by crystal violet staining (n=6/condition, average of n=4 experiments ± SEM). **C)** Representative macroscopic images of the nuclear Hoechst staining in miR-Control, miR-654 overexpression, siR-Control or the corresponding siRNA for each of the target genes at 96h post-transfection of SKOV3 cell line. **D)** Quantification of C. *p<0.05, **p<0.01, ***p<0.001, ****p<0.0001; siR, siRNA: small interfering RNA.

In addition, the levels of the 5 confirmed direct targets were analyzed upon miR-654 overexpression in the 3D patient-derived ascitic cell model presented before, to confirm that these proteins (and their corresponding signaling pathways) are of clinical relevance. Notably, the levels of 3 out of the 5 direct miR-654 targets decreased upon miR-654 overexpression, including CDCP1, PLAGL2 and RAB1B (Figure 35A), thereby suggesting that they are the main mediators of miR-654 effects in this model.

To verify the potential role these three targets in OC progression, their levels were evaluated in human samples from benign ovaries and OC tissues (Table 12). CDCP1 (Figure 35B, left panel) and PLAGL2 (Figure 35B, mid panel) levels were found higher in OC samples compared to benign lesions, while RAB1B levels were similar between benign and tumoral tissues (Figure 35B, right panel). These findings supported the relevance of targeting CDCP1 and PLAGL2 by miR-654 in OC (Figure 34) and, furthermore, suggested a possible role for CDCP1 and PLAGL2 in OC tumorigenesis (Figure 35).

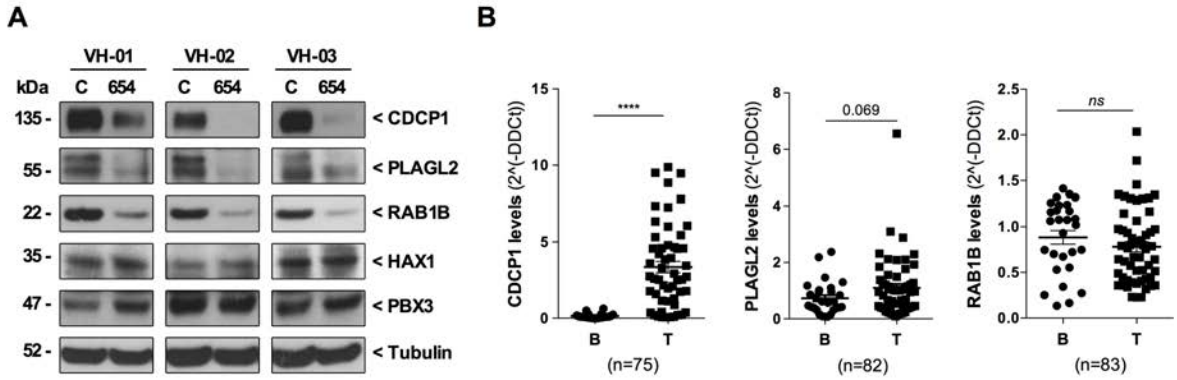

Figure 35: CDCP1 and PLAGL2 are relevant direct miR-654 targets in OC progression. A) Three patient-derived ascitic cells from OC patients cultured under anchorage independent conditions were transfected with miR-Control or miR-654 for 96h and used for Western Blot with the indicated antibodies. **B)** Levels of expression of CDCP1, PLAGL2 and RAB1B analyzed by RTqPCR in n=75, n=82 and n= 83, respectively. Number of samples varied between genes because outlier samples were excluded in the non-parametric statistical analysis. ****p<0.0001.

4.2.9. Microarray analysis revealed MYC and Wnt pathways deregulated in CDCP1 and PLAGL2-depleted cells and miR-654 overexpressing cells

The fact that (i) silencing of CDCP1 and PLAGL2 mimicked the effects observed *in vitro* by miR-654 overexpression; (ii) that the levels of these two direct targets were increased in OC tumors opposite to miR-654 expression; and (iii) that their levels were decreased in spheroids from ascites upon miR-654 overexpression; made to wonder

which downstream signaling pathways of miR-654 were regulated through these two genes. To do that, CDCP1 and PLAGL2 expression was silenced by siRNAs in SKOV3 cells (Figure 36A) and a whole transcriptome analysis was performed. Principal component analysis segregated samples on the basis of treatment (siControl versus siCDCP1 or siPLAGL2), indicating a consistent transcriptional impact of CDCP1 and PLAGL2 silencing (Figure 36B, top and Figure 36B, bottom, respectively). After CDCP1 knockdown, 268 genes were found to be downregulated whereas 148 genes were upregulated (FDR < 0.25, fold change > ± 1.5). For PLAGL2 knockdown, 437 genes were found to be downregulated while 270 were upregulated (FDR < 0.25, fold change > ± 1.5).

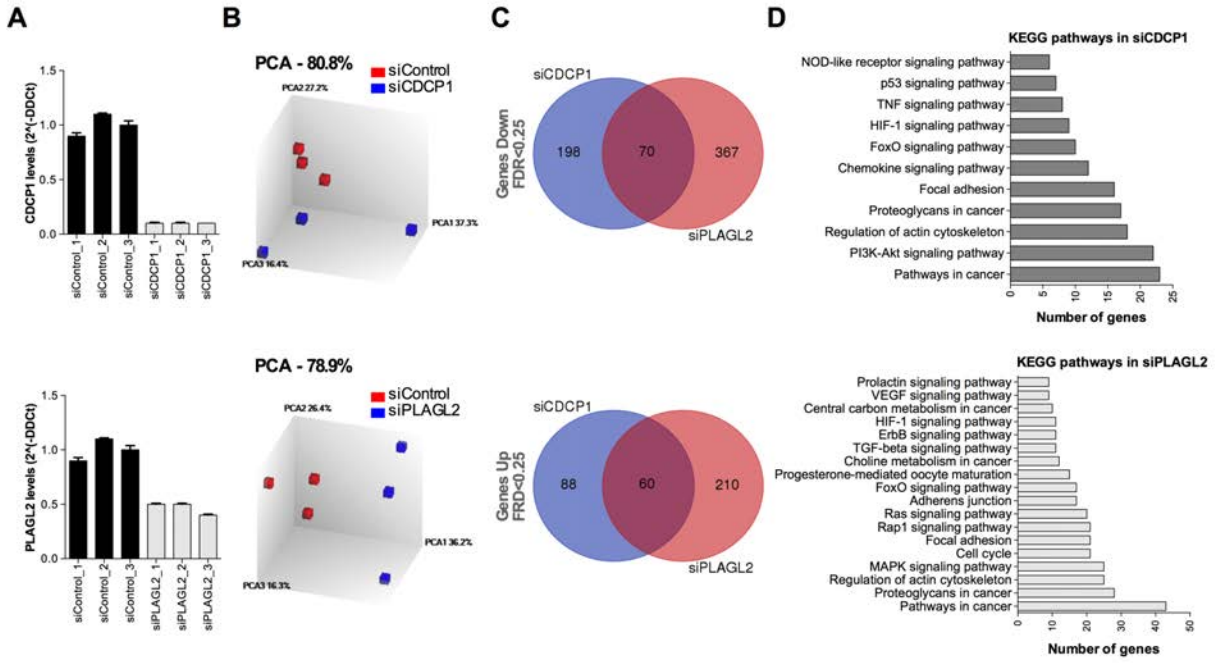

Figure 36: CDCP1 and PLAGL2 knockdown altered multiple pathways related to cancer. A) Levels of CDCP1 (top) and PLAGL2 (bottom) depletions analyzed by RTqPCR before microarray analysis was performed (n=3/condition). **B)** Principal component analysis performed by TAC software showed segregation of distinct expression profiles for the siCDCP1 and siPLAGL2 and the siControl group. **C)** Venn diagram using downregulated (top) and upregulated (bottom) genes upon CDCP1 and PLAGL2 silencing compared to siControl (FDR < 0.05 and fold change > **±** 1.5). **D)** KEGG pathway analysis using DAVID bioinformatic microarray analysis tool using differentially expressed genes with FDR < 0.25 from CDCP1 (top) and PLAGL2 (bottom) depletions compared to siControl.

A Venn diagram analysis showed that 70 genes were downregulated by both CDCP1 and PLAGL2 depletions, while 60 genes were upregulated when CDCP1 and PLAGL2 were silenced (Figure 36C), suggesting that part of the transcriptional changes concomitantly occurred in both gene depletion conditions. Functional annotation using

DAVID bioinformatic tools confirmed that CDCP1 and PLAGL2 depletion impacted on the expression of a significant number of genes associated to canonical pathways in cancer such as PI3K-AKT, MAPK and HIF-1 signaling pathways among others (Figure 36D, > 10 genes and $p < 0.05$). GO term analysis was also found significantly enriched for cellular growth, proliferation and apoptotic processes in both CDCP1 and PLAGL2 depletions (data not shown).

Furthermore, GSEA was performed for both CDCP1 and PLAGL2 depleted transcriptomes. Firstly, major gene sets collections were used to perform the analysis, resulting in a vast number of enriched gene sets for both gene conditions (Figure 37A). To focus on the main altered functions, gene sets related to apoptosis, HIF-1, focal adhesion, WNT/βcat, MYC, actin cytoskeleton, MAPK, AKT, FoxO, Proteoglycan in cancer and angiogenesis were used for the GSEA according to the functions found in the KEGG analysis (Figure 36D) and the relevant enriched gene sets found in the first GSEA (Figure 37A). Both CDCP1 and PLAGL2 knockdown significantly influenced on a high number of gene sets related to apoptosis and hypoxia (Figure 37B and Figure 38). Interestingly, MYC, WNT/βcat, MAPK and AKT signaling pathways appeared to be enriched in both siRNA-silencing conditions, among others (Figure 37B and Figure 38).

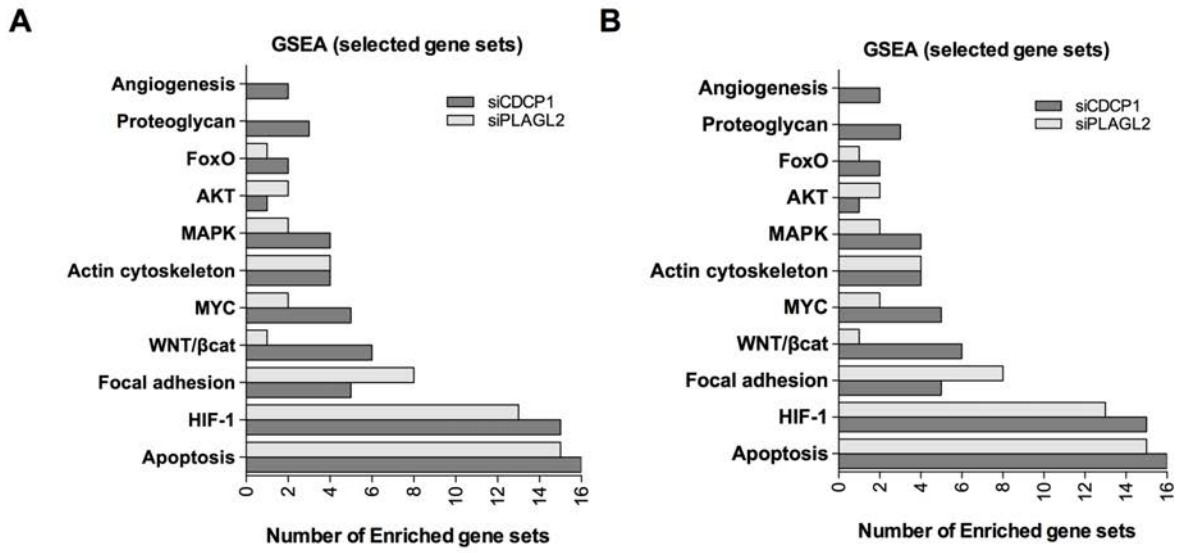

Figure 37: Gene set enrichment analysis. A) Major collections from Hallmarks, KEGG pathways, OS (oncogenic signatures), CP (canonical pathways), CGP (chemical and genetic perturbations) and GO gene sets were downloaded from MSigDB.v6 and used for GSEA. Total number of enriched gene sets with FDR < 0.25 or p< 0.05 were plotted regarding each collection. **B)** Gene sets related to the indicated processes were downloaded form MSigDB.v6 and used for GSEA. Total number of enriched gene sets with FDR < 0.25 or p< 0.05 were plotted regarding each collection.

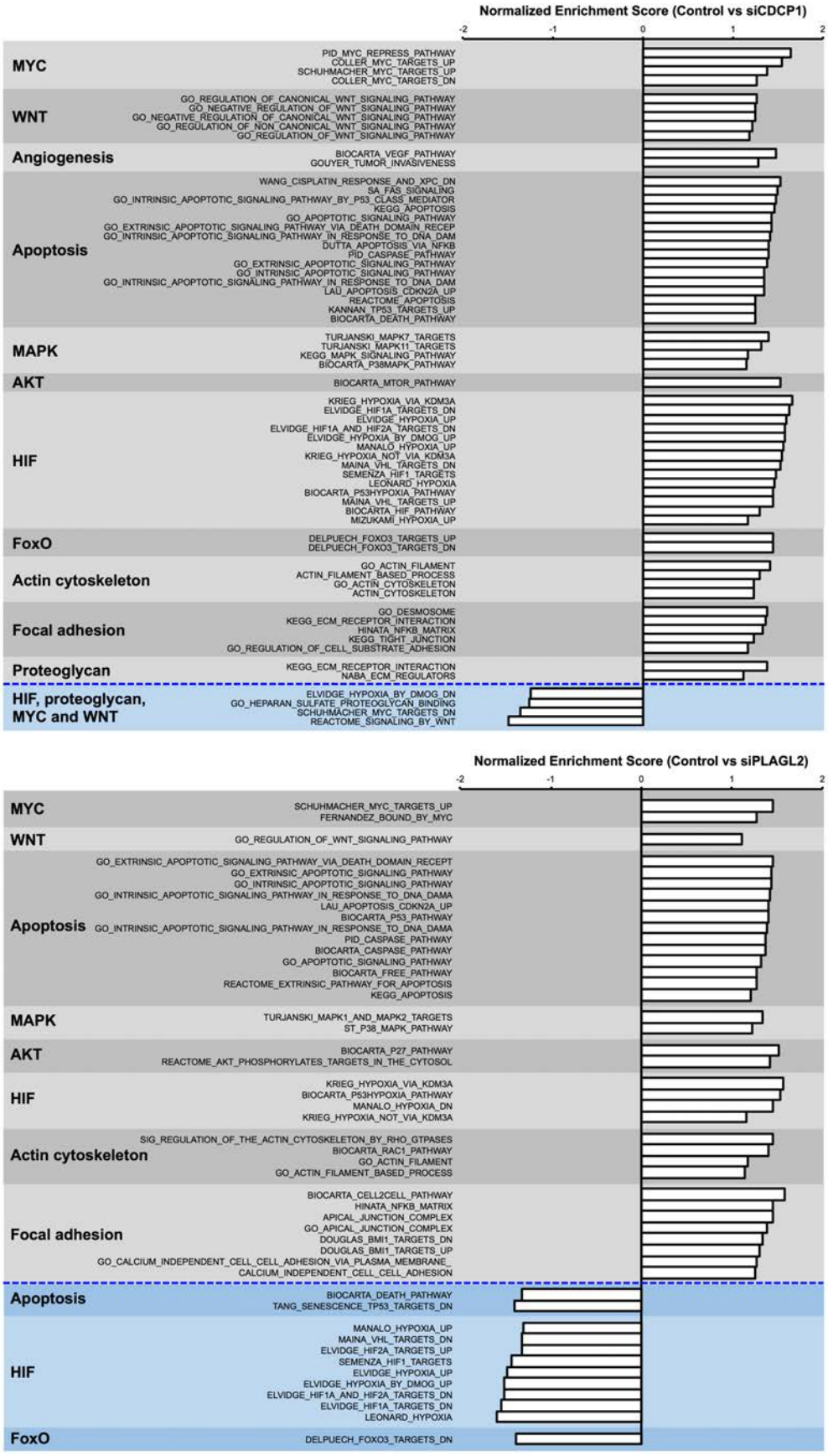

Figure 38: Plot list of enriched gene sets upon CDCP1 and PLAGL2 depletion. Enriched gene sets were plotted regarding normalized enriched score (NES) values, and FDR < 0.25 or p < 0.05 gene sets were included. CDCP1 (top) and PLAGL2 (bottom) enriched gene sets were plotted.

Notably, several processes were commonly altered by CDCP1 and PLAGL2 knockdown (Figure 38). The gene lists of CDCP1 and PLAGL2 silenced transcriptomes (FDR < 0.25 and fold change > ± 1.5) were collapsed with the enriched gene sets for each process (e.g. apoptosis) and heatmaps were generated. Figure 39A showed that many genes related to apoptosis and hypoxia were deregulated upon CDCP1 and/or PLAGL2 depletion. Thus, altered expression of many significant genes related to apoptosis and hypoxia gene sets were found enriched for both CDCP1 and PLAGL2 downregulation (Figure 39B).

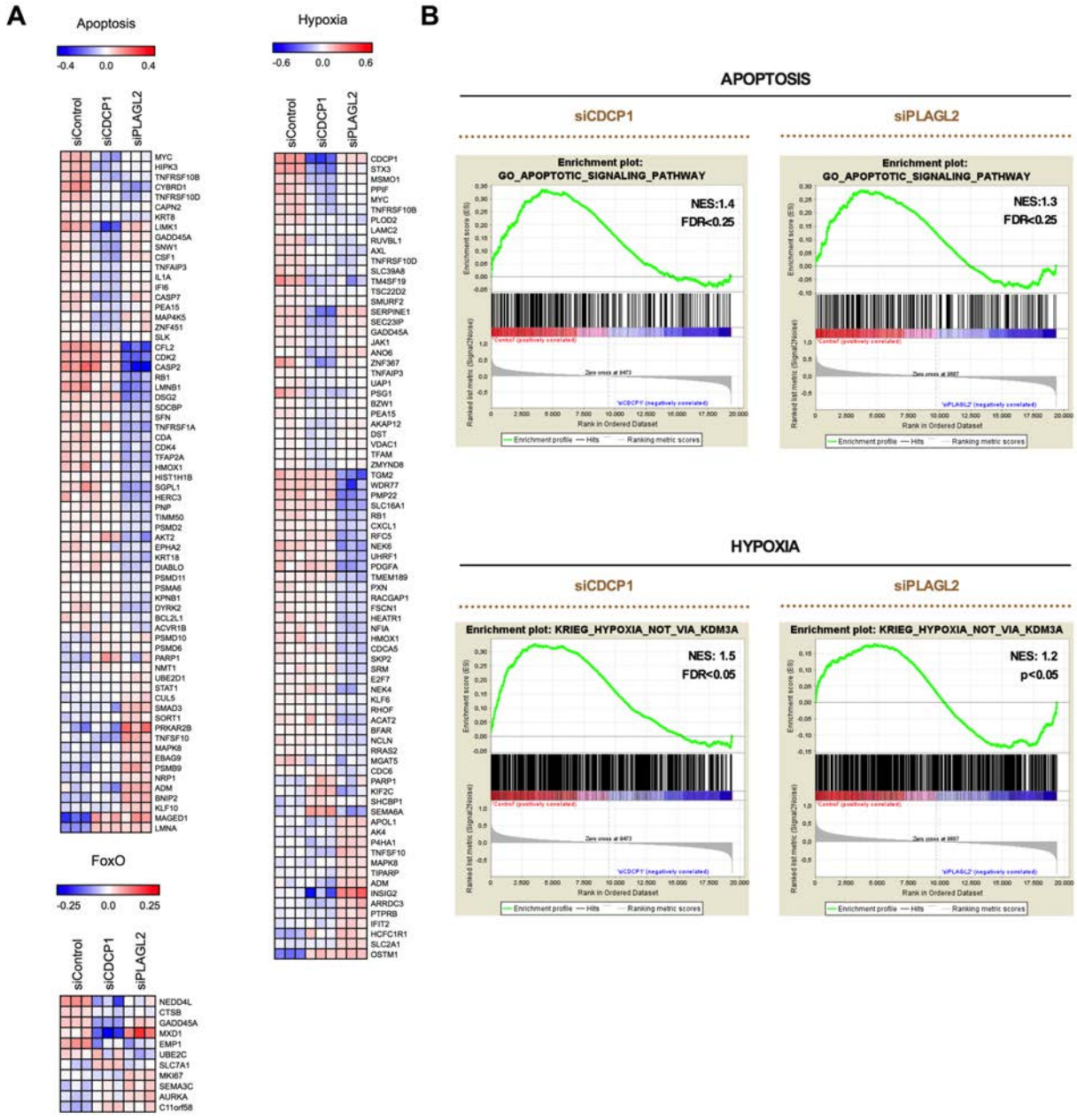

Figure 39: CDCP1 and PLAGL2 knockdown induced changes in apoptosis and hypoxia. A) Heatmap depicting significant genes with FDR < 0.25 and fold change > **±** 1.5 (apoptosis) and > **±**2 (for hypoxia) found in the collapsed gene lists of the enriched gene sets. **B)** Representative GSEA curves for significant enriched gene sets in CDCP1 and PLAGL2 silencing conditions compared to siControl.

In addition to hypoxia and cell death, several enriched gene sets related to MYC, WNT/βcat, MAPK, and AKT pathways were found in both CDCP1 and PLAGL2 depletions (Figure 38). Collapsed gene lists from the enriched gene sets regarding each pathway were used for heatmaps generation, showing only significant DE genes upon CDCP1 and PLAGL2 depletion (Figure 40A). Interestingly, MYC mRNA levels appeared downregulated by both CDCP1 and PLAGL2 depletions (Figure 40A, top left), as well as several regulators of the Wnt/βcat pathway such SMURF2 and DKK1 (Figure 40A, top right). Additionally, several cyclin-dependent kinases (CDKs) such as CDK2 and CDK4 diminished upon PLAGL2 depletion (Figure 40A), as well as the levels of AKT2 and Rb (Figure 40A, bottom), thus suggesting that reduction of the expression of these genes might be contributing to miR-654 effects on cell survival signaling. Representative GSEA curves of MYC and Wnt pathways are shown (Figure 40B).

Following the hypothesis that some of the miR-654 phenotypic effects are through the reduction of CDCP1 and PLAGL2 levels in OC, the levels of MYC, p-AKT, CDK2/4, RB and pRB were analyzed in SKOV3 upon overexpression of miR-654. Indeed, a reduction of MYC was observed upon miR-654 overexpression in SKOV3 cells (Figure 40C), as well as for CDK2 and CDK4 (Figure 40C) confirming the expected molecular events of a reduction in the cell cycle progression. In addition, reduced levels of p-AKT and p-Rb were also observed upon miR-654 overexpression, thereby indicating a diminished activity of survival pathways (Figure 40C).

Currently, it is still under investigation the particular contributions of the relevant direct miR-654 targets (CDCP1 and PLAGL2), by exploiting the influence of the miR-654 on the pathways found in the microarray analysis. For that, the pre-clinical model of patients-derived ascites presented throughout the study is currently used to validate some of the molecular determinants of MYC, WNT/βcat, MAPK, and AKT pathways, in order to illustrate the downstream signaling of miR-654 as a potential therapeutic strategy for OC. Eventually, by establishing an intraperitoneal *in vivo* model using patient-derived ascitic cells, and using inhibitors of these pathways and/or systemic delivery of the miR-654, might prove the therapeutic effect of miR-654 in a closer context to the clinics of OC.

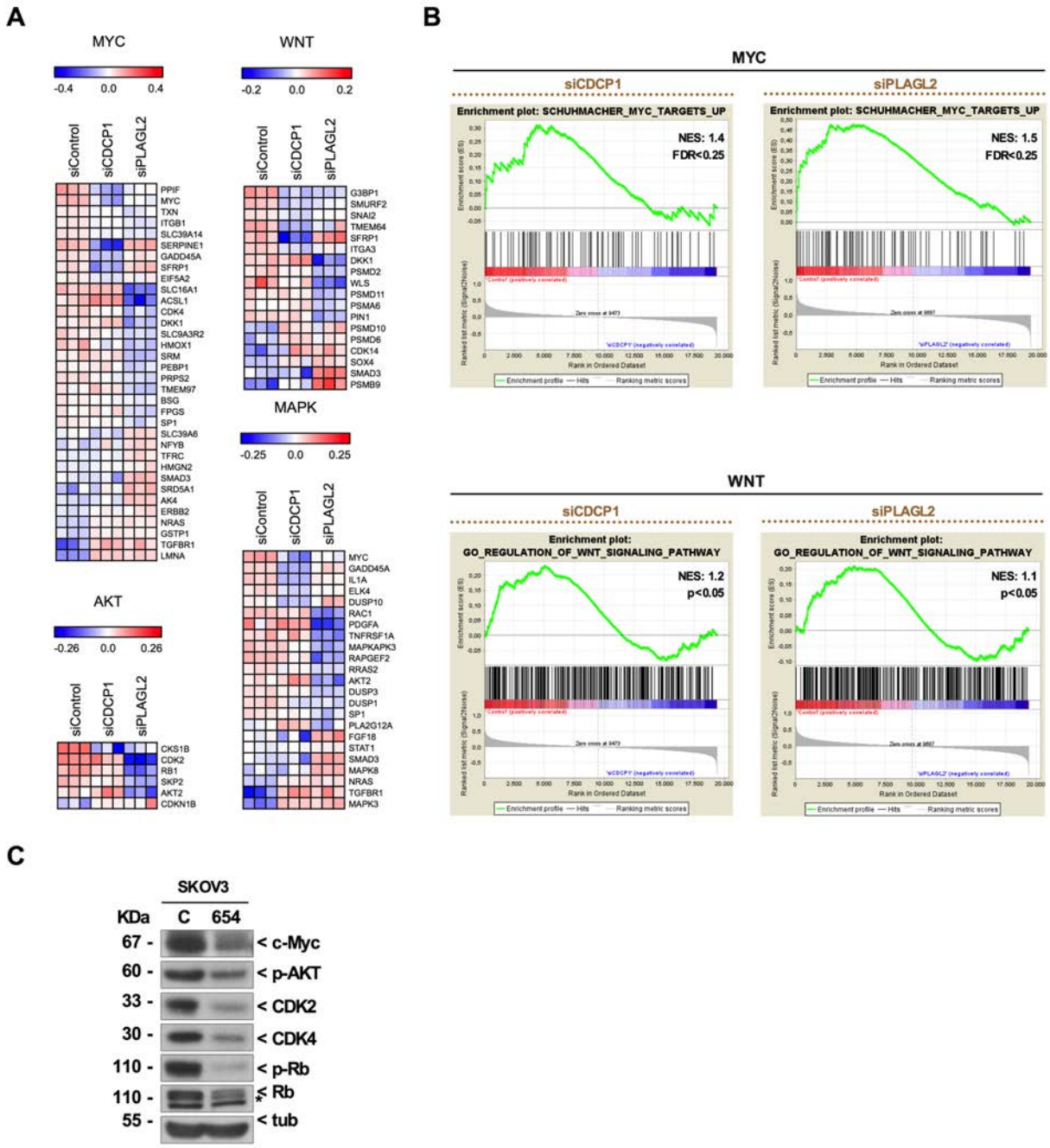

Figure 40: CDCP1 and PLAGL2 silencing reduced MYC, Wnt/βcat, AKT, Rb and CDKs pathways. **A)** Heatmap depicting significant genes with FDR < 0.25 and fold change > ± 1.5 found in the collapsed gene lists of the enriched gene sets for each pathway. **B)** Representative GSEA curves for significant enriched gene sets in CDCP1 and PLAGL2 silencing conditions compared to siControl. **C)** Western Blots of the indicated proteins to verify the alteration in MYC, AKT, Rb and CDKs signaling upon miR-654 overexpression in SKOV3 cell line (96h post-transfection). Tubulin was used as a loading control

5. DISCUSSION

5.1. MIRNAS IN SALIVA AS A DIAGNOSTIC TOOL

5.1.1. Saliva as a source; some considerations

The early diagnosis of OC is crucial to reduce the high mortality rate of this disease. However, early stage OC often causes no apparent severe symptoms, and there are no screening methods to detect the tumor when it is still confined to the ovary, stage of the disease progression in which OC is known as “silent disease”. Thus, the detection of molecular alterations from a liquid biopsy that reflect the initial disease through a non-invasive method is the gold standard to improve OC diagnosis and survival.

Over the last years, most of the studies investigating serum biomarkers other than CA-125 for early OC detection have shown promising results early on, but only no one has proven its value as useful screening test. In this regard, saliva is a highly desirable body fluid for biomarker development in the clinics, constituting a non-invasive, simple and low-cost source for cancer diagnosis tests. Indeed, “early detection of dozens of diseases from a saliva sample” has been addressed as one of the so-called Grand Challenges of the 21st century in President Barack Obama’s Strategy for American Innovation[256,257].

In the last decade, the potential use of salivary mRNA has been demonstrated for detecting various local and systemic diseases including oral cancer[104,105], lung[117,119], pancreatic[121,122] and breast[125] cancers, and only more recently, ncRNAs have also been emerged as putative salivary biomarkers for detecting systemic diseases[133]. In particular for miRNAs, a class of small ncRNAs, increased levels have been found in saliva from colon (miR-21)[258], prostate (miR-21 and miR-141)[259] and pancreatic (miR-17, miR-21, miR-181b and miR-196a[260]; miR-940[261]; miR-21[262]; miR-1246 and miR-4644[263]) cancers.

MiRNAs are stable in circulation and are protected from RNase degradation either by forming ribonucleoproteins complexes or by being contained in extracellular vesicles (EVs)[203,206]. Although salivary miRNAs can provide precise information that could lead to early cancer diagnosis, it is not fully understood how (if so) they arrive to the saliva

in the case that they come directly from the primary tumor, or if miRNAs are solely secreted by the salivary glands or other cells in circulation in response to the presence of a distant tumor to the oral cavity. In support of the latter, there is an *in vitro* model that was used to show that tumor-derived EVs interact with cells of the salivary glands changing the composition of their secretions[264]. However, there are several animal models from melanoma, lung and pancreatic cancer that supported that EVs carry, drive, and deliver tumor markers into the saliva[117,122]. Notably, saliva from mice with pancreatic cancer xenografts showed a molecular signature distinct from the non-tumor bearing mice, that was abolished upon impairment of the exosome biogenesis pathway, in support with the theory that salivary biomarkers arise in the primary tumor and reach saliva travelling through the circulation[122].

In our study, the sequencing of saliva was performed on salivary exRNA from CFS (cell-free saliva) and, despite (i) there was no sub-fractionation between miRNAs contained in EVs or free-miRNAs, (ii) the low RNA abundance, (iii) the small sample volumes and (iv) the highly fragmented RNA, downstream RNA sequencing assays was performed successfully, following the established procedures[87]. Noticeably, salivary exRNAs need different processing methods from other biofluids and the our findings demonstrated that rRNA contamination, which for most biofluids would be presumed to be of cellular origin, was likely due to the high bacterial load in saliva[265].

Although intact prokaryotic peaks were not observed in any of the saliva samples included in the study, an average of 36% of alignment was obtained for the human genome, in accordance with previously published data[244], suggesting that no intact rRNA but maybe free-rRNA (aroused from bacterial lysates and RNAse degradation) were included in the library generation, which reduced the percentage of human alignment. Hereafter, there are two things to take into consideration. On the one hand, when trying to introduce a rRNA removal step before library generation, a big loss of the relative amounts of several human mRNA, miRNAs and piRNAs in the rRNA depleted saliva samples was observed compared to the non-depleted samples[265]. This suggested that a deeper analysis during the sequencing process was achieved in favor of detecting low abundance RNA molecules and higher number of detected genes, but an important amount of human coding and non-coding transcripts were lost by bacterial rRNA removal procedures. Therefore, while for profiling of human salivary coding and non-coding exRNA the bacterial rRNA removal would be recommended,

for biomarker discovery, rRNA removal would introduce a big bias in the quantification of DE transcripts as putative biomarkers (at least in the conditions tested), and was not included in the present study. In addition, the inclusion of the rRNA removal step for clinical applications will not be feasible in hoping for an easy-to-use quick RTqPCR-basted test. As note of interest and although in this study has not been evaluated yet, possible changes in the oral microbiota could be associated to the presence of OC, since it has been seen for other cancer types distant to the oral cavity[88,89].

Quantification of exRNAs is particularly challenging, given that they are typically at low concentrations and have a wide range of lengths, with a prominent population of small RNAs. Therefore, it is important to consider the characteristics of each quantification method, in terms of the limit of detection, dynamic range, and specificity for nucleic acid type. Herein, RiboGreen assay was used to quantify the amount of RNA loaded to each library (RNA input), while Bioanalyzer profiles were used to evaluate the RNA and DNA length as well as a criterion to exclude samples containing bacterial rRNA intact peaks. Due to technical variations in saliva sample processing, RNA extraction and library generation, proper normalization is critical for consistent detection of true biological differences between samples, an issue that has already been pinpointed by the NIH exRNA consortium[266]. They presented a preliminary study suggesting that it may be possible, at least in plasma, to identify a set of exRNAs with relatively stable abundances that may be used as internal reference standards for exRNA quantification following the concept from Vandesompele J. *et al.*[248]. Overall, there is no consensus on validated internal controls for accurate quantification of exRNA levels for saliva body fluid.

This is not a negligible point, as many researchers used reference genes that have not been validated beforehand. With the aim of translating the analysis to the clinics and be able to establish a threshold of expression for a particular biomarker from an established initial volume of sample, the same starting volume of saliva and total RNA was used for RNA extraction and library generation, respectively. Additionally, sequenced libraries were equimolar and DE analyses were performed using normalized reads against the library size (i.e. number of total aligned reads used to count miRNAs by miARma seq pipeline[232]). For the future validation steps, several stable miRNAs across the saliva samples have been obtained following the method of Vandesompele J. *et al.*[248].

5.1.2. Differentially expressed miRNAs in saliva from OC patients

Since an ideal biomarker for cancer diagnosis is a molecule, in this case a miRNA, that is not detected in the control group or it does but its levels rises in the cancer group, the attention was focused on the overexpressed miRNAs in saliva from OC patients. Thus, 32 and 28 known miRNAs appeared overexpressed in early and late stage OC salivas, respectively, when compared with control salivas. Twenty of these appeared commonly overexpressed in both early and late stage highlighting them as putative miRNAs candidate biomarkers. In contrast to other markers such as CA125, primarily detected in blood samples form late stage OC, the number of miRNAs identified as well as miRNA levels, were comparable between late and early salivas, supporting the notion that salivary miRNA in early OC patients were already able to mirror the presence of the tumor.

Of the top 10 overexpressed miRNAs in early stage OC salivas, 3 of them appeared also overexpressed in the late stage salivas (Table 23). These 3 common miRNAs belong to the miR-34 family, namely miR-34c-5p, miR-34c-3p and miR-34b-3p and belong to the same cluster, suggesting a common regulation at transcriptional level[176]. As previously described, the miR-34 family members are direct targets of p53, both acting in concert to block CCNE1, CDK4, MET and p-RB to inhibit inappropriate cell proliferation[192] and, accordingly, all miR-34 family members were increased at transcriptional and post-transcriptional level in wild-type p53 but not in p53-null MEFs[192]. Interestingly, upon p53 activation by genotoxic agents, increased levels of miR-34c and miR-34b but not miR-34a (another family member not found in our screen) were observed in OC cells, inducing cell cycle arrest in G1 phase and reducing the levels of several cell cycle related proteins[245–247]. In addition to the cell cycle regulatory functions, p53 regulated invasion and metastasis through MET receptor tyrosine kinase in part through the miR-34 function[267,268].

5.1.3. The role of miR-34 family in OC and hypotheses of its origin in saliva

The members of the miR-34 family have been described to display a tumor suppressor role in OC[267]. As tumor suppressors, all miR-34a, b and c have been found downregulated in OC with p53 mutation[267], whereas only miR-34a expression was not reduced in tumors with wild-type p53 OC, suggesting a dependent regulation of p53

for miR-34 members[267], but an additional and p53-independent regulation for miR-34a in cancer. Furthermore, reduced expression of miR-34b*/c, but not miR-34a, was found in HGSC p53 mutated tumors compared to LGSC wild-type p53 tumors, levels were even lower in late stage compared to early stages of HGSC, and overall lower expression was found in HGSC than in FTE cells[245,267]. This suggests that the inactivation of miR-34b and miR-34c may contribute to the carcinogenesis and progression of HGSC.

The fact that the salivary miR-34b*/c were increased in OC samples (at early and late stages) seemed then controversial. In the same line, the miR-200 family members have been usually found downregulated in OC tissues (Table 9) but their levels were found increased in plasma in many reports (Table 7). One simple explanation is that miR-34b*/c overexpression in saliva from OC samples and its possible use as diagnosis biomarkers, is not related to the role of these family members in ovarian tumoral cells. However, we favor an alternative possibility as new patterns of post-transcriptional control for miRNA inactivation have been found and may conciliate the results obtained with the already known function for miR-34b*/c. On one hand, it has been identified a new regulatory mechanism for long ncRNA as competitive endogenous RNAs (ceRNAs), more commonly known as miRNA sponges[269]. In particular situations they have been shown to antagonize tumor suppressor miRNAs in cancer[270,271]. For instance, the long ncRNA CCAT2 is overexpressed in OC and has been validated to play a role in OC tumorigenesis, by sponging the tumor suppressor miR-424[272]. Another example is the long ncRNA UCA1, which has also been found upregulated in OC contributing to metastasis through sponging the tumor suppressor miR-485-5p that in turn targets MMP14[273]. Thus, cancer cells might achieve advantages by modulating post-transcriptionally the levels of tumor suppressor miRNAs.

On the other hand, another interesting and recently discovered concept postulated that cells acquire oncogenic capacities by shuttling of the tumor suppressor miRNAs into EVs, boosting the donor cells' tumorigenicity. This could also explain why miR-34b*/c appeared overexpressed in saliva from OC patients. EVs are known to transport miRNAs and RNAs from donor to recipient cells, the most studied cells in this crosstolk[274,275]. However, the effects caused in the donor cells by the selective sorting out of certain miRNAs, is now beginning to be of interest as a post-transcriptional

regulatory mechanism of miRNA activity[276]. In addition, they prove that MVP protein directly interacted with the tumor suppressor miR-193a-3p and mediated its EV sorting, thus promoting colon cancer progression, while knockout of MVP leads to miR-193a-3p accumulation in the donor cells instead of exosomes, inhibiting tumor progression[276]. In this case, cells acquire capacities to selectively sort out miR-193a-3p of the cancer cell to increase its tumorigenic potential[276]. Another example showed that EVs released by mutated KRAS cells contained miRNAs that are different from the ones exported in EVs by cells with a normal copy of the KRAS gene[277]. In particular, several miRNAs that suppress cancer growth in healthy cells were found at lower levels in mutant KRAS cells. Instead, these miRNAs were highly represented in the EVs that were released by the KRAS mutant cells. Interestingly, when cells with a normal copy of the KRAS gene were exposed to the contents of the EVs released from KRAS mutant cells, cell growth was suppressed; not only indicating that the miRNAs exported from cancerous cells can influence gene expression in neighboring cells, but also that eliminating such tumor suppressor miRNAs could give cancer cells a growth advantage over normal cells to promote tumor growth[277]. Interestingly, cells can also acquire the capacity to sort selected oncogenic miRNAs out of the cell through EVs to reduce the tumorigenic potential. This capacity is lost in cancer due to the lack of the machinery responsible for the shuttling of oncogenic miRNA into EVs[278]. Therefore, specific mechanisms seemed to be acquired by cancer cells either by upregulating molecules involved in the shuttling of tumor suppressor miRNAs or by downregulating molecules responsible for the sorting of oncogenic miRNAs out the cell, thus enhancing the proliferative capacities and promoting cancer progression.

One proposed hypothesis is that the elevated levels of the 3 tumor suppressor miRNAs from miR-34 family (miR-34c -5p and -3p, and miR-34b-3p) in saliva from OC patients, would be a consequence of their shuttling out of the OC cell, reaching circulation and thereafter, saliva body fluid. In this context, even though the saliva processing and analysis of the present study did not discriminated between cell-free miRNAs contained in EVs or associated to RNA binding proteins; EVs (i.e. exosomes) have been well characterized in saliva[279,280], as well as their miRNA content for diagnostic purposes of oral diseases[281]. Of note, either free of vesicles or within EVs, it could be hypothesized that the three tumor suppressor miR-34s were shuttled out of the cell in favor of OC carcinogenesis already at an early stage of development, since

they were already detected at high levels in saliva from early stage OC patients. Supporting this notion, it has been shown that the human cell-derived miR-21 was readily detected at high levels in saliva from tumor-bearing mice before tumors were palpable, while undetectable miR-21 levels were obtained in tumor-free animals[262], when using a human pancreatic cancer cell line implanted in the pancreas of athymic mice. For our speculation to be true, one would firstly expect the 3 miRNAs to be usually shuttled by OC cells *in vitro*. Secondly, the hypothesis assumes that miR-34b*/c come directly from the primary tumor, but an animal model with labeled miRNAs/EVs would clarify the mechanisms that support the selective sorting of tumor suppressor miRNAs to the circulation.

Nevertheless, as discussed initially, miR-34s could be secreted by the salivary glands in response to the presence of OC, yet they would still be valuable in reflecting the appearance of the disease. In fact, there is one animal model of melanoma showing that upon systemic disease development, significant changes occurred in the salivary biomarker profile, and that the origins of the disease-induced salivary biomarkers may be both systemic and local[117]. They supported the hypothesis by the observation of several changes in salivary gland cells in mice bearing tumors from the ones of tumor-free mice, which was translated into distinct salivary biomarker profiles[117]. Thus, perhaps less appealing and sophisticated but still valid for our purpose, the biomarkers encountered would account for significant improvements in the early detection of OC, reducing OC mortality and increasing survival.

Last but not least, miR-34s and the other miRNAs found overexpressed in saliva from early OC patients need of further validation in larger independent cohorts (and so are doing next) since the cohorts used for the discovery phase of this study were small, limited not only by the incidence of the disease, but by the fact that the majority off the patients are diagnosed at late stage of dissemination. After validation, possibly also after comparison to a cohort of healthy patients, a point-of-care method will need to be developed in order to translate the findings into a routinely clinical examination. Currently, the unique system to detect salivary miRNAs in an intent to develop a non-invasive diagnostic tool was sett up for prostate cancer detection by Hizir *et al.*[259]. They evaluated the expression of miR-21 and miR-141 (miRNAs over-expressed in early and advanced prostate cancer patients) by using a biosensor that utilizes two

different wavelengths to detect miR-21 and miR- 141 simultaneously[259]. Their approach is faster and easier than multiple and simultaneous RTqPCR detection, and can be performed with a portable spectrofluorometer; however, improved sensitivity is still needed for further clinical application.

Before incorporation into the clinical practice, several criteria for clinical test development will need to be matched: (i) analytical and (ii) clinical validity and (iii) clinical utility[282]: analytical validity showing sufficient assay performance to produce accurate and reproducible technical results; clinical validity referring to the concordance between the test results and the clinical diagnosis before (FDA in vitro diagnostic device) or after (CLIA laboratory-developed test) test clearance/approval; and clinical utility to show that the test has an impact on patient care and includes evaluation of patient outcomes, costs and economic benefits[282].

5.2. MIRNAS AS OC THERAPEUTIC TOOLS

OC is usually diagnosed at a late stage of disease progression were most of the patients become resistant to the therapies and die of recurrence[11]. One of the current alternative is try to find new personalized therapies not only to palliate but hopefully for the disease to become chronic, controlling its progression, and to eradicate the cancer cells from the human body in the best scenario. MiRNAs are trending on the usage as a therapeutic tool as they control multiple targets genes and pathways altered in cancer. They are small molecules that can be modified and encapsulated into several nano-systems, improving accessibility and uptake by cancer cells and reducing side toxicity effects, achieving lower dosage administration[215]. In this study, it has been described the tumor suppressor role of a new miRNA in OC, namely miR-654-5p. Both, increasing the expression of miR-654-5p itself, or the combined inhibition of its immediate downstream effectors appear as novel therapeutic avenues in the management of OC.

5.2.1 Differentially expressed miRNAs in short *vs.* long SV OC patients

Despite it is known that different histological subtypes are considered different entities[2], high-grade histologies generally become resistant to the standard therapies when diagnosed at advanced stages[12]. In this study, advanced stages of high-grade OC patients from different histologies were used to identify new potential miRNA-based therapies for OC. After the multicenter validation, 4 miRNAs were found overexpressed in short SV patients compared to long SV patients: miR-554, miR-409-3p, miR-127-3p and miR-654-5p. Of note, patients with residual disease after PDS were excluded from the study since it is a factor directly related to poor prognosis and shorter SV[11].

In order to evaluate their therapeutic potential of these 4 miRNAs in OC, they were first functionally studied *in vitro* by over- and infra- expressing the 4 miRNAs in multiple OC cell lines. Modulation of miR-554 and miR-409-3p resulted in no consistent and significant effects in the cell lines tested. While the role of miR-554 in cancer is not known, the role of miR-409-3p in cancer has been found highly controversial since it can act as tumor suppressor miRNA in several cancers such as gastric[283,284] and colon[285–287], but it also can act as an oncogene in prostate cancer[288,289]. In contrast,

the effects of modulating miR-127-3p and miR-654-5p *in vitro* suggested a tumor suppressor role for these miRNAs in OC, since overexpression of the miRNAs impaired cell proliferation in all cell lines tested, with more pronounced effects in the case of miR-654-5p overexpression. In accordance, inhibition of their levels slightly increased the proliferation in 3 out of the 4 OC cell lines tested. From the premise that miRNAs levels were in principle found to be higher in short SV patients, one would predict an oncogenic role for miR-127-3p and miR-654-5p, rather than the tumor suppressor role observed *in vitro* upon their overexpression. However, their levels were significantly higher in non-tumoral ovaries compared to OC tumors (regardless of the associated SV) for miR-127-3p[290] and for miR-654-5p (this study) (Figure 24A), thus suggesting that their biological relevance and functional activity might reside in the loss of their expression levels at the initiation of the ovarian tumorigenesis. Indeed, although miR-127-3p has been found to act as an oncogene[291,292], it also has been found to act as a tumor suppressor in several malignancies[293–295], including OC[290] in which inhibited tumor growth through targeting the Bcl-2-associated athanogene 5 (BAG5) gene. Retrospectively, we consider now that including normal (control) tissues in our initial screening would have helped in the understand the role of the found miRNAs, as we suspect that perhaps the identified differences between short and long SV patients might be negligible when compared to the levels in normal (or benign) tissues. However, to obtain normal tissue from a patient affected with HGSC is not trivial. Thus, independent validations using *in vitro*, *in vivo* and patient-derived cells experiments are paramount to establish a definitive role for a particular molecular determinant.

5.2.2. MiR-654-5p location and regulation

In 2006, the sequence of miR-654 was firstly identified and annotated by Miyoshi N. *et al.*[296] as a novel human miRNA in the in the catalogue of “colorectal microRNAome”[296]. MiR-654-5p is located in the 14q32 region[297]. Supporting the notion that miR-654-5p levels were higher in benign ovaries than in tumoral tissues, the CpG islands within this region were found to be highly hypermethylated in OC tissues and cell lines, suggesting that epigenetic regulation would be one of the possible mechanism of miR-654-5p silencing in OC. Indeed, increased expression of miR-654-5p was obtained upon of DNA methyltransferase inhibition. Interestingly, the long ncRNA MEG3, one of

the genes used as a positive control and also located in 14q32 region[297], was found also hypermethylated in the OC tissues and cell lines evaluated (data not shown) and has been related to OC progression[298]. Together, this suggests that the tumor suppressive effect of miR-654-5p might be lost by epigenetic silencing of the 14q32 chromosomal region in OC, thus contributing also to the initiation and progression of OC.

The 14q32 region has been found frequently altered in cancer[249–251], including OC[199], suggesting an important role for its genomic content (either coding and ncRNAs) in the development of cancer. In particular, it has been shown that the 14q32 region is epigenetically silenced in melanoma, with the subsequent reduction of several tumor suppressor miRNAs that are contained in the same cluster as miR-645-5p, such as miR-376a and miR-376c[249]. In OC, it was found that several tumor suppressor miRNAs belonging to the *Dlk1-Gtl2* cluster located in 14q32 (*Gtl2* being the mouse homologue of human MEG3) were epigenetically downregulated in EOC mainly through hypermethylation[199]. Interestingly, the *Dlk1-Gtl2* cluster is structurally conserved between mouse and human, but there is functional divergence on maternally expressed miRNAs, including miR-654 expression that is unique for human[299]. Together, miR-654 is located in an important tightly regulated imprinted region. Furthermore, our results support the idea that the downregulation of the miRNA tumor suppressor cluster is associated with the OC progression[199].

Beyond OC, in 2011 Östling P. *et al*.[300] identified several miRNAs including miR-654-5p, to direct target the androgen receptor (AR) gene. MiR-654-5p overexpression reduced proliferation of prostate cancer cells, pinpointing these miRNAs as novel therapies for androgen-dependent prostate cancer[300]. More recently, downregulation of miR-654-5p levels was also found in classic Hodgkin lymphoma[301] and breast cancer[302] compared to controls, in agreement with our results in OC. Apart from these studies, there is no additional knowledge about its tumor suppressor role and its mechanism of action, and importantly, this is the first study that describes the tumor suppressor role of miR-654-5p in OC.

Additionally, although few more reports exist, little is known about the “-3p” form of pre-miR-654: the miR-654-3p. The seed sequence of miR-654-5p is completely different from the miR-654-3p, thus suggesting different downstream signaling through

an independent spectrum of targeted genes. Interestingly, miR-654-3p has been found downregulated in melanoma cells compared to normal melanocytes supposedly by epigenetic silencing[249]. In addition, reduced levels of miR-654-3p were found in papillary thyroid cancer[303] and in metastatic prostate cancer cells lines[304]. These reports further support the tumor suppressor role of some of the miRNAs located at 14q32.

5.2.3. The tumor suppressor role of miR-654-5p in OC

Here, accompanied to the reduction of the proliferation observed, a marked induction of apoptosis was seen in OC cells, and a reduction of the tumor growth was seen *in vivo* upon overexpression of miR-654-5p. Our first attempt in this study to test *in vivo* the effects of miR-654-5p overexpression, was to stably overexpress miR-654-5p using the constitutive vector system called pGIPZ used to stably overexpress miRNAs in other cancer types[305]. However, we failed in recapitulating the effects shown by miR-654-5p transient overexpression *in vitro*, albeit miR-654-5p levels were 10^4 times higher in SKOV3-pGIPZ-miR-654 cells than in SKOV3-pGIPZ control cells. The cloned miRNA in the pGIPZ vector corresponds to the precursor miRNA of miR-654, thus including the "-3p" form and the "-5p" form. Two explanations for the lack of reproducibility of the miR-654 stable expression could be: (i) the lack of processing of the mature miRNA forms in the cells used, thus being a non-functional miR-654-5p; or (ii) the fact that the presence of miR-654-3p could potentially counteract the effects of miR-654-5p by targeting other genes. Alternatively, our *in vivo* model was set up by using transiently transfected cells, similar to a successful xenograft model of lung cancer performed by reverse transfection or electroporation of let7-f *in vitro* and then injecting the cells into the mice[306]. In the present model, a high reduction of proliferation was observed in mice injected with cells transfected *in vitro* with the miR-654-5p. Interestingly, comparable levels of miR-654-5p were measured in tumors after 5 days of injection supporting the fact that cells still maintain high levels of the transient transfection, which produced visible cellular effects: (i) less cellularity of the tumors containing miR-654-5p, with regressive phenotypes and larger areas with extracellular matrix deposition (produced by the supposedly apoptotic cell death induced by miR-654-5p); (ii) reduction of the proliferation by the ki67 staining in the remaining tumor cells. Due to the low amount of material in tumors at day 5, it was not

possible to be analyzed cell death (e.g. caspase staining by immunohistochemistry). Importantly, and supported by the fact that the levels of miR-654-5p were still high at the end of the *in vivo* model, the tumors were dramatically small (or absent) at the consecution of the experiment, possibly by the maintained miRNA levels, but likely mainly due to the irreversible molecular events originated during the first days after the injection that compromise the fate of the tumors in the miR-654-5p mice group. Thus, the present animal model showed that miR-654-5p reduced tumor growth *in vivo*, supporting the tumor suppressor role observed *in vitro*.

With the aim to verify the results from our *in vitro* experiments and *in vivo* pre-clinical mice model in a patient-derived model, we took advantage of patient-derived ascitic cells (i.e. exfoliated cells from the primary tumor that aggregate and survive forming spheres in the peritoneal cavity) from 4 advanced OC patients.

We were able to culture them in 3D *in vitro*, which represent better the heterogeneity between patients and the characteristic behavior of the progression of the disease[307]. Importantly, while in some reports is shown the modulation of the expression of some miRNAs in patient-derived ascitic cells grown in monolayer (2D)[217,308], this is the first report that tests the effect of modulating a tumor suppressor miRNA, by testing the effects on the sphere forming capacity and sphere viability (i.e. 3D cultures) by using OC patient-derived ascitic cells *ex vivo*. In accordance with the tumor suppressor role observed *in vitro* and *in vivo*, a reduction of the sphere forming capacity was observed upon overexpressing miR-654-5p in 4 patient-derived ascites. Additionally, miR-654-5p reduced the viability of those spheres and induced cell death by the cleavage of PARP and Caspase-3 indicating that the effects seen *in vitro* and *in vivo* upon miR-654-5p overexpression could be of clinical relevance. Indeed, OC models based on orthotopic injection of immortalized OC cell lines that developed ascites or PDX models are proposed systems to evaluate putative therapies against OC[309]. Our next step is to generate mice xenografts using patient-derived ascitic cells injected intraperitoneal, to mimic OC carcinomatosis and further prove the therapeutic benefit of targeting miR-654-5p in a model closest to the clinic. This is not without limitation, as they are primary cultures and its use is limited to 4-6 passages. However, they will be very valuable to test new therapies, such as the potential therapeutic effect of miR-654-5p.

5.2.4. MiR-654-5p target genes

MiRNAs act through targeting specific genes. However, very few targets have been characterized for this miRNA (AR and EPSTI1 for prostate[300] and breast[302] cancer, respectively) and no downstream signaling knowledge has been gathered for miR-654-5p in OC. In this study, 5 gens have been characterized as direct targets of miR-654-5p: HAX1, RAB1B, PBX3, CDCP1 and PLAGL2. All these genes have been associated to cancer-related events, including cell proliferation, apoptosis, migration, vesicle secretion, cancer stem cells, etc.

On one hand, HAX1 is an anti-apoptotic gene that contains two Bcl-2 Homology (BH) domains (BH1 and BH2) and is located in the inner membrane of the mitochondria, in which prevents the accumulation of pro-apoptotic BAX in the outer mitochondrial membrane space through the activation of a serine protease HtrA2, thus preventing apoptosis of neurons and peripheral lymphocytes[310]. Interestingly, its overexpression protects cardiac myocytes and prostate cancer cells from apoptosis through directly binding to and inhibiting of caspase-9[311,312]. It has been described as an oncogene in mantle cell lymphoma, through the acquisitions of phosphodegron mutations which unable the FBXO25 ubiquitin ligase to phosphorylate and send HAX1 for proteasomal degradation[313]. Despite reduced levels seemed to be beneficial for cancer disease, its loss impaired migration of normal skin cells disrupting the wound healing by directly binding to EB2, a microtubule plus ends protein that regulates focal adhesion turnover and directional cell movement[314]. It also impaired neutrophil migration through regulating RhoA activity[315], while mutations in HAX1 induced the sever congenital neutropenia called Kostmann disease[316]. Interestingly, HAX1 deficient women but not man with Kostmann disease showed gonadal insufficiency suggesting that it might play a role in the development and/or function of the normal ovary[317]. In addition, there is one report in OC in which it is explained that HAX1-Rac1/cortactin interactions are required for the induced migration of SKOV3 cells[318], suggesting a possible role in the wound healing during ovulation in the normal ovary and migration capacities in OC. Therefore, its overexpression might not be a tumor driver alteration but it must play a role in preventing cancer-related apoptosis, in accordance with the observation that reduced levels of HAX1 were observed upon miR-654-5p overexpression, which may explain the pro-apoptotic effect caused by the miRNA.

On the other hand, RAB1B is a small GTPase that is essential in endoplasmic reticulum (ER)-to-Golgi vesicle trafficking[319], which also has been related to cancer by enhancing secretion of pro-metastatic factors that lead to a increase in endothelial recruitment and invasion of metastatic cells by binding to and localizing with PITPNC1 in the *trans*-Golgi network[320]. This GTPase is essential for the autophagosome formation[321] and its inhibition by miR-502 reduces colon cancer growth by inhibiting autophagy[322]. RAB1B is also secreted in EV inducing neoplastic transformation of adipose stem cells of the microenvironment surrounding the prostate cancer cells[323], and is overexpressed together with MMP9 in colorectal cancer[324]. Overall, most of the features of RAB1B related it with vesicle-membrane cellular functions in tumorigenesis and metastasis and, although there is no report about RAB1B in OC, its abrogation by miR-654-5p in the context of OC would be beneficial to reduce cell aggressiveness, yet the mechanisms are still not known.

Also, PBX3, pre-B cell leukemia homeobox 3 gene, has been widely found overexpressed in acute myeloid leukemia due to the characteristic chromosomal rearrangements of several subtypes, together with other HOX family genes, such as MEIS and HOXA9[325–328]. Also, several epigenetic regulators have been found to alter the levels of PBX3 in leukemia such as hypomethylation[329] or downregulation of several tumor suppressor miRNAs that target PBX3, such as miR-495[330] and miR-181[331]. Additionally, PBX3 has been found to play an important oncogenic role in solid tumors such as hepatocellular carcinoma[332–334], gastric[335,336] and colorectal cancer[337] promoting proliferation migration, invasion, tumor growth and metastasis, by inducing EMT markers, CDK2, MMP2, p-AKT (Ser473), MMP9, MAPK/ERK signaling, tumor initiating cells (e.g. SOX2 and NOCTH3), etc[332–337]. It is of particular interest that this potent oncogene is targeted by multiple tumor suppressor miRNAs that hare downregulated in distinct malignancies (e.g. miR-320a[332]; miR-33a-3p[333]; let-7c, miR-200b, miR-222 and miR-424[334]; miR-144-3p[336]; let-7c[337]), suggesting that might be a common regulatory network between the downregulated miRNAs that that lead to an increase of the PBX3 oncogenic function.

Although these 3 genes (HAX1, RAB1B and PBX3) together with CDCP1 and PLAGL2 were direct targets of miR-654-5p in OC cells, only CDCP1 and PLAGL2 silencing phenocopied the overexpression of miR-654-5p and therefore we focused our attention in the latter two.

5.2.5. CDCP1 and PLAGL2 are functionally relevant targets of miR-654-5p in OC

CDPC1 and PLAGL2 protein levels were diminished in spheroids from patient-derived ascites when overexpressing miR-654-5p. Despite RAB1B levels were also diminished, its silencing did not produce significant effects on proliferation and cell death as miR-654-5p overexpression did. In addition, CDCP1 and PLAGL2 levels were found increased in tumors compared to benign ovaries, while no differences were found for RAB1B expression levels, suggesting a role for CDCP1 and PLAGL2 in OC progression.

CDCP1, CUB domain-containing protein 1, is type I transmembrane glycoprotein of 140 KDa with a large extracellular domain containing two CUB domains, and an intracellular domain containing five tyrosine phosphorylation sites, mainly substrates of Src family members[338,339]. It is a proto-oncogene widely proposed as an anti-cancer therapy since it was found overexpressed and widely involved in metastasis of melanoma[340], breast[341,342], lung[343,344], gastric[345,346] and prostate[347] cancer, among others. Despite evidence is growing to support the necessity of CDCP1 cleavage for its activity[342,348,349], CDCP1 activity depends on its phosphorylation by Src family kinases[338,339], which activate cell survival through a variety of signaling pathways including the recruitment to the cell membrane of PKCδ[342,350] and Akt[348,349,351], among others. In OC, CDCP1 has been recently found overexpressed in CCC and HGSC, and it mediated migration, spheroid formation and chemoresistance through the activation of p-AKT (S473), and p-ERK, events reversed in vivo by a monoclonal antibody against CDCP1[351,352]. Additionally, CDCP1 and the metaloprotease ADAM12 have been found correlated with poor prognosis in OC, and related to increased angiogenesis[353]. This transmembrane protein is internalized and degraded depended on palmitoylation in OC cells, posttranslational modification that is diminished by EGFR signaling activation increasing the lifespan of membranous CDCP1[354] and therefore its downstream signaling activation, being a possible mechanisms of EGFR-therapy resistant tumors and, therefore, a possible potent anti-cancer therapy[341,354]. In the present model, CDCP1 oncogenic functions might be inhibited by miR-654-5p in OC, and miR-654-5p/CDCP1 axis could be proposed as a potent anti-cancer therapy for OC.

PLAGL2, together with PLAG1 and PLAGL1, constitute the PLAG family of zing finger proteins, able to bind to DNA/RNA sequences[355]. Despite they share homology in the DNA binding domain, they have different DNA binding capacities and, therefore, functions[356]. While PLAGL1 is characterized as a tumor suppressor gene, PLAGL2 and PLAG1 can act as oncogenes by increasing IGF-II gene expression, anchorage independent growth and inducing tumors in mice[356], and its transactivation activity can be modulated by sumoylation and acetylation of 3 lysine residues, reducing IGF-II and impairing the transformation capacity[357,358]. Although there is one report that categorized PLAGL2 as a tumor suppressor by increasing p73 (p53 homologue), which in turn increases pro-apoptotic genes such as p21, DR5, TRAIL and Bax[359], it has been associated with the development of malignancies. In particular, in acute myeloid leukemia, PLAGL2 cooperates with an aberrant fusion gene to promote abnormal growth of hematopoietic progenitors[360,361], as well as inducing the transcription of thrombopoietin receptor Mpl, which promoted Jak2 phosphorylation and increased downstream p-STAT5, p-AKT1, and p-ERK activation in leukemia[362]. Importantly, PLAGL2 has been described to activate Wnt/β-cat pathway in glioblastoma and colon cancer[363,364]. To date, there is only one report about OC and PLAGL2, in which it regulates actin cytoskeleton by modulating the activity of the RhoA (stress fibers and focal adhesions) and Rac1 (lamelipodia) GTPases, decreasing the migratory capacity of OC cells upon PLAGL2 depletion[365].

5.2.6. Signaling pathways controlled by miR-654-5p thought CDPC1 and PLAGL2

Interestingly, the most enriched gene sets in cells depleted of CDCP1 and/or PLAGL2 were composed of genes involved in MYC, WNT/β-cat, AKT and MAPK signaling pathways, indicating an impairment in these processes upon CDCP1 and/or PLAGL2 knockdown at the transcriptional level. Several canonical genes from these pathways were confirmed at protein level by the overexpression of miR-654-5p in SKOV3 cells.

Since AKT signaling is directly implicated in cell cycle regulation[366], some of the altered genes found in this gene set were cell cycle regulatory proteins. First, CSK1B, the cyclin dependent kinase (CDK) regulatory subunit 1, appeared infraexpressed by both PLAGL2 and CDCP1 silencing, at the same time that CDKN1B, the CDK inhibitor 1B (also known as $p27^{Kip1}$), appeared overexpressed upon both depletion conditions. While CSK1B binds to CDKs and is essential for the biological function of the CDKs in

cell cycle progression[367], p27 is a potent therapeutic target by blocking CDKs[368], suggesting that cell cycle progression and survival of OC cells was diminished in part through the defective CDKs by the increased function of p27. In turn, CDK2 appeared infraexpressed at mRNA level upon PLAGL2 depletion, which was confirmed by miR-654-5p overexpression at protein levels. Interestingly, a slight increase in the G1 arrest was observed in OC cells upon overexpression of miR-654-5p concomitant with an increase in protein levels of the tumor suppressor p27 (data not shown). Supporting this fact, the "cell-cycle G1/S checkpoint control'' was described as one of the most enriched canonical pathway regulated by PLAGL2 in glioblastoma[363] and an increase in G1 to S transition by PLAGL2 overexpression was observed in acute myeloid leukemia cells[361]. In addition, SKP2, the S-phase kinase associated protein 2, is also downregulated by PLAGL2 depletion in the present model, which has been found associated with advanced stages and poor prognosis of OC patients and inversely correlated with p27 levels in the same samples[369,370]. Also, SKP2 form complex with CDK2, which is suppressed under serum starvation conditions inducing G1 arrest in SKOV3 OC cells[371]. Altogether, although it awaits further demonstration, it could be hypothesized that the increased levels of p27 in both depletion conditions seemed to be dependent on SKP2 downregulation at least in siPLAGL2 cells, that together with the reduced levels of CKS1B and the increased levels of CDKN1B contributed to the reduction of CDK2, which was confirmed upon miR-654-5p overexpression in SKOV3 OC cells.

MAPK signaling (MEK/ERK) regulates cell cycle regulatory proteins including CDK2 and CDK4[368,372], finding indeed synergistic effects between MEK and CDK inhibitors in preclinical models in neuroblastoma[373]. In addition, ERK can be translocated to the nucleus and phosphorylates many transcription factors including c-MYC, as well as other transcription factors involved in the induction of c-MYC expression[372]. In turn, c-myc can induce gene transcription resulting in increasing proliferation and preventing apoptosis, among other oncogenic functions[374]. For example, c-MYC induced CDK4 expression[368] and induced the activity of CDK2 by promoting the degradation of p27[375], thus promoting proliferation. Here, while p27 was upregulated in SKOV3, c-myc was indeed found downregulated upon CDCP1 and PLAGL2 depletion at mRNA levels, which was further confirmed at protein levels by overexpressing miR-654-5p in

SKOV3 cells, suggesting a reduction of the oncogenic signals by diminishing MAPK, AKT and MYC signaling through miR-654-CDCP1/PLAGL2 axis.

As abovementioned, MAPK/ERK and AKT pathways are regulated by both CDCP1[351,352] and PLAGL2[362]. For CDCP1, its role in proliferation and survival through the regulation of MAPK and AKT signaling is well established and reviewed by He Y. and Harrington BS *et al.*[376], including some reports in OC[351,352]. Despite in the present study we did not found any direct relation between AKT mRNA levels and CDCP1, the CDK regulatory protein CKS1B and the CDK inhibitor CDKN1B, were found infra- and over-expressed, respectively, and together with the reduction of the observed p-AKT levels, it could be suggested a possible contribution of CDCP1 to the reduced proliferation and survival of the OC cells observed upon CDCP1 depletion and miR-654-5p overexpression. Indeed, since MAPK signaling can regulate MYC function[372], and since CDCP1 in turn regulate MAPK cascade[376], it is of important interest to understand how this CDCP1-MAPK-MYC axis may impact on the survival of the OC cells, since reduced levels of MYC were found in CDCP1 depleted cells and miR-654-5p overexpressing cells. Interestingly, not only CDCP1 but also PLAGL2 both reduced MYC levels and increased p27; as p27 mediates addiction of OC cells to MYC[377]; and since MYC has been found mutated and amplified in HGSC[12,15]; and anti-MYC was determined as a good strategy to target platinum-resistant OC[378]; it seems very promising the use of miR-654-5p for the treatment of OC. However, the specific mechanisms of action of miR-654-5p/CDCP1/PLAGL2 axis on MYC should be further investigated.

In regard to AKT and PLAGL2, there is no report about the relation between AKT2 (the AKT isoform downregulated in this study) and PLAGL2. However, it was demonstrated that overexpression of PLAGL2 which promoted Jak2 phosphorylation and increased downstream p-STAT5, p-AKT1, and p-ERK activation in acute myeloid leukemia[362]. Here, the reduced AKT2 mRNA levels by PLAGL2 inhibition and the reduced p-AKT levels confirmed by the miR-654-5p overexpression, suggested that the signaling of the AKT pathway can be altered by the tumor suppressor function of miR-654-5p. AKT2 has been found in HGSC concomitantly amplified with cyclin-E1 (CCNE1)[23,379], so its potential oncogenic function in HGSC could be inhibited by miR-654-5p/PLAGL2 axis in those patients with CCNE1/AKT2 amplification. Indeed, in the recent work

performed by Au-Yeung *et al*. they identified synergistic combinations when treating CCNE1-amplified HGSC, including dinaciclib (a CDK inhibitor) and AKT inhibitors[379], which prompts us to speculate (and it could be test) that miR-654-5p might be a possible therapy for CCNE1-amplified HGSC to target both CDK2 and AKT pathway at the same time.

Finally, active AKT phosphorylates and inactivates p21, another CDK inhibitor, which allows CDK2 and CDK4 to induce DNA replication and cell cycle progression and survival of the cell[366]. To do so, CDK2 and CDK4 in turn phosphorylate retinoblastoma (Rb) protein and send it for degradation[368], thus producing the disassembly of the Rb/E2F complex and allowing the initiation of the transcriptional activity of E2F, DNA replication and cell cycle progression[368]. Here, Rb mRNA levels were reduced upon PLAGL2 depletion, but the decrease at protein levels was more prominent for the phosphorylated form of Rb (p-Rb), suggesting an increase of the stability of Rb/E2F complex, may caused by the reduced levels of p-AKT and its downstream CDK2/4, thus stopping the cell cycle progression and reducing cell survival by miR-654-5p, as observed *in vitro*.

Last but not least, another prominent pathway altered by CDCP1 and PLAGL2 silencing were we have focused our attention was the Wnt/β-cat signaling pathway, in which β-catenin play the central role entering into the nucleus and activating the transcription of a serial of genes[380]. However, multiple receptors, ligands, agonists and antagonists, and post-traductional modifications have been described to regulate the activity of the Wnt/β-cat signaling[381]. Although For CDCP1 there is no report regarding its role in the regulation of Wnt/β-cat, for PLAGL2 it has been described to activate Wnt/β-cat signaling pathway in glioblastoma and colon cancer[363,364]. Interestingly, we confirmed that a downregulation of total β-catenin protein levels was obtained upon miR-654-5p overexpression (data not shown, still under investigation) in OC cells. Accordingly, in glioblastoma, its was obtained that PLAGL2 induced the transcription of a Wnt ligand (Wnt6) and two Wnt receptors (Fzd9 and Fzd2), which induced the upstream activation of the Wnt signaling, also increasing total β-catenin in glioblastoma cells[363]. Here, a possible explanation that lead to a reduced levels of total b-catenin could be the fact p-AKT is reduced, which is known to phosphorylate and inhibit GSK3β (glycogen synthase kinase 3β)[382]. In turn, GSK3β forms a destruction

complex targeting and phosphorylating β-catenin for ubiquitin-proteasomal degradation[383]. So, when AKT is active GSK3β is inhibited and cannot form a complex with β-catenin responsible for its degradation, thus β-catenin enter into the nucleus and perform its transcriptional activity[383]. However, in a situation where p-AKT is diminished (like here upon miR-654-5p), GSK3β could be allowed to form complex with β-catenin sending it for degradation, which may be is happening upon overexpression of miR-654-5p, apart from the direct contribution of PLAGL2 to the Wnt signaling. We are currently testing these hypotheses.

In addition, several regulators of the Wnt pathway such as DKK1 and SMURF2 appeared infraexpressed upon CDCP1 or PLAGL2 depletion. Although DKK1 can antagonize Wnt pathway[384], it seems to have a dual role creating a negative feedback loop, since it has been described a β-catenin binding site in the promoter of DKK1 thus being transcriptionally activated by β-catenin[384]. Therefore, miR-654-5p reduced the levels of total β-catenin (yet the mechanisms are still not known), which is in agreement with the reduced levels of DKK1, since the β-catenin transcriptional activity might be reduced and therefore DKK1 would not be transcribed.

Interestingly, SMURF2 it was found downregulated upon both CDCP1 and PLAGL2 depletion. SMURF2 is the E3 ubiquitin ligase of Axin, one of the members of the destruction complex of β-catenin[385]. It was described that knockdown of endogenous SMURF2 increased the level of endogenous Axin and resulted in reduced β-catenin activity[385]. Thus, the reduction of the SMURF2 by CDCP1 and PLAGL2 suggests a direct regulation of the Wnt pathway through these two genes, increasing the stability of Axin/GSK3β/β-catenin destruction complex, resulting in β-catenin degradation and function. Next step would be to confirm these results by miR-654-5p function and unveil the mechanism of SMURF2 silencing to postulate Wnt signaling as a direct-targeted pathway of miR-654-5p. Some efforts have been done to target the pathway in OC[386], but since the Wnt signaling pathway has multiple “druggable” steps for which there are already many inhibitors developed[380], these studies will help to understand the precise mechanism and the potential therapeutic role of miR-654-5p/PLAGL2/CDCP1 axis as a new inhibitor of Wnt/b-cat pathway in OC.

Additionally, gene sets related to hypoxia appeared enriched in CDCP1 and PLAGL2 depletions and might be altered by the tumor suppressive function of miR-654-5p. This is not out of interest since the important function of hypoxia in OC tumorigenesis and chemoresistance[387,388]. Actually, CDCP1 promoted aggressiveness in hepatocellular carcinoma by increasing Hif-2α through PKC-δ[389], which indeed suggested a potential therapeutic role for OC by miR-654-5p in this context through targeting CDCP1. However, further studies would be needed to reveal whether the reduced hypoxia upon CDCP1 and PLAGL silencing is one of the consequences of the tumor suppressor function of miR-654-5p, or whether it plays and important role in cell death. Overall, it can be hypothesized that the downregulation of MYC, Wnt, AKT and MAPK signaling pathways by miR-654-CDCP1/PLAGL2 axis contributes to a reduction in proliferation and survival of the cells as shown by the high amount of enriched gene sets related to apoptosis.

Combination of targeted therapies for OC could involve either vertical or horizontal pathway blockade[390]. Horizontal pathway blockade means to use targeted agents to inhibit two or more signaling pathways, and vertical pathway blockade involves the inhibition of different steps of a specific pathway and is useful in counteracting negative feedback loops[390]. The use of miRNAs as a therapeutic strategy might result in a more potent effect than the use either two or more selective synergistic targeted agents. In this sense, miR-654-5p would be a suitable therapy to target OC either vertical and horizontally at the same time, since it could act through several targets, including CDCP1 and PLAGL2. These, in turn, control different pathways horizontally, such as of MAPK, AKT, MYC and WNT, but also at different steps of such specific pathways. Our current work focuses on unveiling the specific mechanisms of action of the miR-654-5p targets as well as the use of preclinical models to prove such mechanisms.

6. CONCLUSIONS

6.1. Salivary miRNAs as a diagnostic tool in OC

1. Salivary RNA from HGSC and benign patients was suitable for RNA sequencing; Salivary RNA derived from 1 mL of starting material from all samples included in the study yielded on average 100 ng of RNA, which was sufficient for cDNA library preparation and further RNA sequencing analyses.

2. An average of 36% of the sequenced salivary RNA aligned to the human genome, which resulted in an average of 500 known miRNAs and 65 De Novo miRNAs identified in salivary RNA from HGSC and benign patients.

3. RNA sequencing revealed overexpression of 32 and 28 miRNA in saliva from early- and late- HGSC patients when compared to controls, respectively. Interestingly, 20 miRNAs appeared commonly overexpressed in salivas from early- and late- HGSC patients, suggesting that salivary miRNA in early OC patients were already able to mirror the presence of the tumor.

4. Three members of the miR-34 family (miR-34c-5p, miR-34c-3p and miR-34b-3p) were significantly overexpressed in salivas from early and late HGSC, thus being considered as potential diagnostic biomarkers for OC.

6.1. MiR-654-5p as a therapeutic tool in OC

5. The levels of miR-654-5p were significantly lower in overall tumoral samples compared to benign ovaries; In addition, hypermethylation of the miR-654 locus (14q32) was found in the majority of OC cell lines and ovarian tumors analyzed, respectively, suggesting that miR-654 levels could be decreased in OC due to hypermethylation of its locus.

6. Overexpression of miR-654-5p resulted in reduced cell proliferation and induced caspase-dependent apoptosis, accompanied by a modest cell cycle delay that suggests a tumor suppressor role for miR-654 in vitro.

7. MiR-654-5p overexpression in mice impaired tumor growth and resulted in regressive changes at initial steps of tumor engraftment.

8. MiR-654 overexpression reduced sphere forming capacity and viability of patient-derived ascitic cells.

9. HAX1, RAB1B, CDCP1, PLAGL2 and PBX3 were identified as direct targets of miR-654.

10. CDCP1 and PLAGL2 knockdown recapitulated the effect of miR-654 overexpression in OC cell lines.

11. CDCP1 and PLAGL2 were overexpressed in ovarian tumors, compared to benign ovaries, suggesting a possible role for CDCP1 and PLAGL2 genes in OC tumorigenesis.

12. Whole transcriptome analysis of CDCP1 and PLAGL2 silencing altered multiple pathways related to cancer; including enriched gene sets mainly related to apoptosis, hypoxia, WNT/βcat, MYC, MAPK and AKT. In addition, miR-654-5p overexpression reduced the protein levels of MYC as well as CDK2 and CDK4 confirming a reduction in the cell cycle progression; and reduced the levels of p-AKT and p-Rb, thereby indicating a diminished activity of survival pathways governed by ectopic expression of miR-654.

PUBLICATIONS

During the course of this thesis, several collaborations and additional work has been done and turned into the following publications.

A) **Majem B*,** Rosso M*, Lapyckyj M, Devis L, Abascal Mª F, Llauradó M, Matos Mª L, Besso Mª J, Lanau L, Castellví J,nSánchez-Iglesias JL, Pérez-Benavente A, Santamaria A, Gil-Moreno A, Reventós J, Rigau M, Vazquez-Levin M. The Ups and Downs of Epithelial Cadherin Expression and its Implications in Ovarian Cancer Dissemination (*under revision in Plos One*)

B) Rapado-González O, **Majem B**, Muinelo-Romay L, Álvarez-Castro A, Santamaria A, Lopez-Lopez R, Suarez-Cunqueiro MM. Human salivary microRNAs in Cancer. *(under revision in Journal of Cancer)*

C) **Majem B**, Li F, Sun J, Wong DT. RNA Sequencing Analysis of Salivary Extracellular RNA. Methods Mol Biol. 2017;1537:17-36. *Chapter.*

D) Rapado-González Ó, **Majem B**, Muinelo-Romay L, López-López R, Suarez-Cunqueiro MM. Cancer Salivary Biomarkers for Tumours Distant to the Oral Cavity. Int. J. Mol. Sci. 2016 12;17(9). *Review.*

E) **Majem B**, Rigau M, Reventós J, Wong DT. Non-coding RNAs in saliva: emerging biomarkers for molecular diagnostics. Int J Mol Sci. 2015 Apr 17;16(4):8676-98. doi: 10.3390/ijms16048676. *Review.*

F) Laurent LC, Abdel-Mageed AB, Adelson PD, Arango J, Balaj L, Breakefield X, Carlson E, Carter BS, **Majem B**, Chen CC, Cocucci E, Danielson K, Courtright A, Das S, Abd Elmageed ZY, Enderle D, Ezrin A, Ferrer M, Freedman J, Galas D, Gandhi R, Huentelman MJ, Van Keuren-Jensen K, Kalani Y, Kim Y, Krichevsky AM, Lai C, Lal-Nag M, Laurent CD, Leonardo T, Li F, Malenica I, Mondal D, Nejad P, Patel T, Raffai RL, Rubio R, Skog J, Spetzler R, Sun J, Tanriverdi K, Vickers K, Wang L, Wang Y, Wei Z, Weiner HL, Wong D, Yan IK, Yeri A, Gould S. Meeting report: discussions and preliminary findings on extracellular RNA measurement methods from laboratories in the NIH Extracellular RNA Communication Consortium. J Extracell Vesicles. 2015 Aug 28;4:26533. doi: 10.3402/jev.v4.26533. eCollection 2015.

G) Llauradó M*, **Majem B***, Altadill T, Lanau L, Castellví J, Sánchez-Iglesias JL, Cabrera S, De la Torre J, Díaz-Feijoo B, Pérez-Benavente A, Colás E, Olivan M, Doll A, Alameda F, Matias-Guiu X, Moreno-Bueno G, Carey M, Del Campo JM, Gil-Moreno A, Reventós J, Rigau M. (*Equally contributing). MicroRNAs as prognostic markers in ovarian cancer. Mol Cell Endocrinol. 2014 Jun 5;390 (1-2):73-84. doi: 10.1016/j.mce.2014.03.006. *Review.*

REFERENCES

1. Brennan, J. & Capel, B. One tissue, two fates: molecular genetic events that underlie testis versus ovary development. *Nat. Rev. Genet.* **5,** 509–521 (2004).
2. Karnezis, A. N., Cho, K. R., Gilks, C. B., Pearce, C. L. & Huntsman, D. G. The disparate origins of ovarian cancers: pathogenesis and prevention strategies. *Nat. Rev. Cancer* **17,** 65–74 (2016).
3. Uhlenhaut, N. H. *et al.* Somatic Sex Reprogramming of Adult Ovaries to Testes by FOXL2 Ablation. *Cell* **139,** 1130–1142 (2009).
4. Auersperg, N., Wong, A. S., Choi, K. C., Kang, S. K. & Leung, P. C. Ovarian surface epithelium: biology, endocrinology, and pathology. *Endocr. Rev.* **22,** 255–88 (2001).
5. Auersperg, N., Maclaren, I. A. & Kruk, P. A. Ovarian surface epithelium: autonomous production of connective tissue-type extracellular matrix. *Biol. Reprod.* **44,** 717–24 (1991).
6. Auersperg, N., Edelson, M. I., Mok, S. C., Johnson, S. W. & Hamilton, T. C. The biology of ovarian cancer. *Semin. Oncol.* **25,** 281–304 (1998).
7. Siegel, R. L., Miller, K. D. & Jemal, A. Cancer Statistics, 2017. *CA. Cancer J. Clin.* **67,** 7–30 (2017).
8. Mitra, A. K. in *Tumor Metastasis* (InTech, 2016). doi:10.5772/64700
9. Yin, M. *et al.* Tumor-associated macrophages drive spheroid formation during early transcoelomic metastasis of ovarian cancer. *J. Clin. Invest.* **126,** 4157–4173 (2016).
10. Mutch, D. G. & Prat, J. 2014 FIGO staging for ovarian, fallopian tube and peritoneal cancer. *Gynecol. Oncol.* **133,** 401–404 (2014).
11. Berek, J. S., Crum, C. & Friedlander, M. Cancer of the ovary, fallopian tube, and peritoneum. *Int. J. Gynecol. Obstet.* **131,** S111–S122 (2015).
12. Matulonis, U. A. *et al.* Ovarian cancer. *Nat. Rev. Dis. Prim.* **2,** 16061 (2016).
13. Miller, K. D. *et al.* Cancer treatment and survivorship statistics, 2016. *CA. Cancer J. Clin.* **66,** 271–289 (2016).
14. Lee KR, Tavassoli FA, Prat J, Dietel M , Gersell DJ, Karseladze AI, et al. Surface Epithelial Stromal Tumours: Tumours of the Ovary and Peritoneum. In: Tavassoli FA, Devilee P, editors. World Health Organization Classification of Tumours: Pathology and Genetics of Tumours of the Breast and Female Genital Organs. *IARC Press* 117–45. (2003).
15. Bell, D. *et al.* Integrated genomic analyses of ovarian carcinoma. *Nature* **474,** 609–615 (2011).
16. Patch, A.-M. *et al.* Whole–genome characterization of chemoresistant ovarian cancer. *Nature* **521,** 489–494 (2015).
17. Wentzensen, N. *et al.* Ovarian Cancer Risk Factors by Histologic Subtype: An Analysis From the Ovarian Cancer Cohort Consortium. *J. Clin. Oncol.* **34,** 2888–2898 (2016).
18. Ryland, G. L. *et al.* Mutational landscape of mucinous ovarian carcinoma and its neoplastic precursors. *Genome Med.* **7,** 87 (2015).
19. Romero, I., Sun, C. C., Wong, K. K., Bast, R. C. & Gershenson, D. M. Low-grade serous carcinoma: New concepts and emerging therapies. *Gynecol. Oncol.* **130,** 660–666 (2013).
20. Wiegand, K. C. *et al.* ARID1A Mutations in Endometriosis-Associated Ovarian Carcinomas. *N. Engl. J. Med.* **363,** 1532–1543 (2010).
21. Tan, D. S. P. *et al.* Genomic Analysis Reveals the Molecular Heterogeneity of Ovarian Clear Cell Carcinomas. *Clin. Cancer Res.* **17,** 1521–1534 (2011).
22. Jones, S. *et al.* Frequent Mutations of Chromatin Remodeling Gene ARID1A in Ovarian Clear Cell Carcinoma. *Science (80-.).* **330,** 228–231 (2010).
23. Cho, K. R. & Shih, I.-M. Ovarian cancer. *Annu. Rev. Pathol.* **4,** 287–313 (2009).
24. Banerjee, S. & Kaye, S. B. New Strategies in the Treatment of Ovarian Cancer: Current Clinical Perspectives and Future Potential. *Clin. Cancer Res.* **19,** 961–968 (2013).
25. Powell, S. N. & Kachnic, L. A. Roles of BRCA1 and BRCA2 in homologous recombination, DNA replication fidelity and the cellular response to ionizing radiation. *Oncogene* **22,** 5784–5791 (2003).
26. Bolton, K. L. *et al.* Association between BRCA1 and BRCA2 mutations and survival in women with invasive epithelial ovarian cancer. *JAMA* **307,** 382–90 (2012).
27. Rebbeck, T. R. *et al.* Association of type and location of BRCA1 and BRCA2 mutations with risk of breast and ovarian cancer. *JAMA* **313,** 1347–61 (2015).
28. Norquist, B. M. *et al.* Inherited Mutations in Women With Ovarian Carcinoma. *JAMA Oncol.* **2,** 482–90 (2016).
29. Cools, M., Wolffenbuttel, K. P., Drop, S. L. S., Oosterhuis, J. W. & Looijenga, L. H. J. Gonadal

development and tumor formation at the crossroads of male and female sex determination. *Sex Dev.* **5,** 167–80 (2011).
30. Jeung, Y. J., Ok, H. J., Kim, W. G., Kim, S. H. & Lee, T. H. Krukenberg tumors of gastric origin versus colorectal origin. *Obstet. Gynecol. Sci.* **58,** 32 (2015).
31. Klinkebiel, D., Zhang, W., Akers, S. N., Odunsi, K. & Karpf, A. R. DNA Methylome Analyses Implicate Fallopian Tube Epithelia as the Origin for High-Grade Serous Ovarian Cancer. *Mol. Cancer Res.* **14,** 787–94 (2016).
32. Coscia, F. *et al.* Integrative proteomic profiling of ovarian cancer cell lines reveals precursor cell associated proteins and functional status. *Nat. Commun.* **7,** 12645 (2016).
33. Kipps, E., Tan, D. S. P. & Kaye, S. B. Meeting the challenge of ascites in ovarian cancer: new avenues for therapy and research. *Nat. Rev. Cancer* **13,** 273–282 (2013).
34. Ovarian cancer. Available at: http://simplehealth-healthbeautywellness.blogspot.com.es/2013/03/ovarian-cancer.html. (Accessed: 20th March 2003)
35. Myers, E. R. *et al.* Management of adnexal mass. *Evid. Rep. Technol. Assess. (Full. Rep).* 1–145 (2006).
36. Menon, U. *et al.* Sensitivity and specificity of multimodal and ultrasound screening for ovarian cancer, and stage distribution of detected cancers: results of the prevalence screen of the UK Collaborative Trial of Ovarian Cancer Screening (UKCTOCS). *Lancet. Oncol.* **10,** 327–40 (2009).
37. Skates, S. J., Jacobs, I. J. & Knapp, R. C. in *Ovarian Cancer* 61–73 (Humana Press). doi:10.1385/1-59259-071-3:61
38. Bast, R. C. & Spriggs, D. R. More than a biomarker: CA125 may contribute to ovarian cancer pathogenesis. *Gynecol. Oncol.* **121,** 429–430 (2011).
39. Karimi-Zarchi, M., Dehshiri-Zadeh, N., Sekhavat, L. & Nosouhi, F. Correlation of CA-125 serum level and clinico-pathological characteristic of patients with endometriosis. *Int. J. Reprod. Biomed. (Yazd, Iran)* **14,** 713–718 (2016).
40. Liang, C. *et al.* Oncogenic KRAS Targets MUC16/CA125 in Pancreatic Ductal Adenocarcinoma. *Mol. Cancer Res.* **15,** 201–212 (2017).
41. Guo, N. & Peng, Z. Does serum CA125 have clinical value for follow-up monitoring of postoperative patients with epithelial ovarian cancer? Results of a 12-year study. *J. Ovarian Res.* **10,** 14 (2017).
42. Bast, R. C. *et al.* A Radioimmunoassay Using a Monoclonal Antibody to Monitor the Course of Epithelial Ovarian Cancer. *N. Engl. J. Med.* **309,** 883–887 (1983).
43. Algeciras-Schimnich, A. Ovarian Cancer: A Review of Current Serum Markers and Their Clinical Applications. (2013). Available at: https://www.aacc.org/publications/cln/articles/2013/march/ovarian-cancer. (Accessed: 1st March 2013)
44. Fuzery, A. K., Levin, J., Chan, M. M. & Chan, D. W. Translation of proteomic biomarkers into FDA approved cancer diagnostics: issues and challenges. *Clin. Proteomics* **10,** 13 (2013).
45. Ueland, F. A Perspective on Ovarian Cancer Biomarkers: Past, Present and Yet-To-Come. *Diagnostics* **7,** 14 (2017).
46. Buchen, L. Cancer: Missing the mark. *Nature* **471,** 428–432 (2011).
47. Buys, S. S. Effect of Screening on Ovarian Cancer Mortality. The Prostate, Lung, Colorectal and Ovarian (PLCO) Cancer Screening Randomized Controlled Trial. *JAMA* **305,** 2295 (2011).
48. Jacobs, I. J. *et al.* Ovarian cancer screening and mortality in the UK Collaborative Trial of Ovarian Cancer Screening (UKCTOCS): a randomised controlled trial. *Lancet (London, England)* **387,** 945–56 (2016).
49. Rosenthal, A. N. *et al.* Evidence of Stage Shift in Women Diagnosed With Ovarian Cancer During Phase II of the United Kingdom Familial Ovarian Cancer Screening Study. *J. Clin. Oncol.* JCO.2016.69.933 (2017). doi:10.1200/JCO.2016.69.9330
50. Check, E. Proteomics and cancer: running before we can walk? *Nature* **429,** 496–7 (2004).
51. Petricoin, E. F. *et al.* Use of proteomic patterns in serum to identify ovarian cancer. *Lancet* **359,** 572–577 (2002).
52. Mor G, Visintin I, Lai Y, Zhao H, Schwartz P, Rutherford T, Yue L, Bray-Ward P, W. D. Serum protein markers for early detection of ovarian cancer. *Proc Natl Acad Sci U S A.* **102(21),** 7677–82 (2005).
53. Schwartz PE, Mor G, Visintin I, Feng Z, Longton G, Ward DC, Alvero AB, Lai Y, Tenthorey J, Leiser A, Flores-Saaib R, Yu H, Azori M, R. T. Diagnostic Markers for Early Detection of Ovarian Cancer. *Clin. Cancer Res.* **14,** 1065–1072 (2008).
54. Zhang, Z. *et al.* Three biomarkers identified from serum proteomic analysis for the detection of

early stage ovarian cancer. *Cancer Res.* **64,** 5882–90 (2004).
55. Fung, E. T. A recipe for proteomics diagnostic test development: the OVA1 test, from biomarker discovery to FDA clearance. *Clin. Chem.* **56,** 327–9 (2010).
56. Hellström, I. *et al.* The HE4 (WFDC2) protein is a biomarker for ovarian carcinoma. *Cancer Res.* **63,** 3695–700 (2003).
57. Wu, L. *et al.* Diagnostic Value of Serum Human Epididymis Protein 4 (HE4) in Ovarian Carcinoma. *Int. J. Gynecol. Cancer* **22,** 1106–1112 (2012).
58. Fawzy, A., Mohamed, M. R., Ali, M. A., Abd El-Magied, M. H. & Helal, A. M. Tissue CA125 and HE4 Gene Expression Levels Offer Superior Accuracy in Discriminating Benign from Malignant Pelvic Masses. *Asian Pac. J. Cancer Prev.* **17,** 323–33 (2016).
59. Galgano, M. T., Hampton, G. M. & Frierson, H. F. Comprehensive analysis of HE4 expression in normal and malignant human tissues. *Mod. Pathol.* (2006). doi:10.1038/modpathol.3800612
60. Stiekema, A. *et al.* Human epididymis protein 4 immunostaining of malignant ascites differentiates cancer of Müllerian origin from gastrointestinal cancer. *Cancer Cytopathol.* **125,** 197–204 (2017).
61. Moore, R. G. *et al.* HE4 (WFDC2) gene overexpression promotes ovarian tumor growth. *Sci. Rep.* **4,** (2014).
62. Van Gorp, T. *et al.* HE4 and CA125 as a diagnostic test in ovarian cancer: prospective validation of the Risk of Ovarian Malignancy Algorithm. *Br. J. Cancer* **104,** 863–870 (2011).
63. Vallius, T. *et al.* Postoperative human epididymis protein 4 predicts primary therapy outcome in advanced epithelial ovarian cancer. *Tumor Biol.* **39,** 101042831769118 (2017).
64. Coleman, R. L. *et al.* Validation of a second-generation multivariate index assay for malignancy risk of adnexal masses. *Am. J. Obstet. Gynecol.* **215,** 82.e1-82.e11 (2016).
65. Michael, W. Vermillion Announces FDA Clearance of Overa®, Second Generation OVA1® Test. (2016). Available at: http://www.prnewswire.com/news-releases/vermillion-announces-fda-clearance-of-overa-second-generation-ova1-test-300238668.html.
66. Russell, M. R. *et al.* Protein Z: A putative novel biomarker for early detection of ovarian cancer. *Int. J. cancer* **138,** 2984–92 (2016).
67. Russell, M. R. *et al.* Novel risk models for early detection and screening of ovarian cancer. *Oncotarget* (2016). doi:10.18632/oncotarget.13648
68. Yan, W. *et al.* Systematic comparison of the human saliva and plasma proteomes. *Proteomics. Clin. Appl.* **3,** 116–134 (2009).
69. Loo, J. A., Yan, W., Ramachandran, P. & Wong, D. T. Comparative human salivary and plasma proteomes. *J. Dent. Res.* **89,** 1016–23 (2010).
70. Mandel, I. D. The role of saliva in maintaining oral homeostasis. *J. Am. Dent. Assoc.* **119,** 298–304 (1989).
71. Amerongen, A. V. N. & Veerman, E. C. I. Saliva-the defender of the oral cavity. *Oral Dis.* **8,** 12–22 (2002).
72. Teshima, K. *et al.* Radiation-induced parotid gland changes in oral cancer patients: correlation between parotid volume and saliva production. *Jpn. J. Clin. Oncol.* **40,** 42–6 (2010).
73. Spielmann, N. & Wong, D. T. Saliva: diagnostics and therapeutic perspectives. *Oral Dis.* **17,** 345–54 (2011).
74. Segal, A. & Wong, D. T. Salivary diagnostics: enhancing disease detection and making medicine better. *Eur. J. Dent. Educ.* **12 Suppl 1,** 22–9 (2008).
75. Hu, S. *et al.* Human saliva proteome and transcriptome. *J. Dent. Res.* **85,** 1129–33 (2006).
76. Rapado-Gonzalez, O., Majem, B., Muinelo-Romay, L., L?pez-L?pez, R. & Suarez-Cunqueiro, M. Cancer Salivary Biomarkers for Tumours Distant to the Oral Cavity. *Int. J. Mol. Sci.* **17,** 1531 (2016).
77. Ramachandran, P. *et al.* Identification of N-linked glycoproteins in human saliva by glycoprotein capture and mass spectrometry. *J. Proteome Res.* **5,** 1493–503 (2006).
78. Whitelegge, J. P. *et al.* Protein-Sequence Polymorphisms and Post-translational Modifications in Proteins from Human Saliva using Top-Down Fourier-transform Ion Cyclotron Resonance Mass Spectrometry. *Int. J. Mass Spectrom.* **268,** 190–197 (2007).
79. Sondej, M. *et al.* Glycoprofiling of the Human Salivary Proteome. *Clin. Proteomics* **5,** 52–68 (2009).
80. Hu, S., Jiang, J. & Wong, D. T. Proteomic analysis of saliva: 2D gel electrophoresis, LC-MS/MS, and Western blotting. *Methods Mol. Biol.* **666,** 31–41 (2010).
81. Halgand, F. *et al.* Defining intact protein primary structures from saliva: a step toward the human proteome project. *Anal. Chem.* **84,** 4383–95 (2012).
82. Li, Y., Zhou, X., St John, M. A. R. & Wong, D. T. W. RNA profiling of cell-free saliva using

microarray technology. *J. Dent. Res.* **83,** 199–203 (2004).
83. Hu, Z. *et al.* Exon-level expression profiling: A comprehensive transcriptome analysis of oral fluids. *Clin. Chem.* **54,** 824–832 (2008).
84. Wei, F. *et al.* Electrochemical detection of low-copy number salivary RNA based on specific signal amplification with a hairpin probe. *Nucleic Acids Res.* **36,** e65 (2008).
85. Palanisamy, V. & Wong, D. T. Transcriptomic analyses of saliva. *Methods Mol. Biol.* **666,** 43–51 (2010).
86. Bahn, J. H. *et al.* The Landscape of MicroRNA, Piwi-Interacting RNA, and Circular RNA in Human Saliva. *Clin. Chem.* (2014). doi:10.1373/clinchem.2014.230433
87. Majem, B., Li, F., Sun, J. & Wong, D. T. W. RNA Sequencing Analysis of Salivary Extracellular RNA. 17–36 (2017). doi:10.1007/978-1-4939-6685-1_2
88. Farrell, J. J. *et al.* Variations of oral microbiota are associated with pancreatic diseases including pancreatic cancer. *Gut* **61,** 582–8 (2012).
89. Torres, P. J. *et al.* Characterization of the salivary microbiome in patients with pancreatic cancer. *PeerJ* **3,** e1373 (2015).
90. Lim, Y. *et al.* Salivary DNA methylation panel to diagnose HPV-positive and HPV-negative head and neck cancers. *BMC Cancer* **16,** 749 (2016).
91. Sugimoto, M., Wong, D. T., Hirayama, A., Soga, T. & Tomita, M. Capillary electrophoresis mass spectrometry-based saliva metabolomics identified oral, breast and pancreatic cancer-specific profiles. *Metabolomics* **6,** 78–95 (2010).
92. Barnes, V. M. *et al.* Global metabolomic analysis of human saliva and plasma from healthy and diabetic subjects, with and without periodontal disease. *PLoS One* **9,** e105181 (2014).
93. Ishikawa, S. *et al.* Identification of salivary metabolomic biomarkers for oral cancer screening. *Sci. Rep.* **6,** 31520 (2016).
94. Salivaomics Knowledge Base. *accessed on 23 July 2010* (2012). Available at: www.skb.ucla.edu.
95. Ai, J., Smith, B. & Wong, D. T. Saliva Ontology: an ontology-based framework for a Salivaomics Knowledge Base. *BMC Bioinformatics* **11,** 302 (2010).
96. Wong, D. T. W. Salivaomics. *J. Am. Dent. Assoc.* **143,** 19S–24S (2012).
97. Navazesh, M. Methods for collecting saliva. *Ann. N. Y. Acad. Sci.* **694,** 72–77 (1993).
98. Henson, B. S. & Wong, D. T. Collection, storage, and processing of saliva samples for downstream molecular applications. *Methods Mol. Biol.* **666,** 21–30 (2010).
99. Park, N. J. *et al.* RNAprotect saliva: An optimal room- temperature stabilization reagent for the salivary transcriptome. *Clin. Chem.* **52,** 2303–4 (2006).
100. Jiang, J., Park, N. J., Hu, S. & Wong, D. T. A universal pre-analytic solution for concurrent stabilization of salivary proteins, RNA and DNA at ambient temperature. *Arch. Oral Biol.* **54,** 268–73 (2009).
101. Xiao, H. & Wong, D. T. W. Method development for proteome stabilization in human saliva. *Anal. Chim. Acta* **722,** 63–9 (2012).
102. Hu, S. *et al.* Preclinical validation of salivary biomarkers for primary Sjögren's syndrome. *Arthritis Care Res. (Hoboken).* **62,** 1633–8 (2010).
103. Hall, S. C. *et al.* Alterations in the Salivary Proteome and N-Glycome of Sjögren's Syndrome Patients. *J. Proteome Res.* (2017). doi:10.1021/acs.jproteome.6b01051
104. Li, Y. *et al.* Salivary transcriptome diagnostics for oral cancer detection. *Clin. Cancer Res.* **10,** 8442–8450 (2004).
105. Elashoff, D. *et al.* Prevalidation of salivary biomarkers for oral cancer detection. *Cancer Epidemiol. Biomarkers Prev.* **21,** 664–72 (2012).
106. Gleber-Netto, F. O. *et al.* Salivary Biomarkers for Detection of Oral Squamous Cell Carcinoma in a Taiwanese Population. *Clin. Cancer Res.* **22,** 3340–3347 (2016).
107. Honarmand, M. H., Farhad-Mollashahi, L., Nakhaee, A. & Nehi, M. Salivary Levels of ErbB2 and CEA in Oral Squamous Cell Carcinoma Patients. *Asian Pac. J. Cancer Prev.* **17,** 77–80 (2016).
108. Jiang, W.-W. *et al.* Increased mitochondrial DNA content in saliva associated with head and neck cancer. *Clin. Cancer Res.* **11,** 2486–91 (2005).
109. Wang, Y. *et al.* Detection of somatic mutations and HPV in the saliva and plasma of patients with head and neck squamous cell carcinomas. *Sci. Transl. Med.* **7,** 293ra104-293ra104 (2015).
110. Tamashiro, H. & Constantine, N. T. Serological diagnosis of HIV infection using oral fluid samples. *Bull. World Health Organ.* **72,** 135–43 (1994).
111. Hodinka, R. L., Nagashunmugam, T. & Malamud, D. Detection of human immunodeficiency virus antibodies in oral fluids. *Clin. Diagn. Lab. Immunol.* **5,** 419–26 (1998).
112. Yaari, A. *et al.* Detection of HCV salivary antibodies by a simple and rapid test. *J. Virol. Methods*

133, 1–5 (2006).
113. Cha, Y. J. *et al.* Performance evaluation of the OraQuick hepatitis C virus rapid antibody test. *Ann. Lab. Med.* **33,** 184–9 (2013).
114. Rao, P. V *et al.* Proteomic identification of salivary biomarkers of type-2 diabetes. *J. Proteome Res.* **8,** 239–45 (2009).
115. Lu, L., Mackay, D. F., Newby, D. E. & Pell, J. P. Association Between Salivary Cotinine and Cardiovascular Biomarkers Among Nonsmokers and Current Smokers: Cross-sectional Study of 10,081 Participants. *Eur. J. Vasc. Endovasc. Surg.* **48,** 703–10 (2014).
116. Zheng, H. *et al.* Salivary biomarkers indicate obstructive sleep apnea patients with cardiovascular diseases. *Sci. Rep.* **4,** 7046 (2014).
117. Gao, K. *et al.* Systemic disease-induced salivary biomarker profiles in mouse models of melanoma and non-small cell lung cancer. *PLoS One* **4,** e5875 (2009).
118. Xiao, H. *et al.* Proteomic analysis of human saliva from lung cancer patients using two-dimensional difference gel electrophoresis and mass spectrometry. *Mol. Cell. Proteomics* **11,** M111.012112 (2012).
119. Zhang, L. *et al.* Development of transcriptomic biomarker signature in human saliva to detect lung cancer. *Cell. Mol. Life Sci.* **69,** 3341–50 (2012).
120. Wei, F. *et al.* Noninvasive saliva-based EGFR gene mutation detection in patients with lung cancer. *Am. J. Respir. Crit. Care Med.* **190,** 1117–26 (2014).
121. Zhang, L. *et al.* Salivary transcriptomic biomarkers for detection of resectable pancreatic cancer. *Gastroenterology* **138,** 949-57–7 (2010).
122. Lau, C. *et al.* Role of pancreatic cancer-derived exosomes in salivary biomarker development. *J. Biol. Chem.* **288,** 26888–97 (2013).
123. Xie, Z. *et al.* Salivary HOTAIR and PVT1 as novel biomarkers for early pancreatic cancer. *Oncotarget* (2016). doi:10.18632/oncotarget.8323
124. Brooks, M. N. *et al.* Salivary protein factors are elevated in breast cancer patients. *Mol. Med. Rep.* **1,** 375–8 (2008).
125. Zhang, L. *et al.* Discovery and preclinical validation of salivary transcriptomic and proteomic biomarkers for the non-invasive detection of breast cancer. *PLoS One* **5,** e15573 (2010).
126. Xiao, H. *et al.* Differential Proteomic Analysis of Human Saliva using Tandem Mass Tags Quantification for Gastric Cancer Detection. *Sci. Rep.* **6,** 22165 (2016).
127. Lee, Y.-H., Kim, J. H., Zhou, H., Kim, B. W. & Wong, D. T. Salivary transcriptomic biomarkers for detection of ovarian cancer: for serous papillary adenocarcinoma. *J. Mol. Med. (Berl).* **90,** 427–34 (2012).
128. Yoshizawa, J. M. *et al.* Salivary biomarkers: toward future clinical and diagnostic utilities. *Clin. Microbiol. Rev.* **26,** 781–91 (2013).
129. Vanderburg, B. B. Extracellular Vesicle Detection For Pancreatic Cancer Diagnosis. (2017).
130. GAU, V. & WONG, D. Oral Fluid Nanosensor Test (OFNASET) with Advanced Electrochemical-Based Molecular Analysis Platform. *Ann. N. Y. Acad. Sci.* **1098,** 401–410 (2007).
131. Dong, T. & Matos Pires, N. M. Immunodetection of salivary biomarkers by an optical microfluidic biosensor with polyethylenimine-modified polythiophene-C 70 organic photodetectors. *Biosens. Bioelectron.* (2017). doi:10.1016/j.bios.2017.03.005
132. Mishra, S. *et al.* Recent advances in salivary cancer diagnostics enabled by biosensors and bioelectronics. *Biosens. Bioelectron.* **81,** 181–197 (2016).
133. Majem, B., Rigau, M., Reventós, J. & Wong, D. T. Non-coding RNAs in saliva: emerging biomarkers for molecular diagnostics. *Int. J. Mol. Sci.* **16,** 8676–98 (2015).
134. Chen, D. X., Schwartz, P. E. & Li, F. Q. Saliva and serum CA 125 assays for detecting malignant ovarian tumors. *Obstet. Gynecol.* **75,** 701–4 (1990).
135. Karam, A. *et al.* Fifth Ovarian Cancer Consensus Conference of the Gynecologic Cancer InterGroup: first-line interventions. *Ann. Oncol.* **28,** 711–717 (2017).
136. Minig, L., Padilla-Iserte, P. & Zorrero, C. The Relevance of Gynecologic Oncologists to Provide High-Quality of Care to Women with Gynecological Cancer. *Front. Oncol.* **5,** (2016).
137. Stewart, S. L., Townsend, J. S., Puckett, M. C. & Rim, S. H. Adherence of Primary Care Physicians to Evidence-Based Recommendations to Reduce Ovarian Cancer Mortality. *J. Women's Heal.* **25,** 235–241 (2016).
138. Vergote, I. *et al.* Neoadjuvant Chemotherapy or Primary Surgery in Stage IIIC or IV Ovarian Cancer. *N. Engl. J. Med.* **363,** 943–953 (2010).
139. SEGO. *Oncoguía SEGO: Cancer Epitelial de ovario, trompa y peritoneo 2014. Guías de práctica clínica en cáncer ginecológico y mamario.* (2014).
140. Boone, J. D., Dobbin, Z. C., Straughn, J. M. & Buchsbaum, D. J. Ovarian and cervical cancer

patient derived xenografts: The past, present, and future. *Gynecol. Oncol.* **138,** 486–491 (2015).
141. Heo, E. J. *et al.* Patient-Derived Xenograft Models of Epithelial Ovarian Cancer for Preclinical Studies. *Cancer Res. Treat.* (2017). doi:10.4143/crt.2016.322
142. Kehoe, S. *et al.* Primary chemotherapy versus primary surgery for newly diagnosed advanced ovarian cancer (CHORUS): an open-label, randomised, controlled, non-inferiority trial. *Lancet (London, England)* **386,** 249–57 (2015).
143. Onda, T. *et al.* Phase III Trial of Upfront Debulking Surgery Versus Neoadjuvant Chemotherapy for Stage III/IV Ovarian, Tubal and Peritoneal Cancers: Japan Clinical Oncology Group Study JCOG0602. *Jpn. J. Clin. Oncol.* **38,** 74–77 (2008).
144. Gadducci, A. *et al.* Patterns of Recurrence and Clinical Outcome of Patients With Stage IIIC to Stage IV Epithelial Ovarian Cancer in Complete Response After Primary Debulking Surgery Plus Chemotherapy or Neoadjuvant Chemotherapy Followed by Interval Debulking Surgery. *Int. J. Gynecol. Cancer* **27,** 28–36 (2017).
145. Onda, T. *et al.* Comparison of treatment invasiveness between upfront debulking surgery versus interval debulking surgery following neoadjuvant chemotherapy for stage III/IV ovarian, tubal, and peritoneal cancers in a phase III randomised trial: Japan Clinical Oncology Gr. *Eur. J. Cancer* **64,** 22–31 (2016).
146. Makar, A. P., Tropé, C. G., Tummers, P., Denys, H. & Vandecasteele, K. Advanced Ovarian Cancer: Primary or Interval Debulking? Five Categories of Patients in View of the Results of Randomized Trials and Tumor Biology: Primary Debulking Surgery and Interval Debulking Surgery for Advanced Ovarian Cancer. *Oncologist* **21,** 745–54 (2016).
147. Vaughan, S. *et al.* Rethinking ovarian cancer: recommendations for improving outcomes. *Nat. Rev. Cancer* **11,** 719–725 (2011).
148. Abal, M., Andreu, J. M. & Barasoain, I. Taxanes: microtubule and centrosome targets, and cell cycle dependent mechanisms of action. *Curr. Cancer Drug Targets* **3,** 193–203 (2003).
149. Carboplatin AUC Dose Calculation (Calvert formula). *Medscape Drugs & Diseases* Available at: http://reference.medscape.com/calculator/carboplatin-auc-dose-calvert.
150. Grabosch SM, Edwards RP, H. C. Ovarian Cancer Treatment Protocols. (2016). Available at: http://emedicine.medscape.com/article/2006723-overview.
151. Seagle, B.-L. L. & Shahabi, S. Cost-effectiveness analysis of dose-dense versus standard intravenous chemotherapy for ovarian cancer: An economic analysis of results from the Gynecologic Oncology Group protocol 262 randomized controlled trial. *Gynecol. Oncol.* **145,** 9–14 (2017).
152. Katsumata, N. *et al.* Long-term results of dose-dense paclitaxel and carboplatin versus conventional paclitaxel and carboplatin for treatment of advanced epithelial ovarian, fallopian tube, or primary peritoneal cancer (JGOG 3016): a randomised, controlled, open-label trial. *Lancet Oncol.* **14,** 1020–1026 (2013).
153. Chan, J. K. *et al.* Weekly vs. Every-3-Week Paclitaxel and Carboplatin for Ovarian Cancer. *N. Engl. J. Med.* **374,** 738–748 (2016).
154. Armstrong, D. K. *et al.* Intraperitoneal Cisplatin and Paclitaxel in Ovarian Cancer. *N. Engl. J. Med.* **354,** 34–43 (2006).
155. Foley, Olivia W., Rauh-Hain, J. Alejandro, Del Carmen, M. G. Recurrent Epithelial Ovarian Cancer: An Update on Treatment. (2013). Available at: http://www.cancernetwork.com/oncology-journal/recurrent-epithelial-ovarian-cancer-update-treatment. (Accessed: 15th April 2013)
156. Markman, M. *et al.* Second-line platinum therapy in patients with ovarian cancer previously treated with cisplatin. *J. Clin. Oncol.* **9,** 389–393 (1991).
157. Alvarez, R. D. *et al.* Moving beyond the platinum sensitive/resistant paradigm for patients with recurrent ovarian cancer. *Gynecol. Oncol.* **141,** 405–409 (2016).
158. Burgess, D. J. Genetics: BRCA inequality. *Nat. Rev. Cancer* (2011). doi:10.1038/nrc3177
159. Yang, D. *et al.* Association of BRCA1 and BRCA2 Mutations With Survival, Chemotherapy Sensitivity, and Gene Mutator Phenotype in Patients With Ovarian Cancer. *JAMA* **306,** 1557 (2011).
160. Sehouli, J., Braicu, E. & Chekerov, R. PARP Inhibitors for Recurrent Ovarian Carcinoma: Current Treatment Options and Future Perspectives. *Geburtshilfe Frauenheilkd.* **76,** 164–169 (2016).
161. Chase, D. M., Chaplin, D. J. & Monk, B. J. The development and use of vascular targeted therapy in ovarian cancer. *Gynecol. Oncol.* (2017). doi:10.1016/j.ygyno.2017.01.031
162. Howitt, B. E. *et al.* Clear cell ovarian cancers with microsatellite instability: A unique subset of ovarian cancers with increased tumor-infiltrating lymphocytes and PD-1/PD-L1 expression. *Oncoimmunology* **6,** e1277308 (2017).
163. Oza, A. M. *et al.* Standard chemotherapy with or without bevacizumab for women with newly

diagnosed ovarian cancer (ICON7): overall survival results of a phase 3 randomised trial. *Lancet. Oncol.* **16,** 928–36 (2015).
164. Mullard, A. PARP inhibitors plough on. *Nat. Rev. Drug Discov.* **16,** 229–229 (2017).
165. Leung, A. W. Y., de Silva, T., Bally, M. B. & Lockwood, W. W. Synthetic lethality in lung cancer and translation to clinical therapies. *Mol. Cancer* **15,** 61 (2016).
166. George, A., Kaye, S. & Banerjee, S. Delivering widespread BRCA testing and PARP inhibition to patients with ovarian cancer. *Nat. Rev. Clin. Oncol.* (2016). doi:10.1038/nrclinonc.2016.191
167. Davies, H. *et al.* HRDetect is a predictor of BRCA1 and BRCA2 deficiency based on mutational signatures. *Nat. Med.* (2017). doi:10.1038/nm.4292
168. Kristeleit, R. *et al.* A Phase I-II Study of the Oral Poly(ADP-ribose) Polymerase Inhibitor Rucaparib in Patients with Germline BRCA1/2-mutated Ovarian Carcinoma or Other Solid Tumors. *Clin. Cancer Res.* clincanres.2796.2016 (2017). doi:10.1158/1078-0432.CCR-16-2796
169. Lord, C. J. & Ashworth, A. PARP inhibitors: Synthetic lethality in the clinic. *Science (80-.).* **355,** 1152–1158 (2017).
170. Lheureux, S. *et al.* Somatic BRCA1/2 Recovery as a Resistance Mechanism After Exceptional Response to Poly (ADP-ribose) Polymerase Inhibition. *J. Clin. Oncol.* JCO.2016.71.367 (2017). doi:10.1200/JCO.2016.71.3677
171. Kim, H. *et al.* Targeting the ATR/CHK1 axis with PARP inhibition results in tumor regression in BRCA mutant ovarian cancer models. *Clin. Cancer Res.* (2016). doi:10.1158/1078-0432.CCR-16-2273
172. Delaney, J. R. *et al.* Haploinsufficiency networks identify targetable patterns of allelic deficiency in low mutation ovarian cancer. *Nat. Commun.* **8,** 14423 (2017).
173. Lokadasan, R., James, F. V, Naranayan, G. & Prabhakaran, P. K. Targeted agents in epithelial ovarian cancer: review on emerging therapies and future developments. *Ecancermedicalscience* **10,** (2016).
174. Stover, E. H., Konstantinopoulos, P. A., Matulonis, U. A. & Swisher, E. M. Biomarkers of Response and Resistance to DNA Repair Targeted Therapies. *Clin. Cancer Res.* **22,** 5651–5660 (2016).
175. Zamore, P. D. & Haley, B. Ribo-gnome: the big world of small RNAs. *Science* **309,** 1519–24 (2005).
176. Ha, M. & Kim, V. N. Regulation of microRNA biogenesis. *Nat. Rev. Mol. Cell Biol.* **15,** 509–524 (2014).
177. Hutvagner, G. & Simard, M. J. Argonaute proteins: key players in RNA silencing. *Nat. Rev. Mol. Cell Biol.* **9,** 22–32 (2008).
178. Lin, S. & Gregory, R. I. MicroRNA biogenesis pathways in cancer. *Nat. Rev. Cancer* **15,** 321–333 (2015).
179. Melo, S. A. *et al.* A Genetic Defect in Exportin-5 Traps Precursor MicroRNAs in the Nucleus of Cancer Cells. *Cancer Cell* **18,** 303–315 (2010).
180. Foulkes, W. D., Priest, J. R. & Duchaine, T. F. DICER1: mutations, microRNAs and mechanisms. *Nat. Rev. Cancer* **14,** 662–672 (2014).
181. Meister, G. Argonaute proteins: functional insights and emerging roles. *Nat Rev Genet* **14,** 447–459 (2013).
182. Meister, G. *et al.* Human Argonaute2 Mediates RNA Cleavage Targeted by miRNAs and siRNAs. *Mol. Cell* **15,** 185–197 (2004).
183. Britten, R. J. & Davidson, E. H. Gene regulation for higher cells: a theory. *Science* **165,** 349–57 (1969).
184. Pasquinelli, A. E. *et al.* Conservation of the sequence and temporal expression of let-7 heterochronic regulatory RNA. *Nature* **408,** 86–9 (2000).
185. Lagos-Quintana, M. Identification of Novel Genes Coding for Small Expressed RNAs. *Science (80-.).* **294,** 853–858 (2001).
186. Lu, J. *et al.* MicroRNA expression profiles classify human cancers. *Nature* **435,** 834–838 (2005).
187. Dattilo, V. *et al.* SGK1 affects RAN/RANBP1/RANGAP1 via SP1 to play a critical role in pre-miRNA nuclear export: a new route of epigenomic regulation. *Sci. Rep.* **7,** 45361 (2017).
188. Slade, I. *et al.* DICER1 syndrome: clarifying the diagnosis, clinical features and management implications of a pleiotropic tumour predisposition syndrome. *J. Med. Genet.* **48,** 273–278 (2011).
189. Kumar, M. S. *et al.* Dicer1 functions as a haploinsufficient tumor suppressor. *Genes Dev.* **23,** 2700–2704 (2009).
190. Lopez-Serra, P. & Esteller, M. DNA methylation-associated silencing of tumor-suppressor microRNAs in cancer. *Oncogene* **31,** 1609–1622 (2012).

191. Suzuki, H. I. *et al.* Modulation of microRNA processing by p53. *Nature* **460,** 529–533 (2009).
192. He, L. *et al.* A microRNA component of the p53 tumour suppressor network. *Nature* **447,** 1130–1134 (2007).
193. Tucci, P. *et al.* Loss of p63 and its microRNA-205 target results in enhanced cell migration and metastasis in prostate cancer. *Proc. Natl. Acad. Sci.* **109,** 15312–15317 (2012).
194. Li, Y., Choi, P. S., Casey, S. C., Dill, D. L. & Felsher, D. W. MYC through miR-17-92 Suppresses Specific Target Genes to Maintain Survival, Autonomous Proliferation, and a Neoplastic State. *Cancer Cell* **26,** 262–272 (2014).
195. Li, Y., Casey, S. C., Choi, P. S. & Felsher, D. W. miR-17–92 explains MYC oncogene addiction. *Mol. Cell. Oncol.* **1,** e970092 (2014).
196. Brabletz, S. & Brabletz, T. The ZEB/miR-200 feedback loop—a motor of cellular plasticity in development and cancer? *EMBO Rep.* **11,** 670–677 (2010).
197. Jeon, Y.-J. *et al.* A set of NF-κB–regulated microRNAs induces acquired TRAIL resistance in Lung cancer. *Proc. Natl. Acad. Sci.* **112,** E3355–E3364 (2015).
198. Merritt, W. M. *et al.* Dicer, Drosha, and Outcomes in Patients with Ovarian Cancer. *N. Engl. J. Med.* **359,** 2641–2650 (2008).
199. Zhang, L. *et al.* Genomic and epigenetic alterations deregulate microRNA expression in human epithelial ovarian cancer. *Proc. Natl. Acad. Sci.* **105,** 7004–7009 (2008).
200. Prahm, K. P., Novotny, G. W., Høgdall, C. & Høgdall, E. Current status on microRNAs as biomarkers for ovarian cancer. *APMIS* **124,** 337–355 (2016).
201. Park, S.-M., Gaur, A. B., Lengyel, E. & Peter, M. E. The miR-200 family determines the epithelial phenotype of cancer cells by targeting the E-cadherin repressors ZEB1 and ZEB2. *Genes Dev.* **22,** 894–907 (2008).
202. Yang, D. *et al.* Integrated analyses identify a master microRNA regulatory network for the mesenchymal subtype in serous ovarian cancer. *Cancer Cell* **23,** 186–99 (2013).
203. Schwarzenbach, H., Nishida, N., Calin, G. A. & Pantel, K. Clinical relevance of circulating cell-free microRNAs in cancer. *Nat. Rev. Clin. Oncol.* **11,** 145–156 (2014).
204. Bardelli, A. & Pantel, K. Liquid Biopsies, What We Do Not Know (Yet). *Cancer Cell* **31,** 172–179 (2017).
205. Weber, J. A. *et al.* The microRNA spectrum in 12 body fluids. *Clin. Chem.* **56,** 1733–41 (2010).
206. Mitchell, P. S. *et al.* Circulating microRNAs as stable blood-based markers for cancer detection. *Proc. Natl. Acad. Sci.* **105,** 10513–10518 (2008).
207. Wan, J. C. M. *et al.* Liquid biopsies come of age: towards implementation of circulating tumour DNA. *Nat. Rev. Cancer* **17,** 223–238 (2017).
208. Siravegna, G., Marsoni, S., Siena, S. & Bardelli, A. Integrating liquid biopsies into the management of cancer. *Nat. Rev. Clin. Oncol.* (2017). doi:10.1038/nrclinonc.2017.14
209. Meng, X. *et al.* Diagnostic and prognostic potential of serum miR-7, miR-16, miR-25, miR-93, miR-182, miR-376a and miR-429 in ovarian cancer patients. *Br. J. Cancer* **113,** 1358–1366 (2015).
210. Meng, X. *et al.* Diagnostic and prognostic relevance of circulating exosomal miR-373, miR-200a, miR-200b and miR-200c in patients with epithelial ovarian cancer. *Oncotarget* (2016). doi:10.18632/oncotarget.7850
211. Zhang, Y. *et al.* Serum miRNAs panel (miR-16-2*, miR-195, miR-2861, miR-497) as novel non-invasive biomarkers for detection of cervical cancer. *Sci. Rep.* **5,** 17942 (2015).
212. Zuberi, M. *et al.* Utility of Serum miR-125b as a Diagnostic and Prognostic Indicator and Its Alliance with a Panel of Tumor Suppressor Genes in Epithelial Ovarian Cancer. *PLoS One* **11,** e0153902 (2016).
213. Todeschini, P. *et al.* Circulating miRNA landscape identifies miR-1246 as promising diagnostic biomarker in high-grade serous ovarian carcinoma: A validation across two independent cohorts. *Cancer Lett.* **388,** 320–327 (2017).
214. Zhu, T. *et al.* A Pilot Study of Circulating MicroRNA-125b as a Diagnostic and Prognostic Biomarker for Epithelial Ovarian Cancer. *Int. J. Gynecol. Cancer* **27,** 3–10 (2017).
215. Rupaimoole, R. & Slack, F. J. MicroRNA therapeutics: towards a new era for the management of cancer and other diseases. *Nat. Rev. Drug Discov.* **16,** 203–222 (2017).
216. Chung, V. Y. *et al.* GRHL2-miR-200-ZEB1 maintains the epithelial status of ovarian cancer through transcriptional regulation and histone modification. *Sci. Rep.* **6,** 19943 (2016).
217. Chen, R. *et al.* Regulation of IKKβ by miR-199a affects NF-κB activity in ovarian cancer cells. *Oncogene* **27,** 4712–4723 (2008).
218. Li, S. *et al.* Protein tyrosine phosphatase PTPN3 promotes drug resistance and stem cell-like characteristics in ovarian cancer. *Sci. Rep.* **6,** 36873 (2016).

219. Li, X. *et al.* microRNA-137 promotes apoptosis in ovarian cancer cells via the regulation of XIAP. *Br. J. Cancer* **116,** 66–76 (2017).
220. Wu, J. *et al.* The Fra-1–miR-134–SDS22 feedback loop amplifies ERK/JNK signaling and reduces chemosensitivity in ovarian cancer cells. *Cell Death Dis.* **7,** e2384 (2016).
221. Chang, C. *et al.* MicroRNA-134-3p is a novel potential inhibitor of human ovarian cancer stem cells by targeting RAB27A. *Gene* **605,** 99–107 (2017).
222. Xiang, Y. *et al.* MiR-152 and miR-185 co-contribute to ovarian cancer cells cisplatin sensitivity by targeting DNMT1 directly: a novel epigenetic therapy independent of decitabine. *Oncogene* **33,** 378–386 (2014).
223. Denoyelle, C. *et al.* miR-491-5p-induced apoptosis in ovarian carcinoma depends on the direct inhibition of both BCL-XL and EGFR leading to BIM activation. *Cell Death Dis.* **5,** e1445 (2014).
224. Liu, X. *et al.* MiR-1271 Inhibits Ovarian Cancer Growth by Targeting Cyclin G1. *Med. Sci. Monit.* **21,** 3152–3158 (2015).
225. Chen, X. *et al.* MicroRNA-145 targets TRIM2 and exerts tumor-suppressing functions in epithelial ovarian cancer. *Gynecol. Oncol.* **139,** 513–519 (2015).
226. Mitra, A. K. *et al.* Microenvironment-induced downregulation of miR-193b drives ovarian cancer metastasis. *Oncogene* **34,** 5923–5932 (2015).
227. Yang, Z. *et al.* miR-23a promotes IKKα expression but suppresses ST7L expression to contribute to the malignancy of epithelial ovarian cancer cells. *Br. J. Cancer* **115,** 731–740 (2016).
228. Seviour, E. G. *et al.* Functional proteomics identifies miRNAs to target a p27/Myc/phospho-Rb signature in breast and ovarian cancer. *Oncogene* **35,** 691–701 (2016).
229. Zhao, E. *et al.* Cancer mediates effector T cell dysfunction by targeting microRNAs and EZH2 via glycolysis restriction. *Nat. Immunol.* **17,** 95–103 (2015).
230. Liu, Y., Niu, Z., Lin, X. & Tian, Y. MiR-216b increases cisplatin sensitivity in ovarian cancer cells by targeting PARP1. *Cancer Gene Ther.* (2017). doi:10.1038/cgt.2017.6
231. Shepherd, T. G., Thériault, B. L., Campbell, E. J. & Nachtigal, M. W. Primary culture of ovarian surface epithelial cells and ascites-derived ovarian cancer cells from patients. *Nat. Protoc.* **1,** 2643–2649 (2007).
232. Andrés-León, E., Núñez-Torres, R. & Rojas, A. M. miARma-Seq: a comprehensive tool for miRNA, mRNA and circRNA analysis. *Sci. Rep.* **6,** 25749 (2016).
233. Moran, S. *et al.* Validation of DNA methylation profiling in formalin-fixed paraffin-embedded samples using the Infinium HumanMethylation450 Microarray. *Epigenetics* **9,** 829–833 (2014).
234. Iorio, F. *et al.* A Landscape of Pharmacogenomic Interactions in Cancer. *Cell* **166,** 740–754 (2016).
235. Naldini, L. *et al.* In vivo gene delivery and stable transduction of nondividing cells by a lentiviral vector. *Science* **272,** 263–7 (1996).
236. Soriano, A. *et al.* MicroRNA-497 impairs the growth of chemoresistant neuroblastoma cells by targeting cell cycle, survival and vascular permeability genes. *Oncotarget* **7,** 9271–87 (2016).
237. Jubierre, L. *et al.* BRG1/SMARCA4 is essential for neuroblastoma cell viability through modulation of cell death and survival pathways. *Oncogene* **35,** 5179–5190 (2016).
238. Langmead, B., Trapnell, C., Pop, M. & Salzberg, S. L. Ultrafast and memory-efficient alignment of short DNA sequences to the human genome. *Genome Biol.* **10,** R25 (2009).
239. Liao, Y., Smyth, G. K. & Shi, W. featureCounts: an efficient general purpose program for assigning sequence reads to genomic features. *Bioinformatics* **30,** 923–30 (2014).
240. Friedländer, M. R., Mackowiak, S. D., Li, N., Chen, W. & Rajewsky, N. miRDeep2 accurately identifies known and hundreds of novel microRNA genes in seven animal clades. *Nucleic Acids Res.* **40,** 37–52 (2012).
241. Robinson, M. D., McCarthy, D. J. & Smyth, G. K. edgeR: a Bioconductor package for differential expression analysis of digital gene expression data. *Bioinformatics* **26,** 139–140 (2010).
242. Subramanian, A. *et al.* Gene set enrichment analysis: A knowledge-based approach for interpreting genome-wide expression profiles. *Proc. Natl. Acad. Sci.* **102,** 15545–15550 (2005).
243. Weight to Molar Quantity (for nucleic acids). Available at: http://www.molbiol.ru/eng/scripts/01_07.html.
244. Spielmann, N. *et al.* The human salivary RNA transcriptome revealed by massively parallel sequencing. *Clin. Chem.* **58,** 1314–21 (2012).
245. Zhang, Q. *et al.* [Expression and significance of microRNAs in the p53 pathway in ovarian cancer cells and serous ovarian cancer tissues]. *Zhonghua Zhong Liu Za Zhi* **33,** 885–90 (2011).
246. Yuan, J.-M. *et al.* Downregulation of cell cycle-related proteins in ovarian cancer line and cell cycle arrest induced by microRNA. *Int. J. Clin. Exp. Med.* **8,** 18476–81 (2015).

247. Ma, L. ping, Li, N., He, X. jun & Zhang, Q. [miR-449b and miR-34c on inducing down-regulation of cell cycle-related proteins and cycle arrests in SKOV3-ipl cell, an ovarian cancer cell line]. *Beijing Da Xue Xue Bao.* **43,** 129–33 (2011).
248. Vandesompele, J. *et al.* Accurate normalization of real-time quantitative RT-PCR data by geometric averaging of multiple internal control genes. *Genome Biol.* **3,** RESEARCH0034 (2002).
249. Zehavi, L. *et al.* Silencing of a large microRNA cluster on human chromosome 14q32 in melanoma: biological effects of mir-376a and mir-376c on insulin growth factor 1 receptor. *Mol. Cancer* **11,** 44 (2012).
250. Maire, G. *et al.* Analysis of miRNA-gene expression-genomic profiles reveals complex mechanisms of microRNA deregulation in osteosarcoma. *Cancer Genet.* **204,** 138–146 (2011).
251. Takahashi, M. *et al.* Downregulation of WDR20 due to loss of 14q is involved in the malignant transformation of clear cell renal cell carcinoma. *Cancer Sci.* **107,** 417–423 (2016).
252. Li, J. *et al.* [Reversal effect of 5-aza-2-deoxycytidine on the maternally expressed gene 3 promoter hypermethylation and its inhibitory effect on the proliferation of epithelial ovarian cancer cells]. *Zhonghua Zhong Liu Za Zhi* **37,** 324–9 (2015).
253. Adair, S. J. & Hogan, K. T. Treatment of ovarian cancer cell lines with 5-aza-2′-deoxycytidine upregulates the expression of cancer-testis antigens and class I major histocompatibility complex-encoded molecules. *Cancer Immunol. Immunother.* **58,** 589–601 (2009).
254. Jacob, F. *et al.* Expression of GBGT1 is epigenetically regulated by DNA methylation in ovarian cancer cells. *BMC Mol. Biol.* **15,** 24 (2014).
255. Dweep, H. & Gretz, N. miRWalk2.0: a comprehensive atlas of microRNA-target interactions. *Nat. Methods* **12,** 697–697 (2015).
256. A Strategy for American Innovation: Driving Towards Sustainable Growth and Quality Jobs. Available at: http://www.apr-strasbourg.org/detail-document-411-.html. (Accessed: 5th August 2009)
257. KALIL, T. Grand Challenges of the 21st Century. (2010). Available at: https://obamawhitehouse.archives.gov/blog/2010/02/04/grand-challenges-21st-century. (Accessed: 4th February 2010)
258. Sazanov, A. A., Kiselyova, E. V., Zakharenko, A. A., Romanov, M. N. & Zaraysky, M. I. Plasma and saliva miR-21 expression in colorectal cancer patients. *J. Appl. Genet.* **58,** 231–237 (2017).
259. Hizir, M. S., Balcioglu, M., Rana, M., Robertson, N. M. & Yigit, M. V. Simultaneous detection of circulating oncomiRs from body fluids for prostate cancer staging using nanographene oxide. *ACS Appl. Mater. Interfaces* **6,** 14772–8 (2014).
260. Gao, S., Chen, L.-Y., Wang, P., Liu, L.-M. & Chen, Z. MicroRNA Expression in Salivary Supernatant of Patients with Pancreatic Cancer and Its Relationship with ZHENG. *Biomed Res. Int.* **2014,** 1–8 (2014).
261. Xie, Z. *et al.* Salivary microRNAs show potential as a noninvasive biomarker for detecting resectable pancreatic cancer. *Cancer Prev. Res. (Phila).* **8,** 165–73 (2015).
262. Humeau, M. *et al.* Salivary MicroRNA in Pancreatic Cancer Patients. *PLoS One* **10,** e0130996 (2015).
263. Machida, T. *et al.* miR-1246 and miR-4644 in salivary exosome as potential biomarkers for pancreatobiliary tract cancer. *Oncol. Rep.* (2016). doi:10.3892/or.2016.5021
264. Lau, C. S. & Wong, D. T. W. Breast Cancer Exosome-like Microvesicles and Salivary Gland Cells Interplay Alters Salivary Gland Cell-Derived Exosome-like Microvesicles In Vitro. *PLoS One* **7,** e33037 (2012).
265. Majem, B. Salivary exRNA: towards validated methods for RNA isolation, quality control, and NGS library construction. (2014). Available at: http://exrna.org/2014/11/. (Accessed: 6th November 2014)
266. Laurent, L. C. *et al.* Meeting report: discussions and preliminary findings on extracellular RNA measurement methods from laboratories in the NIH Extracellular RNA Communication Consortium. *J. Extracell. vesicles* **4,** 26533 (2015).
267. Corney, D. C. *et al.* Frequent Downregulation of miR-34 Family in Human Ovarian Cancers. *Clin. Cancer Res.* **16,** 1119–1128 (2010).
268. Hwang, C.-I. *et al.* Wild-type p53 controls cell motility and invasion by dual regulation of MET expression. *Proc. Natl. Acad. Sci.* **108,** 14240–14245 (2011).
269. Thomson, D. W. & Dinger, M. E. Endogenous microRNA sponges: evidence and controversy. *Nat. Rev. Genet.* **17,** 272–283 (2016).
270. Liu, D. *et al.* LncRNA SPRY4-IT1 sponges miR-101-3p to promote proliferation and metastasis of bladder cancer cells through up-regulating EZH2. *Cancer Lett.* **388,** 281–291 (2017).

271. Zeng, H.-F., Qiu, H.-Y. & Feng, F.-B. Long Noncoding RNA LINC01133 Sponges miR-422a to Aggravate the Tumorigenesis of Human Osteosarcoma. *Oncol. Res.* (2017). doi:10.3727/096504017X14907375885605
272. Hua, F., Li, C.-H., Chen, X.-G. & Liu, X.-P. Long Noncoding RNA CCAT2 Knockdown Suppresses Tumorous Progression By Sponging miR-424 in Epithelial Ovarian Vancer. *Oncol. Res. Featur. Preclin. Clin. Cancer Ther.* (2017). doi:10.3727/096504017X14953948675412
273. Yang, Y. *et al.* UCA1 functions as a competing endogenous RNA to suppress epithelial ovarian cancer metastasis. *Tumor Biol.* **37,** 10633–10641 (2016).
274. Valadi, H. *et al.* Exosome-mediated transfer of mRNAs and microRNAs is a novel mechanism of genetic exchange between cells. *Nat. Cell Biol.* **9,** 654–659 (2007).
275. Melo, S. A. *et al.* Cancer Exosomes Perform Cell-Independent MicroRNA Biogenesis and Promote Tumorigenesis. *Cancer Cell* **26,** 707–721 (2014).
276. Teng, Y. *et al.* MVP-mediated exosomal sorting of miR-193a promotes colon cancer progression. *Nat. Commun.* **8,** 14448 (2017).
277. Cha, D. J. *et al.* KRAS -dependent sorting of miRNA to exosomes. *Elife* **4,** (2015).
278. Wei, J. *et al.* Vps4A functions as a tumor suppressor by regulating the secretion and uptake of exosomal microRNAs in human hepatoma cells. *Hepatology* **61,** 1284–1294 (2015).
279. Palanisamy, V. *et al.* Nanostructural and transcriptomic analyses of human saliva derived exosomes. *PLoS One* **5,** e8577 (2010).
280. Sharma, S. *et al.* Structural-mechanical characterization of nanoparticle exosomes in human saliva, using correlative AFM, FESEM, and force spectroscopy. *ACS Nano* **4,** 1921–6 (2010).
281. Michael, a *et al.* Exosomes from human saliva as a source of microRNA biomarkers. *Oral Dis.* **16,** 34–8 (2010).
282. Byron, S. A., Van Keuren-Jensen, K. R., Engelthaler, D. M., Carpten, J. D. & Craig, D. W. Translating RNA sequencing into clinical diagnostics: opportunities and challenges. *Nat. Rev. Genet.* **17,** 257–271 (2016).
283. Zheng, B. *et al.* MicroRNA-409 suppresses tumour cell invasion and metastasis by directly targeting radixin in gastric cancers. *Oncogene* **31,** 4509–4516 (2012).
284. Li, C. *et al.* MicroRNA-409-3p regulates cell proliferation and apoptosis by targeting PHF10 in gastric cancer. *Cancer Lett.* **320,** 189–197 (2012).
285. Tan, S. *et al.* miR-409-3p sensitizes colon cancer cells to oxaliplatin by inhibiting Beclin-1-mediated autophagy. *Int. J. Mol. Med.* (2016). doi:10.3892/ijmm.2016.2492
286. Bai, R. *et al.* MicroRNA-409-3p suppresses colorectal cancer invasion and metastasis partly by targeting GAB1 expression. *Int. J. Cancer* **137,** 2310–2322 (2015).
287. Liu, M. *et al.* Downregulation of microRNA-409-3p promotes aggressiveness and metastasis in colorectal cancer: an indication for personalized medicine. *J. Transl. Med.* **13,** 195 (2015).
288. Josson, S. *et al.* miR-409-3p/-5p Promotes Tumorigenesis, Epithelial-to-Mesenchymal Transition, and Bone Metastasis of Human Prostate Cancer. *Clin. Cancer Res.* **20,** 4636–4646 (2014).
289. Josson, S. *et al.* Stromal fibroblast-derived miR-409 promotes epithelial-to-mesenchymal transition and prostate tumorigenesis. *Oncogene* **34,** 2690–2699 (2015).
290. Bi, L. *et al.* MicroRNA-127-3p acts as a tumor suppressor in epithelial ovarian cancer by regulating the BAG5 gene. *Oncol. Rep.* (2016). doi:10.3892/or.2016.5055
291. Jiang, H. *et al.* MicroRNA-127-3p promotes glioblastoma cell migration and invasion by targeting the tumor-suppressor gene SEPT7. *Oncol. Rep.* (2014). doi:10.3892/or.2014.3055
292. Livingstone, M. C., Johnson, N. M., Roebuck, B. D., Kensler, T. W. & Groopman, J. D. Profound changes in miRNA expression during cancer initiation by aflatoxin B 1 and their abrogation by the chemopreventive triterpenoid CDDO-Im. *Mol. Carcinog.* (2017). doi:10.1002/mc.22635
293. Jiang, H. *et al.* Next Generation Sequencing Analysis of miRNAs: MiR-127-3p Inhibits Glioblastoma Proliferation and Activates TGF-β Signaling by Targeting SKI. *Omi. A J. Integr. Biol.* **18,** 196–206 (2014).
294. Zhang, J. *et al.* MicroRNA-127-3p inhibits proliferation and invasion by targeting SETD8 in human osteosarcoma cells. *Biochem. Biophys. Res. Commun.* **469,** 1006–1011 (2016).
295. Fellenberg, J. *et al.* Restoration of miR-127-3p and miR-376a-3p counteracts the neoplastic phenotype of giant cell tumor of bone derived stromal cells by targeting COA1, GLE1 and PDIA6. *Cancer Lett.* **371,** 134–141 (2016).
296. Cummins, J. M. *et al.* The colorectal microRNAome. *Proc. Natl. Acad. Sci. U. S. A.* **103,** 3687–92 (2006).
297. Miyoshi, N. *et al.* Identification of an imprinted gene, Meg3/Gtl2 and its human homologue MEG3, first mapped on mouse distal chromosome 12 and human chromosome 14q. *Genes*

Cells **5,** 211–20 (2000).
298. Sheng, X. *et al.* Promoter hypermethylation influences the suppressive role of maternally expressedï¿½3, a long non-coding RNA, in the development of epithelial ovarian cancer. *Oncol. Rep.* (2014). doi:10.3892/or.2014.3208
299. Kircher, M., Bock, C. & Paulsen, M. Structural conservation versus functional divergence of maternally expressed microRNAs in the Dlk1/Gtl2 imprinting region. *BMC Genomics* **9,** 346 (2008).
300. Ostling, P. *et al.* Systematic Analysis of MicroRNAs Targeting the Androgen Receptor in Prostate Cancer Cells. *Cancer Res.* **71,** 1956–1967 (2011).
301. Paydas, S. *et al.* Micro-RNA (miRNA) profile in Hodgkin lymphoma: association between clinical and pathological variables. *Med. Oncol.* **33,** 34 (2016).
302. Tan, Y.-Y., Xu, X.-Y., Wang, J.-F., Zhang, C.-W. & Zhang, S.-C. MiR-654-5p attenuates breast cancer progression by targeting EPSTI1. *Am. J. Cancer Res.* **6,** 522–32 (2016).
303. Vieira Geraldo, M., Imoto Nakaya, H. & Teruko Kimura, E. Down-regulation of 14q32-encoded miRNAs and tumor suppressor role for miR-654-3p in papillary thyroid cancer. *Oncotarget* (2016). doi:10.18632/oncotarget.14162
304. Formosa, A. *et al.* MicroRNAs, miR-154, miR-299-5p, miR-376a, miR-376c, miR-377, miR-381, miR-487b, miR-485-3p, miR-495 and miR-654-3p, mapped to the 14q32.31 locus, regulate proliferation, apoptosis, migration and invasion in metastatic prostate cancer cells. *Oncogene* **33,** 5173–82 (2014).
305. Yang, H. *et al.* MicroRNAs regulate methionine adenosyltransferase 1A expression in hepatocellular carcinoma. *J. Clin. Invest.* **123,** 285–298 (2013).
306. Esquela-Kerscher, A. *et al.* The let-7 microRNA reduces tumor growth in mouse models of lung cancer. *Cell Cycle* **7,** 759–764 (2008).
307. Ahmed, N. & Stenvers, K. L. Getting to Know Ovarian Cancer Ascites: Opportunities for Targeted Therapy-Based Translational Research. *Front. Oncol.* **3,** (2013).
308. Wang, L., Mezencev, R., Švajdler, M., Benigno, B. B. & McDonald, J. F. Ectopic over-expression of miR-429 induces mesenchymal-to-epithelial transition (MET) and increased drug sensitivity in metastasizing ovarian cancer cells. *Gynecol. Oncol.* **134,** 96–103 (2014).
309. Scott, C. L., Becker, M. A., Haluska, P. & Samimi, G. Patient-Derived Xenograft Models to Improve Targeted Therapy in Epithelial Ovarian Cancer Treatment. *Front. Oncol.* **3,** (2013).
310. Chao, J.-R. *et al.* Hax1-mediated processing of HtrA2 by Parl allows survival of lymphocytes and neurons. *Nature* **452,** 98–102 (2008).
311. Han, Y. Overexpression of HAX-1 Protects Cardiac Myocytes From Apoptosis Through Caspase-9 Inhibition. *Circ. Res.* **99,** 415–423 (2006).
312. Yan, J., Ma, C., Cheng, J., Li, Z. & Liu, C. HAX-1 inhibits apoptosis in prostate cancer through the suppression of caspase-9 activation. *Oncol. Rep.* **34,** 2776–81 (2015).
313. Baumann, U. *et al.* Disruption of the PRKCD–FBXO25–HAX-1 axis attenuates the apoptotic response and drives lymphomagenesis. *Nat. Med.* **20,** 1401–1409 (2014).
314. Liu, H. *et al.* Regulation of Focal Adhesion Dynamics and Cell Motility by the EB2 and Hax1 Protein Complex. *J. Biol. Chem.* **290,** 30771–30782 (2015).
315. Cavnar, P. J., Berthier, E., Beebe, D. J. & Huttenlocher, A. Hax1 regulates neutrophil adhesion and motility through RhoA. *J. Cell Biol.* **193,** 465–473 (2011).
316. Klein, C. Kostmann's Disease and HCLS1-Associated Protein X-1 (HAX1). *J. Clin. Immunol.* **37,** 117–122 (2017).
317. Carlsson, G., Kristr?m, B., Nordenskj?ld, M., Henter, J.-I. & Fadeel, B. Ovarian failure in HAX1-deficient patients: is there a gender-specific difference in pubertal development in severe congenital neutropenia or Kostmann disease? *Acta Paediatr.* **102,** 78–82 (2013).
318. Gomathinayagam Rohini, Jayaraman Muralidharan , Ha Ji Hee, V. L. and D. D. N. Hax-1 is required for Rac1-Cortactin interaction and ovarian carcinoma cell migration. *Genes Cancer* 84 (2014). doi:10.18632/genesandcancer.8
319. Plutner, H. Rab1b regulates vesicular transport between the endoplasmic reticulum and successive Golgi compartments. *J. Cell Biol.* **115,** 31–43 (1991).
320. Halberg, N. *et al.* PITPNC1 Recruits RAB1B to the Golgi Network to Drive Malignant Secretion. *Cancer Cell* **29,** 339–353 (2016).
321. Kakuta, S. *et al.* Small GTPase Rab1B is associated with ATG9A vesicles and regulates autophagosome formation. *FASEB J.* fj.201601052R (2017). doi:10.1096/fj.201601052R
322. Zhai, H., Song, B., Xu, X., Zhu, W. & Ju, J. Inhibition of autophagy and tumor growth in colon cancer by miR-502. *Oncogene* **32,** 1570–9 (2013).
323. Abd Elmageed, Z. Y. *et al.* Neoplastic Reprogramming of Patient-Derived Adipose Stem Cells by

Prostate Cancer Cell-Associated Exosomes. *Stem Cells* **32,** 983–997 (2014).
324. Yang, X.-Z. *et al.* Overexpression of Rab1B and MMP9 predicts poor survival and good response to chemotherapy in patients with colorectal cancer. *Aging (Albany. NY).* (2017). doi:10.18632/aging.101200
325. Qin, H., Malek, S., Cowell, J. K. & Ren, M. Transformation of human CD34+ hematopoietic progenitor cells with DEK-NUP214 induces AML in an immunocompromised mouse model. *Oncogene* **35,** 5686–5691 (2016).
326. Li, Z. *et al.* PBX3 and MEIS1 Cooperate in Hematopoietic Cells to Drive Acute Myeloid Leukemias Characterized by a Core Transcriptome of the MLL-Rearranged Disease. *Cancer Res.* **76,** 619–629 (2016).
327. Zhou, J. *et al.* PU.1 is essential for MLL leukemia partially via crosstalk with the MEIS/HOX pathway. *Leukemia* **28,** 1436–1448 (2014).
328. Huang, H. *et al.* TET1 plays an essential oncogenic role in MLL-rearranged leukemia. *Proc. Natl. Acad. Sci.* **110,** 11994–11999 (2013).
329. Hájková H, Fritz MH, Haškovec C, Schwarz J, Šálek C, Marková J, Krejčík Z, Dostálová Merkerová M, Kostečka A, Vostrý M, Fuchs O, Michalová K, Cetkovský P, B. V. CBFB-MYH11 hypomethylation signature and PBX3 differential methylation revealed by targeted bisulfite sequencing in patients with acute myeloid leukemia. *J. Hematol. Oncol.* **7,** 66 (2014).
330. Jiang, X. *et al.* miR-495 is a tumor-suppressor microRNA down-regulated in MLL-rearranged leukemia. *Proc. Natl. Acad. Sci.* **109,** 19397–19402 (2012).
331. Li, Z. *et al.* Up-regulation of a HOXA-PBX3 homeobox-gene signature following down-regulation of miR-181 is associated with adverse prognosis in patients with cytogenetically abnormal AML. *Blood* **119,** 2314–2324 (2012).
332. Zhang, Z. *et al.* Loss of exosomal miR-320a from cancer-associated fibroblasts contributes to HCC proliferation and metastasis. *Cancer Lett.* **397,** 33–42 (2017).
333. Han, S.-Y. *et al.* MicroRNA-33a-3p suppresses cell migration and invasion by directly targeting PBX3 in human hepatocellular carcinoma. *Oncotarget* (2016). doi:10.18632/oncotarget.9886
334. Han, H. *et al.* PBX3 is targeted by multiple miRNAs and is essential for liver tumour-initiating cells. *Nat. Commun.* **6,** 8271 (2015).
335. Wang, S., Li, C., Wang, W. & Xing, C. PBX3 promotes gastric cancer invasion and metastasis by inducing epithelial-mesenchymal transition. *Oncol. Lett.* (2016). doi:10.3892/ol.2016.5305
336. Li, B., Zhang, S., Shen, H. & Li, C. MicroRNA-144-3p suppresses gastric cancer progression by inhibiting epithelial-to-mesenchymal transition through targeting PBX3. *Biochem. Biophys. Res. Commun.* **484,** 241–247 (2017).
337. Han, H.-B. PBX3 promotes migration and invasion of colorectal cancer cells via activation of MAPK/ERK signaling pathway. *World J. Gastroenterol.* **20,** 18260 (2014).
338. Bhatt, A. S., Erdjument-Bromage, H., Tempst, P., Craik, C. S. & Moasser, M. M. Adhesion signaling by a novel mitotic substrate of src kinases. *Oncogene* **24,** 5333–43 (2005).
339. Wong, C. H. *et al.* Phosphorylation of the SRC epithelial substrate Trask is tightly regulated in normal epithelia but widespread in many human epithelial cancers. *Clin. Cancer Res.* **15,** 2311–22 (2009).
340. Liu, H. *et al.* CUB-domain-containing protein 1 (CDCP1) activates Src to promote melanoma metastasis. *Proc. Natl. Acad. Sci. U. S. A.* **108,** 1379–84 (2011).
341. Alajati, A. *et al.* Interaction of CDCP1 with HER2 enhances HER2-driven tumorigenesis and promotes trastuzumab resistance in breast cancer. *Cell Rep.* **11,** 564–76 (2015).
342. Wright, H. J. *et al.* CDCP1 cleavage is necessary for homodimerization-induced migration of triple-negative breast cancer. *Oncogene* **35,** 4762–72 (2016).
343. Zeng, X.-J., Wu, Y.-H., Luo, M., Cong, P.-G. & Yu, H. Inhibition of pulmonary carcinoma proliferation or metastasis of miR-218 via down-regulating CDCP1 expression. *Eur. Rev. Med. Pharmacol. Sci.* **21,** 1502–1508 (2017).
344. Chiu, K.-L. *et al.* ADAM9 enhances CDCP1 by inhibiting miR-1 through EGFR signaling activation in lung cancer metastasis. *Oncotarget* (2017). doi:10.18632/oncotarget.17648
345. Uekita, T. *et al.* CUB-Domain-Containing Protein 1 Regulates Peritoneal Dissemination of Gastric Scirrhous Carcinoma. *Am. J. Pathol.* **172,** 1729–1739 (2008).
346. Nakashima, K. *et al.* Novel small molecule inhibiting CDCP1-PKC pathway reduces tumor metastasis and proliferation. *Cancer Sci.* **108,** 1049–1057 (2017).
347. Siva, A. C. *et al.* Targeting CUB domain-containing protein 1 with a monoclonal antibody inhibits metastasis in a prostate cancer model. *Cancer Res.* **68,** 3759–66 (2008).
348. Casar, B. *et al.* Blocking of CDCP1 cleavage in vivo prevents Akt-dependent survival and inhibits metastatic colonization through PARP1-mediated apoptosis of cancer cells. *Oncogene* **31,**

3924–3938 (2012).
349. Casar, B. *et al.* In vivo cleaved CDCP1 promotes early tumor dissemination via complexing with activated β1 integrin and induction of FAK/PI3K/Akt motility signaling. *Oncogene* **33,** 255–268 (2014).
350. Razorenova, O. V. *et al.* VHL loss in renal cell carcinoma leads to up-regulation of CUB domain-containing protein 1 to stimulate PKC?-driven migration. *Proc. Natl. Acad. Sci.* **108,** 1931–1936 (2011).
351. He, Y. *et al.* Elevated CDCP1 predicts poor patient outcome and mediates ovarian clear cell carcinoma by promoting tumor spheroid formation, cell migration and chemoresistance. *Oncogene* **35,** 468–478 (2016).
352. Harrington, B. S. *et al.* Cell line and patient-derived xenograft models reveal elevated CDCP1 as a target in high-grade serous ovarian cancer. *Br. J. Cancer* **114,** 417–426 (2016).
353. Vlad, C. *et al.* Expression of CDCP1 and ADAM12 in the ovarian cancer microenvironment. *J. BUON.* **21,** 973–978
354. Adams, M. N. *et al.* EGF inhibits constitutive internalization and palmitoylation-dependent degradation of membrane-spanning procancer CDCP1 promoting its availability on the cell surface. *Oncogene* **34,** 1375–1383 (2015).
355. Kas, K., Voz, M. L., Hensen, K., Meyen, E. & Van de Ven, W. J. M. Transcriptional Activation Capacity of the Novel PLAG Family of Zinc Finger Proteins. *J. Biol. Chem.* **273,** 23026–23032 (1998).
356. Hensen, K., Van Valckenborgh, I. C. C., Kas, K., Van de Ven, W. J. M. & Voz, M. L. The tumorigenic diversity of the three PLAG family members is associated with different DNA binding capacities. *Cancer Res.* **62,** 1510–7 (2002).
357. Zheng, G. & Yang, Y.-C. Sumoylation and Acetylation Play Opposite Roles in the Transactivation of PLAG1 and PLAGL2. *J. Biol. Chem.* **280,** 40773–40781 (2005).
358. Ning, J., Zheng, G. & Yang, Y.-C. Tip60 modulates PLAGL2-mediated transactivation by acetylation. *J. Cell. Biochem.* **103,** 730–739 (2008).
359. Hanks, T. S. & Gauss, K. A. Pleomorphic adenoma gene-like 2 regulates expression of the p53 family member, p73, and induces cell cycle block and apoptosis in human promonocytic U937 cells. *Apoptosis* **17,** 236–247 (2012).
360. Castilla, L. H. *et al.* Identification of genes that synergize with Cbfb-MYH11 in the pathogenesis of acute myeloid leukemia. *Proc. Natl. Acad. Sci.* **101,** 4924–4929 (2004).
361. Landrette SF, Kuo YH, Hensen K, Barjesteh van Waalwijk van Doorn-Khosrovani S, Perrat PN, Van de Ven WJ, Delwel R, C. L. Plag1 and Plagl2 are oncogenes that induce acute myeloid leukemia in cooperation with Cbfb-MYH11. *Blood* **105,** 2900–2907 (2005).
362. Landrette, S. F., Madera, D., He, F. & Castilla, L. H. The transcription factor PlagL2 activates Mpl transcription and signaling in hematopoietic progenitor and leukemia cells. *Leukemia* **25,** 655–662 (2011).
363. Zheng, H. *et al.* PLAGL2 Regulates Wnt Signaling to Impede Differentiation in Neural Stem Cells and Gliomas. *Cancer Cell* **17,** 497–509 (2010).
364. Wang, Y.-P. *et al.* Pleomorphic adenoma gene like-2 induces epithelial-mesenchymal transition via Wnt/b-catenin signaling pathway in human colorectal adenocarcinoma. *Oncol. Rep.* (2017). doi:10.3892/or.2017.5485
365. Sekiya, R. *et al.* PLAGL2 regulates actin cytoskeletal architecture and cell migration. *Carcinogenesis* **35,** 1993–2001 (2014).
366. Chang, F. *et al.* Involvement of PI3K/Akt pathway in cell cycle progression, apoptosis, and neoplastic transformation: a target for cancer chemotherapy. *Leukemia* **17,** 590–603 (2003).
367. Hamdi, A. *et al.* Tampering with cell division by using small-molecule inhibitors of CDK-CKS protein interactions. *Chembiochem* **16,** 432–9 (2015).
368. Otto, T. & Sicinski, P. Cell cycle proteins as promising targets in cancer therapy. *Nat. Rev. Cancer* **17,** 93–115 (2017).
369. Sui, L. *et al.* Clinical significance of Skp2 expression, alone and combined with Jab1 and p27 in epithelial ovarian tumors. *Oncol. Rep.* **15,** 765–71 (2006).
370. Hafez, M. M. *et al.* SKP2/P27 Kip1 pathway is associated with Advanced Ovarian Cancer in Saudi Patients. *Asian Pacific J. Cancer Prev.* **16,** 5807–5815 (2015).
371. Shin, J.-S. *et al.* Serum starvation induces G1 arrest through suppression of Skp2-CDK2 and CDK4 in SK-OV-3 cells. *Int. J. Oncol.* **32,** 435–9 (2008).
372. ZHANG, W. & LIU, H. T. MAPK signal pathways in the regulation of cell proliferation in mammalian cells. *Cell Res.* **12,** 9–18 (2002).
373. Hart, L. S. *et al.* Preclinical Therapeutic Synergy of MEK1/2 and CDK4/6 Inhibition in

Neuroblastoma. *Clin. Cancer Res.* **23,** 1785–1796 (2017).
374. Coller, H. A. *et al.* Expression analysis with oligonucleotide microarrays reveals that MYC regulates genes involved in growth, cell cycle, signaling, and adhesion. *Proc. Natl. Acad. Sci. U. S. A.* **97,** 3260–5 (2000).
375. Yang, W. *et al.* Repression of transcription of the p27Kip1 cyclin-dependent kinase inhibitor gene by c-Myc. *Oncogene* **20,** 1688–1702 (2001).
376. Yaowu He, Brittney S. Harrington, and J. D. H. New crossroads for potential therapeutic intervention in cancer - intersections between CDCP1, EGFR family members and downstream signaling pathways. *Oncoscience* (2016). doi:10.18632/oncoscience.286
377. Prathapam, T., Aleshin, A., Guan, Y., Gray, J. W. & Martin, G. S. p27Kip1 Mediates Addiction of Ovarian Cancer Cells to MYCC (c-MYC) and Their Dependence on MYC Paralogs. *J. Biol. Chem.* **285,** 32529–32538 (2010).
378. Reyes-Gonzalez, J. M. *et al.* Targeting c-MYC in Platinum-Resistant Ovarian Cancer. *Mol. Cancer Ther.* **14,** 2260–2269 (2015).
379. Au-Yeung, G. *et al.* Selective Targeting of Cyclin E1-Amplified High-Grade Serous Ovarian Cancer by Cyclin-Dependent Kinase 2 and AKT Inhibition. *Clin. Cancer Res.* **23,** 1862–1874 (2017).
380. Kahn, M. Can we safely target the WNT pathway? *Nat. Rev. Drug Discov.* **13,** 513–532 (2014).
381. Niehrs, C. The complex world of WNT receptor signalling. *Nat. Rev. Mol. Cell Biol.* **13,** 767–779 (2012).
382. Fang, X. *et al.* Phosphorylation and inactivation of glycogen synthase kinase 3 by protein kinase A. *Proc. Natl. Acad. Sci.* **97,** 11960–11965 (2000).
383. Anastas, J. N. & Moon, R. T. WNT signalling pathways as therapeutic targets in cancer. *Nat. Rev. Cancer* **13,** 11–26 (2012).
384. Mazon, M., Masi, D. & Carreau, M. Modulating Dickkopf-1: A Strategy to Monitor or Treat Cancer? *Cancers (Basel).* **8,** 62 (2016).
385. Kim, S. & Jho, E. -h. The Protein Stability of Axin, a Negative Regulator of Wnt Signaling, Is Regulated by Smad Ubiquitination Regulatory Factor 2 (Smurf2). *J. Biol. Chem.* **285,** 36420–36426 (2010).
386. Boone, J. D. *et al.* Targeting the Wnt/?-catenin pathway in primary ovarian cancer with the porcupine inhibitor WNT974. *Lab. Investig.* **96,** 249–259 (2016).
387. Nakai, H., Watanabe, Y., Ueda, H. & Hoshiai, H. Hypoxia inducible factor 1-α expression as a factor predictive of efficacy of taxane/platinum chemotherapy in advanced primary epithelial ovarian cancer. *Cancer Lett.* **251,** 164–167 (2007).
388. Horiuchi, A. *et al.* Hypoxia upregulates ovarian cancer invasiveness via the binding of HIF-1 to a hypoxia-induced, methylation-free hypoxia response element of S100A4 gene. *Int. J. Cancer* **131,** 1755–1767 (2012).
389. Cao, M. *et al.* HIF-2α regulates CDCP1 to promote PKCδ-mediated migration in hepatocellular carcinoma. *Tumor Biol.* **37,** 1651–1662 (2016).
390. Yap, T. A., Carden, C. P. & Kaye, S. B. Beyond chemotherapy: targeted therapies in ovarian cancer. *Nat. Rev. Cancer* **9,** 167–181 (2009).